MOLECULAR INTERACTIONS OF ADIPOCYTE FATTY ACID-BINDING PROTEIN WITH ACTIVATING AND NON-ACTIVATING LIGANDS: PROTEIN OLIGOMERIZATION AND LIGAND BINDING SITES

by

SAMAR HELMY RIZK

A dissertation submitted to the Graduate Faculty in Biochemistry in partial fulfillment of the requirements for the degree of Doctor of Philosophy, The City University of New York

2013

This manuscript has been read and accepted for the
Graduate Faculty in Biochemistry in satisfaction of the
dissertation requirement for the degree of Doctor of Philosophy.

Prof. Ruth E. Stark

Date — Chair of Examining Committee

Prof. Edward J. Kennelly

Date — Executive Officer

Prof. Ranajeet Ghose, City College

Prof. Ronald Koder, City College

Prof. Probal Banerjee, College of Staten Island

Prof. Judith Storch, Rutgers University
Supervision Committee

THE CITY UNIVERSITY OF NEW YORK

Abstract

MOLECULAR INTERACTIONS OF ADIPOCYTE FATTY ACID-BINDING PROTEIN WITH ACTIVATING AND NON-ACTIVATING LIGANDS: PROTEIN OLIGOMERIZATION AND LIGAND BINDING SITES

by

Samar Helmy Rizk

Adviser: Professor Ruth E. Stark

Intracellular lipid binding proteins involved in fatty acid transport and metabolism include adipocyte fatty acid-binding protein (AFABP), a 15 kDa polypeptide that plays a central role in the development of diabetes and atherosclerotic cardiovascular disease in experimental animals; the significant degree to which the protein is released into the bloodstream is thought to predict the development of Metabolic Syndrome. Upon binding of activating ligands such as linoleate and troglitazone (TDZ) or inactivating ligands such as oleate, AFABP has been proposed to adopt two alternative modes of self-association that activate or deactivate a nuclear localization signal. The goal of this study is to develop a molecular rationale for these contrasting ligand-associated signals. Both apo and liganded AFABP proteins were shown to maintain an overwhelmingly monomeric form in solution using size exclusion chromatography and static light scattering methods. Multidimensional solution-state nuclear magnetic resonance experiments were used to make sequential resonance assignments of the polypeptide backbone ^{1}H and ^{15}N nuclei. These assignments made possible ligand titration

experiments that identified the key protein residues involved in the binding and the defined binding site. Comparative analysis of the binding sites in the three holo proteins demonstrated that oleate and linoleate bind similarly in a U-shaped configuration within the protein binding cavity despite their contrasting functional behavior, whereas the activating linoleate and TDZ ligands bind at dissimilar sites with the AFABP protein.

ACKNOWLEDGMENTS

I would like to express my heartfelt gratitude and appreciation for my mentor, Prof. Ruth E. Stark, who generously provided guidance, mentorship and feedback for me every step of my Ph.D and whose gracious mentorship never stopped at academia but covered all aspects of life.

I would like to extend my appreciation to Dr. Cedric Bernard, who brought me to the learning of the NMR field and whose attention to detail and countless discussions were deeply valuable for my learning experience.

I would like to thank my committee members, Prof. Ranajeet Ghose, Prof. Ronald Koder, Prof. Probal Banerjee and Prof. Judith Storch, for their constructive feedback and unwavering support.

I give my thanks to both Dr. Hsin Wang who provided me detailed help in working in the NMR field with great patience and sincere attention, and to Dr. Shibani Bhattacharya for her assistance and discussions while performing the diffusion experiments at the New York Structural Biology Center. I also give my sincere appreciation to Dr. Subhasish Chatterjee for the countless discussions and his valuable friendship.

I would like to give my special thanks to all members of the Stark, Ghose and Tu's labs who helped me greatly in experimentation, analysis, friendly discussions and advice.

I would like give my deep thanks to my husband, Mohamed, and my daughter, Jannah, who were were there for me every step of the way; my parents who made it possible; and my brothers who made it fun and worthwhile.

Finally, I give many thanks to all members of my wonderful family and friends who gave me their help and support in this amazing journey.

DEDICATION

To *my* loving *husband, Dr. Mohamed Saad*, *the love of my life*, whose love and dedication carried me all way through this journey and are what I continuously count on.

To *my lovely daughter*, *Jannah Saad, the light of my life*, who inspires me and surprises me constantly.

To *my adoring mother and father, Mervat Abdelaty Abdelaty and Helmy Awad Rizk, my rock and my sanctuary*, who are always there for me and inspire me to strive higher.

To *my amazing brothers, Mohamad and Ahmed Helmy Rizk, my life companions*, who shower me with their generous and endless love and continuous support.

Table of Contents

List of Acronyms

3D	3 Dimensional
AFABP	Adipocyte Fatty Acid Binding Protein
B, K, L, IFABP	Brain, Keratinocyte, Liver, Intestinal Fatty Acid Binding Protein
ANS	2-anilino-8-naphthalene sulfonate
AUC	Area under the curve
BSA	Bovine Serum Albumin
CARLA	Coactivator-dependent Receptor Ligand Assay
cDNA	Complementary Deoxyribonucleic Acid
DMSO	Dimethyl Sulfoxide
dRI	differential Refractive Index
FA	Fatty Acid
GF	Gel filtration
GFP	Green Fluorescent Protein
HSQC	Heteronuclear Single Quantum Correlation
SRC	Steroid Receptor Coactivator
iLBP	Intracellular Lipid Binding Protein
ILBP	Ileal Lipid Binding Protein
IPTG	Isopropyl ß-D-1-thiogalactopyranoside
LB broth	Luria-Bertani broth
LBD	Ligand Binding Domain
LCFA	Long-Chain Fatty Acid
LOLA	Linoleic acid (linoleate)
MALS	Multi-Angle Light Scattering

MHz	Mega Hertz
mRNA	Messenger Ribonucleic Acid
MSDS	Material Safety Data Sheet
N_A	Avogadro's number
NLS	Nuclear Localization Signal
NMR	Nuclear Magnetic Resonance
NOE	Nuclear Overhauser Effect
NOESY	2D Nuclear Overhauser Effect Spectroscopy
OD	Optical density
OLA	Oleic acid (oleate)
PAP	Placental Alkaline Phosphatase
PMSF	Phenylmethylsulfonyl Fluoride
PPAR	Peroxisome Proliferator Activated Receptor
PPM	Parts Per Million
SAXS	Small-Angle Light Scattering
SEC	Size Exclusion Chromatography
SLS	Static Light scattering
TDZ	Troglitazone
TOCSY	Total Correlation Spectroscopy
TZD	Thiazolidinediones
UV	UltraViolet
VNMRS	Varian Nuclear Magnetic Resonance

List of Tables

List of Figures

I. Introduction

A. The Calycin Superfamily

The Calycin proteins are a structural superfamily (Flower 1993; Flower *et al.,* 1993), whose protein members bind hydrophobic ligands inside and outside the cell (Flower 1996). This superfamily is composed of three distinct families of ligand binding proteins: the lipocalins, avidins and intracellular lipid binding proteins (**Figure I. 1**).

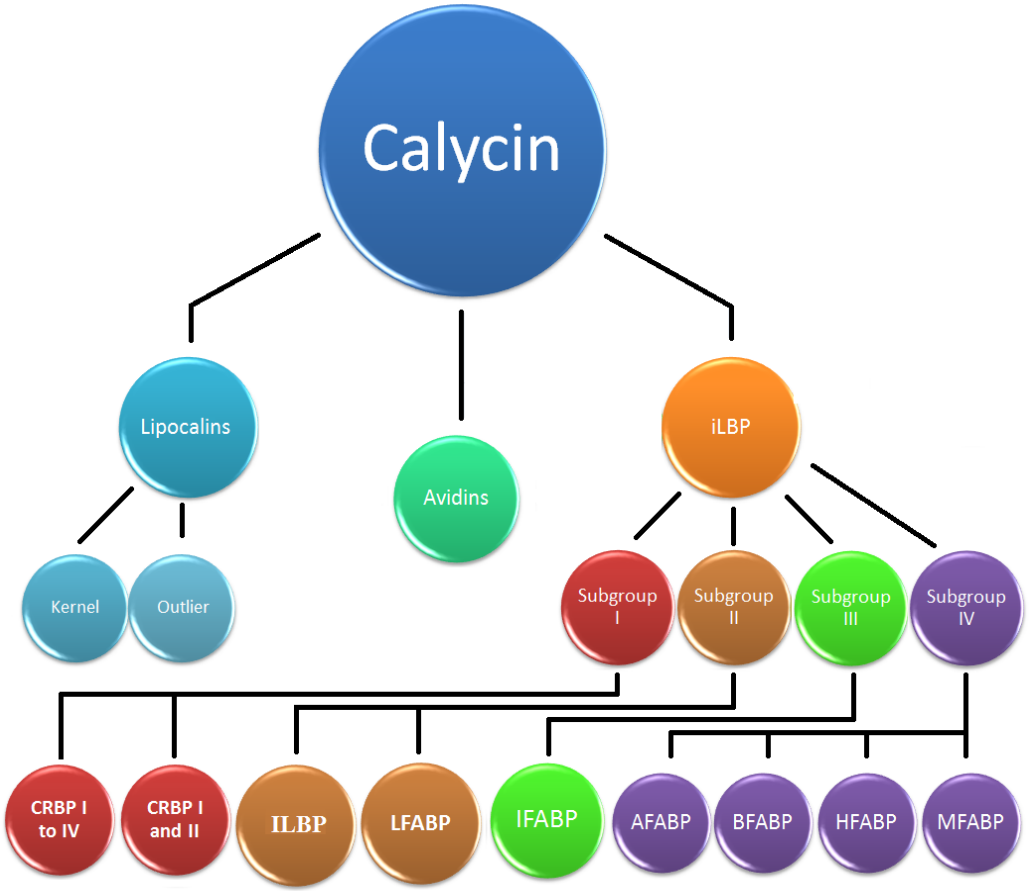

Figure I. 1. The Calycin superfamily classification.

Even though the primary sequence of its protein members shows great disparity, the calycin structural superfamily is characterized by a conserved fold, ensuring that the three dimensional structure can be superimposed to a great extent (**Figure I. 2,top**). This common structure of its protein members is composed of an antiparallel β-barrel fold

enclosing an internal ligand binding cavity, with repeated loop connections between the β-strands (**Figure I. 2, bottom**) (Flower 1993; Flower *et al.* 1993)**.**

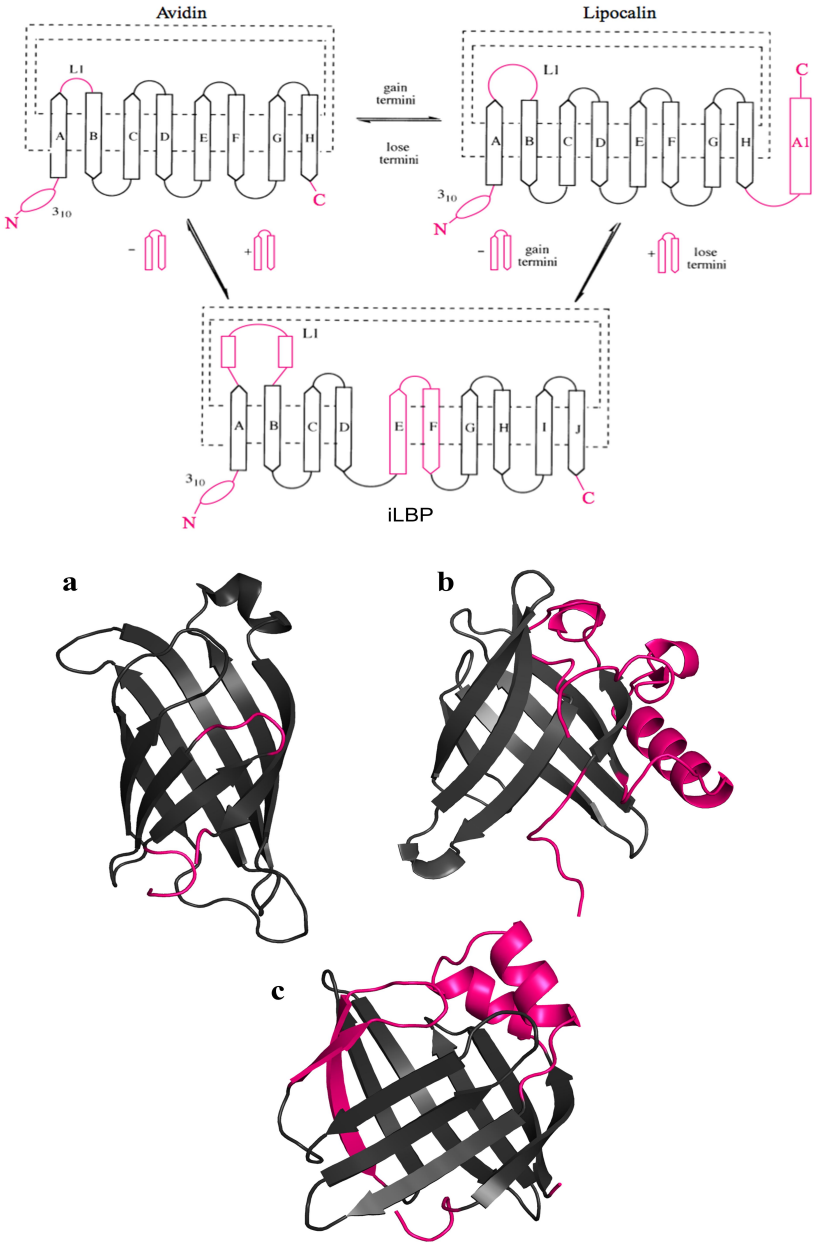

Figure I. 2. Top: a schematic representation showing the topology of secondary structural elements in each member of the calycin triumvirate (avidin, lipocalin and iLBP families). Common features are colored black, while differences among the families are colored in pink (Flower 1996). Bottom: the structures of three proteins (avidin, odorant binding protein and AFABP) from the avidin, lipocalin and iLBP families, respectively. The respective PDBs are 3RY2, 1E02 and 1LIB. Structures are color coded following the graphical representation at the top.

1. Lipocalin Family

The lipocalin fold is characterized by a symmetrical β-barrel composed of eight β-strands connected by seven turns. Six of the seven connecting β-turns are short β-hairpins, except for the first one which forms a loop that folds back and partially closes the ligand binding cavity at one end of the β-barrel. In cross section, the β-barrel structure has a flattened or elliptical shape and encloses a ligand binding site.

The lipocalins comprise a diverse protein family of extracellular transport proteins whose members exhibit high affinity for hydrophobic molecules and are thought to have diverse functions in addition to ligand transport (Blaner 1989; Cowan *et al.,* 1990) such as olfaction (Snyder *et al.,* 1988), mediation of pheromone activity (Cavaggioni *et al.,* 1987) and immunomodulation (Akerstrom and Logdberg 1990; Akerstrom 1992) among others. Based on protein sequence, lipocalins are divided into 'kernel' and 'outlier' groups based on whether the protein members share three or one conserved sequence motifs in the protein sequence, respectively (Flower 1996). The family includes a huge number of proteins including retinol binding protein (RBP) and odorant binding proteins that belong to the kernel and outlier protein groups of the lipocalin family, respectively.

2. Avidin Family

Similar to the lipocalins, the avidin family β-barrel is composed of eight hydrogen bonded β-strands, linked by a succession of β-turns, but demonstrating less ellipticity in

the cross section of the β-barrel and C-terminal helix. The avidin protein family includes proteins such as streptavidin, a soluble protein from the bacterium *Streptomyces avidinii* and its homolog hen egg-white avidin (Flower 1993) among others. Both proteins demonstrate a very high affinity for biotin (vitamin B_7) (Richards 1990), and other catalytic functions in addition to applications in the field of biotechnology where immobilized avidin can be used to purify, extract or identify biotinylated compounds (Bayer and Wilchek 1990; Kohanski and Lane 1990).

3. The iLBP Family

The iLBP family shares the same β-barrel structure but forms from ten β-strands, including a discontinuity of hydrogen bonding between β-strands β_D and β_E termed "the gap." The β-strands are connected by eight turns and two α helices (α_I and α_{II}) encompassing a loop between the first two β-strands and forming a cap that closes one end of the β-barrel.

The intracellular lipid binding proteins (iLBP) bind hydrophobic molecules and perform a host of different functions (that will be discussed later) in addition to being involved in lipid transport and metabolism. Protein members of this family share a common evolutionary origin (**Figure I. 3**). Based on evolutionary relationship, sequence identity and ligand binding characteristics, the iLBP family is categorized into four subfamilies: (I, II, III and IV; **Figure I. 3)** (Hohoff and Spener 1998). Subfamily I

includes retinoid binding iLBP such as cellular retinol binding proteins (CRBP I - IV) and cellular retinoid acid binding proteins (CRABP I and II) which bind retinoids (Vitamin A and its derivatives); while subfamily II includes LFABP (liver fatty acid-binding protein) and ILBP (ileal lipid-binding protein), both of which bind bulky ligands. ILBP binds both conjugated and unconjugated bile acids (Sacchettini *et al.,* 1990), while LFABP is the only FABP that binds two ligands including fatty acids, bile acids, eicosanoids, cholesterol and heme among others inside its cavity (Veerkamp *et al.,* 1991). Moreover, subfamily III includes only IFABP and subfamily IV includes HFABP, BFABP, AFABP, MFABP and EFABP that bind a single ligand and show a 3_{10} helical loop as an additional secondary structural element at the N-terminus (Hohoff *et al.* 1998).

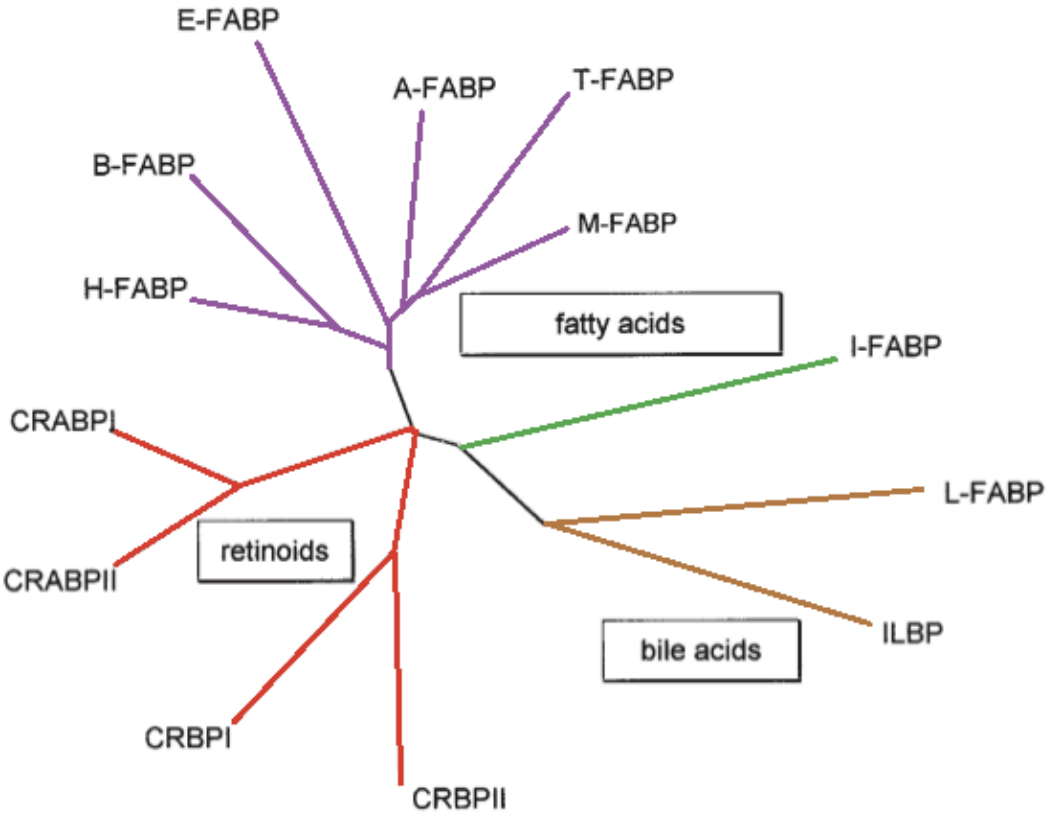

Figure I. 3. Radial rootless phylogenetic tree of the gene family of intracellular lipid binding proteins (iLBP). The branch length represents the evolutionary distance between the proteins. Members subfamilies I, II, III and IV) are colored red, tan, green and purple, respectively. Main ligands for each subfamily are displayed in a square, where subfamilies IIII and IV share a common ligand (fatty acids). Figure modified from Hohoff *et al.* (1998).

B. The iLBP family in focus

Intracellular long-chain fatty acids (LCFA) serve many functions in mammalian cells. They are of particular importance in cell homeostasis, in formation of biological membranes, and as fuels for energy production, specifically in the heart and skeletal muscle (Glatz *et al.,* 2010). FAs also take part in modulation of gene expression, growth and survival pathways, and inflammatory and metabolic responses (Saltiel and Kahn

2001; Hotamisligil 2006). Nevertheless, FA metabolites may exert toxic effects on cellular functions and cause cell injury if left unregulated. Therefore, fatty acid uptake and transportation inside the cell is carefully controlled (Glatz *et al.* 2010). Within the iLBP family, retinoid binding proteins are specialized in binding vitamin A and its derivatives (retinol, retinal and retinoic acid) and delivering these ligands to different enzymes and binding sites inside the cell (Ong 1987). FABPs within the iLBP family may play an important role in biological processes by modulating the cellular concentrations of FAs and their derivatives and ultimately affect the FA's physiological interactions with membranes, various enzymes inside the cell, and genes inside the nucleus by interacting with nuclear hormone receptors (Sorof 1994).

1. Members of the FABP Family

FABPs are named after the tissue from which they were first isolated. The same FABP is often expressed in different tissues, in some cases more predominantly in certain tissues than others. Additionally, in a specific tissue, more than one type of FABP may be expressed, indicating that each FABP type has a unique specialized function. A numerical nomenclature for the different FABP genes has been introduced (Hertzel *et al.*, 2000) as summarized in **Table I.1**. To date, there have been nine types of FABPs identified from tissues including adipocyte, liver, intestine, heart, brain, keratinocyte, myelin, testis and ileum (Storch and Corsico 2008) as indicated in Table I.1.

Table I.1 FABP types, genes, alternative names and tissues of expression. Adapted from (Furuhashi and Hotamisligil 2008; Storch *et al.* 2008).

Gene	FABP type	Alternative names	Tissues of expression
FABP1	Liver FABP	LFABP	Liver, small intestine, kidney
FABP2	Intestinal FABP	IFABP	Small intestine
FABP3	Heart FABP	HFABP, MDGI	Cardiac and skeletal muscle, brain, mammary tissue, kidney, adrenals, ovaries, testis, placenta, lung and stomach
FABP4	Adipocyte FABP	AFABP, ap2, ALBP	Adipocyte, macrophage
FABP5	Epidermal FABP	EFABP, PAFABP, cutaneous, keratinocyte, mal_1	Epidermis, adipocyte, macrophage, mammary tissue, tongue, testis, liver, lung, brain, heart, skeletal muscle, retina and kidney
FABP6	Ileal FABP	IlFABP, IBABP, ILBP, gastropin	Ileum, ovary, adrenal gland, stomach
FABP7	Brain FABP	BFABP, MRG	Central nervous system, retina
FABP8	Myelin FABP	MFABP, PMP_2	Peripheral nerve myelin
FABP9	Testis FABP	TFABP	Testis

2. Primary Sequence and Tertiary Structure of FABPs

Though present in invertebrates as well as vertebrates (Schaap *et al.,* 2002; Lucke *et al.,* 2006) and 126 - 134 amino acid residues in length, the same FABP types extracted from different organisms have a higher sequence homology than different FABP types extracted from the same organism. For instance, the sequence homology between human and murine AFABP is 92 %, versus 64 % between human AFABP and human HFABP. In general, the sequence similarities between different types of FABPs range between 22 and 70 %, which demonstrates very low convergence in sequence homology (Banaszak *et al.,* 1994). This low similarity of primary amino acid sequence is highlighted in **Figure I. 4**, showing a sequence alignment of different murine FABPs obtained using ClustalX (Thompson *et al.,* 1997).

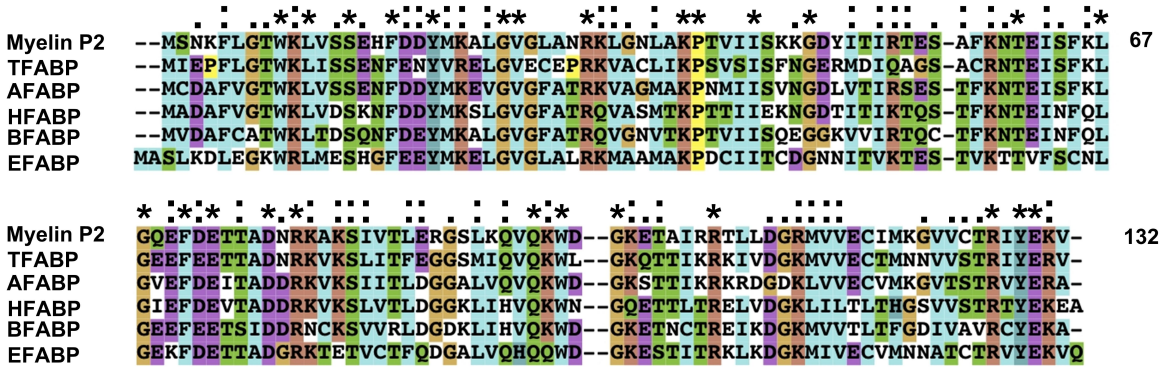

Figure I. 4. Sequence alignment of different murine iLBPs. Sequences are formatted and aligned using ClustalX (Thompson *et al.* 1997). UniProt (Consortium 2012) entry numbers are P24526, O01786, P04117, P11404, P51880, Q05816 for Myeline P2, TFABP, HFABP, BFABP and EFABP, respectively. Residues are indicated as strictly conserved (*), strongly conserved (:) or weakly conserved (.) and alignment gaps as dashes (-).

Despite such variations in amino acid sequence between FABPs, all protein members share a conserved tertiary structure. As noted above, the tertiary structures of FABPs share a β-barrel structure composed of 10 anti parallel β-strands connected via a network of hydrogen bonding to form a β-sheet structure that wraps around to create the β-barrel structural appearance. Between β-strands β_D and β_E is a "gap" due to absence of hydrogen bonding between the two β-strands, but they are connected instead via a network of conserved water molecules that are present in between. Two α helices (α_I and α_{II}) forming a helix-turn-helix domain exist between β-strands β_A and β_B and form a cap on the top part of the β-barrel. The two α helices along with residues 55-58 and 74-78 (Figure I. 4) located in the neighboring reverse turns between β-strands β_C-β_D and β_E-β_F, respectively, are called the 'portal', presumed to be the region where ligand entrance and exit takes place (Reese-Wagoner *et al.,* 1999).

FABPs have a molecular weight of 14 -15 kDa and a binding capacity of one FA ligand, except for the liver type (LFABP), which binds two FAs inside its cavity. While LFABP and ILBP are the only FABP members that bind bulky ligands, most FABPs bind specific fatty acids with similar affinity, showing differences in K_d of no more than one order of magnitude. The protein cavity is a very hydrophobic environment and provides an excellent medium for binding of fatty acids and other hydrophobic ligands. However, ligand binding has also been shown to be influenced by internal cavity waters (Likic *et al.,* 2000; Likic and Prendergast 2001).

Inside the protein cavity, conserved water molecules are present, both in the apo (unliganded) and holo (liganded) forms. In the holo proteins, some water molecules were found in the same position as in the apo, while others were missing after ligand binding. Water molecules that are found in the holo structures of FABPs are thought to facilitate the binding of the ligand by creating a hydration shell (Sacchettini *et al.,* 1992).

The number of water molecules inside the protein cavity differs for different subfamilies within the iLBP protein family. For instance for subfamily IV, an intricate network of highly ordered water molecules has been described inside the protein cavities of AFABP (LaLonde *et al.,* 1994), HFABP (Young *et al.,* 1994) and IFABP (Scapin *et al.,* 1992) and is suggested for EFABP and MFABP since they have similar cavity residues. In subfamily III, even though fewer water molecules are present inside the

protein cavity of IFABP, those water molecules are positioned as a hydration shell surrounding the ligand in the holo structure and thus are thought to facilitate and stabilize ligand binding (Sacchettini *et al.* 1992; Zimmerman *et al.,* 2001). By contrast LFABP and ILBP lack the intricate network of ordered water molecules inside the cavity, in addition to exhibiting greater sequence divergence than protein members in other iLBP subfamilies. These two observations combined could be the reason for the greater versatility of these proteins in accommodating bulkier ligands inside their cavities, in contrast with FABPs in subfamilies III and IV (Lucke *et al.,* 2002).

Additionally a specific water molecule has been reported by several groups to have a specific importance in stabilizing the tertiary fold of FABPs (Mesgarzadeh *et al.,* 1998; Likic *et al.* 2000). This water molecule is present in the gap area and facilitates the formation of three hydrogen bonds between backbone atoms of residues on β-strand β_F and the β-turn between β_D-β_E (Likic *et al.* 2000).

3. Function of FABPs

The physiological functions of FABPs are not fully established. Initially these proteins were thought to be merely a functional albumin equivalent in the cytoplasm. *In vitro* studies suggest that FABPs transport FAs around the cell in a regulated manner. For instance, AFABP has been shown to interact with hydrogen sensitive lipase (HSL) and possibly translocate the fatty acid produced from the hydrolysis process away and possibly to other cellular organelles. FABPs may transfer these fatty acids across

membranes inside the cell. *In vitro* studies have shown that different FABPs transfer FAs to membranes by two different transfer mechanisms (Storch and Thumser 2000). Some FABPs such as the liver type protein transfer the ligand to and from membranes primarily by aqueous phase diffusion (Kim and Storch 1992; Hsu and Storch 1996), while others such as the adipocyte, keratinocyte, intestinal, brain, myelin, and heart types, transfer the FA by directly interacting with a membrane (Kim and Storch 1992; Wootan *et al.,* 1993).

Strong evidence suggests other important physiological functions for FABPs. They are thought to play a central role in lipid homeostasis, and recent theories postulate that some FABPs play a role in signal transduction pathways, cytoprotection, cell cycle, and cell growth and differentiation (Zimmerman *et al.* 2000). Through use of FABP-deficient mouse models, consequences of genetically altered FABP expression in cells or whole animals have improved our understanding of FABP functions. For example, E-deficient mice that are also deficient for AFABP showed protection from atherosclerosis, suggesting a role in development of atherosclerosis (Makowski *et al.,* 2001), and AFABP deficiency was found to generate dramatic protection from dietary lipid–induced cardiovascular disease (Boord et al., 2004). I-FABP null mice demonstrated alterations in body weight based on gender, leading to the hypothesis that IFABP functions as a lipid sensor of energy homeostasis that alters body weight gain in a gender-specific fashion (Vassileva *et al.,* 2000).

C. AFABP

AFABP is also known as FABP4, ALBP or aP2. It was named as aP2 due to its high sequence similarity (67 %) to myelin P2 protein (Hunt *et al.,* 1986). AFABP was first detected in mature adipocytes but is also expressed in macrophages. Expression of AFABP is highly regulated during differentiation of adipocytes, and its mRNA is transcriptionally controlled by fatty acids, peroxisome proliferator activated receptor (PPARγ) agonists and insulin (Reese-Wagoner *et al.* 1999).

1. Function of AFABP

In addition to the functions mentioned previously for AFABP, it has also been established as a biomarker for type 2 diabetes (Reese-Wagoner *et al.* 1999). Some studies suggest that the role of AFABP in pathogenesis of type 2 diabetes may involve the regulation of insulin resistance through its impact on lipolysis as well as insulin secretion. Experiments with obese AFABP-deficient mice demonstrated improved peripheral insulin resistance and demonstrated reduced hyperinsulinemia. AFABP deficiency also preserves pancreatic β cell function and has beneficial effects on lipid metabolism (Zimmermann *et al.,* 1998; Scheja *et al.,* 1999; Yu and Reddy 2007). However, the physiological role of AFABP in cancer is poorly understood. For instance, AFABP synthesis was detected in lipoblasts in lipoblastoma and liposarcoma, but not in other benign adipose tissue tumors or malignant connective tissue or epithelial tumors. By contrast, AFABP expression by normal bladder urothelium was lost at various stages of carcinoma progression (Yu *et al.* 2007).

2. Structure of AFABP

Similar to other members of the iLBP family, the structure of AFABP consists of a 10-stranded (A through J) antiparallel β-barrel, two α helices (α_I and α_{II}), and an internal ligand binding cavity (**Figure I. 5**). As discussed for the general structure of FABPs, AFABP has the same β-clam shell with a cap formed by helix-turn-helix loop, but has a 3_{10} loop as an additional secondary structure element at the N-terminus (Reese-Wagoner *et al.* 1999).

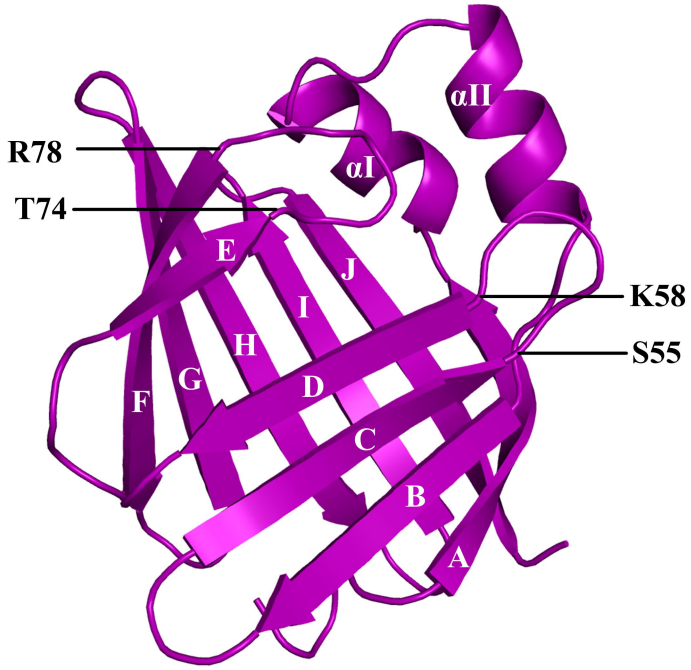

Figure I. 5. The crystal structure of apo AFABP demonstrating ten β-strands (β_A - β_J) forming a β-barrel and two α-helices (α_I and α_{II}). PDB:1LIB (Xu *et al.*, 1993).

3. AFABP Functional Modulation by Ligand Binding

AFABP binds various hydrophobic ligands inside the cell and is thought to be

involved in facilitating two way trafficking of fatty acids that are broken down by lipolysis and produced through lipogenesis inside the cell. Among these ligands are saturated and unsaturated long chain fatty acids such as oleic and linoleic acids, respectively, in addition to troglitazone (TDZ), which is a member of the thiazolidinedione (TZD) class of synthetic antidiabetic drugs. While TZDs have been associated with numerous health risks that led to subsequent withdrawal from the pharmaceutical market, their mode of action and possible role in signal transduction pathways involving Peroxisome Proliferator Activated Receptorγ (PPARγ) have kept them in the research field until today. For instance, troglitazone, a ligand for both AFABP and PPARγ, was used as an insulin sensitizing agent but removed from the US pharmaceutical market in 2000 due to its association with risk of liver failure. Nevertheless, it has been used in numerous subsequent studies to investigate the role of ligands in affecting the mechanisms by which PPARγ and possibly AFABP regulate gene transcription inside the cell (Tan *et al.,* 2002; Adida and Spener 2006; Gillilan *et al.,* 2007). The TZD class of drugs proved to be not only ligands for PPARγ, but also to be good agonists that activate the receptor (Ibrahimi *et al.,* 1994; Tontonoz *et al.,* 1994; Lehmann *et al.,* 1995).

Cytosolic FA and TZD concentrations have been shown to control expression of many genes, probably by acting as ligands that modulate the transcription of the peroxisome proliferator activated receptors (PPAR) (Fruchart et al., 1999; Meadus et al., 2002). PPARs are transcription factors that belong to the nuclear hormone receptor

(NHR) family consisting of three subtypes (PPARα, PPARβ and PPARγ). FABPs can access the nucleus under certain conditions and may interact with members of the PPAR family or may potentially target fatty acids to these transcription factors inside the nucleus, thereby influencing the gene transcription process. Since PPARγ is expressed predominantly in the adipocytes and is involved in regulation of adipose differentiation and adipogenesis (Devchand *et al.,* 1996), it is presumed to partner with AFABP and control signal transduction for certain genes in the adipose tissue. Tso *et al.* indicated that nucleocytoplasmic shuttling may underlie transcriptional activation of PPARγ by AFABP, where AFABP is thought to deliver ligands from the cytosol to PPARγ in the nucleus, thereby enhancing the transcriptional activity of the receptor, as shown in Figure I. 6 (Tso *et al.,* 2007; (Haunerland 2003). This activity has also been mentioned by Gillilan *et al*. (2007).

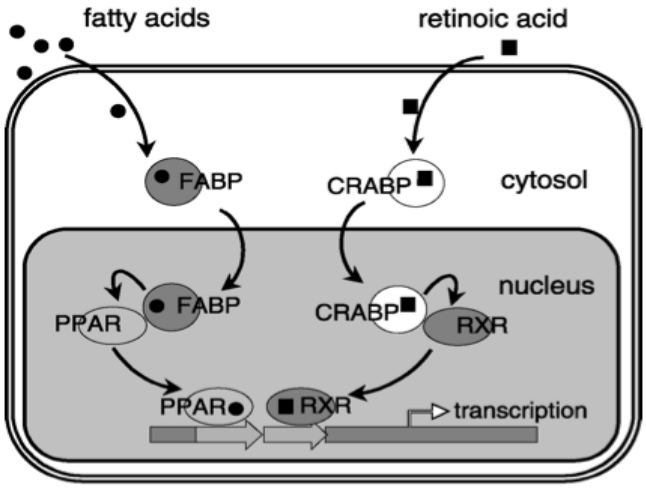

Figure I. 6. Scheme showing FABP- PPAR interaction in the nucleus. Figure adapted from Haunerland *et al.* (2003).

While oleic and linoleic acids along with troglitazone (**Figure I. 7**) are ligands

that bind both PPARγ and AFABP, the three ligands do not all activate the nuclear hormone receptor. A coactivator-dependent receptor ligand assay (CARLA) was used for both fatty acids to show that linoleic acid activated the receptor while oleic acid does not (Krey *et al.,* 1997). CARLA is based on ligand-induced binding of transcription coactivators such as steroid receptor coactivator (SRC-1), where SRC-1 is known to promote transcriptional activity through direct interaction with the ligand-activated form of some nuclear hormone receptors (Onate *et al.,* 1995).

Additionally, Gottlicher *et al.* measured PPARγ activation through the expression of a reporter gene for Placental Alkaline Phosphatase, (PAP) upon the addition of linoleic acid. PAP expression was induced by the presence of ligand and was proportional to the amount of linoleic acid added (Gottlicher *et al.,* 1992). Oleate and troglitazone were not included in that study. Troglitazone was also shown to activate PPARγ and upregulate PPARγ expression (Davies *et al.,* 2002) as part of the TZD family as mentioned previously (Ibrahimi *et al.* 1994; Lehmann *et al.* 1995). It is not understood how these ligands perform these diverse actions toward the receptor.

Gillilan *et al*. (2007) investigated the effect of ligand on the activation of the receptor from a different angle. They claim that these ligands become more readily available to the receptor inside the nucleus via manipulation of AFABP's ability to translocate into the nucleus. Gillilan *et al*. proposed a model whereby apo AFABP self associates and forms two different homodimers interacting either through the alpha

helices or beta barrel in such a way that a nuclear localization signal (NLS) sequence is either masked or revealed depending on the dimerization mode. The NLS is composed of three residues (K21 on helix α_I and R30 and K31 on helix α_{II}) (Ayers *et al.,* 2007) and is thought to facilitate translocation into the nucleus when revealed.

The first model speculates dimer formation based on crystallographic data for apo and holo (oleate) forms that were deposited by Xu *et al.* (1996), even though the structure was deposited as a monomer by Xu *et al*.. The other model of the dimer is proposed to form upon binding of the protein to activating ligands such as linoleate and TDZ, based on a crystallographic dimer and deposited by Gillilan et al. (2007), formed in 20 mM Tris HCl buffer. The group only solved the structures of the protein bound to linoleic acid and TDZ (both activating ligands) but not bound to non-activating ligands such as oleic acid or even the unbound form of the protein. The fact that the latter group deposited data for only two forms of the protein but not the others presents a challenge in comparing the two different proposed dimer models consistently. The structures of the two groups were derived at different concentrations and salt concentrations; even their own model is based on a crystalline lattice and may not be realistic under physiological conditions. Use of data from Xu *et al.* (1996) to propose a contrasting mode of dimerization is speculative.

Notably, the self association of the protein was tested using fluorescence anisotropy experiments in 100 mM KCl and small angle X-ray scattering (SAXS) in 20

mM Tris HCl, again considering apo and holo (TDZ) AFABP but not holo (oleate or linoleate). Additionally, the fluorescence anisotropy experiment was done at a very low protein concentration ranging up to a maximum of 1.6 μM protein concentration and did not reach an anisotropy plateau that is needed to rule out protein nonspecific aggregation. This experiment was not done on a range of ligands; it was only performed on apo and holo (TDZ) AFABP but not oleate or linoleate and therefore the experiment does not provide solid proof of the dimerization hypothesis. Thus the physical data supporting dimer formation are incomplete and pertain in some instances to conditions of very low ionic strength that artificially favor self association and are not physiologically realistic.

Gillilan's hypothesis of protein dimerization claims that upon binding of non-activating ligands such as oleic acid, the NLS remains sequestered and the homodimer is maintained in the same apo conformation so that the protein is retained in the cytosol (**Figure I. 8.a**). However, upon binding of activating ligands such as troglitazone or linoleic acid, the inactive homodimer dissociates and then reassociates in a different conformation (**Figure I. 8.b**) for which the NLS would be accessible and the protein would be transported into the nucleus via interactions with the importin type of protein machinery.

The protein is presumed to undergo this translocation upon binding to activating ligands (such as linoleate and troglitazone) where this interaction allows the side chain of F57 to exist in a closed conformation and therefore is available to interact with V32,

which in turn interacts with the residues involved in the nuclear localization signal. However, Gillilan *et al*. also reported that a portion of the apo AFABP was localized in the nucleus upon mutation of the nuclear export signal (NES), that facilitates export of the protein from the nucleus using CRM1 export machinery (Ayers *et al.,* 2007). They suggested that a fraction of the apo protein was inherently present in an activated mode (Gillilan *et al.* 2007), a seemingly contradictory statement about the role of dimerization in nuclear translocation. Moreover, they based this activation hypothesis on transfection of the gene containing AFABP fused with green fluorescent protein (GFP) in cells, followed by measurements of the ratio of fluorescence in the nucleus and cytosol in apo protein and upon addition of ligand. The only ligand that was used was ANS (another activating ligand) and not oleate, linoleate or TDZ. They supplemented their incomplete information with experimental results obtained by another group (Tan *et al.* 2002) without ligand and upon adding TZD and linoleic acid but not oleic acid. The results of this latter experiment show that the protein localized in the nucleus to great extent upon the addition of TDZ and linoleic acid, when compared with the presence of the ligand in the whole cell with no ligand addition. After mutating residue F57, they added TDZ to the cell medium and found that the protein nuclear import in response to TDZ was abolished, but they did not show the TDZ effect on protein import with wild type protein. Unfortunately, they did not perform analogous experiments using oleate as a non-activating ligand to check the extent of localization of the protein in the cytosol. These experiments in total do not provide a confident picture of activation of nuclear translocation. The lack of complete information presents a challenge to the complete understanding of the role of ligand in the interaction between AFABP and PPARγ

through the nuclear translocation process.

Additionally, the role of the ligand in the interaction between AFABP and PPARγ, once inside the nucleus, remains unclear. Some reports suggest that AFABP interacts with PPARγ regardless of ligand binding, judged by immunostaining with microscopy (Adida *et al.* 2006). By contradiction another study demonstrated that AFABP interacts physically with PPARγ and that this interaction is enhanced by binding of specific ligands (Tan *et al.* 2002). The latter study used a stopped-flow apparatus to determine the reaction rate (in subsecond range) for transfer of ligand from holo AFABP to pyrene-labeled PPARγ at different AFABP/ PPARγ molar ratios, concluding that physical interaction between AFABP and PPARγ occurs in order to facilitate ligand transfer (Tan *et al.* 2002). Tan *et al.* also show activation of PPARγ by measuring the activity of luciferase, which is an enzyme that is activated by PPARγ. They show that the addition of AFABP to PPARγ increases luciferase activity twofold, and by threefold in presence of both AFABP and linoleic acid. These experiments were also not performed with oleic acid or TDZ. It is possible that the discrepancies between those two articles could be due to the difference in experimental approaches where in the first report, a construct of the PPAR ligand binding domain PPAR-LBD was used while in the second one it was the full PPAR protein. Moreover, Adida *et al.* (2006) compared GST pull down assays to test the physical binding, while Tan *et al.* measured luciferase activity, which is an effect of the activation of the nuclear receptor. Nevertheless, there is evidence that AFABP is up-regulated by PPAR during adipocyte differentiation. This supports the hypothesis that AFABP is not only present in the nuclear compartment as

shown in various research articles, but that it is a modulator of the nuclear hormone receptor activity (Tontonoz *et al.* 1994). The fact that these two proteins (AFABP and PPARγ) are tissue specific and are predominantly expressed in the adipose tissue (Devchand *et al.* 1996) strengthens this hypothesis.

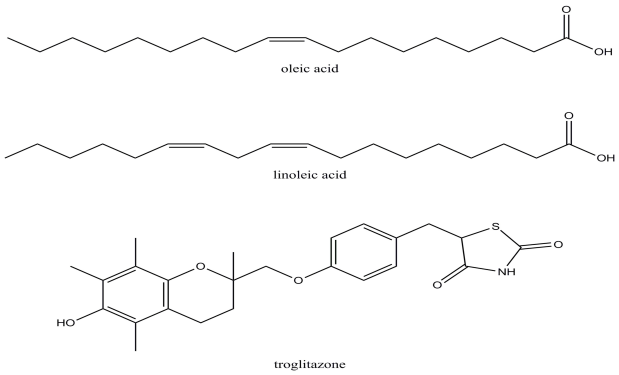

Figure I. 7. Structures of oleic acid, linoleic acid and troglitazone.

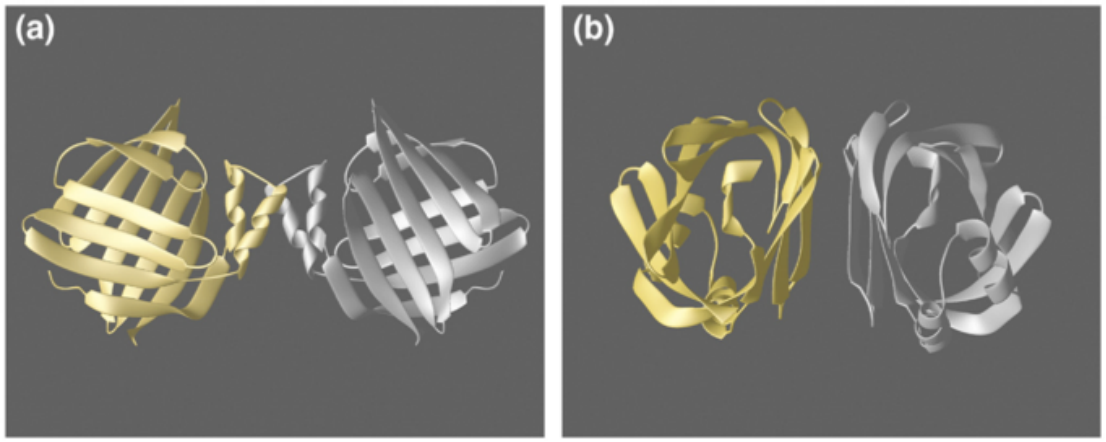

Figure I. 8. Two homodimers proposed of AFABP: (a) speculation that dimer interface is through the α helix region and the NLS is masked, (b) proposed dimer interface is through the β barrel where the NLS is revealed based on crystal lattice of structures deposited by Gillilan group with activating ligands (linoleate and TDZ). The homodimers shown above (a) and (b) are based on the crystal structures reported by two different groups, Xu *et al.* (1993) for (a) and Gillilan *et al.* (2007) for (b) even though the two crystal structures were derived from crystals made with different buffers and solvents. Figure from Gilillan *et al.* (2007).

It is interesting to ask whether AFABP functions in the nucleus to transport these

ligands to PPARγ or interacts itself with the nuclear receptor as a secondary messenger. Additionally, it is not clear how these ligands elicit such a contrasting functional effect on the protein and why a certain percentage of the apo protein should be activated automatically as Gillilan *et al.* proposed. Their hypothesis would imply the presence of a percentage of apo AFABP that homodimerizes in a way that is revealing the NLS without ligand binding. Moreover, it is intriguing that oleic and linoleic acids have similar structures (both are composed of an 18-carbon hydrocarbon chain, with linoleic acid processing two double bonds compared with one double bond in oleate), yet they engender different AFABP homodimers and in turn different functional outputs from the protein. Additionally even though troglitazone is much bulkier than linoleate, it is interesting to investigate how those two different ligands produce such a similar structural/functional effect on the AFABP protein.

Our goal in this study is to investigate the interaction of these three ligands with AFABP, as a prelude to understanding nuclear receptor activation. Given that two fatty acids (oleate and linoleate) of similar structure elicit different functional attributes of the AFABP and lead to either activation or inactivation of PPAR in the nucleus, while two activating ligands possess stark differences in structure yet similar functional modulation of AFABP, we would expect the resulting protein-ligand complexes to provide essential insights into the functional trends.

Our aim is to study the interaction of these three ligands with AFABP at the molecular level. First, biophysical methods such as size exclusion chromatography and

laser light scattering can clarify the dependence of AFABP oligomerization state on ligand binding and buffer composition. As detailed below, NMR is an ideal method to study protein-ligand interaction in close to the native environment and at physiological salt concentration. Once all resonance assignments of the backbone residues of the apo protein have been made, a ligand can be titrated into the protein and the chemical shifts of the backbone resonances can be recorded. Changes in the magnetic and chemical environment of residues due to ligand binding will result in changes in the NMR signal, as intensity and/or chemical shift perturbations. This is an excellent method to highlight residues that are involved in the binding (discussed in Chapter II). Mapping these chemical shift perturbations onto the three dimensional crystal structure of the protein, provisionally assumed similar to the solution-state structure, reveals the binding site for each ligand. Comparing the residues involved in the ligand binding and the pocket in each case is expected to shed light on how these three ligands produce similar or contrasting functions of the protein.

II. Materials and Methods

A. Protein Expression of mAFABP

Transformed *E. coli* host strain BL21 (DE3) cells (Novagen, Madison, WI) with expression vector pET-11a containing the cDNA of mAFABP, a generous gift from the lab of Prof. Judith Storch (Rutgers University), were inoculated into a small culture of 50 ml Luria Broth (LB) medium containing 200 μg/ml ampicillin (Sigma, St. Louis, MO) and incubated at 37 ºC in a C25 incubator shaker (New Brunswick Scientific, Enfield, CT) with constant shaking at 225 rpm. The optical density (OD_{600}) of the culture was measured periodically at 600 nm with a Thermo UV1 spectrophotometer until it reached a value of 0.6, at which point the small culture was scaled up to two liters of LB medium containing 200 μg/ml ampicillin and incubated under the same conditions.

Once the OD_{600} reached the value 0.6, the culture medium was centrifuged at 4 ºC and 7,000 x g for 15 minutes, after which the pellet containing the cells expressing the protein was thawed and re-suspended in one liter of minimal media enriched with either $^{15}NH_4Cl$ (nitrogen labeled protein), or $^{15}NH_4Cl$ and ^{13}C glucose (double labeled protein) (Marley *et al.,* 2001) and then incubated under the same conditions as previously described. Induction of protein synthesis in the cells was initiated after one hour by addition of isopropyl β-D-1-thiogalactopyranoside (IPTG) (Goldbio Technology, St. Louis, MO) to make a concentration of 0.1 mM, after which the culture was re-incubated for three more hours. The culture was centrifuged using a fixed angle centrifuge (Beckman Coulter, Danvers MA) at 4 ºC and 4,000 x g for 15 minutes, and the cells were

harvested and stored at - 80 ºC until protein purification. 50 µL aliquots were collected before and after induction in order to check the protein expression using 16 % SDS-PAGE (Laemmli 1970) and stored in - 20 ºC (**Figure II.1**).

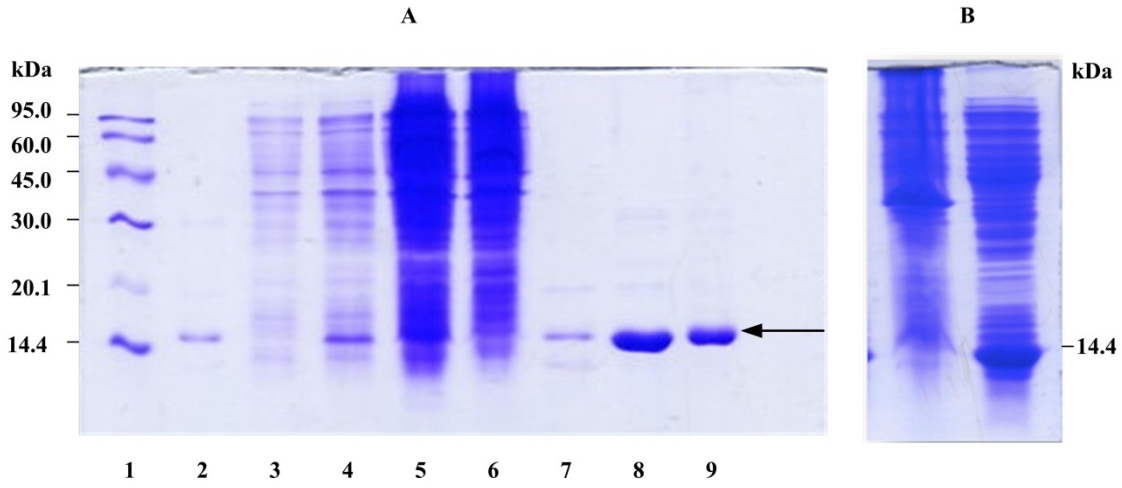

Figure II.1. (A) 16 % Acrylamide SDS - PAGE of some fractions collected during expression and purification of AFABP. The gel was stained with Coumassie Blue. Lane 1, molecular weight standards; lane 2, control AFABP (purified by the Storch group); lane 3, fraction collected before induction of protein with IPTG; lane 4, fraction collected four hours after induction with IPTG; lanes 5 and 6, supernatant and cell lysate, respectively, after sonication; lane 7, eluted fraction from G50 column; lane 8, eluted fraction from DE52; lane 9, purified protein after passing through Lipidex column. (B) 16 % acrylamide SDS - PAGE gel showing pellet and supernatant of the lysed cells after sonication, with better demonstration of protein in the supernatant. Arrow points to pure AFABP after delipidation.

B. Purification of AFABP Protein

The cells were thawed in a water bath and then resuspended in 25 ml $T_{10}E_1K_{100}$ lysis buffer (10 mM Tris, 1 mM EDTA, 100mM KCl, pH 7.7) with addition of phenylmethylsulfonyl fluoride (PMSF) so that the final concentration was 0.1 mM, then split into two small beakers for sonication in an ice/water bath in pulse mode for a total of 15 minutes (cycles of 0.5 s of pulse on and 1 s pulse off using a 50 % duty cycle and

output amplitude of 50 %). The solution was then centrifuged for 30 minutes at 44,000 x g at 4 ºC. The supernatant was collected and loaded on a Sephadex G50 size exclusion column (GE Healthcare Biosciences, Piscataway, NJ) equilibrated with 150 mM KCl in a 10 mM phosphate buffer (pH 7.7) (Kim *et al.* 1992; Hsu *et al.* 1996). Fractions of 8 ml were collected and the optical density (λ=280 nm) of each fraction was measured. Fractions containing the protein appearing in the second peak of OD_{280} (Kim *et al.* 1992) were pooled and concentrated to 40 ml by ultrafiltration using a 5 kDa cutoff Millipore membrane (Millipore, Billerica, MA). The concentrate was loaded on a DE52 anion exchange column (Whatman Inc., Clifton, NJ) equilibrated with 10 mM Tris phosphate buffer (pH 8.3). The elution profiles of G50 and DE52 columns are illustrated in **Figure II.2**. The fractions containing the protein were directly collected and pooled based on OD_{280} measurements of 5-µL samples made with a Nanodrop spectrophotometer (courtesy of the Ghose lab, CCNY) and concentrated as described above. 50 µL aliquots were collected after each purification step in order to check the protein purification using 16 % SDS-PAGE and stored in - 20 ºC (**Figure II.1**).

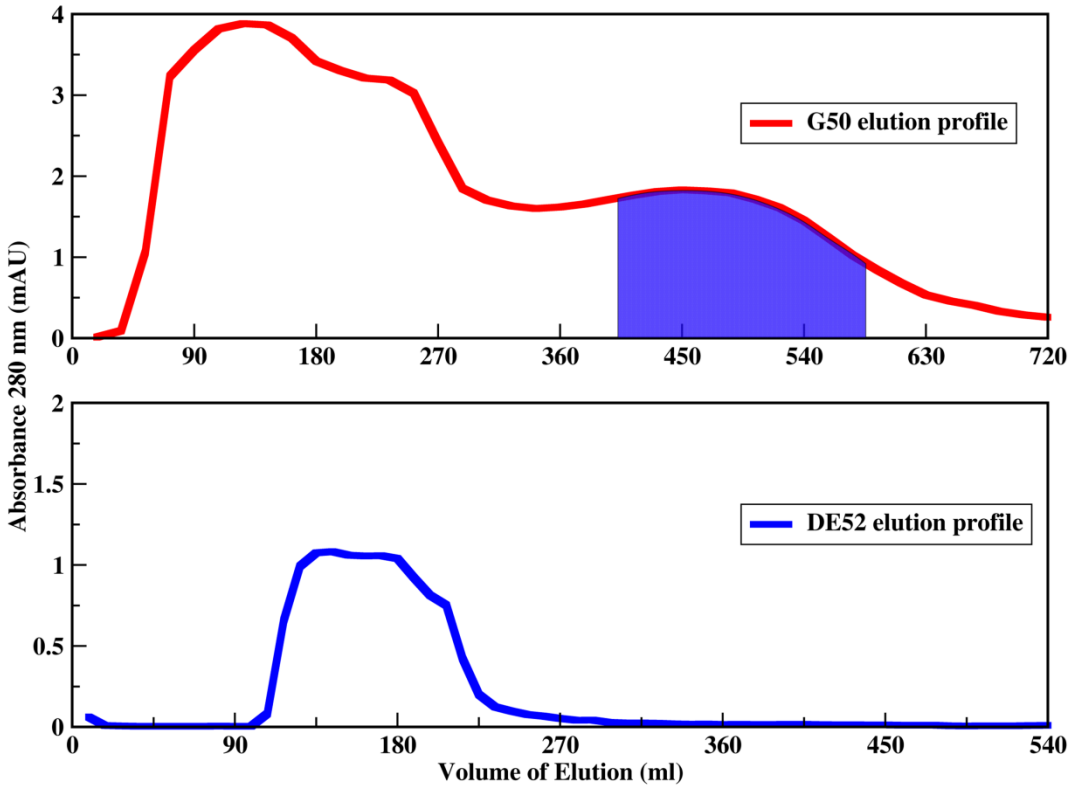

Figure II.2. Elution profile of AFABP passing through G50 size exclusion and DE52 ion exchange columns, respectively. The second peak in the G50 elution profile (highlighted in blue) was pooled, concentrated and injected into DE52 for further purification. Profiles were drawn from samples collected at 9-ml intervals and assayed by UV absorbance at 18-ml intervals.

C. Protein Delipidation

The purified protein was injected into a Lipidex-1000 column packed with hydroxyalkoxypropyl Sephadex Type II beads (Sigma, St. Louis, MO) that were equilibrated with a phosphate buffer (150 mM KCl, 10 mM Pi, pH 7.4) at 37 °C, in order to remove any intracellular fatty acid that may have bound to the protein during bacterial growth (Glatz *et al.,* 1985) (**Figure II.3**). Fresh unused beads are stored in 4 °C then

presoaked in 100 % methanol for 30 minutes before use. Beads are then washed with 300 ml of 100 % methanol followed by one liter solutions of 50, 30, 15 % methanol/water (v/v), then finally one liter phosphate buffer (150 mM KCl, 10 mM Pi, pH 7.4) before packing into pre-warmed column. After delipidation, the beads are regenerated washing with one-liter solutions of 15, 30, 50 and 100 % methanol/water (v/v), then stored in 100 % methanol at -20 °C. At each step of the growth and purification process, aliquots of 50 µL were saved for subsequent analysis of protein purity by 16 % SDS-PAGE (Laemmli 1970) (illustrated in **Figure II.1**). The protein was stored at 4 °C until needed for physical measurements. Prior to use, the protein was concentrated to reach the desired concentration (depending on each experiment) using a Centricon-3 kDa cutoff ultrafiltration membrane (Millipore).

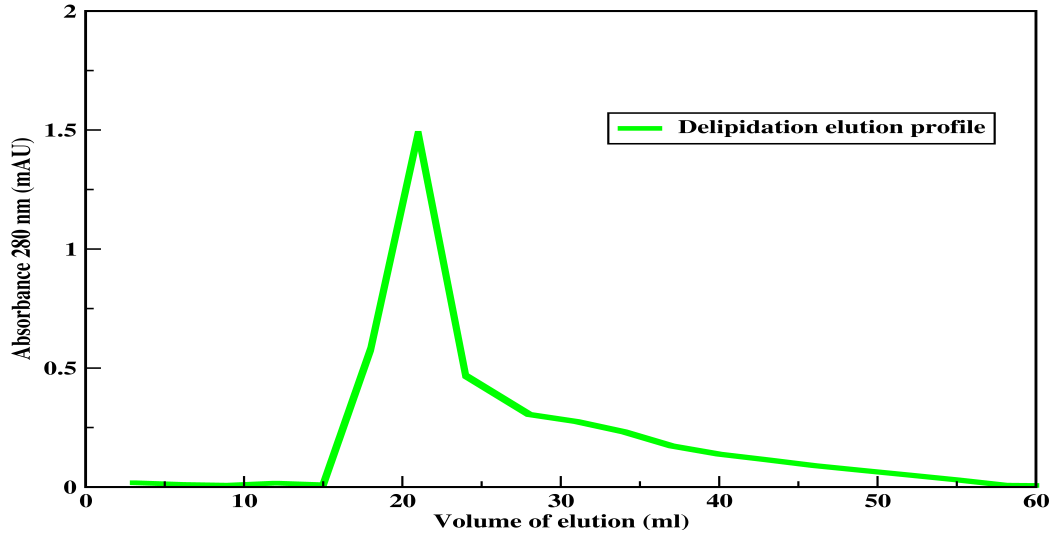

Figure II.3. Elution profile of AFABP passing through Lipidex column. Profile was drawn from samples collected at 3-ml intervals and assayed by UV absorbance at 3-ml intervals.

D. NMR Spectroscopy

1. Two dimensional [^{1}H-^{15}N] heteronuclear single quantum correlation (HSQC)

[^{1}H-^{15}N] HSQC is a two-dimensional experiment that utilizes through-bond (scalar or *J coupling*) magnetization transfer between pairs of atoms, which provides chemical shift and correlation information on the heteronucleus (^{15}N) and a proton (^{1}H) that is directly coupled through one bond to that same nitrogen (Cavanagh *et al.,* 2007). HSQC provides a fingerprint map for the protein, where each proton that is directly coupled to nitrogen in the protein will appear as a peak in the spectrum. All backbone amides of protein residues (except for the first N-terminal residue and proline) typically appear in the spectrum as single peaks. The first N-terminal residue does not yield an observable signal due to exchange with the solvent, and proline lacks an amide proton. Additionally peaks may be doubled or missing due to exchange between multiple protein conformations; the HSQC spectrum also contains peaks for nitrogen containing side chains such as Arginine, Asparagine, Glutamine, Lysine, Histidine and Tryptophan. Each cross-peak in the spectrum can be defined by chemical shifts on the ^{1}H and ^{15}N axes, as illustrated in **Figure IV.8**.

Running [^{1}H-^{15}N] HSQC experiments require the appropriate isotope labeling using an ^{15}N ammonium chloride enriched medium as the only source of nitrogen during protein expression. This allows all the amino acids produced by the *E. coli* to be properly and uniformly labeled. Running an HSQC experiment provides an ideal technique to

check protein quality, sample denaturation, and ligand binding. For instance, a dispersion of chemical shifts indicates a properly folded protein with distinctive amide magnetic environments. A change in the local environment of the amino acid residues of the protein will result in changes in the chemical shifts, making an HSQC experiment ideal to study protein-ligand interactions in solution.

2. Multidimensional NMR Experiments

Three dimensional NMR experiments were used to obtain backbone resonance assignments for apo and holo (oleate) AFABP.

(a) Triple Resonance Experiments

3D heteronuclear triple resonance experiments that correlate backbone ^{1}HN, ^{15}N, ^{13}C, and ^{13}CO included [^{15}N-^{13}C] CBCA(CO)NH (Grzesiek and Bax 1992), HNCACB (Grzesiek and Bax 1992), HNCACO (Bax and Ikura 1991) and HNCO (Kay *et al.,* 1990). The correlations obtained between spins of intra- and interresidue atoms in the protein allow for site-specific protein backbone assignments. (HNCACB and CBCA(CO)NH) and (HNCO and HNCACO) were used as complementary pairs to facilitate these correlations. For example, the HNCACB experiment correlates the chemical shifts of ^{1}H, ^{15}N, ^{13}Cα and ^{13}Cβ of residue (*i*) with those of ^{13}Cα and ^{13}Cβ of (residue *i*-1), while CBCA(CO)NH correlates the chemical shifts ^{1}H, ^{15}N of residue (*i*) with only the chemical shift of ^{13}Cα and ^{13}Cβ for the previous residue (*i*-1). Similarly, (HNCO and HNCACO) experiments can be used as a pair since the HNCO experiment correlates ^{1}H, ^{15}N chemical shifts of residue (*i*) with the ^{13}CO of residue (*i*-1), while the HNCACO experiment shows the same information in the HNCO with the addition to ^{13}CO of

residue (*i*).

Collectively, these experiments facilitated making the backbone assignments of AFABP. The strategy of utilizing these experiments to make assignments is illustrated in more detail in Chapter IV and a schematic representation describing correlation diagrams illustrating triple resonance 3D NMR experiments is shown **Figure IV.2**.

(b) Double Resonance Experiments [^{1}H-^{15}N] NOESY-HSQC and TOCSY-HSQC

3D [^{1}H-^{15}N] TOCSY-HSQC and [^{1}H-^{15}N] NOESY-HSQC experiments (Marion *et al.,* 1989; Zhang *et al.,* 1994) were used as a pair to correlate intra- and interresidue spin systems correlated through bonds and through space, respectively. The 3D [^{1}H-^{15}N] TOCSY experiment enables investigation of intra-residue spin systems that are scalar coupled through bonds and therefore provides correlations between ^{15}N and the amide and side chain protons in the same residue. This facilitates amino acid typing via identification of the set of resonances for each individual amino acid residue (Cavanagh *et al.* 2007).

Additionally, the 3D [^{1}H-^{15}N] NOESY experiment provides intra and inter-residue spin systems. It provides important structural information about the protein by investigating the short, medium, and long-range Nuclear Overhauser Effect (NOE) interactions. Intra-residue, sequential, medium, and long range NOEs correlate protons

that are located on the same residues (i), consecutive residues (i+1), separated by two, three or four ($2 < i \leq 4$), or more than four residues ($i > 4$) in the polypeptide sequence, respectively. NOE connectivity patterns between antiparallel β-strands or α-helices can be differentiated and identified. A schematic representation describing correlation diagrams illustrating double resonance 3D NMR experiments is shown in **Figure IV.2**.

E. NMRViewJ

NMRViewJ (Johnson 2004), a computer program for the visualization and analysis of NMR data, displays ".nv" files, and helps in analyzing NMR data such as peak picking, obtaining peak intensities, and semi-automatic assignments through the Runabout feature

F. Protein Oligomerization State

1. NMR Self-diffusion Experiments

NMR spectroscopy is one of the techniques used to determine the oligomerization state. Since self association and oligomerization usually involves changes in molecular weight and hydrodynamic properties of single molecules, diffusion of these molecules change as a consequence. Using spatially well defined magnetic field gradients to spatially encode the traslatioonal motion of spins enable us to study of the diffusion of molecules in solution by NMR. Self-diffusion is the random translational motion of molecules driven by internal kinetic energy (Hawlicka 1995) and reflects the molecular size of the (assumed spherical) molecule as given in the Stokes Einstein equation

(Equation III.1).

$$D = \frac{kT}{6\pi\eta r} \qquad \textbf{Equation II.1}$$

where k is the Boltzmann constant, T is the temperature (Kelvin) and η is the viscosity of the buffer containing the particles (in centipoise). Detailed analysis of the process is given in Chapter III.

2. Gel Filtration Experiments

Gel filtration chromatography is a high efficiency technique that separates different proteins or peptides based on the size of the molecules (Andrews 1962; Sun *et al.,* 2004; Wang *et al.,* 2010). Columns packed with the appropriate beads are used to separate molecules of a certain size range. Depending on the size of the biomolecules, they may diffuse into the pores of the beads if they are small in size, and therefore are eluted from the column slowly, or travel between the beads more quickly if they are large (**Figure II.4**). Both molecular weight and three-dimensional shape contribute to the retention volume and time. Gel filtration chromatography may be used for analysis of molecular size, for separations of components in a mixture, or for buffer exchange of protein solutions.

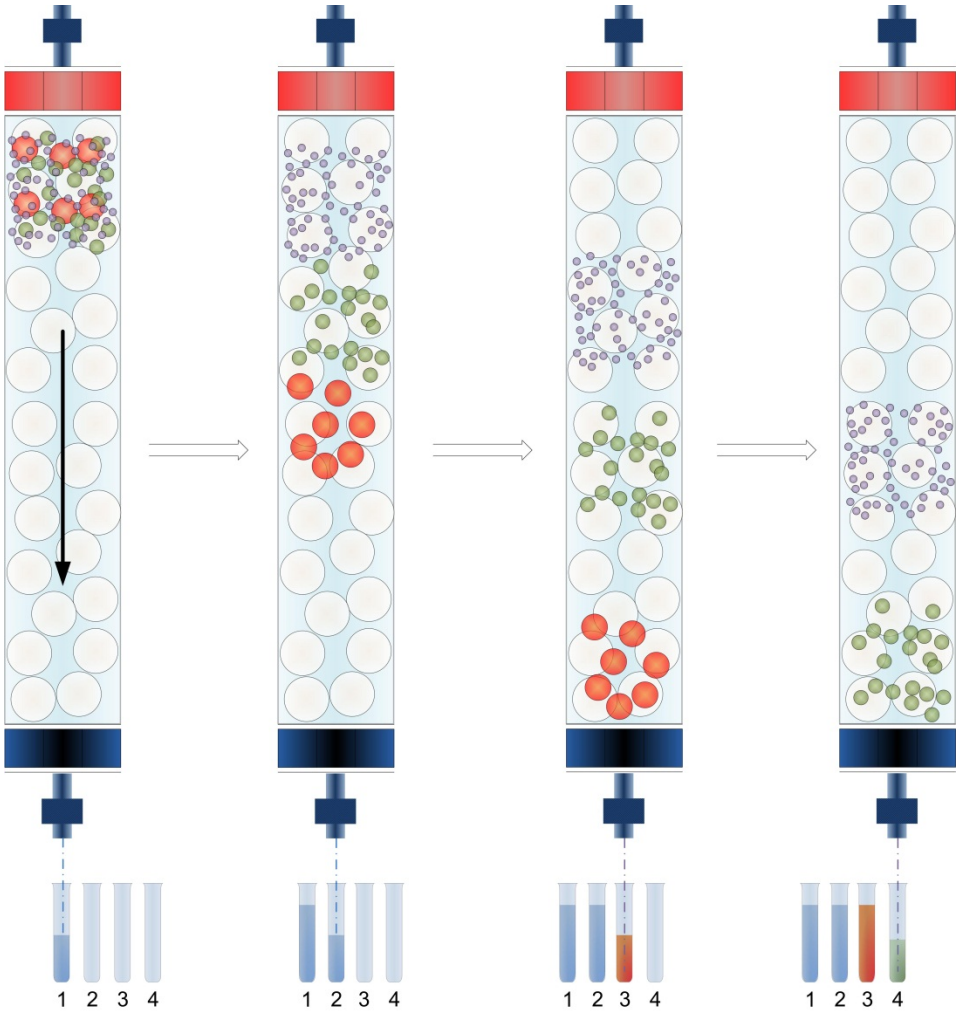

Figure II.4. Graphical representation of gel filtration column. Molecules that are larger in size (colored red) elute first followed by intermediate (colored green) and smaller molecules (purple), allowing for separation of these different molecules by size by collecting the different eluted fractions. Arrow shows the direction of flow of molecules inside the column. Figure was prepared with the Microsoft Visio program.

A Superdex 75 column (GE Healthcare Biosciences, Piscataway, NJ) is ideal for separation of protein and biomolecules of molecular weight in the range of 3 to 75 kDa. Superdex 75 (courtesy of the Ghose lab, CCNY) was used to investigate the oligomerization of AFABP (mol. wt. 15 kDa) at near physiological conditions and further enabled investigation of the oligomerization under varying conditions of buffer, protein

concentration, and salt concentration. **Figure II.5** is a schematic representation of the automated fast protein liquid chromatography (FPLC) system that was used in these experiments.

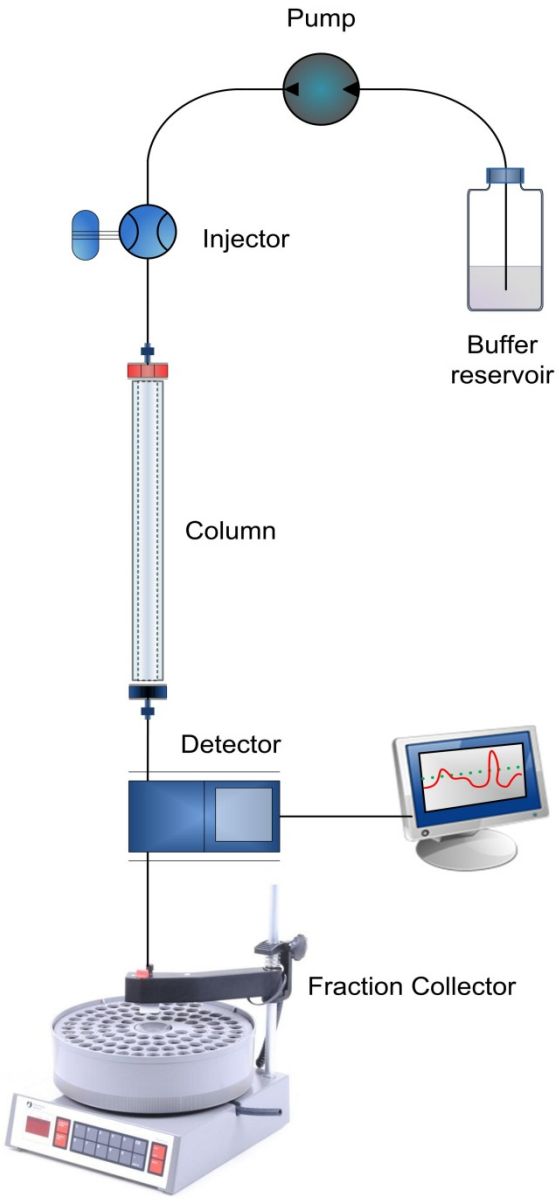

Figure II.5. A scheme demonstrating the automated FPLC system used in sizing experiments. Protein is injected into the column while the pump draws buffer as the mobile phase onto the stationary phase (Superdex 75 beads) inside the column. The eluted protein fractions are collected in fixed volumes by an automated fraction collector, while a detector reads the absorbance of the eluted protein and displays it onto an attached display monitor. Figure was prepared with the Microsoft Visio program.

Prior to performing the experiments, the column was equilibrated with 2 column volumes of phosphate buffer (pH 7.4, 150 mM KCl, 10 mM Pi and 0.02 NaN_3). Blue Dextran (mol wt. 2,000 kDa) was passed through the column to obtain the void volume (V_o). 100 µL of sample containing 5 known proteins (3 mg/mL Conalbumin (75 kDa), 3 mg/mL Ovalbumin (43 kDa), 3 mg/mL Carbonic Anhydrase (29 kDa), 3 mg/mL Ribonuclease A (13 kDa) and 3 mg/mL Aprotinin (6.5 kDa)) (GE Healthcare, and courtesy of Prof. Ghose's lab, CCNY), was passed through the column to make a standard profile. These standards were eluted based on their size. The elution volume (V_e) was recorded and used to calculate the partition coefficient (K_{av}) of each eluted protein, where

$$K_{av} = (V_e - V_o)/ (V_c - V_o) \qquad \textbf{Equation II.2}.$$

V_e, V_o and V_c are the elution volume, void volume and column volume (equivalent to the volume of the packed bed), respectively. Molecules of similar shape and density demonstrate a sigmoidal relationship between their K_{av} values and the logarithms of their molecular weights (Whitaker 1963; Andrews 1964). The linear portion of this sigmoidal curve yields a direct relationship between the partition coefficients of eluted proteins and their molecular weights. This linear relationship is specific to the column volume and the gel filtration medium and can be used to determine the molecular weight of an unknown molecule that is similar in shape to the standards and eluted from the same column.

Calibration curves were made following the GE Healthcare manual by plotting

K_{av} against log (mol. wt.) of the standard proteins and fit by a straight line. The equation of the straight line could then be used to estimate the size of AFABP. The elution volume and profile for AFABP samples are presented in Chapter III.

3. Static Light Scattering Experiments

Static light scattering is a technique that can be used to obtain the molecular weight of a macromolecule or a protein by measuring the intensity of the scattered light as a function of angle. A high intensity monochromatic light, usually a laser, is directed into a solution, while detectors placed at fixed angles are used to measure the scattering intensity. Measurement of the scattering intensity at many angles allows calculation of the molecular weight. This process is discussed in more detail in Chapter III.

III. Oligomerization state of AFABP in solution

A. Introduction

It is important to investigate whether AFABP exists as a monomer or a dimer in solution, specifically since Gillilan *et al*. proposed that the protein exists mainly as either one of functionally significant homodimer models depending on whether it was in an activating or inactivating state. They used anisotropic fluorescence experiments in very low concentration range (0.1-1.6 μM) in 100 mM KCl, to show that the protein self associates with a K_d of 120 nM. They also showed that SAXS profile of the apo protein fits with a dimer model more than a monomer one. They proposed two models of homodimers based on the X-ray crystal lattice of the protein bound to activating (linoleate and TDZ) (Gillilan *et al.*) and non activating (oleate), (Xu *et al.*) ligands despite the two structures being crystallized by two different groups under different conditions. With that in mind and preceding further binding studies on the protein, it was vital to explore the dimeric/monomeric state of the protein. Several samples of apo and holo AFABP with various buffer conditions and salt concentrations were examined using numerous techniques to reach a verdict in that respect.

B. NMR Self-Diffusion

1. Principles

Self-diffusion is the random translational motion of molecules driven by internal kinetic energy (Hawlicka 1995) and reflects the molecular size of the (assumed spherical)

molecule as given in the Stokes Einstein equation (Equation III.1).

$$D = \frac{kT}{6\pi\eta r} \qquad \textbf{Equation III.1}$$

where k is the Boltzmann constant, T is the temperature (Kelvin) and η is the viscosity of the buffer containing the particles (in centipoise).

NMR spectroscopy is one of the tools used for studying diffusion of molecules in solution, thereby offering a means to determine oligomerization state. This process will be discussed in detail in the Results section.

2. Materials and Methods

^{15}N AFABP at 130 and 400 μM concentrations, 500 μM [^{15}N ^{13}C] AFABP, and 100 and 300 μM (unlabeled) apo AFABP along with 630 μM ^{15}N holo (linoleate) AFABP samples were used to carry out more than 20 self-diffusion experiments. Samples were inserted into a 4 mm Shigemi tube (Shigemi Inc., Allison Park, PA) and pulsed field gradient (PFG) NMR spectra were acquired at 20 °C on a Bruker Avance 500 MHz spectrometer equipped with a TCI cryo-probe. Gradients were applied in the same direction as the field from the spectrometer magnet. ^{1}H NMR spectra were acquired by applying pulsed field gradient - heteronuclear stimulated echoes (PFGX-STE) (Ferrage *et al.,* 2003) and Pulsed field gradient - longitudinal eddy-current delay (PFGLED) (Yao *et al.,* 2000) pulse sequences. With the help of Dr. Shibani Bhattacharya at the NYSBC, 15 experiments were recorded using those two pulse sequences at each protein concentration, and varying the delay for diffusion time (d20) in PFGX-STE pulse sequence and the gradient recovery (d16) and gradient pulse (p30) in

the PFGLED pulse sequence that are used in the experiments. The pulse sequences were successfully used previously on peptides of known molecular weight.

3. Results

The obtained data were processed using TopSpin™ (Bruker Biospin) by identifying the limits of a region of peaks in the 1D spectrum (Figure III. 1) over which the signal is integrated to obtain a plot of the effective gradient intensity decay as a function of the amplitude of the gradients (Figure III. 2).

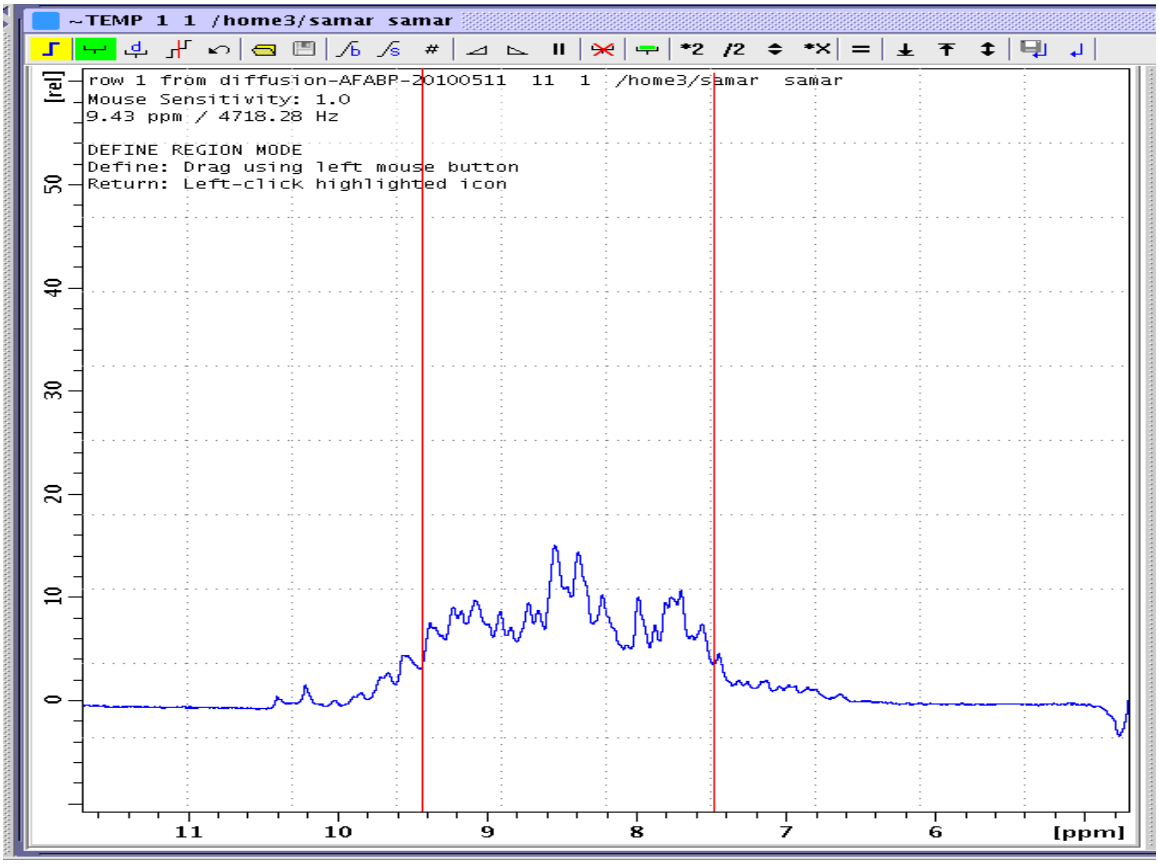

Figure III. 1. Screenshot of the processing of typical data of the proton spectrum from 0.63 mM ^{15} N holo (linoleate) AFABP, pH 7.4 at 20 °C. The region indicated by the red line between (7.5 - 9.4 ppm) over which signals was integrated as a function of amplitude to obtain a plot of the effective gradient intensity decay shown in Figure III. 2.

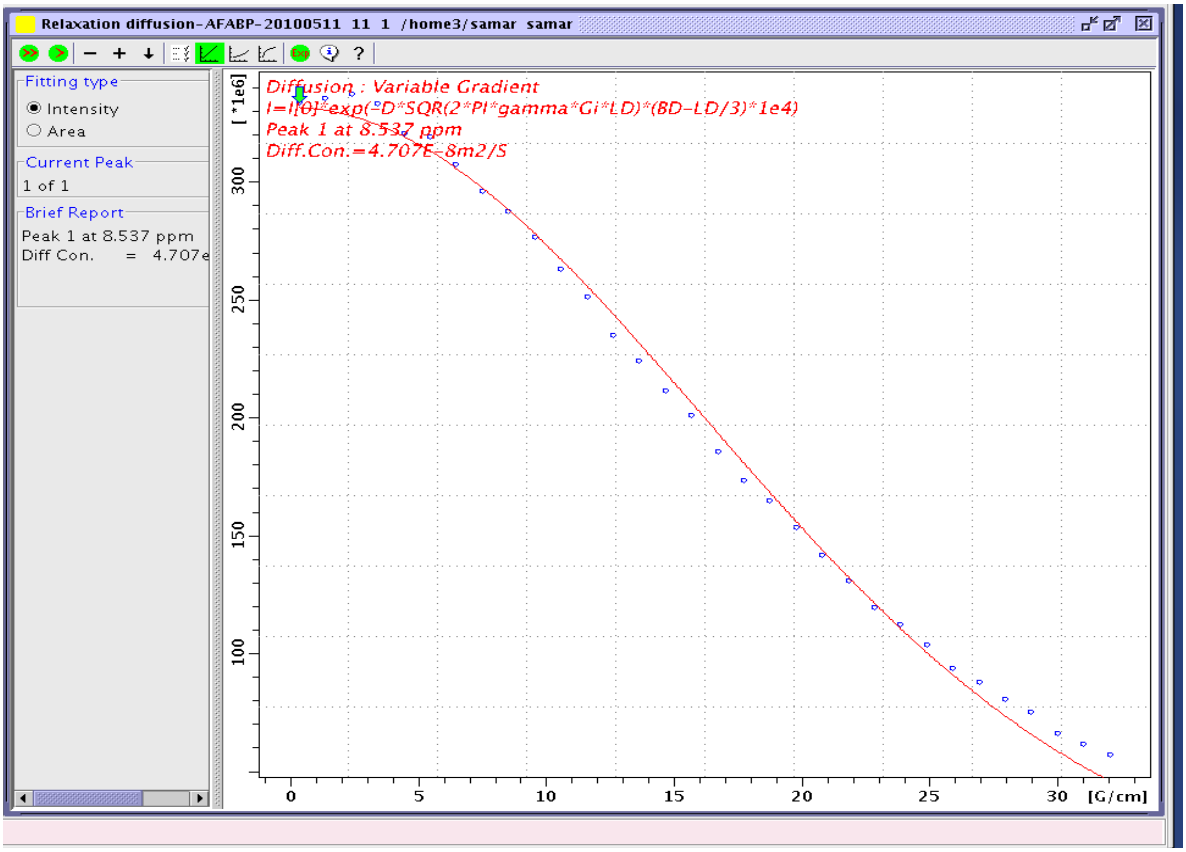

Figure III. 2. Plot from TopSpin software showing the decay of the integrated signal of ^{15}N holo (linoleate) AFABP as a function of the amplitude of gradients. Proton signals were integrated over the amide region indicated in Figure III.1.

The diffusion coefficient can be determined by fitting the signal from the data output (S/S_0) to Equation III.2.

$$S / S_0 = \exp\left[-4Dk^2\left(\Delta + 6\tau\right)\right] \qquad \textbf{Equation III.2,}$$

where $k = \gamma g \delta$; sg is the gradient strength, γ is the gyromagnetic ratio (26752 rad sec^{-1} $gauss^{-1}$) and δ = 0.01 sec. The quantity (Δ+6τ) is one of the delay times d20 (0.4 sec).

by which equation III.6 could be converted in such a way to allow derivation of the D = (1.49723) X 10^{-10} m^2 sec^{-1} from the slope of the linearized equation (Equation III.3, Figure III. 3):

$$\ln(S/S_0) = -4D\gamma(sg)^2\delta^2(\Delta + 6\tau) \qquad \textbf{Equation III.3.}$$

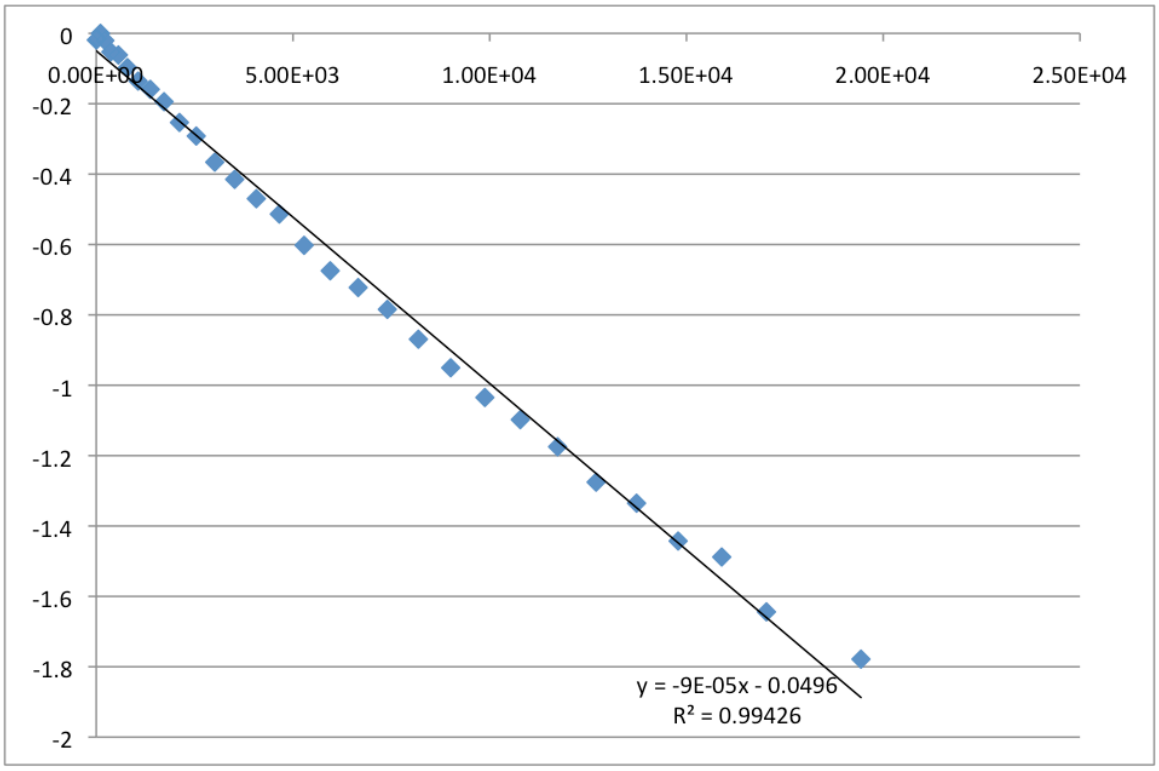

Figure III. 3. Chart showing the derivation of the diffusion coefficient (D) by plotting ln (S/S_0) against $(sg)^2$. D = (1.49723) X 10^{-10} m^2 sec^{-1}

The molar mass M = 9.02 kDa for AFABP was obtained from one of the experiments by utilizing the diffusion coefficient in Equation III.4 (Yao *et al.* 2000). This is one of many experiments that were processed and fitted in the same manner.

$$M = \left(kT/6\pi\eta FD\right)^3 \left[4\pi N_A \Big/ \left[3\left(\nu_2 + \delta\nu_1\right)\right]\right] \qquad \textbf{Equation III.4}$$

where k is the Boltzmann constant, T is the temperature (in Kelvin), η is the viscosity of the solution, δ_1 is the fractional amount of water bound to the molecule (hydration number, 0.2756), ν_1 and ν_2 are the partial specific volumes of the solvent water (1.0 X10^{-3} m^3 kg^{-1}) and of AFABP (7.2 X 10^{-3} m^3 kg^{-1}), respectively, while F is the shape factor (1.005). The shape factor is defined as the friction coefficient of the molecule (f) compared to that of a hard sphere (f_0) where both possess equivalent mass and partial specific volume. Because AFABP is an oblate ellipsoid, judged by its axial ratio: (p >1; $p = b/a = 1.19$; a is the semi axis of revolution and b is the equatorial radius), therefore F can be defined by **Equation III.5**.

$$F = f \Big/ f_0 = \left(p^2 - 1\right)^{1/2} \Big/ \left[p^{2/3} \tan^{-1}\left[\left(p^2 - 1\right)^{1/2}\right]\right] \qquad \textbf{Equation III.5}$$

14 more experiments were processed and fitted in order to derive the molecular weight of AFABP. The results of those 15 experiments are summarized in **Table III.1**, showing that the molecular weights obtained from these experiments after both linear and

exponential fitting were discrepant and unreliable as they gave molecular weights ranging from 0.1 – 36 kDa (Table III.1).

Table III.1 Summary of the results obtained for 15 diffusion experiments.

Pulse Program	Sample type	C (µM)	P30 (µs)	d20 (ms)	d16 (µs)	D ($m^2 s^{-1}$)	MW (kDa)
PFGX-STE	Apo	130	120	350	150	$1.94E^{-10}$	4.121
PFGX-STE	Apo	130	120	400	150	$1.65E^{-10}$	6.697
PFGX-STE	Apo	400	120	350	150	$1.61E^{-10}$	7.298
PFGX-STE	Apo	400	120	400	150	$1.50E^{-10}$	9.016
PFGX-STE	Apo	700	120	350	150	$2.86E^{-10}$	1.295
PFGX-STE	Apo	700	120	320	150	$2.70E^{-10}$	1.533
PFGLED	Apo	700	500	100	200	$4.75E^{-10}$	0.282
PFGLED	Apo	700	800	100	200	$5.23E^{-10}$	0.211
PFGLED	Apo	700	750	100	200	$5.15E^{-10}$	0.221
PFGLED	Apo	700	900	100	200	$4.77E^{-10}$	0.278
PFGLED	Apo	700	1000	100	200	$6.26E^{-10}$	0.123
PFGX-STE	Holo (linoleate)	630	600	600	150	$1.66E^{-10}$	6.643
PFGX-STE	Holo (linoleate)	630	120	500	150	$2.49E^{-09}$	0.002
PFGLED	Apo	100	1000	500	200	$1.11E^{-10}$	22.050
PFGLED	Apo	300	1000	500	200	$9.36E^{-11}$	36.931

C. Gel Filtration

1. Principles

In gel filtration chromatography molecules and proteins of different molecular weights can be separated based on size. Moleules with similar shape or size elute at similar times and have comparable migration profiles (Andrews 1962; Sun *et al.* 2004; Wang *et al.* 2010). Depending on the size of the biomolecules, they may diffuse into the pores of the beads if they are small in size, and therefore are eluted from the column slowly, or travel between the beads more quickly if they are large. This method can be used to roughly determine the molecular weight of proteins assuming they are globular

protein and posess similar shape as the protein standards used to plot the calibration curve. The principle of this technique is described in detail in Chapter II.

2. Materials and Methods

A Superdex 75 column (GE Healthcare Biosciences, Piscataway, NJ) (courtesy of the Ghose lab, CCNY) was used in the sizing experiments. The column was calibrated using 100 μL Blue Dextran as void volume protein, and 100 μL of a mixture of known proteins (Conalbumin, Ovalbumin, Carbonic Anhydrase, Ribonuclease, Aprotinin) with concentrations of 3 mg/ml each. The elution profile of those known proteins is illustrated in Figure III. 4**.**

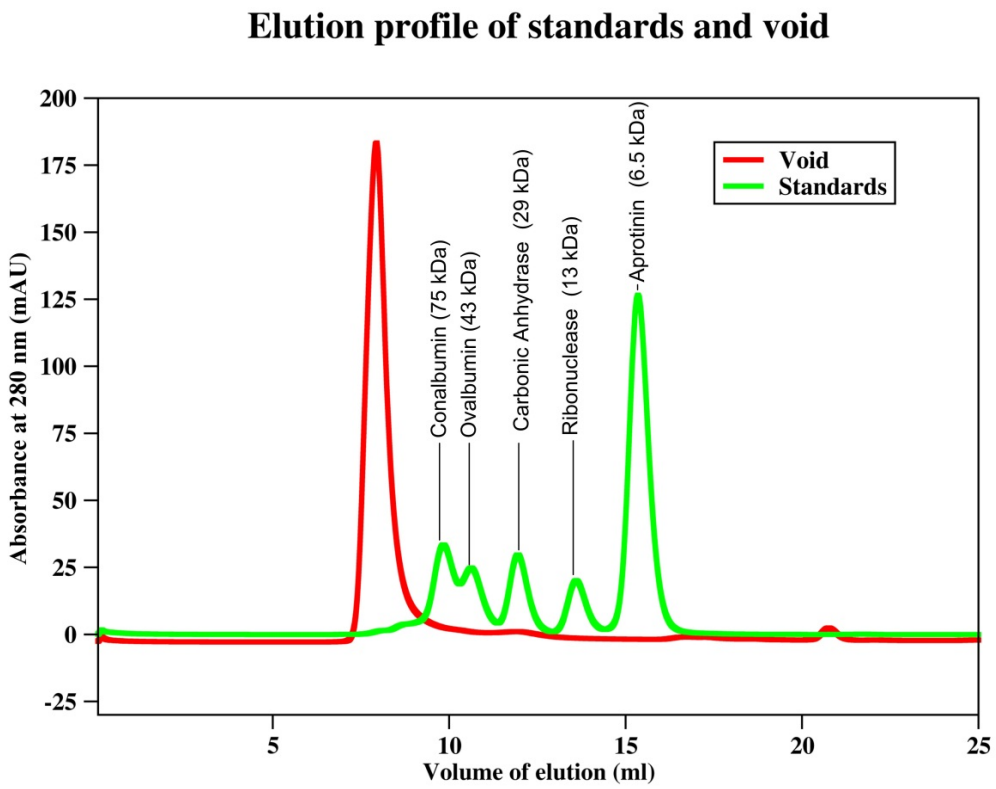

Figure III. 4. Elution profile of void volume protein (Blue Dextran (2,000 kDa)) colored red, and standard proteins (Conalbumin (75 kDa), Ovalbumin (43 kDa), Carbonic Anhydrase (29 kDa), Ribonuclease (13 kDa), Aprotinin (6.5 kDa)) colored green.

A calibration curve was then plotted between the partition coefficient (known as the gel-phase distribution coefficient) (K_{av}) and logarithm of molecular weight of each eluted protein (Figure III. 5), where K_{av} is calculated using the following equation (Equation III.6) involving the elution volumes of the proteins (V_e), void volume (V_o) and column volume (V_c, equivalent to the volume of the packed bed) (Andrews 1964):

$$K_{av} = (V_e - V_o)/(V_c - V_o) \qquad \textbf{Equation III.6}$$

The equation of the straight line obtained from the plot can be used to estimate the molecular weight of an unknown protein.

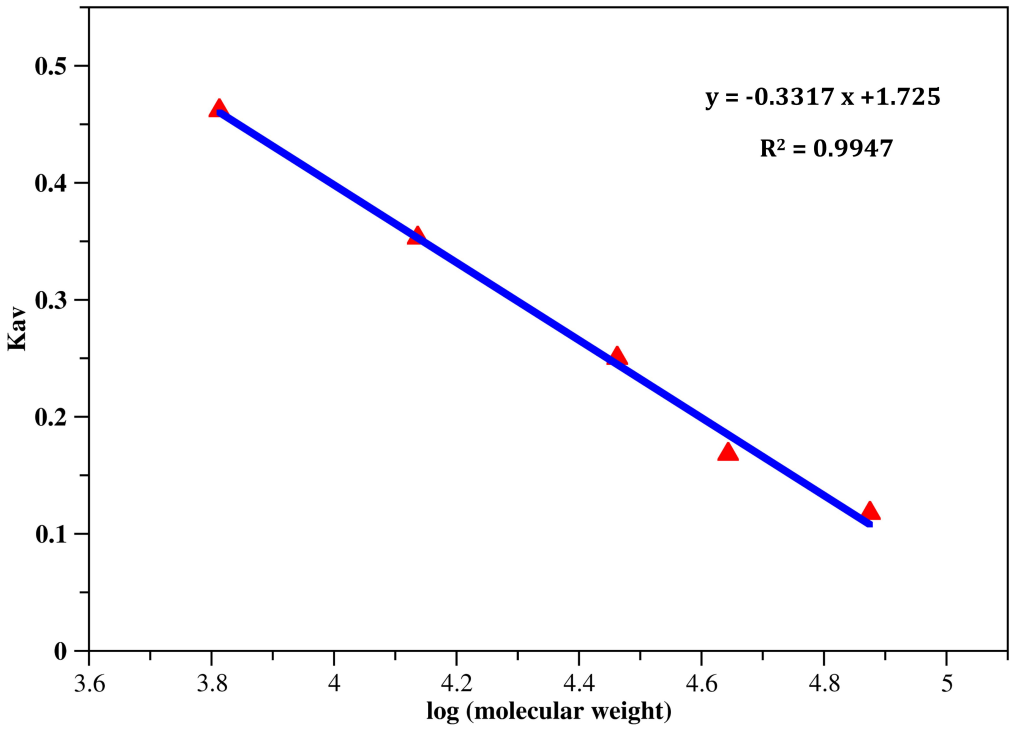

Figure III. 5. Calibration curve obtained by plotting the partition coefficient (K_{av}) against logarithm of molecular weights corresponding to five known protein standards (Conalbumin, Ovalbumin, Carboonic Anhydrase, Ribonuclease, Aprotinin).

Apo and holo AFABPs of different concentrations were loaded onto the Superdex 75 column. Series dilutions were prepared for each of the apo and holo proteins from 0.5 mM to 0.05 mM. Apo protein was prepared as mentioned in Chapter I. Samples for each experiment were concentrated to 0.4 – 0.5 mM concentration and then diluted in a series using the same buffer to prepare different concentrations of the protein. Oleate, linoleate and TDZ (dried from ethanol) were added prior to the series dilution in the molar ratio (2:1) ligand to protein in order to prepare their respective holo proteins.

These samples were run through the column and the elution profiles were plotted. Peaks were analyzed based on their elution volumes to determine the corresponding protein molecular weight. This procedure can help to identify the monomeric or oligomeric state of the protein. In the case that more than one peak is detected, the ratio of areas under the curve (AUC) of these peaks determines the ratio of the two protein states.

3. Results

In order to test the reproducibility of the measurment, 100 µl of 0.5, 0.4, 0.3, 0.1, 0.06 and 0.04 mM old samples of apo AFABP were loaded onto the column and the elution profiles were plotted. The samples were repeated multiple times with the number of repeats (n) and the standard deviation calculated for each experiment. The experiment shows a proportion of monomer that ranges between 64 and 70 % and dimer formation that decreases with the concentration. The percent error does not exceed 2 % in repeated trials. For convenience this experiment was conducted using an old sample that was available and standing for a long time increasing the likelihood of aggregation to produce dumers and higher oligomers. The aim was to ascertain reproducibility of experimental results using size exclusion experiments on an abundant sample.

Table III.2 Apo AFABP monomer as a function of concentration from size exclusion chromatography

Concentration (mM)	0.5	0.4	0.3	0.1	0.06	0.04
Average Percentage % of monomer	63	64	65	66	67	70
Standard deviation	N/A	0.62	1.44	1.66	1.14	N/A
Number of trials	n=1	n= 3	n=2	n=3	n=2	n=1

(a) Apo AFABP

100 µl of 0.4, 0.32, 0.1, 0.06 and 0.04 mM of apo AFABP in a 10 mM phosphate buffer (pH 7.4) containing 150 mM KCl were loaded onto the column and the elution profiles were plotted. On average 90 % monomeric AFABP was calculated, based on the average ratio of AUC for the second and first peaks, respectively, that eluted at 13.26 and 11.66 ml, respectively, and corresponded to molecular weights of 15.8 and 31.6 kDa, respectively. Because the migration profile of the molecules depend mainly on their shape (ellipsoid versus spherical), some slight differences may be found between the estimated molecular weights and the derived ones. While the expected molecular weight of the protein monomer and dimer are 15 and 30 kDa, respectively, the differences between those molecular weight values and derived ones (15.8 and 31.6 kDa) are modest and could be attributed to a difference in the shape of AFABP as compared with the standard proteins. However, it is still possible to distinguish between monomeric and dimeric protein states from size exclusion results despite slight inaccuracies.

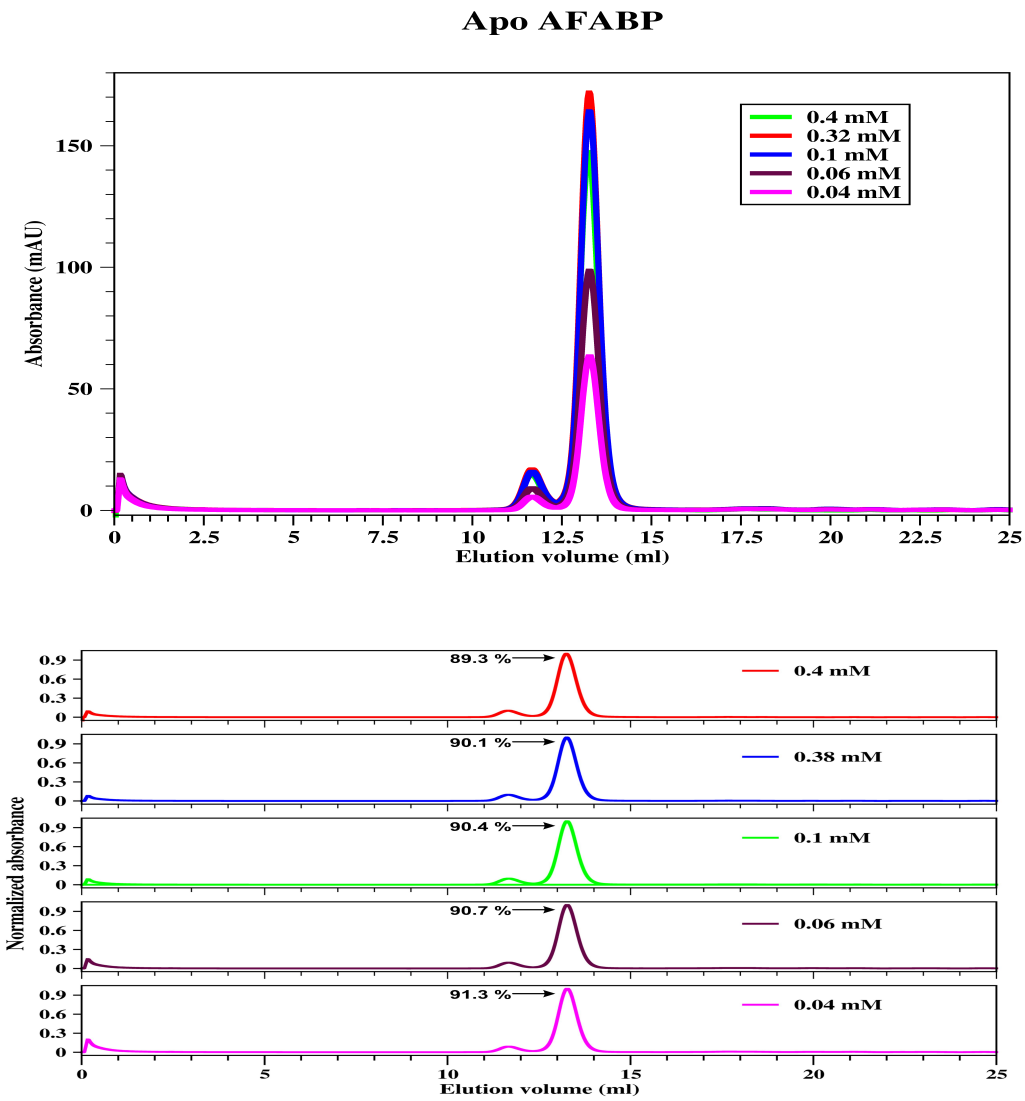

Figure III. 6. (top) Superimposed elution profiles of 0.4, 0.32, 0.1, 0.06 and 0.04 mM apo AFABP loaded on Superdex 75 column. Two peaks elute at 11.66 and 13.26 ml, respectively corresponding to 31.6 and 15.8 kDa molecular sizes. (bottom) Normalized elution profiles displaying the ratio of the AUC of the second peak with respect to the first peak representing the percentage of monomeric AFABP at each concentration.

(b) Holo (oleate) AFABP

Holo (oleate) AFABP eluted as a monomer. The elution profile of 100 µl of each of 0.3, 0.2, 0.1, 0.07 and 0.01 mM holo oleate AFABP in a 10 mM phosphate buffer (pH 7.4) containing in 150 mM KCl show a single major peak eluting at 13.22 ml and corresponding to 16.1 kDa protein, and a much smaller peak eluting at 11.65 ml and corresponding to 31.8 kDa. The average percentage of monomer form of holo AFABP is 98.4 % over the entire concentration range.

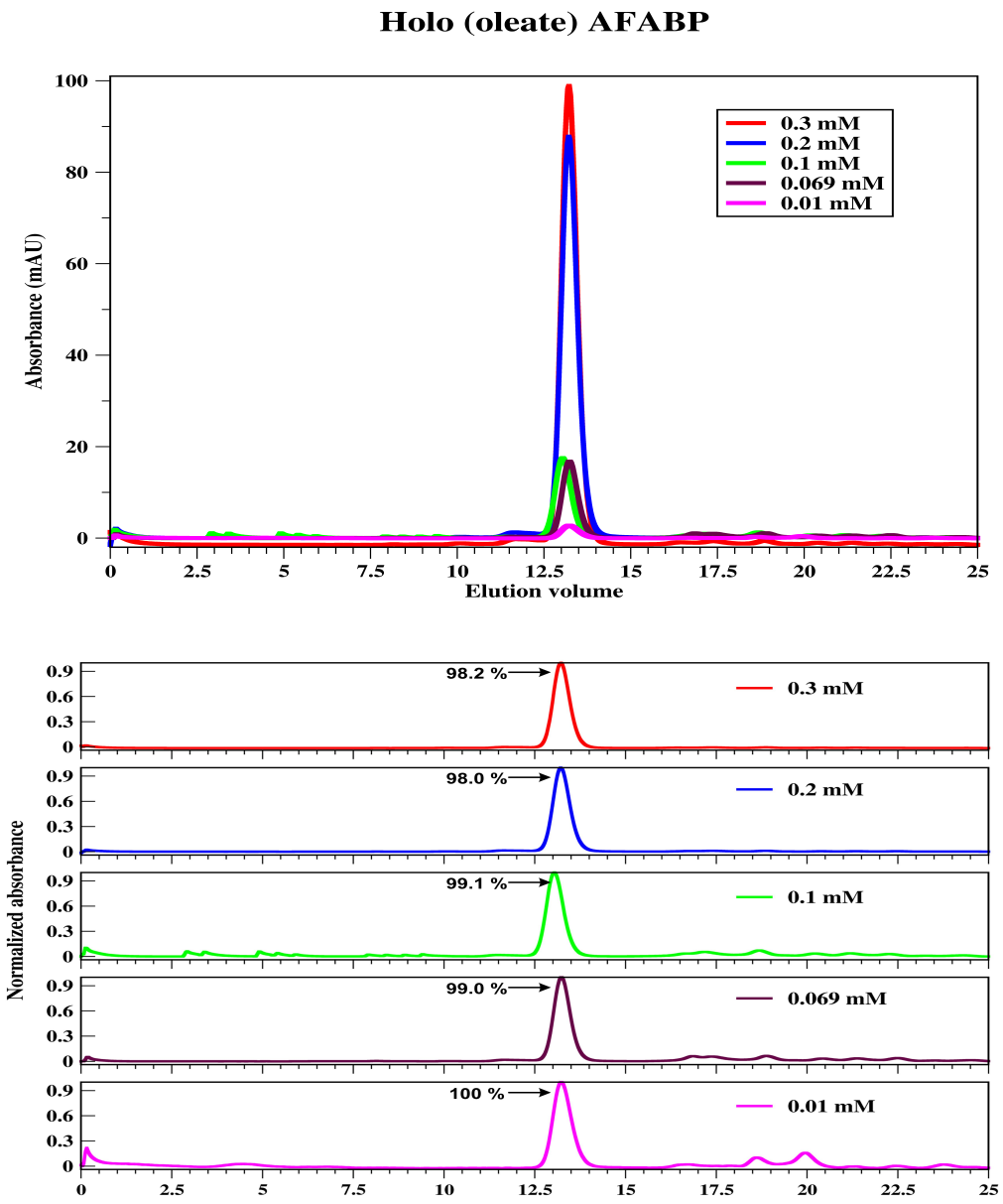

Figure III. 7. (top) Superimposed elution profiles of 0.3, 0.2 0.1 0.069 and 0.01 mM holo (oleate) AFABP loaded on Superdex 75 column. Two peaks elute at 11.66 and 13.22 ml, respectively corresponding to 31.8 and 16.1 kDa molecular sizes. (bottom) Normalized elution profiles displaying the ratio of the AUC of the second peak in respect to the first peak, and corresponding to the percentage of monomeric AFABP at each concentration. The slowly eluting peaks in the most dilute samples are attributed to buffer contaminants.

(c) Holo (linoleate) AFABP

100 µl of 0.3, 0.21, 0.12, 0.07 and 0.035 mM of holo (linoleate) AFABP in a 10 mM phosphate buffer (pH 7.4) containing in 150 mM KCl were loaded onto the column and the elution profiles were plotted. 94.1 % monomer form of AFABP was calculated, based on the average ratio of AUC of the second and first peaks. The peaks eluting at 13.25 and 11.63 ml, respectively correspond to the molecular weights of 15.9 and 32.1 kDa. A third small peak eluting at 9.54 ml and corresponding to 79.1 kDa is observed in all the elution profiles of holo (linoleate) AFABP preceding the other two peaks. The percentage of that peak considered as an oligomer ranged between 0.5 % at 0.035 mM increasing to 7.6 % in 0.35 mM protein. The concentration dependence of these values is discussed below.

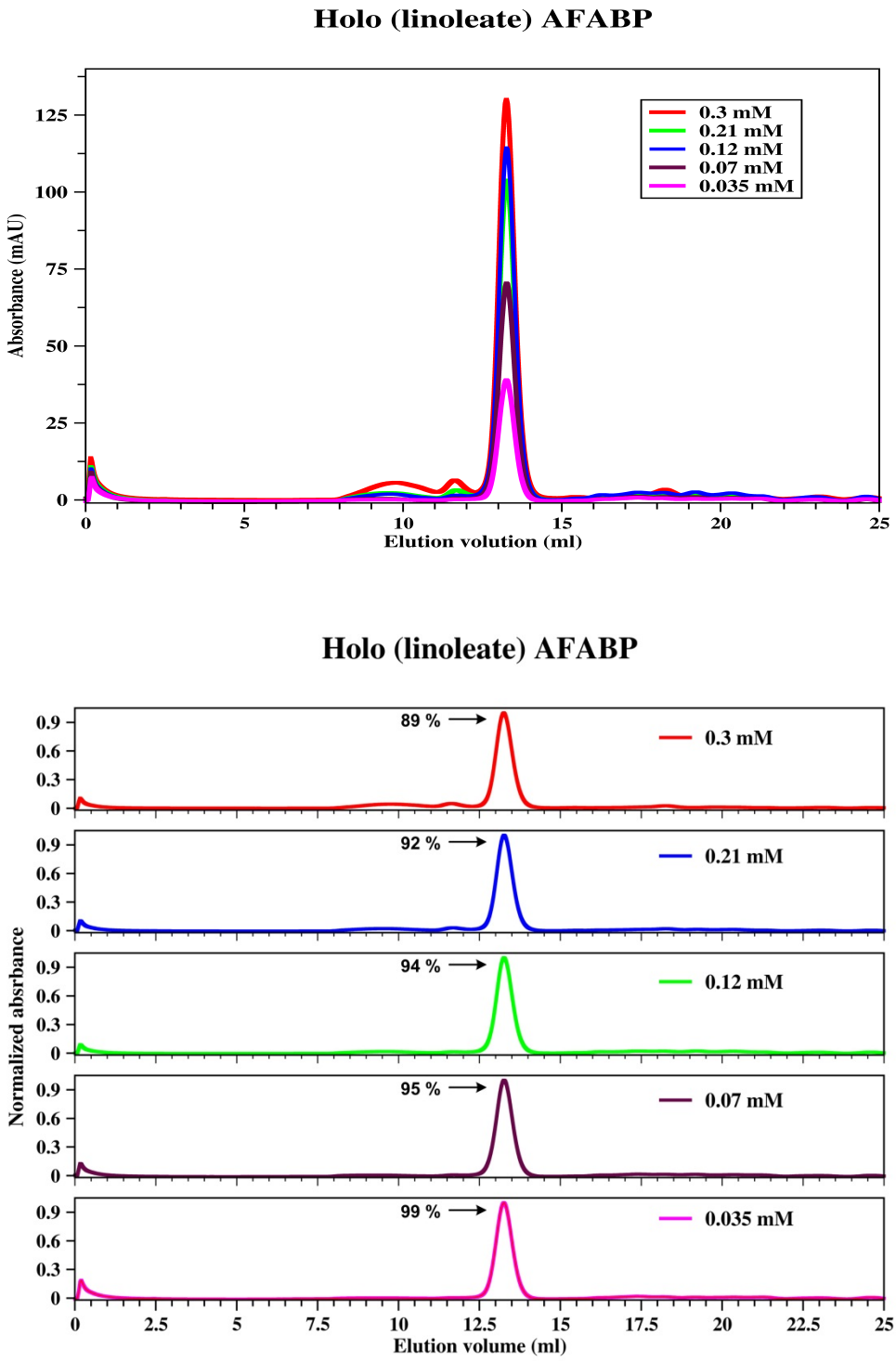

Figure III. 8. (top) Superimposed elution profiles of 0.3, 0.21, 0.12, 0.07 and 0.035 mM holo (linoleate) AFABP loaded on Superdex 75 column. Two peaks elute at 11.63 and 13.25 ml, respectively corresponding to 32.1 and 15.9 kDa molecular sizes. (bottom) Normalized elution profiles displaying the ratio of the AUC of the second peak with respect to the first peak, and corresponding to the percentage of monomeric AFABP at each concentration.

(d) Holo (TDZ) AFABP

100 µl of 0.47, 0.32, 0.15, 0.1 and 0.05 mM of holo (TDZ) AFABP in a 10 mM phosphate buffer (pH 7.4) containing 150 mM KCl were loaded onto the column and the elution profiles were plotted. An average of 91.5 % monomeric AFABP was calculated, based on the average ratio of AUC of the second and first peaks, eluting at 13.24 and 11.64 ml, respectively, and corresponding to the molecular weights of 16.0 and 31.9 kDa, respectively. The concentration dependence of these values is discussed below.

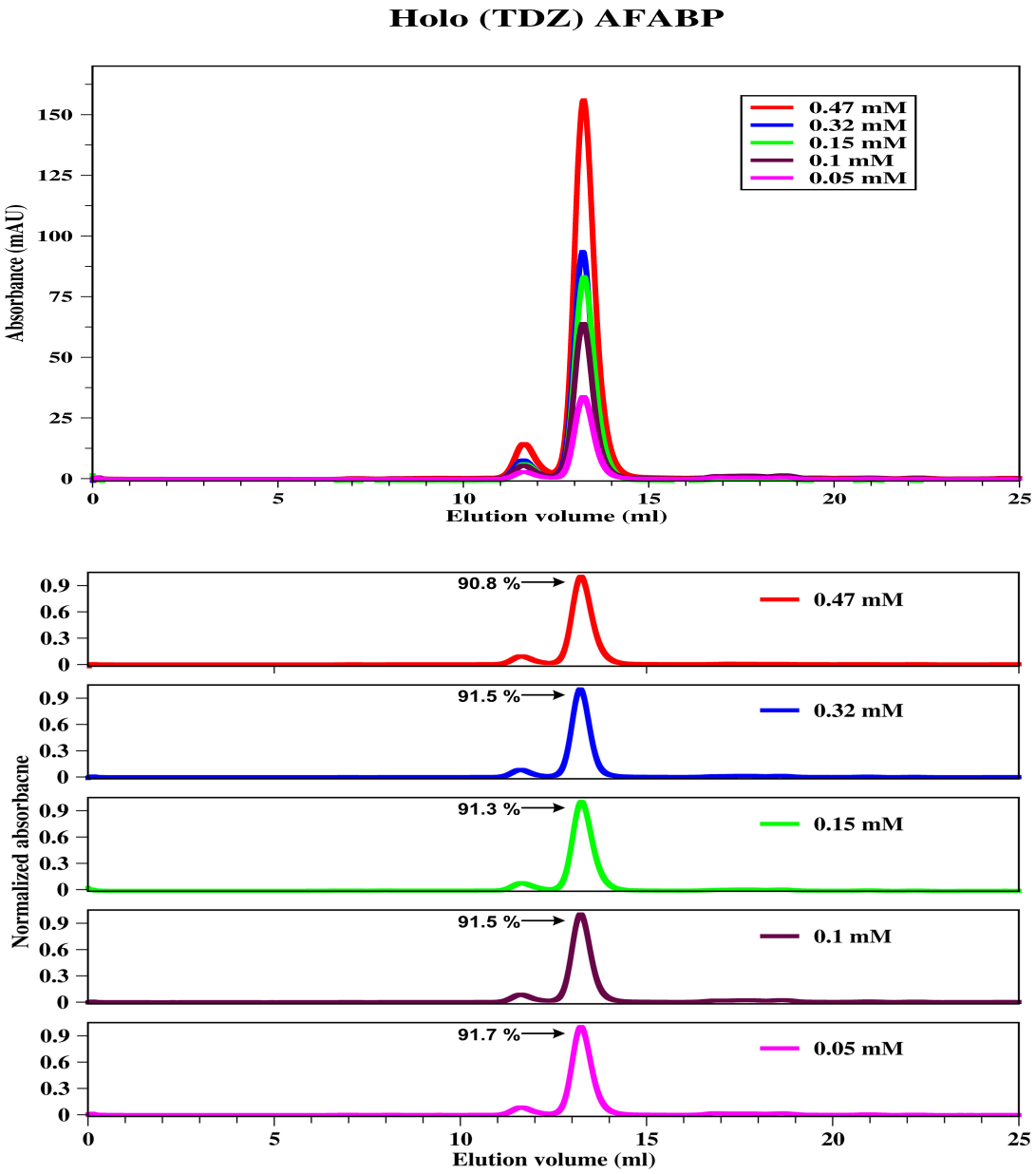

Figure III. 9. (top) Overlaid elution profiles of 0.47, 0.32, 0.15, 0.1 and 0.05 mM holo (TDZ) AFABP loaded on Superdex 75 column. Two peaks elute at 11.64 and 13.24 ml, respectively, corresponding to 16.0 and 13.9 kDa molecular weights. (bottom) Normalized elution profiles displaying the ratio of the AUC of the second peak in respect to the first peak, and corresponding to the percentage of monomeric AFABP at each concentration.

(e) Apo AFABP in 20 mM TRIS

100 µl of 0.25, 0.2 mM of both apo and holo (TDZ) AFABP in 20 mM Tris-HCl buffer (pH 7.8) were loaded onto the column and the elution profiles were plotted. Apo AFABP showed 84 % monomer form, calculated based on the average ratio of AUC of the second and first peaks, eluting at 13.33 and 11.85 ml, respectively, and corresponding to molecular weights of 15.4 and 29.2 kDa, respectively. The holo (TDZ) AFABP the protein showed 85 % average monomer AFABP, based on the two peaks eluting at 13.33 and 11.88 ml and corresponding to 15.4 and 28.8 kDa, respectively.

These measurements have been done for apo AFABP and holo (TDZ) AFABP only and will be done for the other holo (oleate and linolate) AFABP proteins in the future to confirm monomeric versus dimeric species ratio at low ionic strength.

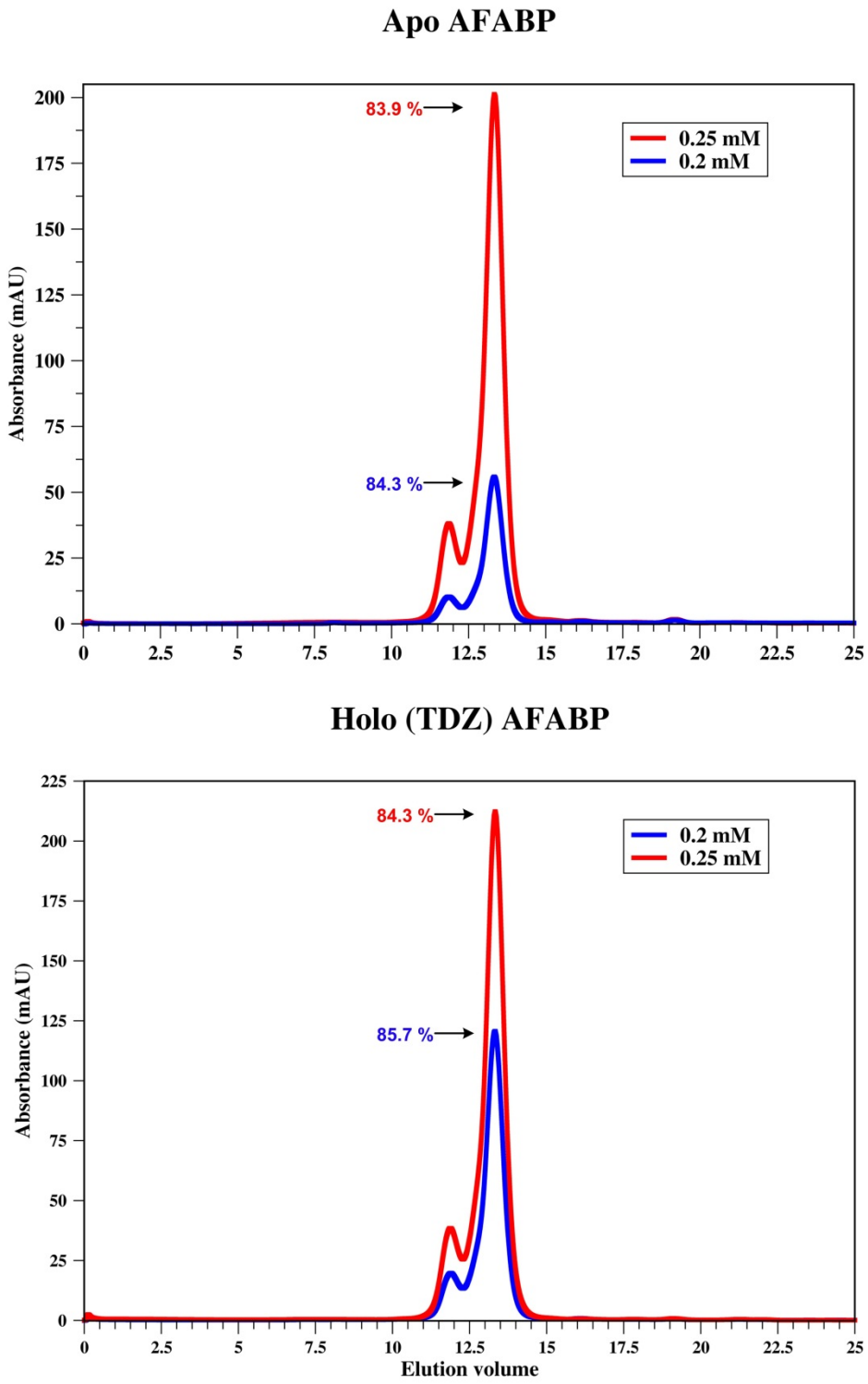

Figure III. 10. (top) Overlapped elution profiles of 0.25 and 0.2 mM apo AFABP showing two peaks eluting at 11.85 and 13.33 ml, respectively. (bottom) Overlapped elution profiles of holo (TDZ) AFABP showing two peaks eluting at 11.88 and 13.33 ml, respectively, corresponding to and kDa molecular weights.

D. Static Light Scattering

1. Principles

Static light scattering (SLS) is a technique that measures the intensity of the scattered light in relation to the scattering angle to obtain information on the size of the particle. Usually the scattering intensity is measured at different angles using fixed detectors. This procedure can be used to acquire the molecular mass, the root mean square radius and the second virial coefficient related to the particle-particle interactions in solution. The basis for this procedure is the Zimm plot equation (Equation III.7) (Zimm 1948),

$$Kc/I(\theta) = \left[1/MP(\theta)\right] + 2A_2c \qquad \textbf{Equation III.7}$$

where c is the solution concentration, M is the molecular weight, A_2 is the second virial coefficient and K is an optical constant defined as:

$$K = 4\pi^2 n_0^2 \left(dn/dc\right)^2 \lambda_0^{-4} N_A^{-1} \qquad \textbf{Equation III.8}$$

where λ_0 is the incident radiation (vacuum) wavelength, n_0 is the refractive index of the solvent at λ_0, N_A is Avogadro's number and dn/dc is the differential refractive index (dRI) increment of the solvent-solute solution with rspect to a change in solute concentration, expressed in ml/g (measured using dRI detector during the experiment).

P(θ) and I(θ) in Equation III.7 describe the angular dependence and the intensity of the scattered light, and can be related to the root mean square radius (rms radius):

$$P(\theta) \approx 1 - \frac{16\pi^2\eta_0^2}{3\lambda_0^2}\left\langle r_g^2 \right\rangle \sin^2\left(\frac{\theta}{2}\right) \qquad \textbf{Equation III.9}$$

η_0 is the index of refraction of the solvent, λ_0 is the vacuum wavelength of laser, and r_g is the rms radius. If θ goes to zero, then the term $P(\theta)$ will equal unity. In this case one can obtain the molecular mass by plotting the value derived from intensity and experimental parameters (K) on the y-axis against the squared scattering vector (Sin^2 (θ/2)) on the x-axis (Equation III.7). The molar mass can be calculated from the reciprocal of the y-intercept. This can be demonstrated by Figure III. 11.

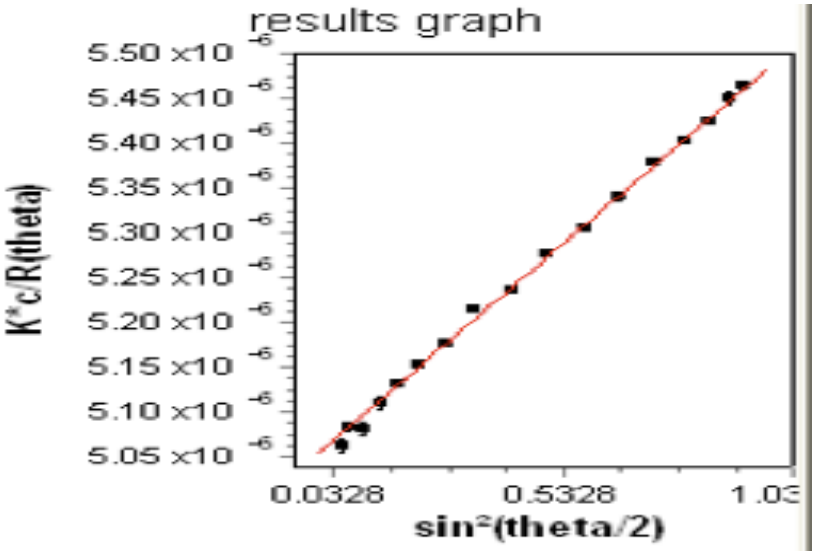

Figure III. 11. Plot from Wyatt Technology manual, showing linear fitting used to obtain the molecular mass (reciprocal of the y-intercept).

2. Materials and Methods

Experiments were conducted in Prof. Ranajeet Ghose's lab using a Wyatt MALS system that includes a miniDAWN TREOS multi angle light scattering (MALS) instrument (Wyatt, Santa Barbara, CA) equipped with ASTRA software and connected to an Optilab T-rEX refractometer, as well as a SEC column preceding the UV/Vis at the inlet. The sample is injected into the instrument and a UV detecor records the signal.

A protein purification method designed by Dr. Cedric Bernard and Mr. David Kam used a His-tagged protein on a Ni affinity column. In this specific experiment holo (oleate) His-tagged protein was used prior to cleavage of the tag. The molecular weight of the protein is slightly bigger in size (18.1 kDa) and has 29 additional residues. More experiments will be done on the cleaved protein in the future.

3. Methods

A 100 µL sample of each of 2 mg/ml BSA and 30 mg/ml Lysozyme and 200 µM ^{15}N labeled holo (oleate) AFABP were injected into the MALS instrument. Calibration was performed using 2mg/ml BSA (66.5 kDa) and 30 mg/ml Lysozyme (16 kDa) as standards prior to performing the experiments. While BSA (66.5 kDa) is almost four times the molecular weight of His- tagged AFABP (18.1 kDa), BSA is a well studied water soluble protein of a known molecular weight (Hirayama *et al.,* 1990) with good stability and therefore is a suitable protein standard in this experiment. Lysozyme was also used since it has a molecular weight similar to that of AFABP. The data obtained were analyzed using ASTRA software to obtain the protein molecular weights.

4. Results

(a) Lysozyme and BSA

After injecting 30 mg/ml lysozyme and 2 mg/ml BSA, SLS data were analyzed by the ASTRA software to derive the molecular weights **(**Figure III. 12**)**. Lysozyme and BSA gave molecular weights that are very close to those reported in literature (Table III.3). These experiments gave us confidence to move forward and determine the molecular weight of holo (oleate) AFABP.

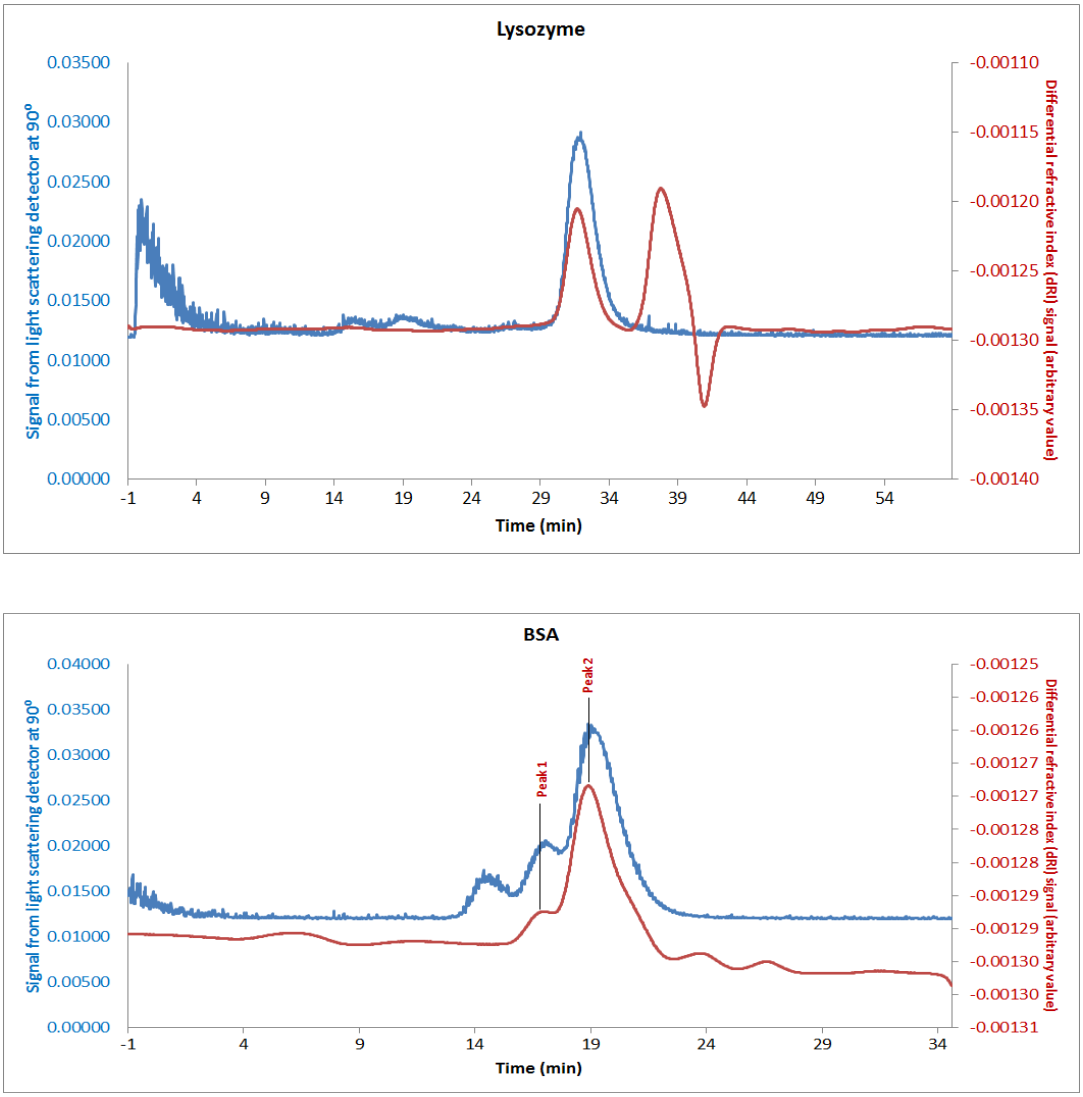

Figure III. 12. Elution profiles of Light scattering and dRI(in blue and red, respectively) for lysozyme and BSA.

(b) Holo (oleate) AFABP

As noted above, His-tagged holo (oleate) AFABP was used in this experiment prior to cleavage of the tag. The protein has an additional 29 residues and has a molecular weight of 18.1 kDa (Figure III. 13**,** Table III.3**)** whereas the measured molecular weight was 17.5 kDa. This molecular weight shows that holo (oleate) AFABP exists as a monomer in physiological salt concentration. Future experiments will be performed on apo and holo (linoleate and TDZ) AFABP samples, but these preliminary data provide supportive evidence to the size exclusion data (both discussed below).

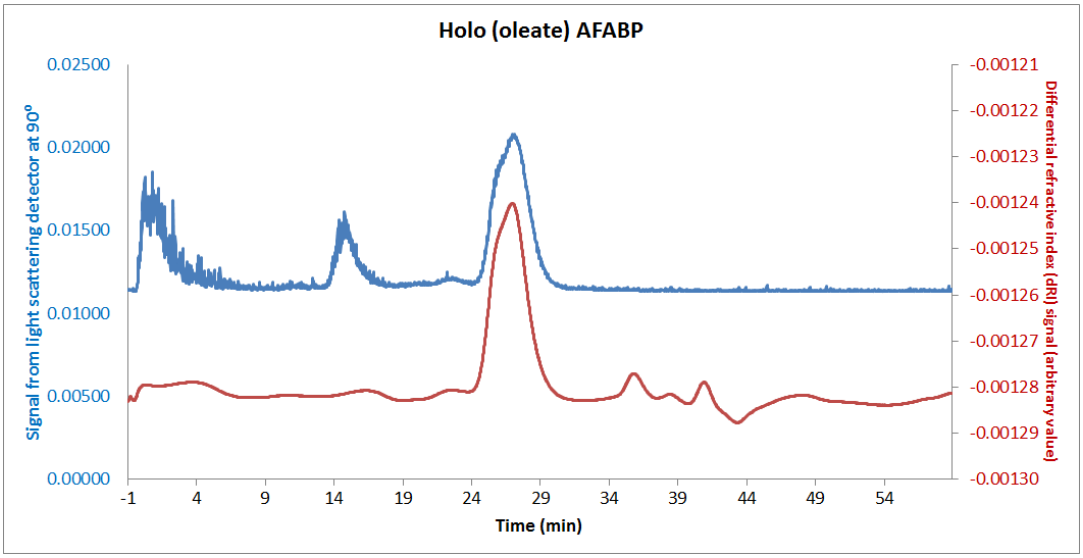

Figure III. 13. Elution profile of Light scattering data and dRI (in blue and red, respectively) of holo (oleate) AFABP.

Table III.3 Summary of molecular weights calculated from light scattering data and molecular weights of these proteins from literature for comparison.

Protein	Molecular weight from instrument	Molecular weight from publication
Lysozyme	15.6 kDa	14.3 kDa
BSA (Peak 1)	112 kDa	124 kDa (Hirayama *et al.* 1990)
BSA (Peak 2)	68 kDa	67.5 kDa (Hirayama *et al.* 1990)
Holo AFABP	17.5 kDa	18.1 kDa (Obtained herein)

E. Discussion

Our results from size exclusion with both protein standards and SLS detection show that AFABP exists predominantly in monomeric form. Performing the size exclusion experiments on the apo protein using numerous concentrations showed the same consistent result that the apo protein is at least 90 % monomer in physiological salt as shown in Table III.4. Using size exclusion to estimate size depends on a standard calibration curve from globular proteins of an array of molecular weights. While our protein is assumed spherical, estimating the protein size of a dimer form could be challenging since the shape of the protein could change as well and may not be globular anymore. In this case, the standard calibration curve may not fit properly with the protein. In addition, re-equilibration between monomer and dimer forms as the protein solution passes through the column could throw off the measured percentages. By

contrast, light scattering techniques provide the absolute molecular mass of the protein and do not require a calibration curve, though the protein was still passed through a column. Even though size exclusion technique could have a pitfall in estimating the size of the protein, performing the SLS on holo AFABP gives us confidence in our results and confirms the monomer form essentially as the sole species of holo (oleate) AFABP in 150 mM salt.

AFABP bound to activating ligands linoleate and TDZ showed a slightly smaller percentage of monomer (94.7 and 91.3 %) than for the non activating ligand oleate (99.1). With linoleate bound protein, some higher oligomers of the protein were also observed (7.6 %). Nonetheless, we found no significant oligomerization for either activating or non-activating ligands. Experiments performed on the apo protein at different salt concentrations also showed more dimers as the salt decreases. The protein exists as at least 90 % monomer in physiological salt (150 mM KCl) versus 85 % monomer in 20 mM Tris HCl. This result is expected since a decrease in salt concentration will decrease the electrostatic shielding between protein molecules and thus promote an increase in oligomerization **(**Figure III. 14**)**. This low ionic strength corresponds to the conditions used by Gillilan *et al.* (2007) in their SAXS and crystallography experiments, that were run in 20 mM Tris-HCl. The fact that our data shows predominant monomer formation even at lower salt concentration gives us confidence in our assertion that AFABP exists mainly in monomer form rather than dimer. As noted above, it was noticed that the percent monomer did not vary in a concentration dependent manner, which may suggest incomplete monomer/dimer

thermodynamic equilibrium in our samples. Approaches that avoid elution through a chromatographic column, as well as replicate measurements, should be performed in order to investigate this issue further.

Table III.4 Summary of the size exclusion results showing percentage of monomer form of AFABP for the concentrations between 100 and 200 µM in each experiment.

Protein sample	Percentage of Monomer form
Apo AFABP	90.4 %
Holo (oleate) AFABP	99.1 %
Holo (linoleate) AFABP	94.7 %
Holo (TDZ) AFABP	91.3 %
Apo AFABP in 20 mM Tris	84.3 %
Holo (TDZ) AFABP in 20 mM Tris	85.7 %

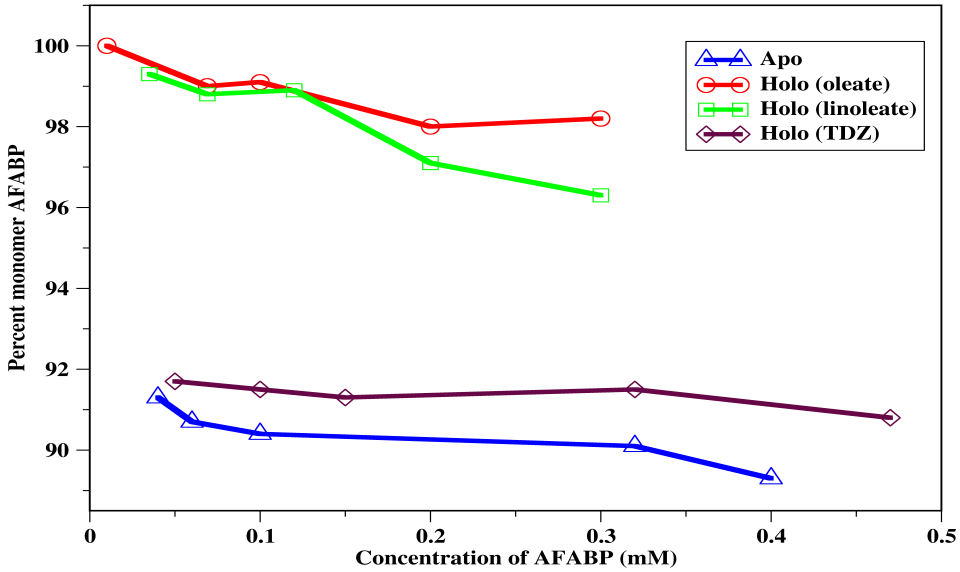

Figure III. 14. Concentration dependence of monomer proportion for apo, holo (oleate), (linoleate) and TDZ AFABP shown in blue, red, green and maroon, respectively.

Our size exclusion results provided the important insight that apo and holo AFABP exist predominantly as monomer under physiological salt conditions in solution.

While estimation of the mass using chromatography techniques depends on a premade calibration curve using the relationship between globular proteins of known molecular mass and their elution volumes and could lead to slight inaccuracies in the estimated molecular weights, SLS detection for the holo (oleate) AFABP allowed us to confirm our size exclusion experiments on holo (oleate) AFABP and suggested that other size exclusion results are also valid. Given the success and the accuracy of the SLS experiment, more measurements will be done on a newly designed preparation of apo and holo AFABP after cleavage of the His-tag. Additionally, the sizing experiments will be repeated using other physical methods in order to ascertain monomer-dimer equilibrium in solution and to investigate % monomer dependence on protein concentration more thoroughly.

IV. Assignments of Apo and holo (oleate) murine mAFABP

A. Introduction

The sequence assignments of murine AFABP have never been published, however, Constantine *et al*. obtained 92 % of the backbone and side chain assignments for human AFABP (Constantine *et al.,* 1998). Even though the sequence similarity between human and murine AFABP is 91.7 %, it was not possible to transfer the human protein assignments to the murine AFABP HSQC spectrum. Fewer than 30 % of the chemical shift assignments of human AFABP could be made by inspection of the murine AFABP resonances, but the remainder were too ambiguous to apply. Therefore it was evident that assigning the apo protein was the first necessary step to understand the effect of binding different ligands. Following this task, ligand binding will cause changes in some of those resonance positions (or linewidths), leading to identification of the binding site. After adding the oleate to apo AFABP, only 20 resonances that overlapped clearly with apo resonance could be identified by inspection. However, the remaining resonances had to be assigned independently. To help in assigning the apo and holo (oleate) AFABP, a series of 2D and 3D experiments were conducted towards that end as discussed in this chapter. For linoleate and TDZ, possible transfer of assignments was also possible as discussed herein. Murine AFABP (mAFABP) will be referred to as AFABP in the following text.

B. Materials and Methods

1. Preparation of NMR Sample

Uniformly ^{15}N labeled murine adipose fatty acid binding (AFABP) samples were obtained as described previously in Chapter II. Unlabeled sodium oleate was obtained from Sigma (St. Louis, MO) and used in a molar ratio of 1:1 protein to ligand in the holo experiments.

2. Double and Triple Resonance NMR Experiments for Apo AFABP

The [^{1}H-^{15}N]-HSQC, [^{1}H-^{15}N]-NOESY-HSQC and [^{1}H-^{15}N]-TOCSY-HSQC spectra were acquired on a Bruker Avance III 700 spectrometer equipped with a TCI cryoprobe. 1024, 240 and 64 complex points were acquired in the direct ^{1}H, indirect ^{1}H, and indirect ^{15}N dimensions with sweep widths of 9765, 9803 and 2483 Hz, respectively. The NOESY-HSQC mixing time was 150 ms, while the TOCSY-HSQC spinlock was 70 ms. The HN(CA)CO and HNCO spectra were acquired on a Varian VNMRS 600 spectrometer. 512, 32 and 32 complex points were acquired in the direct ^{1}H, indirect ^{13}C, and indirect ^{15}N dimensions with sweep widths of 9058, 1959 and 2200 Hz, respectively. The number of scans for the HN(CA)CO and HNCO experiments were 32 and 8 respectively. The HNCACB and CB(CA)CONH spectra were acquired on a Bruker Avance III 600 spectrometer. 512, 64 and 32 complex points were acquired in the direct ^{1}H, indirect ^{13}C and indirect ^{15}N dimensions with sweep widths of 9058, 11457 and 2200 Hz, respectively. The number of scans for the HNCACB and CBCA(CO)NH experiments were 32 and 16 respectively.

3. Double Resonance NMR Experiments for Holo (oleate) AFABP

The [^{1}H-^{15}N]-HSQC, [^{1}H-^{15}N]-NOESY-HSQC and [^{1}H-^{15}N]-TOCSY-HSQC spectra were acquired on a Bruker Avance 600 MHz spectrometer equipped with a TCI cryo-probe. 1024, 128 and 80, and 1024, 256 and 80 complex points were acquired for the NOESY and TOCSY experiments, respectively, with sweep widths of 8389, 8403 and 2128 Hz in the direct ^{1}H, indirect ^{1}H, and indirect ^{15}N dimensions, respectively. The NOESY-HSQC mixing time was 100 ms, while the TOCSY-HSQC spinlock was 120 ms.

All spectra were processed using the NMRPipe package (Delaglio *et al.,* 1995) and were analyzed using NMRViewJ software (Johnson 2004). Coordinates for apo and holo (oleate) AFABP were obtained from Protein Data Bank (PDB) entries 1LIB and 1LID, respectively (Xu *et al.* 1993). All structure representations of AFABP were displayed graphically with PyMOL (The PyMOL Molecular Graphics System), and all figures were prepared with either GIMP (http://www.gimp.org/) or Microsoft Visio (http://visio.microsoft.com) softwares.

C. Results

1. Apo and Holo (oleate) AFABP Two Dimensional ^{1}H-^{15}N HSQC Spectra

As described in Chapter II, spectra are derived from through-bond (scalar or *J*

coupling) magnetization transfer between pairs of atoms. Each peak in the HSQC spectrum represents a proton that is bound to a nitrogen atom, and the two-dimensional coordinates relate the chemical shifts of a proton and a heteronuclear atom (^{15}N) (Cavanagh *et al.* 2007). Therefore peaks in the HSQC spectrum can be assigned either to backbone NH groups in each amino acid residue or to side chains containing nitrogen-bound protons such as those in Asn, Gln, Trp, His, Lys, and Arg. The side chains could be detected at their corresponding ^{15}N chemical shifts, which lie outside of the conventional HSQC spectral width of 30 PPM (Ulrich *et al.,* 2008). Nevertheless, they may appear weak or missing due to rapid exchange of the protons with the solvent. Nevertheless, they could be investigated at their corresponding ^{15}N chemical shifts (Iwahara *et al.,* 2007; Esadze *et al.,* 2011).

Since AFABP is 131 residues long, we expect to find 129 backbone cross peaks in the HSQC spectrum, representing the backbone amide groups (excluding the first residue and P37, since the proton of the first residue exchanges rapidly with the solvent and is not observable while proline residues have no amide protons) and 14 side chain cross peaks: eight side chain resonances for four Asn, four side chain resonances for two Gln, and two side chain resonances for two Trp residues.

Each one of the apo and holo (oleate) HSQC spectra showed well resolved peaks indicating a well-folded protein. An overlay of the two spectra shows that some of resonances overlap while others show spectral deviations (**Figure IV.1**). Typically, the residues that are involved in the interaction experience a change in chemical

environment, due to interaction with the ligand, which results in an alteration in the NMR spectrum in the form of chemical shift changes in those residues. Additionally, there may be protein conformational changes that produce chemical shift perturbation and linewidth changes associated with complexation. In order to identify the residues that are involved in the interaction, it was important to assign each peak in the apo and holo spectra to its corresponding backbone or side chain amide group.

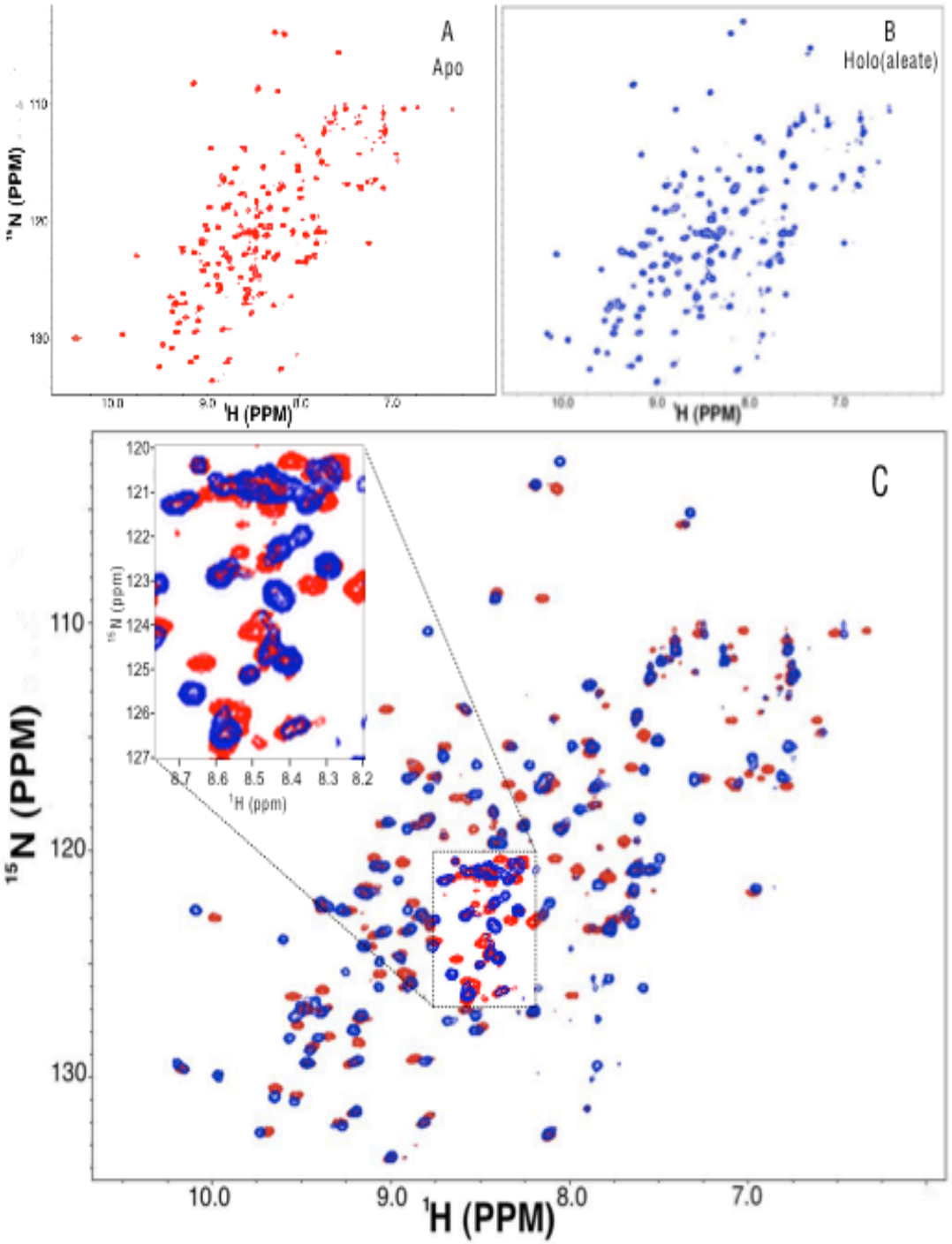

Figure IV.1. [^{1}H-^{15}N] HSQC spectra of (A) 0.9 mM apo AFABP collected on a Bruker spectrometer with ^{1}H frequency of 700 MHz; (B) 0.63 mM holo (oleate) AFABP of the protein to ligand ratio of (1:1) collected on Bruker spectrometer with ^{1}H frequency of 600 MHz; and (C) an overlay of apo (red) and holo (blue) AFABP showing overlapping holo and apo resonances as well as spectral deviations. Spectra were recorded at 20 °C and pH 7.4. The inset illustrates chemical shift changes in a crowded spectral region.

2. Sequential Assignments of Apo AFABP

Since the sequence similarity between human and murine AFABPs is 91.7 %, the published 92 % complete chemical shift assignments of human AFABP (Constantine *et al.* 1998) were investigated for possible assistance in assigning resonances in the murine AFABP HSQC spectrum. Some (less than 30 %) of the chemical shift assignments of human AFABP were similar to those of the murine AFABP resonances, but the remainder were too ambiguous to utilize.

To obtain the sequence specific assignments of murine apo AFABP, two sets of [^{1}H-^{15}N] and [^{15}N-^{13}C] edited three-dimensional experiments, respectively, were carried out. By performing [^{15}N-^{13}C] 3D HNCO (Kay *et al.* 1990), HNCACO (Bax *et al.* 1991), HNCACB (Grzesiek *et al.* 1992), and CBCA(CO)NH (Grzesiek *et al.* 1992) experiments, 91 % of the assignments could be made. The Runabout semi-automatic feature in the NMRviewJ software (Johnson 2004) was used, followed by manual confirmation of assignments.

In the parameters panel of Runabout, four experiments were loaded along with their respective peaklists, with the HNCO peaklist as the reference list for all the others. Runabout operates through three main modes: 1) Edit peaks, 2) Edit clusters, and 3) Edit links. In the edit peaks mode, Runabout filters and trims the peaklists that were loaded for the four 3D experiments by taking into consideration the number of residues in the protein and tolerance value (conservativeness). In this mode, the number of peaks of

each experiment are either deleted or added to the spectra in accordance to the original number of protein residues, level of peak picking and strength of the peak. Peaks that have the same ^{1}H and ^{15}N coordinates based on the reference peak list (HNCO) are then grouped into clusters. Edit clusters mode allows the user to go over cluster by cluster to confirm the number of peaks available (should be nine peaks for four 3D experiments: (four HNCACB, two CBCA(CO)NH, two HNCACO, and one HNCO). At this stage, clusters that have more than the expected number of peaks could be trimmed again by manual investigation of peak alignments, and could be labeled to belong to either residues (*i*-1) or (*i*). After that, edit links mode automatically connects up the clusters by aligning the peaks in such a way that the peaks can be assigned to protein residues. For each cluster, a given set of peaks are given as possible matches for preceding or following residues based on peak connectivities and alignment and number of peaks that could be aligned. A score is provided by the program based on the probability of a good match for each provided cluster. These clusters are investigated manually and sequential connections are either "extended" if there is a good match or not extended if they seem not to match perfectly; other clusters are investigated for better connectivities.

The success of this strategy is dependent mainly on the pairs of experiments used and their ability to provide important chemical shift correlations needed to deduce the sequential assignments for the protein. The pairs of complementary 3D NMR experiments used in this process were (HNCACB and CBCA(CO)NH) and (HNCO and HNCACO), where the HNCACB experiment correlates the chemical shift of the amide of residue (*i*) with the chemical shift of the Cα and Cβ carbons of residue (*i*) and the (Cα)

and (Cβ) carbons of (residue *i*-1), while (CBCA(CO)NH) correlates the chemical shift amide of residue (*i*) with only the chemical shift of Cα and Cβ for the previous residue (residue *i*-1). By using alternating strips of both experiments we were able to make sequential assignments of Cα and Cβ in AFABP. Figure IV.2 displays a schematic representation of the 3D experiments used for the apo AFABP protein assignments.

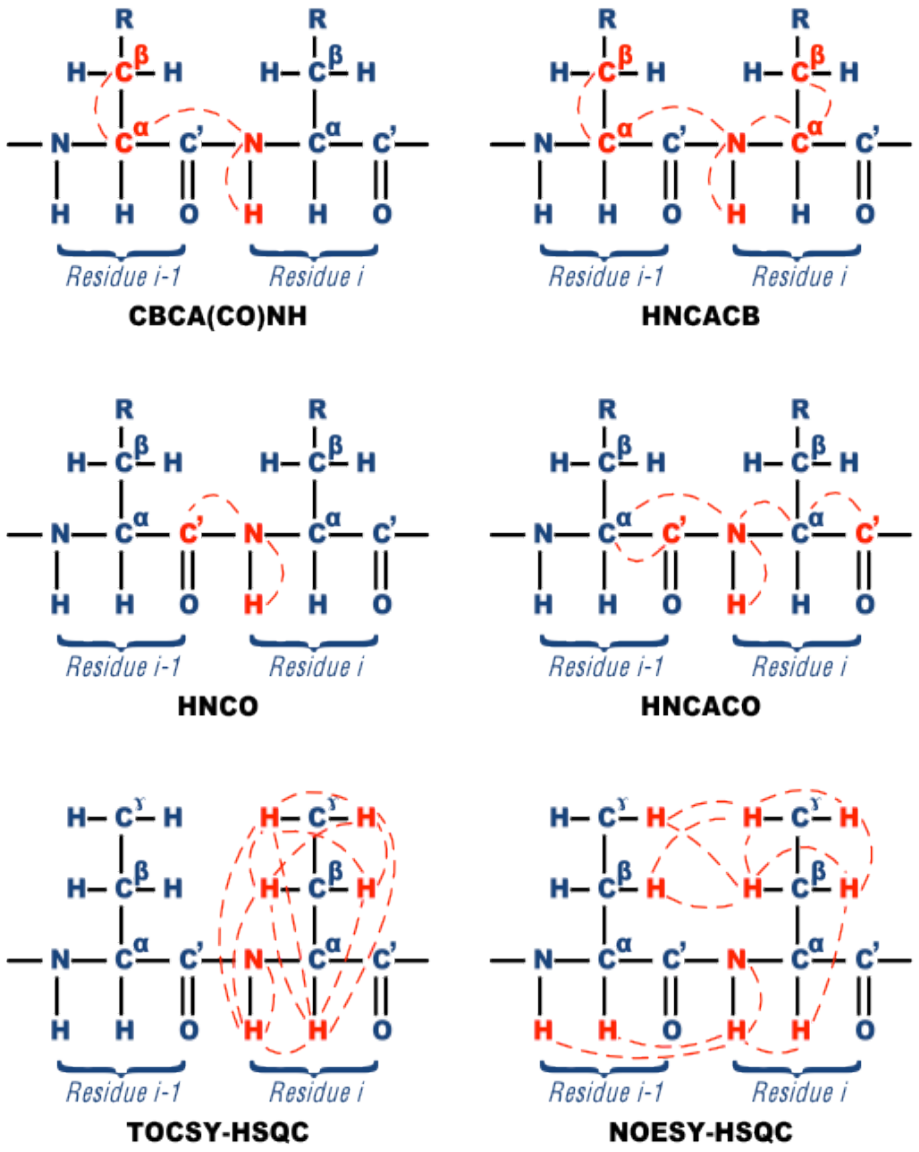

Figure IV.2. Schematic representation of six double and triple resonance 3D experiments used for AFABP sequence assignments, indicating intra and inter- residue correlations available from these experiments. The nuclear spins are designated as H-N for amide proton, N for the amide ^{15}N spin, and H for aliphatic proton and Cα, Cβ and C' for the carbonyl ^{13}C spin. Adapted from (Wuthrich 1986; Cavanagh *et al.* 2007). Only sequential NOE correlations are illustrated in this figure.

Similarly, (HNCO and HNCACO) experiments were used as a pair to make sequential assignments, where the HNCO experiment correlates amide chemical shifts of residue *i* with the CO of residue *i*-1, while the HNCACO experiment shows the same

information in the HNCO with the addition of the CO of residue *i*, which allows for ready assignments of sequential residues. Starting by identifying amino acid residues that carry side chains with distinct chemical shifts and using the 30 % of the backbone assignments made by inspection from human AFABP, these experiments facilitated connections to sequential amino acid residues. **Figure IV.3** shows an example of the strategy used to connect sequential residues.

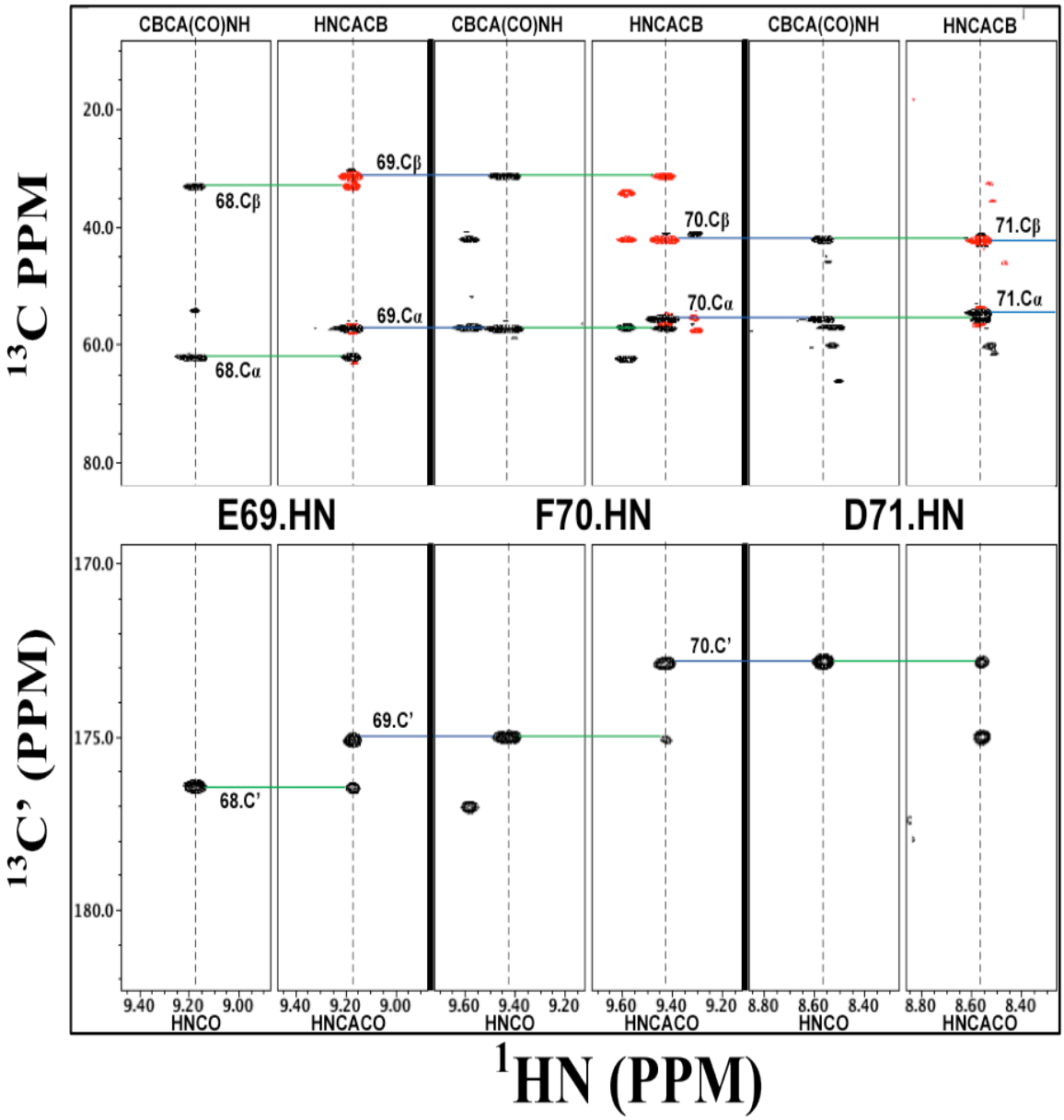

Figure IV.3. Extracted strips of CBCA(CO)NH and HNCACB in the top panel and of HNCO and HNCACO in the bottom panel, respectively, showing ^{15}N planes of residues E69, F70 and D71. Dashed lines represent the ^{1}HN chemical shift of each residue. Connecting lines demonstrating intra-residue and sequential connections are colored green and blue, respectively. Cβ resonances are colored red, indicating negative peaks in HNCACB. Details of the assignment strategy are provided in the text.

Figure IV.3 shows alternating strips of [^{15}N-^{13}C] HNCACB and CBCA(CO)NH in the top panel, and of [^{15}N-^{13}C] HNCO and HNCACO in the bottom panel for residues

E69, F70 and D71. Each strip from a pair of experiments was used as a pair. Each strip is a plot from the ^{15}N plane centered at the HN chemical shift (indicated by a dashed line) for each of the three residues, while each ^{15}N plane for respective pairs of 3D experiments is separated by a thick black line. Intra-residue and sequential correlations are denoted in blue. In the top panel, by examining the HN shift (dashed line) in the ^{15}N plane of CBCA(CO)NH and HNCACB strips for residue E69, Cα and Cβ of residue V68 (*i-1*) are observed as strong peaks in CBCA(CO)NH and weaker peaks in the HNCACB strips, and therefore the other two (slightly stronger) peaks in the HNCACB strip could be identified as Cα and Cβ of residue E69 (*i*). The latter two peaks could be matched in different ^{15}N or ^{1}HN planes of CBCA(CO)NH to find connectivities that would identify the sequential (*i*+1) residue. In a similar strategy, the carbonyl peak of residue V68 can be seen as a strong peak in the HNCO strip and as a weak one in the HNCACO strip for the ^{15}N plane of residue E69. The strong additional peak in the HNCACO strip belongs to E69, and could be connected to the sequential residues in the HNCO and HNCACO of the F70 strips.

Additionally, 3D [^{1}H-^{15}N] TOCSY-HSQC and [^{1}H-^{15}N] NOESY-HSQC experiments (Marion *et al.* 1989; Zhang *et al.* 1994) were used as a pair to investigate intra- and inter- residue spin systems correlated through bonds and through space, respectively. The 3D [^{1}H-^{15}N] TOCSY experiment provides through-bond correlations between amide nitrogen and side chain protons in the same residue and serves as an identification tool for the set of resonances of each individual amino acid residue and for amino acid typing via intra-residue (through bond) spin systems. 3D [^{1}H-^{15}N] NOESY

spectra are used to investigate the short, medium and long-range nuclear Overhauser Effect (NOE) peaks, which provide important through-space structural information for the protein.

NOE peaks result from dipole-dipole coupling between two protons that are separated by less than 5 Å through space. According to the location of the two coupled protons, NOEs are categorized into intra-residue, sequential, medium, and long range NOEs where protons are located on the same residues (*i*), consecutive residues (*i*+1), separated by two, three or four ($2 < i \leq 4$), or more than four residues ($i > 4$) in the polypeptide sequence, respectively.

NOE connectivity patterns between antiparallel β-strands were observed between β-strands β_A through β_J as well as between β_J and β_A, except for the β_D-β_E interface (**Figure IV.4**), indicating a long distance (greater than 5 Å) between those latter two β-strands. The distance between β-strands β_D-β_E is known as the 'gap', whereby an increased separation is attributed to substitution of the conventional inter-strand hydrogen bonding by a network of conserved water molecules and side chain interactions between them (Reese-Wagoner *et al.* 1999).

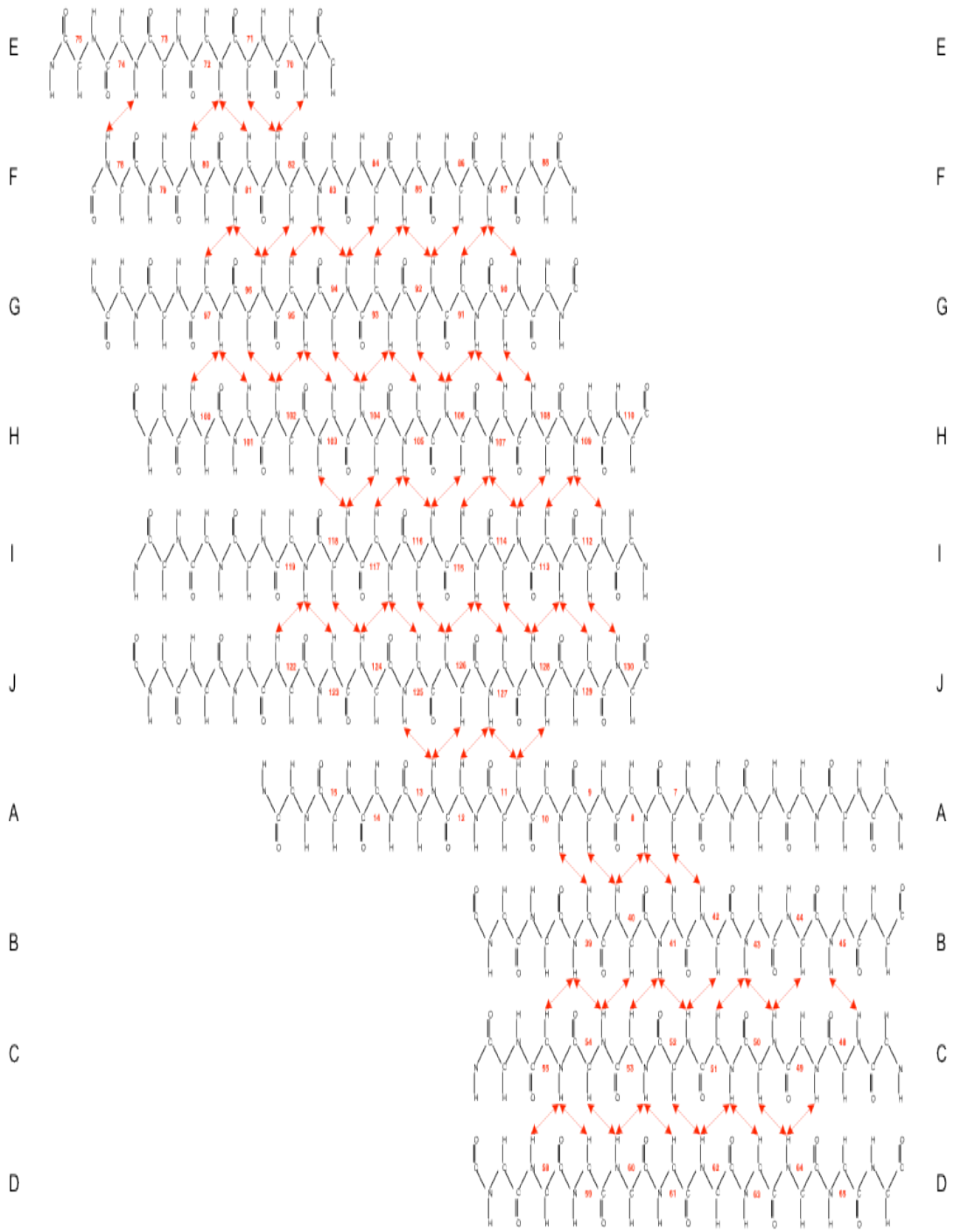

Figure IV.4. Schematic representation of apo AFABP backbone atoms of anti parallel β-strands β_A through β_J demonstrating long-range NOE connections between residues located on different β-strands. β-strands β_D and β_E do not interact via hydrogen bonding.

By studying sequential NOE connectivities between backbone Hα(*i*)-HN(*i*+1) and HN(*i*)-HN(*i*+1) on the NOESY strips, sequential chemical shift assignments obtained from the triple resonance experiments were further confirmed. Moreover, it was possible to infer the secondary structural elements of the protein. For example, α-helices are characterized by short distances between sequential backbone amide protons (HN(*i*)–HN(*i*+1)) that consequently demonstrate a strong NOE, while β-strands show NOEs between sequential α protons of residue (*i*) and amide protons of residue (*i*+1) (Hα*i* - HN*i*+1). α-helical structures also exhibit short distances between residues (*i*) and (*i*+4), which result in observing (Hα(*i*)- HN(*i*+2), (Hα(*i*)- HN(*i*+3) and (Hα(*i*)- HN(*i*+4) NOEs. These NOE connectivities for apo AFABP and the consequent secondary structure elements are illustrated in **Figure IV.5**. This NMR data analysis confirms that AFABP, like other proteins in the FABP family, is comprised of two α-helices and ten β-strands (Marcelino *et al.,* 2006).

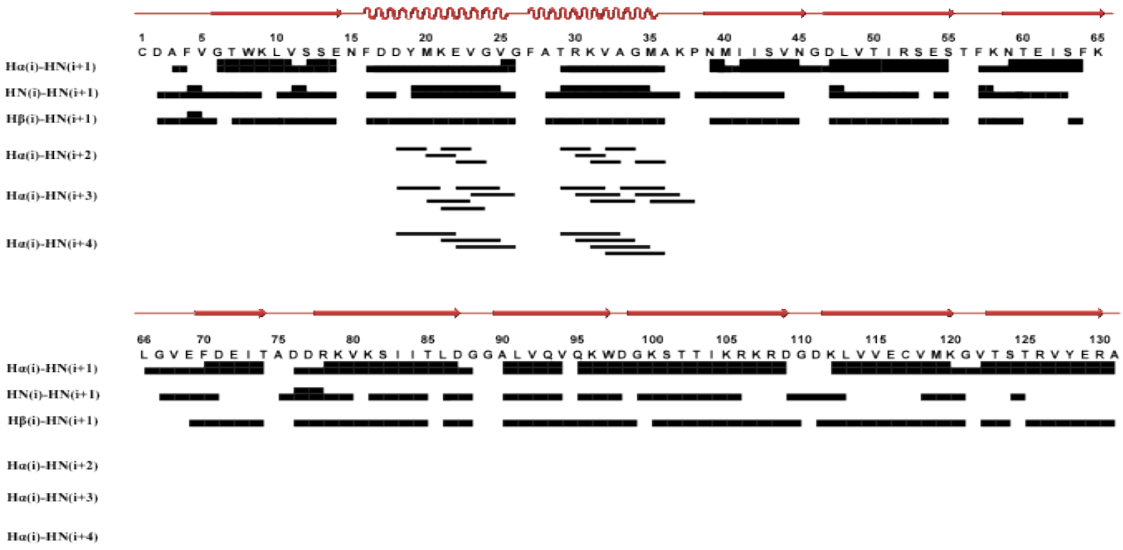

Figure IV.5. Schematic representation of short, medium and long range NOEs along the protein sequence of AFABP, demonstrating ^{1}H NMR sequential interactions for apo AFABP. Block height represents the strength of the NOE signal. Secondary structure of the protein can be predicted from this scheme, since a strong Hα(*i*)-HN(*i*+1) NOE connectivity indicates residues in an extended secondary structure (β-strands), while strong HN(*i*)-HN(*i* +1) indicates residues in a helical secondary structure element or a loop. The Hα(*i*)-HN(*i*+2), Hα(*i*)-HN(*i*+3) and Hα(*i*)-HN(*i*+4) connectivities are represented by lines, and are characteristic specifically for helical secondary structures. The figure was prepared with the Microsoft Visio program.

A long stretch of Hα(*i*)-HN(*i*+1) NOE connections between residues A90 and D109, interrupted by a missing Hα(*94*)-HN(*95*) NOE, could be interpreted as a long β-strand. However, by studying the long range NOEs delineated in **Figure IV.4**, residues 90-95 demonstrate strong signals with residues 100-108 on one β-strand and residues 81-87 on the other β-strand, suggesting that residues (90-109) form two β-strands separated by a short β-turn composed of one or two residues. Together, the combined data from short, medium and long -range NOEs summarized in **Figure IV.4** and **Figure IV.5** agree with previously published data regarding the secondary structure of AFABP (Reese-Wagoner *et al.* 1999) and show that the protein is composed two α-helices (αI:16-25 and

αII:27-35) and ten β-strands (β_A:6-16, β_B:39-45, βc:47-55, β_D:59-65, β_E:70-74, β_F:78-87, β_G:90-97 and β_H:99-109 , β_I:112-120, β_J:122-130).

By combining this information with the assignments obtained from both sets of 3D experiments, 124 out of 129 (96 %) backbone, and 13 out of 14 side chain resonances were successfully assigned for apo AFABP **(Table IV.1)**. Five residues remain unassigned (N15, F27, T56, G88, G110), excluding C1 and P37 since they do not produce detectable resonances in the HSQC spectrum as mentioned earlier. The remaining five unassigned residues are located either in the portal region (N15 and F27) or in the turns connecting β-strands (T56, G88 and G110).

3. Sequential Assignments of Holo (oleate) AFABP

After assigning the apo protein, it was essential to assign the holo (oleate) spectrum in order to identify the residues that are involved in the interaction with the ligand and map them onto the structure to finally deduce the binding locus. Since there are 20 peaks in the HSQC spectrum of the apo protein that overlap with those in the spectrum of holo (oleate) and do not undergo chemical shift changes, it was possible to assign them readily by visual inspection from the apo assignments. 3D [^{1}H-^{15}N] edited TOCSY-HSQC and [^{1}H-^{15}N] NOESY-HSQC experiments were carried out for the purpose of assigning the remaining backbone and side chain amide resonances of holo AFABP. With the initial assignments in hand, [^{1}H-^{15}N] NOESY and [^{1}H-^{15}N] TOCSY strips were used to confirm the identity of the remaining amino acids, by connecting the

identified amino acid residues to sequential ones through proper matching of NOE connectivities in the NOESY strips. More connectivities were made until 118 out of 129 (91 %) of the expected backbone resonances, and eleven out of 14 side chain assignments were made successfully for the holo (oleate) AFABP. Eleven residues remained unassigned (D2, N15, F16, D17, F27, K37, G46, T56, G88, G89, G110), excluding C1 and P38 but including the five unassigned apo AFABP residues. **Table IV.2** lists the chemical shift assignments of holo (oleate) AFABP.

Identifying long-range NOE signals between β-strands aided in confirming the assignments of the holo protein (**Figure IV.6**). Similar to the apo protein, these observable NOE signals between residues on different β-strands demonstrate that they are in close proximity (less than 5 Å) in space. As for the apo protein, no NOE signals were identified between residues on β-strands β_D and β_E, which means they are further away in space, confirming previously published reports (Marcelino *et al.* 2006).

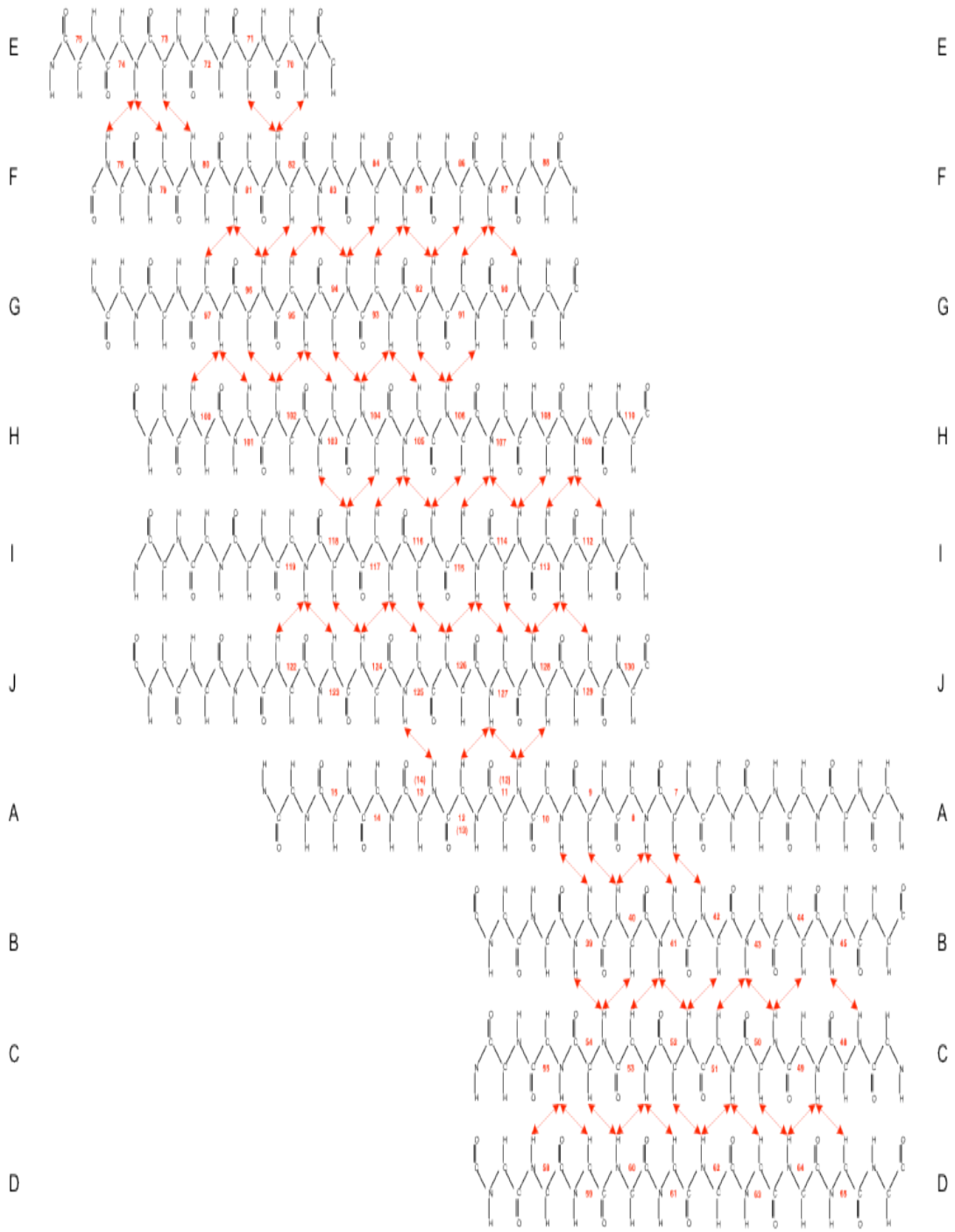

Figure IV.6. Schematic representation of holo (oleate) AFABP backbone atoms of anti parallel β-strands β_A through β_J demonstrating long-range NOE connections between residues located on different β-strands, where β-strands β_D and β_E do not interact via hydrogen bonding.

Moreover, the short and medium -range NOEs between sequential residues helped to make the sequential assignments and establish the secondary structural elements of the protein structure (**Figure IV.7**). Strong Hα(*i*)-HN(*i*+1) NOE signals between sequential residues indicate the presence of residues in a β-strand structural motif, while strong HN(*i*)-HN(*i*+1) NOE signals between sequential residues indicate residues in an alpha helical structure.

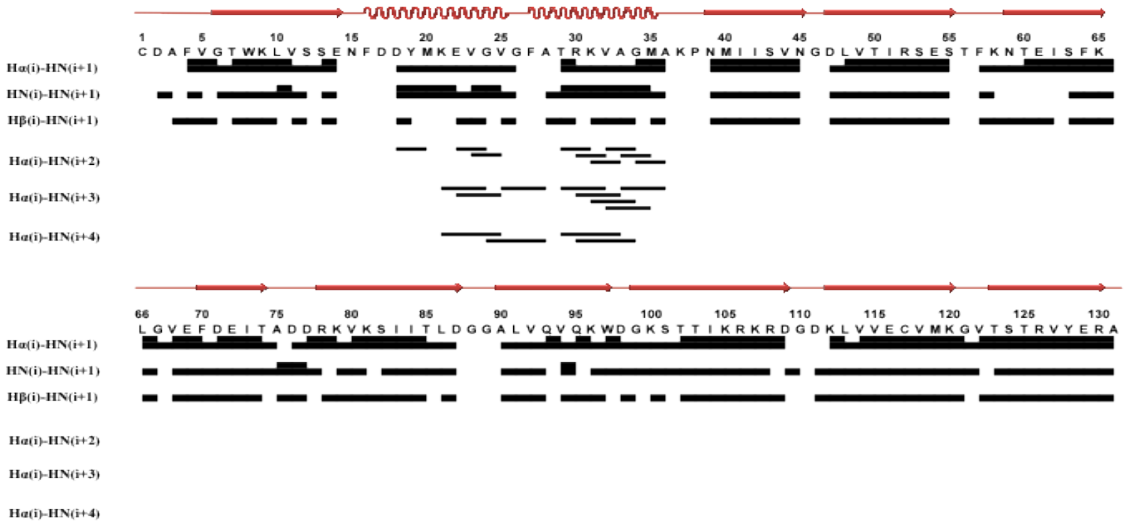

Figure IV.7. Schematic representation of short, medium and long range NOEs along the protein sequence of AFABP, demonstrating ^{1}H NMR sequential interactions for holo (oleate) AFABP. Block height represents the strength of NOE connectivity signal.

As discussed previously for apo AFABP, short, medium and long range NOE data for holo (oleate) AFABP collectively confirm the secondary structure known for FABP protein family (Marcelino *et al.* 2006) two α-helices and ten β-strands. Although Hα (*i*)-HN(*i*+1) connectivities between residues 90-101 do not show strong NOE signals, long range NOEs illustrated in **Figure IV.6** show that residues 91-97 interact with residues 81-87 on β-strand β_F on one side and residues 100-106 on β-strand β_H on the other side and

therefore exist in a β-sheet conformation.

D. Discussion

The site-specific apo and holo (oleate) assignments are necessary to study the effect of ligand binding on the protein. The human AFABP protein was 92 % assigned previously (Constantine *et al.* 1998) at 20°C and in a pH 7.5 phosphate buffer with 25 mM Pi. Although the sequence similarity between murine and human type proteins is 91.7 %, and the NMR recording conditions were similar, it was not possible to use all of the published backbone or side chain chemical shifts. The two proteins differ in eleven residues, which evidently changed the local environment of neighboring residues and therefore produced a significant disparity between human and murine AFABP spectra. By utilizing the strategies discussed previously, it was possible to assign 124 of 129 (96 %) of the expected backbone residues for the murine apo AFABP protein (**Figure IV.8**). Five residues remained unassigned despite efforts to match them up with ten unassigned resonances in the apo [^{1}H-^{15}N] HSQC spectrum due to their weak 3D [^{1}H-^{15}N] NOESY-HSQC signals and the absence of triple resonance [^{15}N-^{13}C] HNCACB and CBCA(CO)NH, HNCO and HNCACO connectivities. The five unassigned residues (N15, F27, T56, G88, G110) are located in the α helices and in the turns connecting the ten β strands, four of which were among ten unassigned residues (N15, F27, A28, K37, E54, T56, A75, G88, R108, D111) reported by Constantine *et al.* (1998).

In the [^{1}H-^{15}N] HSQC holo (oleate) AFABP spectrum, 118 (91 %) of the backbone assignments were made successfully out of the expected 129, and eleven out of

thirteen side chain resonances were assigned. Despite the observation of ten unassigned resonances in the [^{1}H-^{15}N] HSQC holo (oleate) spectrum, eleven residues remained unassigned (D2, N15, F16, D17, F27, K37, G46, T56, G88, G89, G110), excluding C1 and P38. It was impossible to correlate any of the remaining peaks with any of the eleven unassigned residues because of a lack of matching in the connectivity pathways of the double resonance [^{1}H-^{15}N] NOESY-HSQC and TOCSY-HSQC experiments, and a lack of triple resonance [^{15}N-^{13}C] experiments.

The HSQC spectra displayed 155 and 139 resonances for apo and holo (oleate) AFABP, respectively. While the apo spectrum displayed additional peaks beyond what was expected, the holo spectrum displayed fewer. The additional peaks in the apo spectrum will be addressed in Chapter V, while the missing peaks in the holo spectrum may be due to some residues exhibiting intermediate exchange, which resulted in less assignments made for the holo (oleate) protein than apo AFABP. The obtained apo and holo (oleate) assignments nevertheless, provide the necessary information for studying the effect of ligand binding on the protein.

AFABP	**Backbone assignments** (out of 129 assignments)	**Side chain assignments** (out of 14 assignments)
Apo	**124 (96 %)**	**13**
Holo (oleate)	**118 (91 %)**	**11**

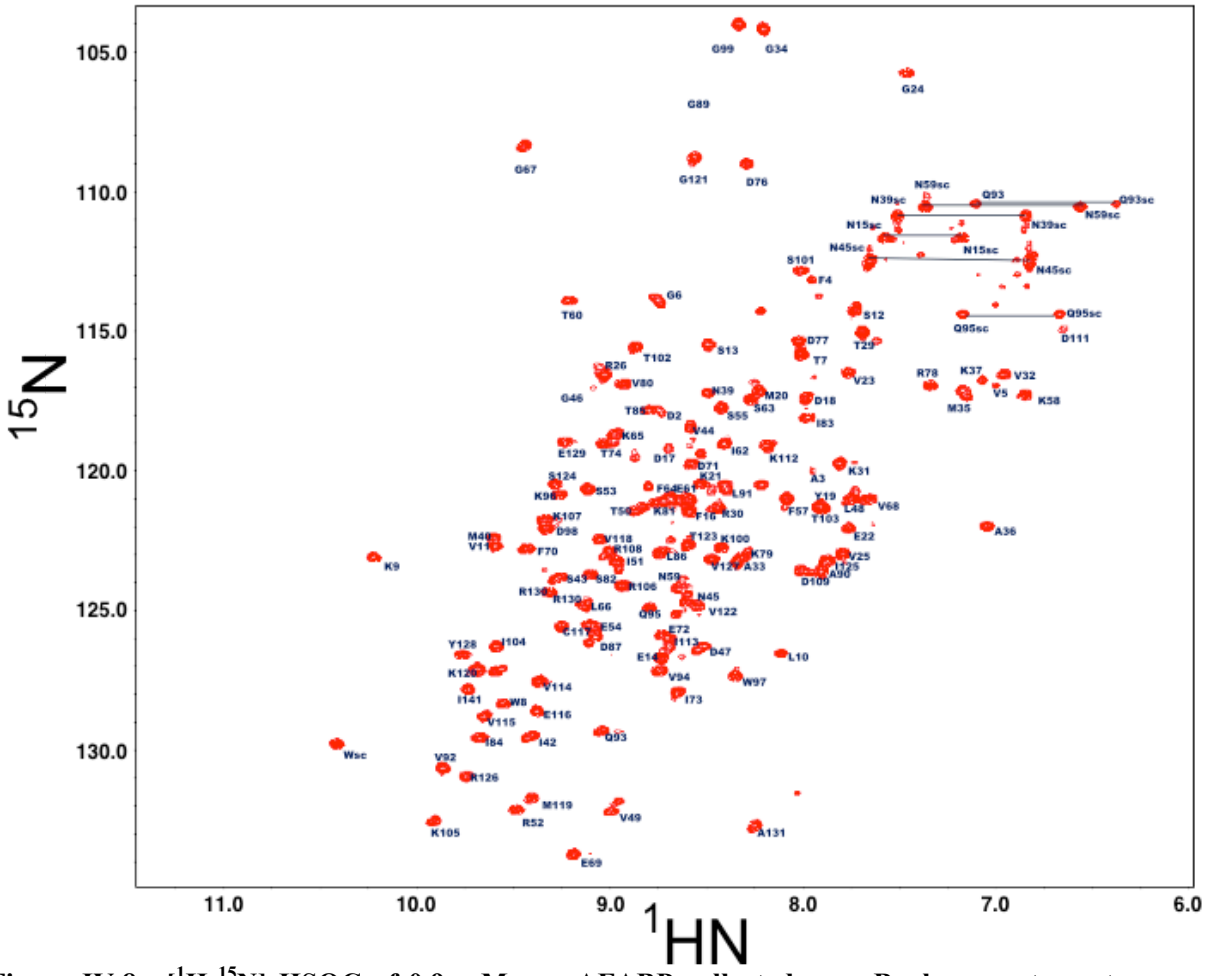

Figure IV.8. [^{1}H-^{15}N] HSQC of 0.9 mM apo AFABP collected on a Bruker spectrometer with a ^{1}H frequency of 700 MHz at 20 °C and pH 7.4.

Table IV.1 1H, 15N, and 13C chemical shifts for apo AFABP at pH 7.4 and 20 °C.

Spin	^{1}HN	^{15}N	^{13}CO	^{1}H$^{\alpha}$	^{13}C$^{\alpha}$	^{1}H$^{\beta}$	^{13}C$^{\beta}$	Other ^{1}H
C1					61.6		27.4	
D2	8.72	118.0	177.6	4.23	57.0		40.1	
A3	7.93	120.0	177.6	4.13	53.8	1.09	18.6	
F4	7.95	113.1	175.2	4.25	59.2	3.15, 2.79	40.4	
V5	7.06	116.6	176.5	3.67	64.2	2.16	32.6	
G6	8.74	113.8	171.1	4.11, 3.79	44.0			
T7	7.99	115.7	173.0	4.96	62.4	3.87	69.5	^{1}Hγ 1.12
W8	9.54	128.2	175.2	5.27	55.4	3.32, 2.98	32.1	
K9	10.22	123.0	175.7	5.44	54.5	1.88	36.1	^{1}Hγ 1.45
L10	8.11	126.4	177.0	3.41	57.1		42.1	
V11	9.58	122.6	176.1	4.47	62.2	2.08	34.1	^{1}Hγ 0.91
S12	7.73	114.2	176.0	4.66		3.88, 3.70	65.3	
S13	8.45	115.5	172.9	4.98				
E14	8.70	126.7		4.87		2.17, 1.99		
N15								
F16	8.56	121.4		4.57				
D17	8.66	119.2	177.9	4.09	58.7		41.6	
D18	7.96	117.3	179.0	4.26	57.2	2.57	39.9	
Y19	7.90	121.2	175.5	3.84	62.3	3.02	39.0	
M20	8.21	117.0	178.3	3.48	58.8		34.2	
K21	8.52	120.3	179.6	3.84	60.1	1.94	32.5	
E22	7.76	121.8	178.5	3.95	58.6	1.88	29.2	
V23	7.76	116.3	175.5	3.79	64.7	1.93	32.0	^{1}Hγ 0.59, 0.48
G24	7.45	105.7	174.5	4.30, 3.61	44.8			
V25	7.78	122.9	177.1	3.81	63.0	1.45	31.9	^{1}Hγ 0.99, 0.81
G26	9.00	116.6		4.01, 3.61				
F27								
A28	8.67	121.1	180.7	4.79		3.05		
T29	7.67	115.0	175.5	3.91	65.7		68.0	^{1}Hγ 1.11
R30	8.44	121.2	179.5	3.61	60.3		30.0	
K31	7.78	119.7	178.6	3.85		1.52		
V32	6.93	116.5	178.7	3.77		1.96		^{1}Hγ 0.94
A33	8.31	123.3	180.8	3.44		0.86		
G34	8.17	104.2	179.0	3.98, 3.86				
M35	7.12	117.3	176.2	4.48		2.17, 2.04		
A36	7.01	121.9		4.23		1.50		
K37	7.12	117.1						
P38			176.3					
N39	8.51	117.2	175.0	5.81		2.92, 2.73		
M40	9.57	122.4	174.3	5.49		1.76		
I41	9.72	127.9	176.5	5.15	61.4		41.2	
I42	9.40	129.4	175.6	5.33	60.6	2.41	38.6	^{1}Hγ 0.69
S43	9.25	123.7	171.2	4.89	56.9		66.1	
V44	8.57	118.4	174.7	4.65	60.9	1.81	35.4	^{1}Hγ 0.77
N45	8.61	124.7		4.84		2.69, 2.57		
G46	9.21	117.0	173.6	3.94, 3.56	47.3		47.4	
D47	8.51	126.2	174.1	4.46	53.6		40.7	
L48	7.74	120.9	175.7	4.46	53.8		44.2	
V49	8.98	132.0	174.2	4.22	60.9		32.0	
T50	8.86	121.4	173.8	5.31	61.1	3.72	71.5	
I51	8.95	123.2	175.1	4.68	61.3	1.72	40.1	^{1}Hγ 0.64
R52	9.48	132.0	174.4	5.28	54.2	1.97	33.7	
S53	9.10	120.6	173.8	5.43	56.8	3.89, 3.67	64.2	
E54	9.07	125.6	176.0	5.26		1.95		^{1}Hγ 2.21
S55	8.39	117.7		4.88		4.15, 3.98		

Spin	^{1}HN	^{15}N	^{13}CO	^{1}H$^{\alpha}$	^{13}C$^{\alpha}$	^{1}H$^{\beta}$	^{13}C$^{\beta}$	Other ^{1}H
T56			170.7					
F57	8.05	121.0	174.1	4.73		3.11		
L58	6.82	117.3	173.9	4.14		1.26, 1.06		
N59	8.61	124.2	175.5	5.80				
T60	9.20	113.8	173.4	4.78	59.9		72.3	
E61	8.58	121.0	174.5	5.07	56.7		33.7	
I62	8.40	119.0	174.0	4.85	59.8		42.5	
S63	8.26	117.3	172.9	3.47	57.2		65.4	
F64	8.67	120.9	172.0	4.58	55.5		41.5	
K65	8.96	118.6	177.9	4.90	54.0		34.9	
L66	9.12	124.8	179.3	4.52	56.2		41.0	
G67	9.44	108.3	173.4	4.25, 3.42	46.2			
V68	7.65	120.9	176.4	4.39	62.1	2.25	33.1	^{1}Hγ 1.1, 0.90
E69	9.17	133.6	175.0	4.95	57.2	2.02	31.3	
F70	9.42	122.8	172.8	5.21	55.6	3.26	42.2	
D71	8.56	119.7	175.0	5.11	54.5	2.65	42.3	
E72	8.73	125.8	173.9	4.59	54.7	2.65, 1.78	33.1	
I73	8.64	127.9	177.9	4.48	59.7	1.62	37.6	
T74	9.02	119.0	177.0		61.9		70.6	
A75	9.32	123.4	176.5	3.81	55.0	1.42, 1.41	18.5	
D76	8.27	109.0	172.8	4.54	52.7	2.91, 2.10	39.8	
D77	8.02	115.2	176.3	4.08	56.2	2.70	38.7	
R78	7.33	116.8	175.3	4.13	56.1	1.35	31.5	
K79	8.29	123.0	176.1	4.84	55.9		31.8	^{1}Hε 2.95577
V80	8.92	116.8	175.4	5.15	57.9	2.01	34.9	^{1}Hγ 0.53, 0.25
K81	8.75	121.0	176.8	4.98	54.2	1.82, 1.63	34.3	
S82	9.10	123.6	171.7	5.73	57.3	2.87, 2.18	68.3	
I83	7.97	118.0	173.6		61.3		42.0	
I84	9.67	129.5	174.9	5.29	60.2		38.1	
T85	8.79	117.7	172.5	4.65	59.3		38.1	
L86	8.72	122.8	176.2	5.23	53.9	1.83, 1.23	43.9	
D87	9.08	126.0	177.3	4.92	54.2	2.64, 2.44	43.9	
G88								
G89	8.61	106.7	173.0	4.21			45.1	
A90	7.89	123.5	176.2	5.08	50.5		21.0	
L91	8.39	120.5	177.3	4.92	53.5		43.3	
V92	9.85	130.6	172.8	4.18	63.4		32.7	
Q93	9.03	129.3	174.0	5.39	52.9		30.8	
V94	8.73	127.1	176.4	4.95	61.1		34.0	
Q95	8.78	124.8	175.9	5.15	54.0		34.0	
K96	9.26	120.8	176.7	5.56	55.7	1.77	36.3	
W97	8.34	127.2	172.5	4.88	57.7	3.21, 2.78	32.6	
D98	9.31	122.0	175.2	4.23	55.3	2.75, 2.27	41.1	
G99	8.32	103.9	174.1	3.92	46.0			
K100	8.41	122.6	175.6	4.26	54.7	0.80, 0.23	34.1	
S101	8.00	112.7	172.4	5.82	57.3	3.66	66.2	
T102	8.86	115.6	170.8	5.16	59.4		71.0	
T103	7.90	121.4	173.0	5.55			71.2	
I104	9.56	126.3	175.9	4.91	60.7		41.9	
K105	9.91	132.5	174.5	5.16	55.1		35.2	
R106	8.92	124.1	173.4	5.24	54.4		31.8	
L107	9.35	121.7	174.6	5.07			36.7	
R108	8.99	122.8	175.9	4.69	53.3		28.8	
K109	7.96	123.6	175.8	4.70	53.2		42.8	
G110								
D111	6.62	115.0	175.6					
K112	8.16	119.1	175.5	5.12				
L113	8.67	126.1	174.2	4.63	54.7	0.73, -0.44	43.7	
V114	9.36	127.4	174.4	4.66	61.8	1.86	34.1	^{1}Hγ 1.00, 0.90
V115	9.64	128.9	175.2	5.07	60.7	2.21	33.7	^{1}Hγ 0.79

Spin	^{1}HN	^{15}N	^{13}CO	^{1}H$^{\alpha}$	^{13}C$^{\alpha}$	^{1}H$^{\beta}$	^{13}C$^{\beta}$	Other ^{1}H
E116	**9.37**	**128.5**	**175.7**	**5.34**	**54.2**	**2.06, 1.92**	**33.4**	
C117	**9.25**	**125.6**	**173.5**	**5.19**	**56.3**	**1.86, 1.77**	**27.7**	
V118	**9.04**	**122.4**	**177.5**	**5.31**	**61.1**	**1.99**	**35.1**	**^{1}Hγ 0.91**
M119	**9.40**	**131.6**	**173.4**	**5.07**	**55.4**		**35.0**	
K120	**9.68**	**127.0**	**176.2**	**3.78**	**58.1**	**2.01**	**30.4**	
G121	**8.56**	**108.9**	**174.1**	**3.99, 3.88**	**45.7**			
V122	**8.54**	**124.7**	**174.7**	**4.18**	**62.8**	**2.29**	**33.2**	**^{1}Hγ 0.97, 0.88**
T123	**8.58**	**122.6**	**174.5**	**5.36**	**62.8**	**3.92**	**33.2**	
S124	**9.28**	**120.6**	**173.8**	**5.19**	**55.7**	**3.21**	**65.6**	
T125	**7.87**	**123.2**	**174.2**	**5.28**	**62.2**	**3.83**	**70.3**	**^{1}Hγ 1.06**
R126	**9.74**	**130.8**	**173.6**	**5.03**	**54.8**	**1.71**	**34.1**	
V127	**8.47**	**123.2**	**174.1**	**4.73**	**62.3**	**2.05**	**33.5**	
Y128	**9.75**	**126.5**	**175.2**	**5.56**	**56.4**	**3.15**	**42.1**	
E129	**9.22**	**118.9**	**175.8**	**5.34**	**53.7**	**2.30, 2.08**	**34.1**	
R130	**9.30**	**124.3**	**176.3**	**3.80**	**53.7**	**1.53**	**34.1**	
A131	**8.24**	**132.7**	**182.2**	**4.02**	**53.4**	**1.17**		

Table IV.2 1H, 15N, and 13C chemical shifts for holo (oleate) AFABP at pH 7.4 and 20 °C.

Spin	^{1}HN	^{15}N	^{1}Hα
C1			
D2			
A3	7.94	120.0	
F4	7.94	113.2	4.25
V5	7.03	116.4	3.68
G6	8.74	113.8	4.15
T7	7.98	115.5	5.02
W8	9.59	128.4	5.33
K9	10.32	122.7	5.58
L10	7.68	126.2	3.25
V11	9.57	122.4	4.48
S12	7.71	114.1	4.67
S13	8.46	115.5	4.89
E14	8.68	127.5	4.89
N15			
F16			
D17			
D18	7.97	117.3	4.28
Y19	7.68	121.0	
M20	8.26	117.0	5.48
K21	8.52	119.8	3.81
E22	7.74	121.9	3.93
V23	7.67	116.6	3.75
G24	7.41	105.2	4.33, 3.58
V25	7.74	123.3	3.76
G26	9.07	116.9	4.05
F27			
A28	8.72	121.0	4.82
T29	7.59	115.3	3.94
R30	8.47	121.3	3.62
K31	7.70	118.7	3.82
V32	6.82	115.5	3.83
A33	8.57	123.3	3.46
G34	8.17	102.9	4.02, 3.93
M35	7.04	116.0	4.54
A36	7.01	121.8	
K37			
P38			
N39	8.66	116.3	6.03
M40	9.80	124.0	5.59
I41	9.77	128.4	5.20
I42	9.37	129.4	5.33
S43	9.21	123.7	4.89
V44	8.56	118.5	4.67
N45	8.58	124.6	4.86
G46			
D47	8.49	126.2	4.47
L48	7.73	120.9	4.48
V49	8.97	132.1	4.23
T50	8.85	121.4	5.33
I51	8.91	123.1	4.64
R52	9.46	132.3	5.33
S53	9.13	121.4	5.46
E54	9.24	125.0	5.36
S55	8.35	116.3	4.92
T56			
F57	7.58	120.5	4.57
L58	6.87	116.8	4.10
N59	8.49	122.0	6.02
T60	9.34	114.3	4.83
E61	8.54	121.0	5.13
I62	8.38	119.0	4.86
S63	8.28	117.3	5.73
F64	8.64	120.9	4.56
K65	8.94	118.7	4.91
L66	9.12	124.8	4.55
G67	9.44	108.3	4.25, 3.42
V68	7.63	121.0	4.40
E69	9.17	133.6	4.95
F70	9.46	122.7	5.20
D71	8.56	119.7	5.10
E72	8.70	126.3	4.71
I73	8.68	128.0	5.10
T74	9.07	119.2	4.29
A75	9.53	122.6	
D76	8.95	110.4	4.61
D77	8.10	115.5	4.09
R78	7.37	117.0	4.20
K79	8.23	122.4	4.85
V80	8.94	117.4	5.12
K81	8.60	120.8	4.98
S82	9.05	123.6	5.71
I83	8.05	118.3	4.23
I84	9.66	129.5	5.34
T85	8.67	117.6	4.66
L86	8.73	122.9	5.26
D87	9.04	126.0	
G88			
G89			
A90	7.88	123.6	5.09
L91	8.42	120.7	4.90
V92	9.85	131.0	4.13
Q93	8.96	129.4	5.33
V94	8.83	127.6	4.94
Q95	8.80	125.6	5.25
K96	9.21	120.8	5.56
W97	8.32	127.2	4.88
D98	9.31	122.1	4.24
G99	8.31	103.9	3.92
K100	8.41	122.7	4.25
S101	8.00	112.8	5.83
T102	8.86	116.0	5.19
T103	7.95	121.6	5.57
I104	9.62	126.8	4.91
K105	9.94	132.6	5.13
R106	8.93	124.3	5.19
L107	9.35	121.9	5.08
R108	8.99	123.0	4.72
K109	8.00	123.6	4.72
G110			
D111	6.62	114.9	
K112	8.17	119.2	5.10
L113	8.72	126.4	4.61
V114	9.34	127.4	4.63
V115	9.64	128.9	5.05
E116	9.39	128.0	5.32
C117	9.24	126.1	5.02
V118	9.07	122.7	5.35
M119	9.37	131.6	5.06
K120	9.70	127.1	3.77
G121	8.55	109.0	4.01
V122	8.53	124.8	4.18
T123	8.55	122.3	5.36
S124	9.26	120.8	5.21
T125	7.76	122.8	5.19
R126	9.74	131.2	4.99
V127	8.54	123.5	4.67
Y128	9.74	127.5	5.48
E129	9.18	118.9	5.35
R130	9.33	124.3	3.77
A131	8.24	132.6	4.02

V. Binding Interactions of AFABP with Different Ligands

A. Introduction

AFABP, as inferred from its abbreviation, exhibits a binding preference for fatty acids, specifically long-chain fatty acids (LCFA) that bind AFABP with high affinity. The AFABP protein binds and sequesters within its cavity a single hydrophobic ligand. Affinity for fatty acids is related to chain length, with 16–20 carbon analogs having the lowest dissociation constants (Richieri *et al.,* 1994) and therefore the highest affinities. It has been suggested that depending on the type of ligand that binds inside the protein cavity (activating or nonactivating ligand), the protein is either translocated from the nucleus or remains localized in the cytosol (Gillilan *et al.* 2007). Based on their data, binding of linoleate and troglitazone (a member of the synthetic thiazolidinedione antidiabetic family) are both activating ligands and allow the protein to localize mainly in the nucleus where it is putatively involved in the activation of the PPARγ signal transduction pathway. By contrast, oleate binding promotes localization of AFABP in the cytosol where it cannot activate PPARγ. The Gillilan group attributes this distinction to contrasting modes of AFABP dimerization in solution and solid state: activating ligands are thought to be associated with formation of a homodimer that facilitates translocation of the protein to the nucleus, while inactivating ligand binding stimulates formation of a different homodimer that hides the nuclear localization signal (Gillilan *et al.* 2007). As detailed in a prior chapter, neither our size exclusion chromatography and static light scattering measurements provided supporting evidence for dimer formation.

While oleate and linoleate are both 18-carbon fatty acids, linoleate has an extra double bond, but based on Gillilan's reports they have differing effects on the function of

AFABP. The X-ray crystal structures of holo (oleate and linoleate) AFABP show that linoleate is present in a U-shaped conformation (Gillilan *et al.* 2007) while oleate is present in a slightly kinked position inside the protein cavity with the carboxylate group inside the cavity and the other end protruding out (Xu *et al.,* 1992). The crystal structure of holo (TDZ) AFABP shows the ligand in a similar position to other FA ligands bound in the protein cavity. Investigating protein-ligand interaction by NMR allows for study of these interactions in solution and at near-physiological condition by contrast to a crystal for which formation depends on buffer constituents and where every atom is locked in a particular state and loses the normal flexibility it would have in solution. Studying the interactions between these ligands in solution by NMR allows for identifyication of similar and dissimilar aspects of each ligand binding with AFABP.

Since the resonance frequencies of the nuclei in each protein residue are exquisitely sensitive to the local environment, NMR is an ideal technique to study protein-protein and protein-ligand interaction in solution. With the NMR backbone resonance assignments of apo AFABP in hand (Chapter IV), ligands can be gradually titrated into the protein and the chemical shift perturbation of each residue can be monitored. Residues that are involved in the interaction will encounter a change in local environment as a result of direct interaction or a conformational change in the protein (Zuiderweg 2002). These changes in local environment in the affected residues can be apparent as a chemical shift perturbation and/or linewidth changes. Composite chemical shift perturbations are then calculated by taking into consideration the changes in proton and nitrogen shifts of each residue and used to highlight the most affected residues upon

ligand addition, establishing the protein-ligand interaction surface or revealing global conformational changes. Studying the protein in solution and at physiological salt concentrations provide an advantage to study protein – ligand interaction as compared to crystallography techniques.

The exchange rate between free (apo) and bound protein states exhibits a fundamental interplay with the observation of chemical shift perturbations during the titrations. Usually the exchange rate relates to ligand affinity, but in all cases the dissociation constant is a collective net ratio between k_1 (association reaction rate) and k_{-1} (dissociation reaction rate) of the interaction between the protein (P) and ligand (L)

$$P + L \underset{k_{-1}}{\overset{k_1}{\rightleftharpoons}} PL \qquad \textbf{Equation V.1}$$

The exchange rate k_{ex} can be defined by (**Equation V.2**) describing the relationship between the association and dissiociation reaction rates, the ligand concentration and the exchange rate

$$k_{ex} = k_1[L] + k_{-1} \qquad \textbf{Equation V.2}$$

For instance, fast chemical exchange regime suggests a weak binding while slow chemical exchange regime suggests a strong binding. Fast chemical exchange between apo and holo protein species results in averaging of their corresponding resonances into one set of peaks corresponding to a weighted average chemical shift of both species and

occurs when the rate of exchange is much larger than the observed chemical shift perturbation.

$$k_{ex} >> |\Delta\nu| \qquad \textbf{Equation V.3}$$

$\Delta\nu$ is the difference between ν_p and ν_{PL}, where ν_P and ν_{PL} are the resonance frequencies of nuclear spin in the unbound and bound proteins, respectively (Cavanagh *et al.* 2007).

Slow exchange between apo and holo protein species results in the existence of two sets of resonances corresponding to both the bound and free states, observed when the chemical shift perturbation is much larger than the rate of exchange (Equation V.4).

$$k_{ex} \sim |\Delta\nu| \qquad \textbf{Equation V.4}$$

Intermediate exchange is characterized by disappearance of resonances during the interaction (Zuiderweg 2002) and indicates that the rate of exchange is comparable to the magnitude of the chemical shift perturbation (Equation V.5).

$$k_{ex} << |\Delta\nu| \qquad \textbf{Equation V.5}$$

The NMR titration experiment is quite valuable as it enables us to identify the key residues that are involved in protein-ligand interaction. By mapping these changes on the protein 3D structure, it is possible to define the binding site for each of the three AFABP ligands offering the potential to identify the similarities and the differences in each interaction that bring about the contrasting functional behavior of AFABP.

B. AFABP Binding Interactions with Oleic Acid

1. Materials and Methods

(a) Preparation of NMR Sample

Unlabeled sodium oleate was obtained from Sigma (St. Louis, MO). Uniformly ^{15}N labeled murine adipose fatty acid binding (AFABP) samples were obtained as described previously in Chapter III.

(b) ^{1}H-^{15}N HSQC NMR Experiments

Aliquots from an 8.2 mM oleate stock solution were added successively to 550 µL of 0.23 mM apo AFABP in phosphate buffer (pH 7.4 with 10 mM Pi/150 mM KCl and 0.02 % NaN_3) in a 5 mm NMR tube. The protein concentration was calculated from optical density measurements at 280 nm using a UV1 spectrophotometer (ThermoFisher Scientific, Pittsburgh, PA) and an extinction coefficient 1.55 x 10^4 $M^{-1}cm^{-1}$ (Matarese and Bernlohr 1988). Aliquots of oleate were added in 0.4 molar equivalent steps until the protein-to-oleate ratio reached 1:2.4. Three more steps were added thereafter to reach 1:3.2, 1:4, and 1:6.0.

^{15}N-edited Heteronuclear Single-Quantum Coherence (HSQC) spectra were recorded at each titration step on a Varian 600 MHz VNMRS Spectrometer (Agilent Technologies, Santa Clara, CA) with a conventional 5 mm inverse detection triple resonance (HCN) probe. Experiments were measured with 32 transients, and with 128

and 1024 complex points in the indirect (t1) and direct (t2) dimensions, respectively. The sweepwidths of the direct ^{1}H and indirect ^{15}N dimensions were 15 ppm and 36 ppm, respectively. The water signal (4.821 ppm) was set on resonance in the proton dimension, and the ^{15}N carrier was set in the middle of the amide region (119 ppm). NMR spectra were processed using NMRPipe (Delaglio *et al.* 1995) and were analyzed using NMRViewJ (Johnson 2004) software.

Composite chemical shift perturbations (ΔPPM) for each backbone cross-peak were calculated with the formula $[(\Delta N/6.5)^2 + \Delta H^2]^{1/2}$ (Mulder *et al.,* 1999) where ΔN and ΔH denote the chemical shift differences of ^{15}N and ^{1}H in ppm, respectively.

(c) Molecular Structures

Coordinates for apo and holo mAFABP were obtained from Protein Data Bank (PDB) entries 1LIB and 1LID, respectively (Xu *et al.* 1993), and for apo hBFABP (PDB) entry 1JJX (Rademacher *et al.,* 2002) and displayed graphically with PyMOL software (The PyMOL Molecular Graphics System) (DeLano and Lam 2005), and with LigPlot software (Wallace *et al.,* 1995). Figures were prepared with GIMP software (http://www.gimp.org/), and plots were prepared with Grace software (http://plasma-gate.weizmann.ac.il/Grace/).

2. Results

The chemical shift perturbation method was used to analyze changes in the magnetic and chemical environment of the protein residues at each titration point. Throughout the titration, each 2D spectrum showed single HN resonances from residues of either the apo or holo protein (but not both) but displayed no gradual shifts in peak positions. This is illustrated in **Figure V.1** which shows the evolution of the ^{1}H-^{15}N HSQC of residue S53 as an example, because its apo and holo crosspeaks are distinct and do not overlap on the spectrum. A possible explanation is discussed below.

Many apo HN peaks disappeared below the noise level when the first 0.4 equivalents of oleate were added, whereas holo peaks continued to grow and reached a plateau at 0.8 - 1.2 equivalents, after which a gradual decline in intensity was observed. The decrease in the intensity was observed for the HN cross-peaks was small in the first experiments, then increased for the last few points of the titration. This observation may be attributed to both the excessive precipitation, and to a dilution factor. We calculated the total volume of ligand stock solution that was added to total protein through the titration steps to be 91.3 µL. The sample volume at the end of the titration was 641.4 µL corresponding to a 14.2 % dilution factor. Even after correcting the intensities in the last point with the calculated dilution factor, the peak intensities were still much lower than those in apo spectrum. Therefore this drop in intensity could be attributed to the precipitation that was visible through the titration; it was small at first then increased in the last points, probably in relation to the quantity of ligand added.

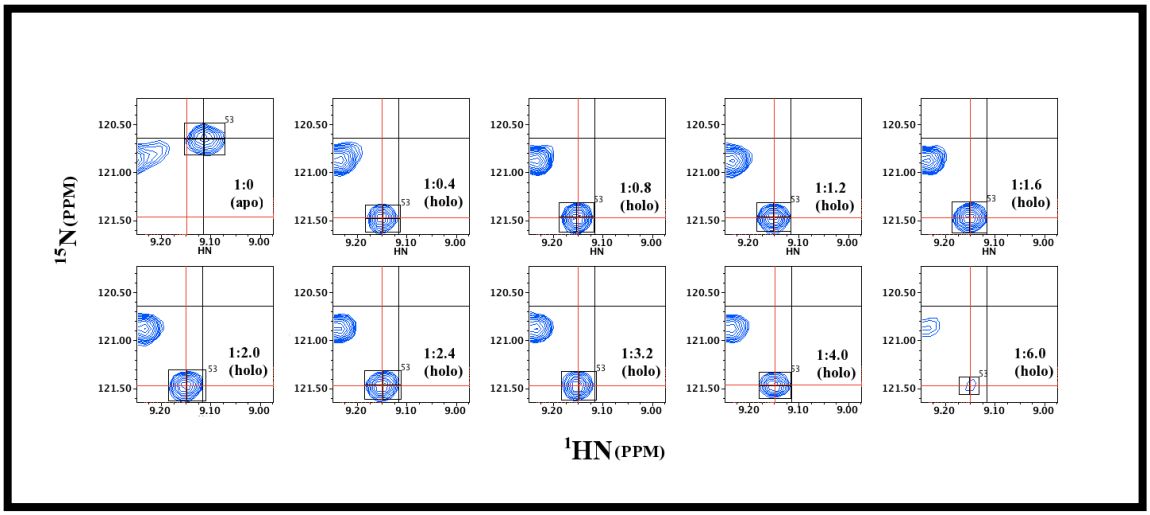

Figure V.1. Expanded regions of ^{1}H ^{15}N HSQC contour plots for residue S53 in AFABP upon titration with oleate. The apo peak is centered at the black cursor, and holo peaks are centered at the red cursor. The plots show 10 titration points (1:0, 0.4, 0.8, 1.2, 1.6, 2.0, 2.4, 3.2, 4.0, and 6.0). The intensity of the last point shows a dramatic decrease (probably due to precipitation).

As noted in Chapter IV, each one of the apo and holo spectra shows a well-folded protein, and an overlay of the two spectra shows that some of the HN cross-peaks overlap while others show spectral deviations (**Figure V.2.a**). The apo protein (96 % assigned) displayed 45 more peaks than expected from the polypeptide sequence, which we tried to match up with five unassigned residues (N15, F27, T56, G88, G110) but were unable to assign due to the weak 3D NOESY signal corresponding to these peaks. Some of these additional peaks were located at the same or close to the same position as the holo (oleate) peaks (**Figure V.2.b**). These additional peaks did not hinder the analysis of the data or the comparison of apo and holo AFABP, because in most cases it was possible to distinguish between apo and 'holo like' HN resonances in the apo spectrum based on apo and holo (oleate) AFABP assignments. These additional peaks in the apo spectrum can be categorized as follows: (i) three cross-peaks appeared at the same position as the holo protein, (ii) 19 were 'holo like' peaks (**Figure V.2.b**); (iii) eleven were elongated apo

peaks (which may be a peak or two overlapped); (iv) the remaining 12 additional peaks were scattered in the spectrum. In the holo (OLA) AFABP (91 % assigned), ten cross-peaks remained unassigned despite all effort to identify them with the 11 unassigned residues (D2, N15, F16, D17, F27, K37, G46, T56, G88, G89, G110) due to lack of matching in the connectivity pathways of the double resonance experiments.

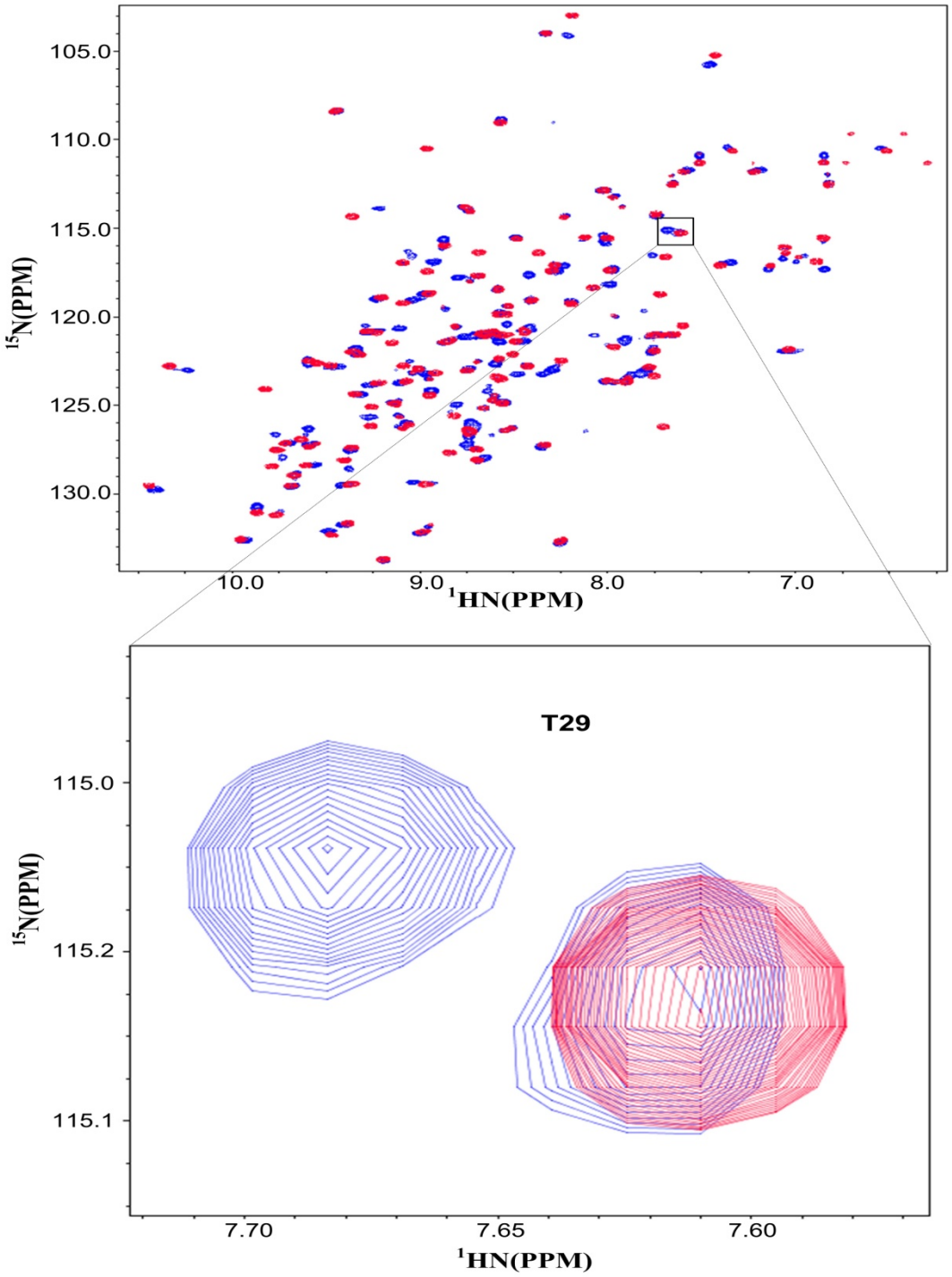

Figure V.2 Overlaid [^{1}H-^{15}N] spectra of apo and holo (oleate) AFABP with the peaks colored in blue an. d red, respectively. b: Apo and holo peaks of residue T29 in blue and red respectively, showing an additional 'holo like' peak in the apo spectrum colored in blue but located close to the holo position. Apo and holo (oleate) aFABP concentration was 0.23 mM and the protein to ligand molar ratio was 1:2.0 in the latter.

The composite chemical shift perturbations (ΔPPM) between apo and holo states are plotted and presented in **Figure V.3**. Chemical shift perturbations were omitted for 11 residues (residues D2, N15, F16, D17, F27, K37, G46, T56, G88, G89, and G110), as they remain unassigned either in apo, and/or holo states due to lack of matching of connectivity pathways in 3D experiments, as described in Chapter IV. These residues are given a negative value of -0.02.

A red dashed line is drawn across the chart at 0.18 ppm to delineate residues with perturbations greater than one standard deviation (0.102) above the average (0.078) (significant perturbations), while a green one is drawn at 0.078 ppm to differentiate between residues with moderate perturbations whose values are greater than the average, but less than standard deviation plus the average, and those with subtle perturbations less than average. Eleven residues have significant chemical shift perturbations that lie above one standard deviation plus the average (L10, Y19, A33, M35, N39, M40, S55, F57, N59, A75, and D76). Residues D76, F57, and L10 display the highest deviation: 0.71, 0.5 and 0.42 ppm, respectively, whereas perturbations for the other eight residues lie in the range of 0.2 - 0.35 ppm.

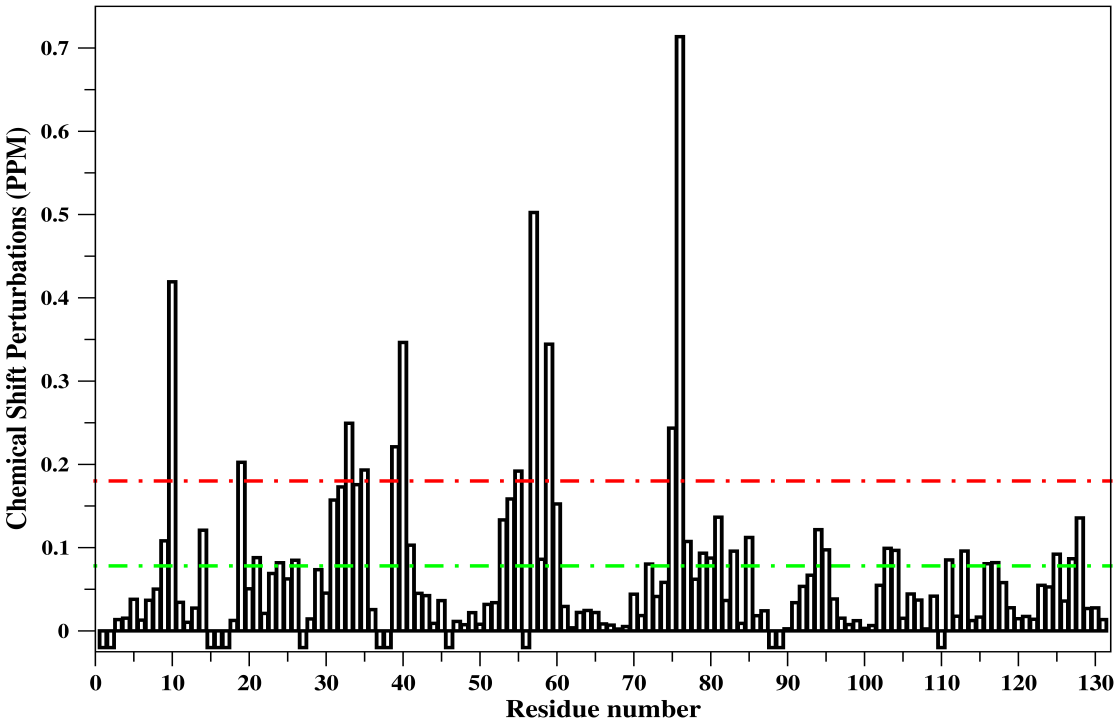

Figure V.3. Composite ^{1}H ^{15}N chemical shift perturbations plotted along the protein sequence for AFABP. The red dashed line is set at one standard deviation above the average chemical shift perturbation, highlighting the residues with the largest (significant) perturbation, while the green dashed line is set at the average chemical shift perturbation of 0.078 ppm, differentiating between residues with moderate (greater than average ppm, and less than standard deviation above the average) ppm, and residues with subtle perturbations (less than average) ppm. Negative values indicate residues that are unassigned in one or both protein forms.

It is notable that the magnitude of perturbation in the latter 40 % of protein sequence is modest **(Figure V.3)**. No significant perturbations were observed for residues located beyond D76 in the AFABP protein sequence (residues 88, 89, 110 are unassigned). By mapping the chemical shift perturbation as well as the unassigned residues onto the crystal structure of holo AFABP **(Figure V.4),** it can be seen that most of the changes occur in or near the segments between secondary structure elements, particularly between β_A and α_I, α_{II}-β_B loops, and β_C-β_D, β_E-β_F turns. The rear side of the

β-barrel, (β-strands β_H through β_J) displays smaller perturbations in magnitude when compared with perturbations in the front side of the β-barrel (β-strands β_A through β_G).

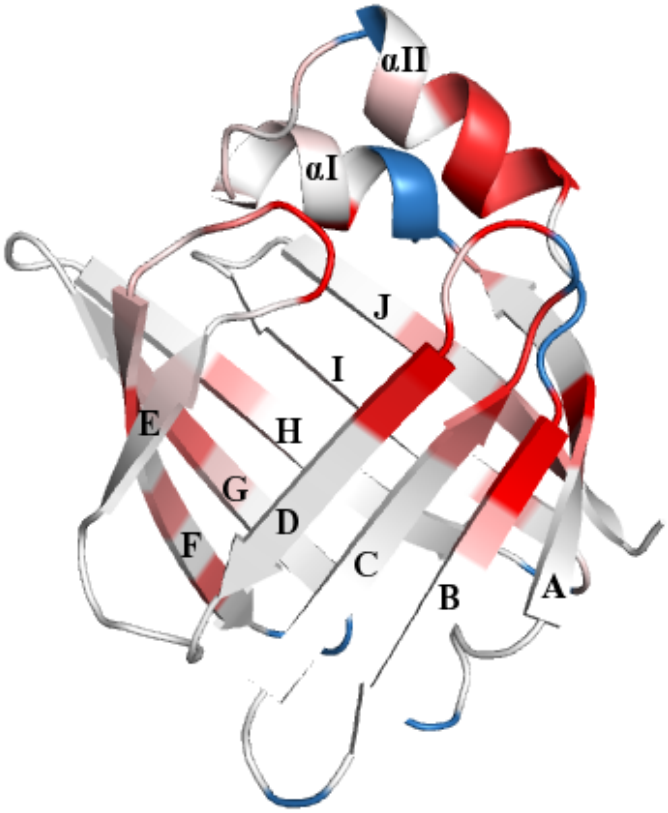

Figure V.4. Chemical shift perturbation mapping. The chemical shift perturbations are mapped onto the x-ray structure of holo AFABP (PDB: 1LID, Xu *et al.* 1993). The protein residues are colored based on a color gradient spanning from white to red to represent an increase in chemical shift perturbation, while unassigned residues are colored blue. Ligand is not shown. The 3D structure is labeled to demonstrate β-strands (A-J) and helices αI and αII.

3. Discussion

Titration of oleate into AFABP was used to investigate the binding mechanism and location of the ligand with respect to the protein. Studying the binding by NMR rather than by X-ray crystallography allows the protein to be in its native environment near physiological conditions. Although the protein may exist in different concentration and is present among other biomolecules, performing these experiments on the protein in solution and at physiological salt concentration (150 mM KCl), provides a medium similar to the one where the protein exerts its function *in vivo*.

The apo spectrum displayed a greater number of crosspeaks than the number of residues in the protein. Those crosspeaks decreased in number upon addition of oleate to the protein but were not assigned to holo protein residues. The chemical shift perturbation method was used in order to identify residues that showed a significant perturbation in their magnetic environment as a result of the binding. Spectral deviations of these residues due to ligand binding were studied and analyzed since these perturbations gave insight about the binding site. Upon addition of the ligand to the protein, eleven residues are perturbed more than one standard deviation above the average. Those residues comprised a contiguous area and are discussed in detail below.

(a) Extra Peaks in the Apo AFABP Spectrum

As noted above, the apo spectrum displays 45 additional weak HN resonances, some of which coincide with the resonances of the holo state of particular residues. This phenomenon could have either one of two explanations: (i) the protein was not fully delipidated or (ii) some of the residues exist in multiple conformations. As mentioned in Chapter II, the delipidating agent Lipidex-1000 was used previously to remove sequestered fatty acids from the protein at 310 K for 6 h (J. Storch personal communication). They demonstrated by using ^{3}H-oleate that after a single delipidation, the counts of radioactive oleate go back to baseline counts, indicating that one delipidation was enough to obtain apo AFABP.

Nevertheless, the above-mentioned possibilities have been described previously in the literature. For instance, Marr *et al.* published a crystal structure (pdb: 2HNX, Marr *et al*. 2006) for human AFABP in 2006; although they delipidated the protein using two agents (Lipidex-1000 and Lipidex-5000), they noted that the resulting AFABP still contained a bound fatty acid. Their crystal structure showed electron density in the cavity of the protein consistent with either a palmitate or an oleate along with two citrate and one phosphate molecules. In a different case, Xu *et al*. (1993) demonstrated that Arg 126 exists in two different conformations in the crystal structure, one of which corresponds to the holo conformation although the protein is unliganded. Additionally, Lucke *et al*. used NMR to demonstrate distinct conformational states of protein residues in certain regions of HFABP (Ruterjans *et al.,* 2001), and moreover, He observed several doubled apo LFABP NMR resonances (He, 2000; PhD thesis).

Attempts were made to identify the additional peaks of the ^{15}N HSQC by analyzing their corresponding strips in the ^{15}N-NOESY-HSQC, and ^{15}N-TOCSY-HSQC data. Although the protein concentration was a reasonable value of 700 μM, the 3D NOESY strips of the corresponding additional HSQC peaks either did not show any structural information or were too congested with information. It was therefore not possible to unambiguously connect to previously assigned residues and identify the amino acid type to which they belong. In order to investigate whether the additional peaks belong to a partially undelipidated population of the protein bound to a lipid that was sequestered by the protein *in vivo* during protein expression in *E. coli*, we carried out a second delipidation. By comparing the ^{15}N HSQC between the second and first protein delipidation, the extra peaks were found to decrease by 75 % in number compared with the first delipidation. This decrease in the number of peaks is not attributed to low protein concentration since AFABP concentration at this stage was high enough (200 μM) to give a decent intensity for the peaks. In light of the prior reports and our own procedures, a possible explanation for the extra HSQC peaks involves protein residues existing in multiple conformations in solution as reported by Xu *et al.* (1993) in the crystalline form. Nevertheless it was not possible to rule out incomplete delipidation of AFABP since radioactive oleate was not used in the delipidation process. It is possible that a proportion of AFABP was still bound to endogenous lipids and therefore in a holo-like state when the titration was performed, and consequently shows extra peaks in the apo spectrum.

(b) Titration Analysis

1) Exchange Rate and Ligand Stoichiometry

By observing the HSQC spectra of the titration points, we noted that the intensities of the holo HN signals at 0.8 equivalent showed an increase in magnitude compared with those of 0.4 equivalent. We did not observe two sets of apo and holo resonances that co-exist in one spectrum after the addition of the ligand at the first few points of the titration, which would indicate slow exchange on the NMR time scale, nor did we observe HN resonances shift after 0.4, or 0.8 or more equivalents of ligand, which would indicate fast exchange due to signal averaging between apo and holo resonances. Thus, our observations did not fit the expectations of either exchange regime. The fact that we saw evidence for neither fast, intermediate or slow exchange mechanisms indicates that we probably underestimated our ligand concentration or overestimated our protein concentration, and that the protein may be close to saturation with oleate at our first titration point. However, our experiments nevertheless reveal the structural differences between apo and holo states of the protein, that is the location and the effect of ligand binding on AFABP under near - physiological conditions in solution.

2) Mapping the Binding Site

The chemical shift perturbation method and mapping allowed us to highlight the residues that are affected by ligand binding (**Figure V.5**). Eleven residues (L10, Y19, A33, M35, N39, M40, S55, F57, N59, A75, and D76) have perturbation values greater than one standard deviation above the average (0.18 ppm). Together the eleven highly perturbed residues constitute the binding site, which can be described as a contiguous localized area, specifically the loops and turns connecting β_A and α_I, α_{II}-β_B, β_C-β_D, and

β_E-β_F. Part of this region coincides with the portal region, which involves helix αII (27-35) and β-turns between β-strands β_C-β_D (55-58), and β_E-β_F (74-78) (Xu *et al.* 1993; Reese-Wagoner *et al.* 1999). While AFABP does not go through a global conformational change upon ligand binding, the portal region is thought to act as a pathway to facilitate ligand binding, exit and entry (Ory *et al.,* 1995).

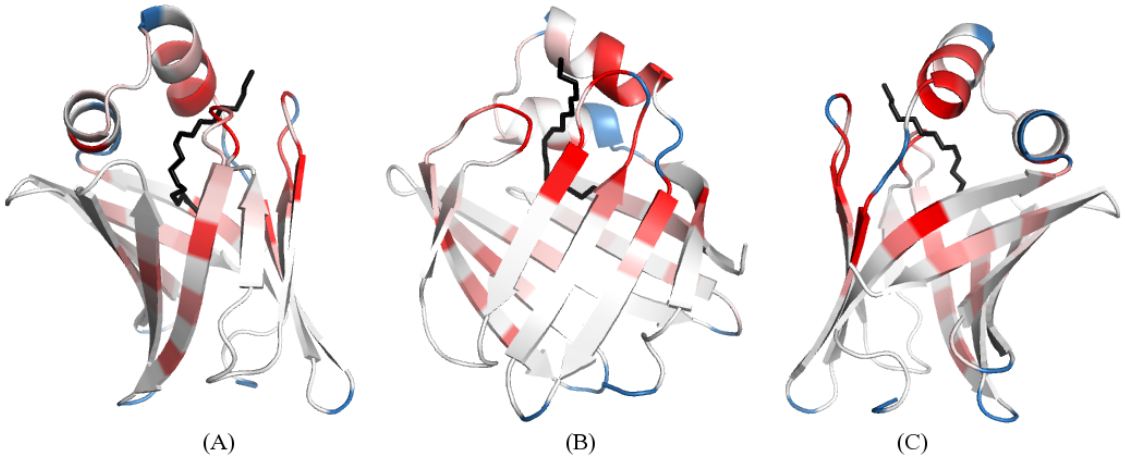

Figure V.5. Visual representation of the chemical shift perturbation plot. The chemical shift perturbations were mapped onto the x-ray structure of holo AFABP in complex with oleate (PDB: 1LID, Xu *et al.* 1993). The protein residues are colored based on a color gradient spanning from white to red colors to represent an increase in chemical shift perturbation, while unassigned residues are colored blue. Alternate views of AFABP-oleate complex (B), and (C) are rotated by 90°, and 180° about the Y-axis relative to (A) to facilitate viewing the positioning of the ligand inside the protein cavity. Ligand is shown in black.

The NMR results may be compared with the oleate - liganded crystal structure (Xu *et al.* 1993). Based on the crystal structure of AFABP (pdb: 1LID, Xu *et al.* 1993), at least one atom of 18 residues (F16, Y19, M20, V25, T29, V32, A33, M40, F57, K58, A75, D76, R78, I104, R126, Y128, V115, C117) lies in close proximity (within 4.5 Å) to the ligand. Since X-ray distances often reflect distances from side chains or center of the electron density of the residues rather than backbone, and since the chemical shift

perturbation method depends on changes in the chemical environment at the backbone of the residues, distances between the amide nitrogen of these 18 residues and the closest carbon atom in the ligand in the crystal structure were measured using PyMOL software (Table V.1) to compare proximity to the ligand with extent of chemical shift perturbation by NMR.

Table V.1 Amide nitrogen - ligand carbon distances and chemical shift perturbations in holo AFABP. (A): the extent of chemical shift perturbations where (++) indicates significant perturbation with a value greater than one standard deviation above average (0.18 ppm), (+) indicates moderate perturbation with a value greater or equal to average (0.08 ppm), and (–) indicates subtle perturbation with a value less than average. (B): residue type and name, (C): distance between amide nitrogen of the residue and the closest atom in the ligand.

(A) Extent of Perturbation by NMR	(B) Residue Type and Number	(C) X-ray Distance (Å) between N of residue & atom of the ligand	
Unassigned	F16	C11:9.1	
++	Y19	C7:9.2	
-	M20	C9:6.6	
-	V25	C9:7.1	
-	T29	C18:6.5	
+	V32	C16:6,4	
++	A33	C14:4.4	
++	M40	C1-O2:7.3	
++	F57	C16:5.9	
-	K58	C16:4.7	
++	A75	C9:5.6	C10:5.8
++	D76	C9:4.8	C10:4.7
-	R78	C9:8	
-	I104	C4:7	
-	V115	C1-O1:6.9	
-	C117	C3:7	
-	R126	C1-O1:6.5	
+	Y128	C1-O1:8	

As shown in **Table V.1**, with the exception of F16, which is unassigned in holo many of the distances are larger than the reported 4.5 Å and range between 4.4 and 9.2 Å.

This variation between the X-ray crystal structure and NMR could be due to the fact that the protein is in solution, which allows the residues additional freedom. Distances show that the amide groups of only three residues (A33, K58, and D76) lie within 5 Å of the ligand. D76 and A33 titration results show significant chemical shift perturbation values (0.71 and 0.25 ppm), while K58 does not. Although the perturbation of D76 and A33 seems logical due to their proximity to the ligand, it is unclear why K58 is not perturbed significantly. The extent of the perturbation by NMR was consistent with the distances measured from the crystal structure except for Y19, K58, and Y128.

Several of the highly perturbed residues are involved in hydrophobic interactions with the ligand. A33, F57, A75, and D76 demonstrate significant perturbation and interact hydrophobically with the ligand. A LigPlot schematic representation (Wallace *et al.* 1995) (**Figure V.6**), which gives 2D views of the protein-ligand hydrophobic and hydrogen bonding interactions based on the crystal structure (pdb: 1LID, Xu *et al*. 1993) as an input, shows which residues are involved in these interactions. The schematic representation illustrates nine residues interacting hydrophobically with oleate (M20, V32, A33, F57, K58, A75, D76, and C117) and two (R126 and Y128) forming H-bonds with the ligand. Theses eleven residues are among the 18 residues reported by Banaszak group to have at least one atom within 4.5 Å from the ligand in the crystal structure.

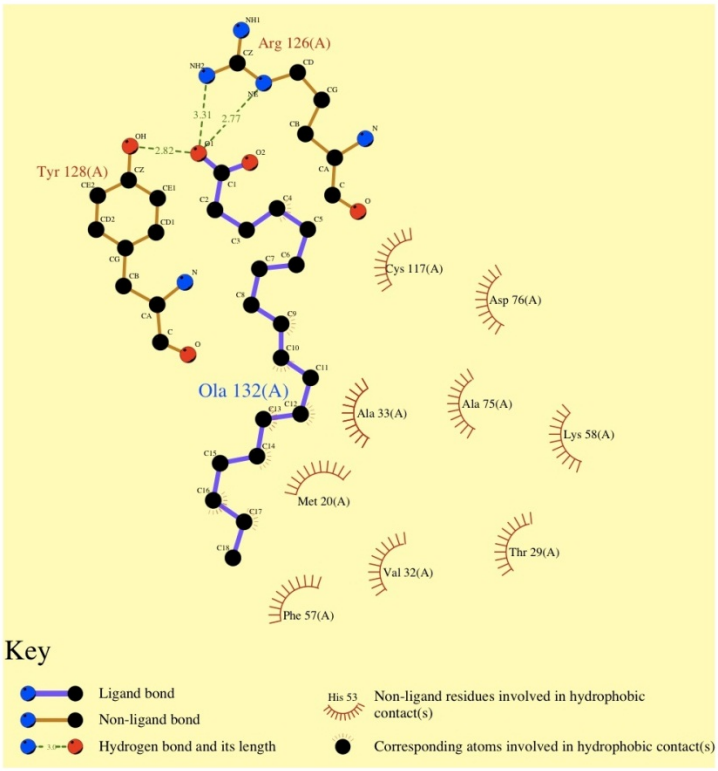

Figure V.6 Ligplot schematic diagram illustrating polar and non-polar interactions between oleate and protein residues.

While M20, V32, and K58 are not significantly perturbed, the three residues lie adjacent to at least one significantly perturbed residue. Y19, A33, M35, F57, and N59 are neighboring residues and undergo high chemical shift perturbation. V32 demonstrates a moderate deviation, while M20 and K58 show a subtle perturbation. It appears that the chemical environments of these three residues were not strongly affected by the hydrophobic interaction with the ligand.

In the crystal structure, the tail of oleate is shown to extend from between helix αII and β-turns between β_C-β_D and β_E-β_F that define the portal, while its carboxylate head is seen to extend towards residues N39 and M40 and their amide groups lie at distances

of 8.1 Å and 7.3 Å, respectively, from the carboxyl group. Therefore, observation of chemical shift perturbation in the observed pattern is in agreement with the positioning of the ligand in crystal structure of the holo complex.

The β-turn between β_C-β_D, which is part of the defined portal, is composed of residues E55 – N58. With the exception of T56, which is unassigned, and K58, which shows subtle perturbation, residues S55 and F57 along with neighboring residues S53, E54, N59, and T60 undergo either a moderate or a significant perturbation. Together these residues form a contiguous perturbed site that is in close proximity to the bound oleate.

The effect of ligand binding on residues F57 and K58 is dissimilar. While K58 shows a subtle perturbation (0.07 ppm), F57 undergoes a significant perturbation of (0.5 ppm). F57 is thought to be involved in the portal region of the protein and to be one of the residues that facilitates ligand entry and exit to the cavity by changing the side chain orientation in holo as compared with apo (**Figure V.7**) (Xu *et al.* 1993). The tail of the oleate in the holo complex occupies the space where the phenylalanine side chain was lying in the apo, and the F57 side chain is rotated to the side to accommodate the ligand tail. Upon overlaying the apo and holo structures in PyMOL, the K58 side chain remained in the same position and is unchanged except for a slight rotation. Despite lying in the portal region within 4.7 Å from the ligand and residing between two significantly perturbed residues (F57 and N59), the chemical environment of K58 is not greatly affected by the presence of the oleate in the holo form and therefore did not show

significant perturbation. It could be the fact that the protein is in solution and the side chains behave differently than in crystalline form. It is also possible that the effect of F57 side chain rotation counteracts the effect of ligand binding on K58, thus resulting in a subtle chemical shift perturbation.

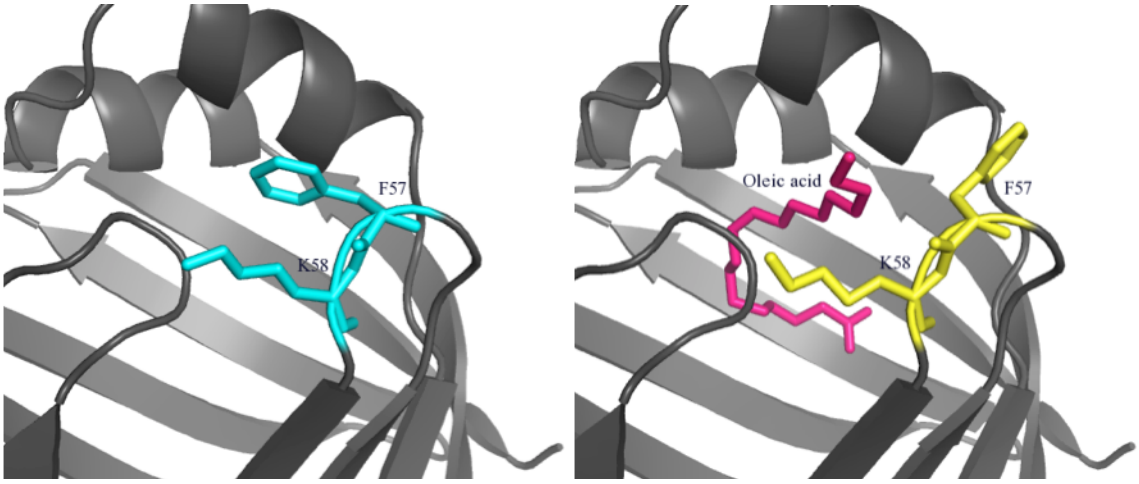

Figure V.7 Apo (cyan) and holo oleate (yellow) AFABP to compare the position of the F57 ring. Ligand is shown in pink in the holo complex.

This type of hypothesis could explain as to why a direct correlation between the proximity of the residues to the ligand and the extent of the chemical shift perturbations was not observed in some cases. For example, Y19 shows a significant perturbation although it lies 9.2 Å away from the ligand. This may be attributed to a secondary, and indirect effect on the amide groups of the significantly perturbed residues from spatially neighboring residues. M20 is adjacent to Y19 and interacts hydrophobically with oleate. Although it is itself not significantly perturbed due to this interaction, the hydrophobic interaction may exert an indirect effect on the amide nitrogen of Y19 resulting in the significantly observed perturbation.

D76 and A75 undergo a significant chemical perturbation and reside within less than 6 Å from the ligand. The amide nitrogen of residue D76 lies at 4.8 Å and 4.7 Å away from C9 and C10 of the oleate molecule, respectively, while the amide nitrogen of A75 lies 5.6 Å and 5.8 Å away from the same two carbons, respectively. $D76_N$ is closer to the ligand double bond and shows the highest shift perturbation of 0.71 ppm, while $A75_N$ shows a perturbation of 0.24 ppm. Thus the significant chemical shift perturbation found for both residues is likely to result from the effect of proximity and interaction of the electron cloud of the π orbital with these amide groups.

Additionally, residue L10, which lies in the β_A strand and is outside but in close proximity to the portal region, shows a significant chemical shift perturbation. The L10 amide nitrogen was shown to form a hydrogen bond with the carbonyl group of P38, but the $L10_{HN}$ - $P38_{CO}$ hydrogen bond is missing in the apo protein. This could be due to a flip in the peptide bond in the holo complex that was reported by the Banaszak group (Xu *et al.* 1993). This flip between A36 and K37 results in tilting of helix II by 5° (**Figure V.8**) and also rotation of the carbonyl group of A36 to the opposite direction in the holo form compared with the apo protein. The distance between these atoms involved in hydrogen bonding is shortened to 2.3 from 3.6 Å in holo compared with apo, facilitating formation of the hydrogen bond. The structural difference in A36, K37, and P38 resulting from this flip of the main chain between apo and holo is likely to affect the chemical environment of the amide nitrogen of the structurally close L10 residue.

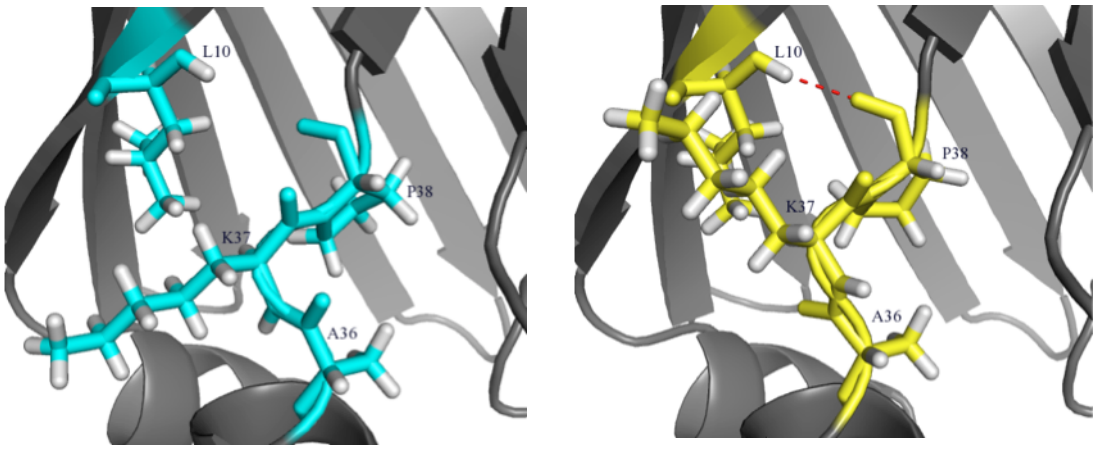

Figure V.8. Comparative PyMOL representation of apo and holo (oleate) structures, highlighting a flip in the peptide bond between A36 and K37 leading to a tilt in helix II. Apo AFABP is represented in Cyan while holo (oleate) is represented in yellow. Hydrogen bonding between L10 and P38 is shown in red while the ligand is not shown.

Moreover, residues 31 – 41 are adjacent to the structural flip between A36 and K37 and are either in or close to the portal region. Each one of these residues either shows a significant (A33, M35, N39, and M40), or a moderate (K31, V32, G34, A36, and I41) perturbation with the exception of P38, which is unobservable in this particular NMR experiment, and K37, which is unassigned (both lie in the loop region connecting αII and β_B). The observed chemical shift perturbations are rational and could be attributed to the effect of the main chain flip and the consequent helix rotation.

Furthermore, it is intriguing that residues R126 and Y128 show no significant perturbation upon binding even though they interact directly via hydrogen bonding with the carboxylate of the ligand. The holo three-dimensional structure (Xu *et al.* 1993) shows that R126 and Y128 both lie in the rear side of the protein and that the amide

nitrogens of these residues lie 6.5 Å, and 8 Å, respectively, away from the carboxylate of the ligand. It is not obvious why residues R126, and Y128 were not perturbed significantly in the titration. It is possible that although the ligand forms hydrogen bonds with the side chains of these residues, the effect of ligand binding is not significant at the amide region and therefore their chemical environment is only slightly changed.

Studying the binding by NMR allowed for investigation of the AFABP-ligand interaction and location in solution and close to physiological conditions of the protein. The chemical shift perturbation mapping enabled for identification of the binding site as a contiguous localized area, specifically the loops and turns connecting β_A and α_I, α_{II}-β_B, β_C-β_D, and β_E-β_F. The eleven residues that undergo significant perturbation and are involved in the binding were located within the portal region, or were involved in hydrophobic or hydrogen bonding with the ligand.

(c) Comparing AFABP with Other Members in the Protein Family

The murine adipocyte FABP may be compared to other members of the FABP family for which oleate binding has been studied. The only published NMR data of FABPs with oleate ligand is for liver and brain type proteins. Since LFABP binds two ligands it is not an ideal candidate for comparison with AFABP.

Oeemig *et al.* studied the human brain type (BFABP) by NMR and determined the 3D structure of apo and various holo forms of the protein including holo oleate (Oeemig *et al.,* 2009). This data was deposited in BMRB erroneously. Although the sequence identity between murine adipocyte and human brain type FABP(s) is fairly high (54 %), and both proteins are composed of 131 residues, it was not possible to confidently compare the chemical shift perturbations of both proteins. The chemical shift perturbations were recalculated in (ppm) for BFABP using the chemical shifts deposited for apo and holo (OLA) BFABP (Oeemig *et al.* 2009) in the BMRB (Biological Magnetic Resonance Bank). The chemical shift perturbations for BFABP displayed smaller magnitudes than the those of AFABP, with a maximum magnitude of 0.15 ppm for residue N59 (BFABP) versus 0.69 ppm in residue D76 (AFABP) (**compare Figure V.3 and Figure V.9**). With three residues unassigned (K37, T56, D110) in BFABP, 14 are significantly perturbed (E2, F27, R30, N34, T39, K58, L54, S55, N59, A75, N79, D89, M113, V125) lying above one standard deviation (0.018) plus the mean (0.020). It is notable that those 14 residues are scattered along the protein sequence while no significant perturbation was observed beyond residue D76 in AFABP.

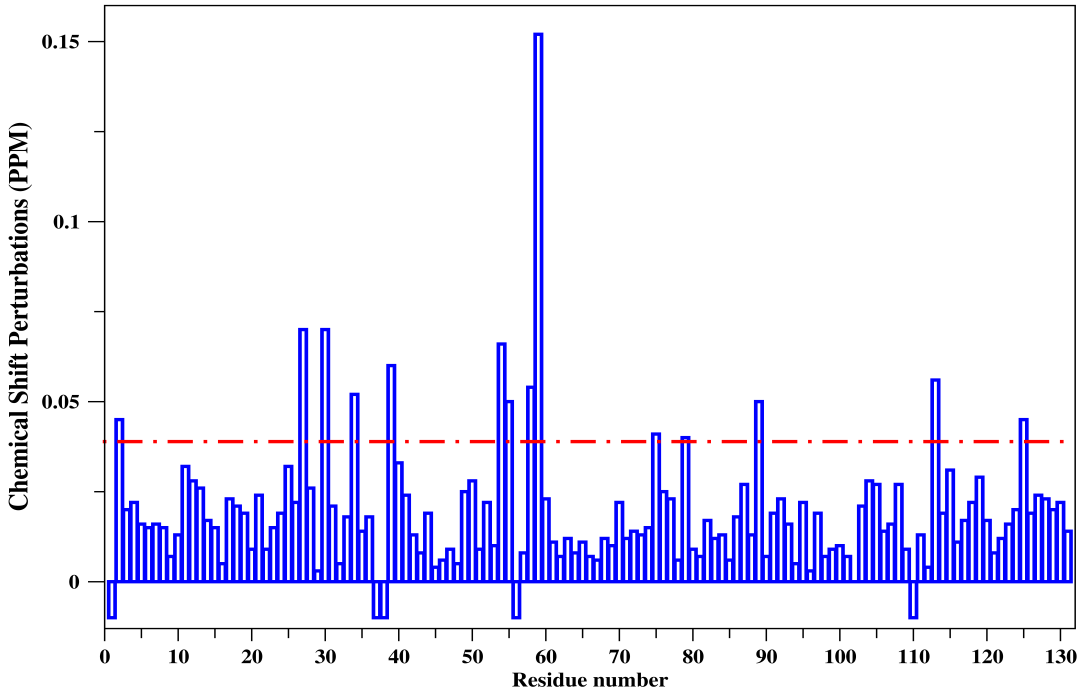

Figure V.9. Composite ^{1}H ^{15}N chemical shift perturbations plotted along the protein sequence for BFABP. The dashed line is set at one standard deviation above the average of chemical shift deviations, and highlights the residues with significant chemical shift deviations due to significant change in the chemical environment of these residues. (Data recalculated from Oeemig et al. (Oeemig *et al.* 2009).

Given the small scale of the magnitudes of the chemical shift perturbations and the fact that the some of the deposited data in BMRM was erroneous, it was not possible to confidently compare the data acquired from BFABP published data to AFABP-oleate titration results.

(d) Conclusions

Studying the binding between AFABP and oleic acid by NMR enabled for investigation of the AFABP-ligand interaction and location in solution close to physiological conditions of the protein. Although it was not possible to identify whether

the binding mechanism is slow or fast, probably due to overestimated protein concentration, the chemical shift perturbation mapping enabled identification of the binding site location and the effect of the ligand binding on AFABP. Eleven residues undergo significant chemical shift perturbation and constitute the binding site as a contiguous localized area involving the loops and turns connecting β_A and α_I, α_{II}-β_B, β_C-β_D, and β_E-β_F, which are mainly located within the portal region. Based on the comparisons with previously published results, some of these perturbations fit with these published reports, while others that were expected to show significant perturbations did not. This discrepancy could be due to the difference in the medium in which the protein existed and was studied in each case. Studying the protein-ligand interaction in solution allows the protein residues to adopt multiple conformations, by comparison with the crystal where the intermolecular crystalline lattice locks the protein residues into a particular state.

C. AFABP Binding Interactions with Linoleic Acid

1. Materials and Methods

(a) Preparation of NMR Sample

Unlabeled linoleic acid was obtained from Spectrum (San Pedro, CA). Uniformly ^{15}N labeled murine adipose fatty acid binding protein (mAFABP) was purified as described previously in Chapter III.

(b) ^{1}H- ^{15}N HSQC NMR Experiments

Aliquots from a 3.6 mM linoleic acid stock solution were added sequentially to 550 μL of 0.4 mM apo AFABP in phosphate buffer (pH 7.4 with 10 mM Pi/ 150 mM KCl and 0.02 NaN_3) in a 5 mm NMR tube. Aliquots of linoleic acid were added in 0.1 molar equivalents until the protein-to-linoleate ratio reached 1:0.6. Three more steps were added thereafter to reach 1:0.8, 1:1, and 1:1.5. The total volume of ligand added to total volume of protein throughout the titration was 92 to 642 μL, respectively. All experiments were conducted at 20 °C.

^{15}N-edited Heteronuclear Single-Quantum Coherence (HSQC) spectra were recorded on a Bruker Advance 600 MHz spectrometer (equipped with a cryoprobe). Experiments were recorded using 16 scans, measured with 256 increments in t_1 and 1024 complex points in t_2 using a sweep-width of 14 ppm for the direct dimension and a sweep-width of 35 ppm for the indirect dimension. The water signal (4.7 ppm) was set

on resonance in the proton dimension, and the ^{15}N carrier was set in the middle of the amide region (118.6 ppm). The NMR spectra were processed using the program NMRPipe (Delaglio *et al.* 1995) and were analyzed using NMRViewJ (Johnson 2004) software.

Composite chemical shift perturbations (ΔPPM) for each backbone cross-peak were calculated with the formula $[(\Delta N/6.5)^2 + \Delta H^2]^{1/2}$ (Mulder *et al.* 1999), where ΔN and ΔH denote the chemical shift differences of ^{15}N and ^{1}H in ppm, respectively.

(c) Molecular Structures

Coordinates for apo and holo mAFABP were obtained from (PDB) entries 1LIB (Xu *et al.* 1993) and 2Q9S (Gillilan *et al.* 2007), respectively, and displayed graphically with PyMOL software (The PyMOL Molecular Graphics System) (DeLano *et al.* 2005), and with LigPlot software (Wallace *et al.* 1995). Figures were prepared with GIMP software (http://www.gimp.org/), and plots were prepared with Grace software (http://plasma-gate.weizmann.ac.il/Grace/).

2. Results

Studying the spectral deviations resulting from changes in the magnetic and chemical environment of the protein residues at each titration point was done by using the chemical shift perturbation method. At the first two points (1:0, and1:0.1) of the titration, the 2D spectra showed single HN backbone resonances from residues in the apo form of

the protein. When 0.1 equivalent of linoleate was added at the second titration point, two sets of HN resonances were observed corresponding to both apo and holo forms of AFABP. The existence of both apo and holo HN resonances in the spectrum is indicative of a slow exchange process on the NMR time scale. The resonances corresponding to apo AFABP decreased in intensity upon the addition of 0.3 (nominal) equivalents linoleate, while those corresponding to holo increased in intensity. The apo peaks disappeared from the spectrum at 0.4 (nominal) equivalents, while the holo peaks reached maximum intensity at 0.5 equivalents and plateaued at 0.6, followed by a decline in intensity (but no change in position) at the last three points of the titration. This trend is illustrated in **Figure V.10** with D76 as an example. The intensity of the peaks at final titration point showed 48 % of original peak intensity. This loss of peak intensity may be attributed to both excessive precipitation, and to a dilution factor. Even after correcting the intensities in the last point with the calculated dilution factor of 14.3 %, the peak intensities were still much lower than those in the apo spectrum. This could occur as a result of the precipitation, which was visible throughout the titration and was dramatic in the last points.

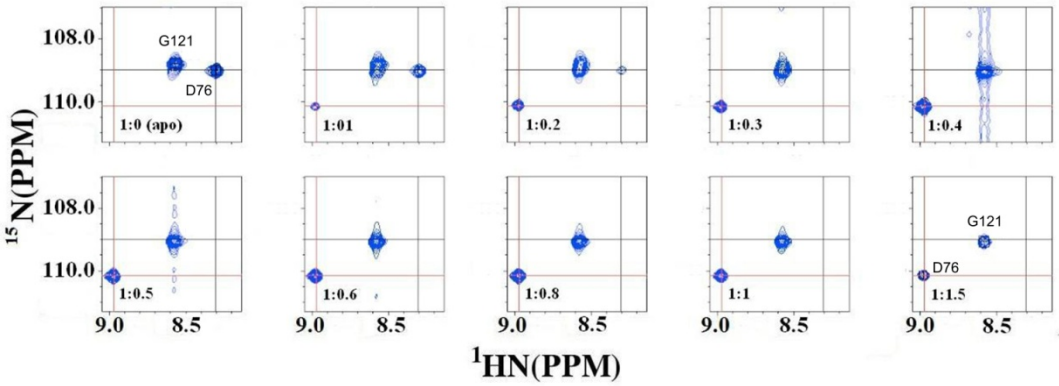

Figure V.10. Expanded regions of ^{1}H ^{15}N HSQC contour plots for residue D76 in AFABP upon titration with linoleic acid. The apo peak is centered at the black cursor, and holo peaks are centered at the red cursor. The plots show 10 titration points of nominal protein to ligand ratios (1:0, 0.1, 0.2, 0.3, 0.4, 0.5, 0.6, 0.8, 1.0, and 1.5) demonstrating a slow exchange regime where the apo and holo peaks coexist in one spectrum in 1:0.2 molar ratio of the titration. The intensity of the last point shows a dramatic decrease (probably due to precipitation). The ratios of protein to ligand and the protein concentration will be discussed below. The implications of these intensity trends for a determination of protein-ligand stoichiometry are discussed below.

As noted in Chapter IV, each one of the apo and holo spectra shows a well-folded protein, and an overlay of the two spectra shows that some of the HN cross-peaks coincide while others show spectral deviations (**Figure V.11**). The apo protein (96 % assigned with five unassigned residues (N15, F27, T56, G88, G110) displayed 10 more peaks than expected from the polypeptide sequence. Some of these additional peaks were located at the same or close to the same position as the holo (linoleic acid) peaks. Most of these peaks were scattered randomly in the spectrum except for three peaks, which appeared as broadened apo peaks.

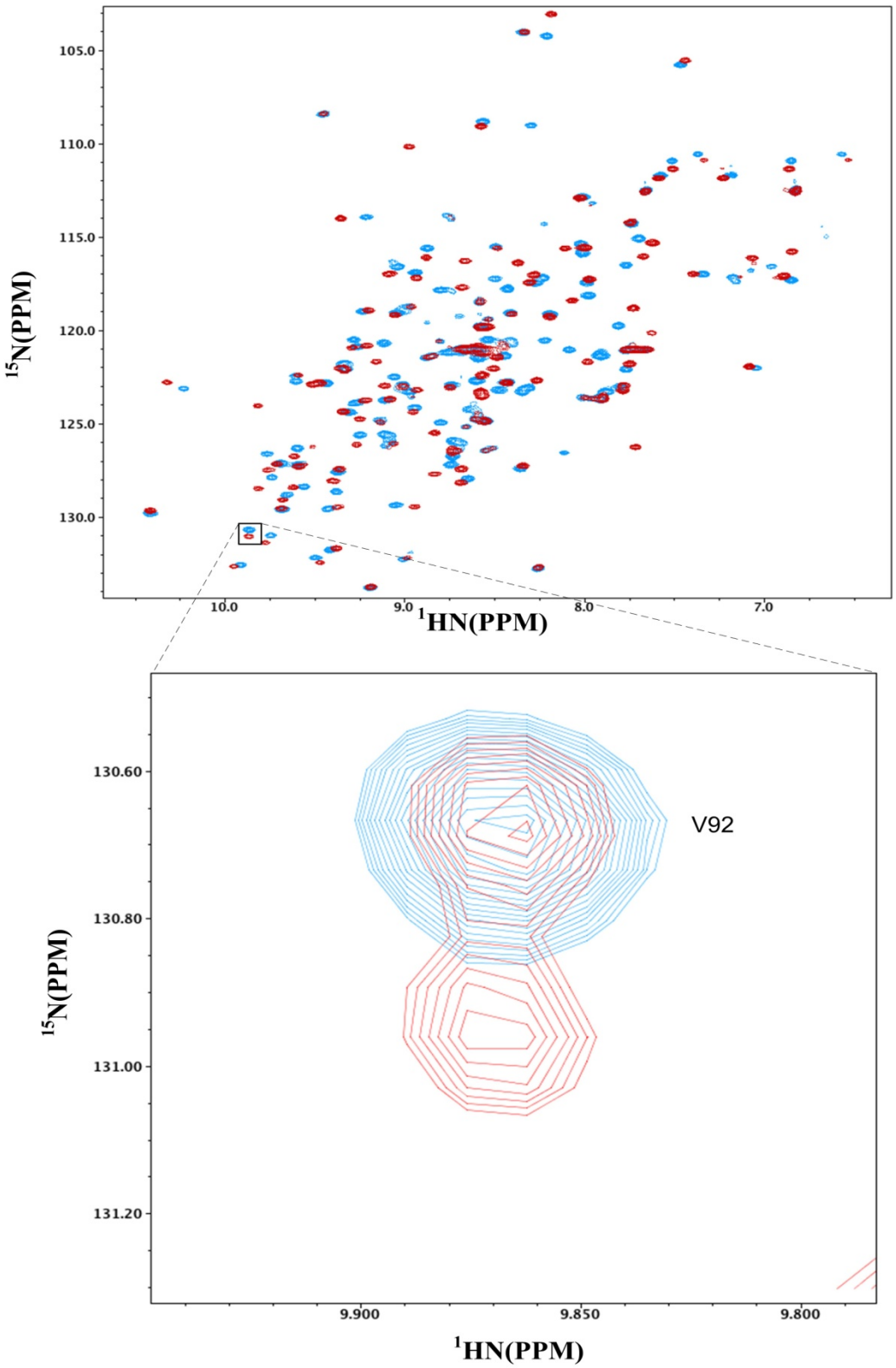

Figure V.11. (top) Overlaid spectra of apo and holo (linoleate) AFABP with the peaks colored in blue and red, respectively. (bottom) Apo and holo peaks of residue V92, showing slow exchange mechanism for 1:0.3 nominal ratio of AFABP to ligand.

By overlaying spectra of apo samples that were used in titrating the two ligands (oleate and linoleate), it was possible to compare both spectra (**Figure V.12 top**). Although the apo sample used in the oleate titration displays a bigger number (42) of extra peaks, all of the other peaks overlap, demonstrating that the assigned residues exhibit similar chemical shifts and therefore the proteins have the same folded conformation. Moreover, upon overlaying the holo spectra (**Figure V.12 bottom**), it could be noted that most of the residues in bound state exhibited similar chemical shifts for linoleate-bound, compared with oleate-bound proteins. Therefore, it was possible to transfer the assignments from holo (oleate) to holo (linoleate) for 91 % of the protein residues, except for the eleven residues that remain unassigned in holo oleate and consequently remain unassigned in holo linoleate. Those residues are: D2, N15, F16, D17, F27, K37, G46, T56, G88, G89, G110. As shown in **Figure V.12 (bottom)**, the holo spectra of oleate- and linoleate- bound AFABP are very similar though not identical. As the exchange rate of the interaction is slow for holo (linoleate) AFABP, it is impossible to unambiguously identify residues visually that are not identically affected by the ligand binding. The only way to remove such ambiguity would be to record a set of 3D experiments in order to assign those residues.

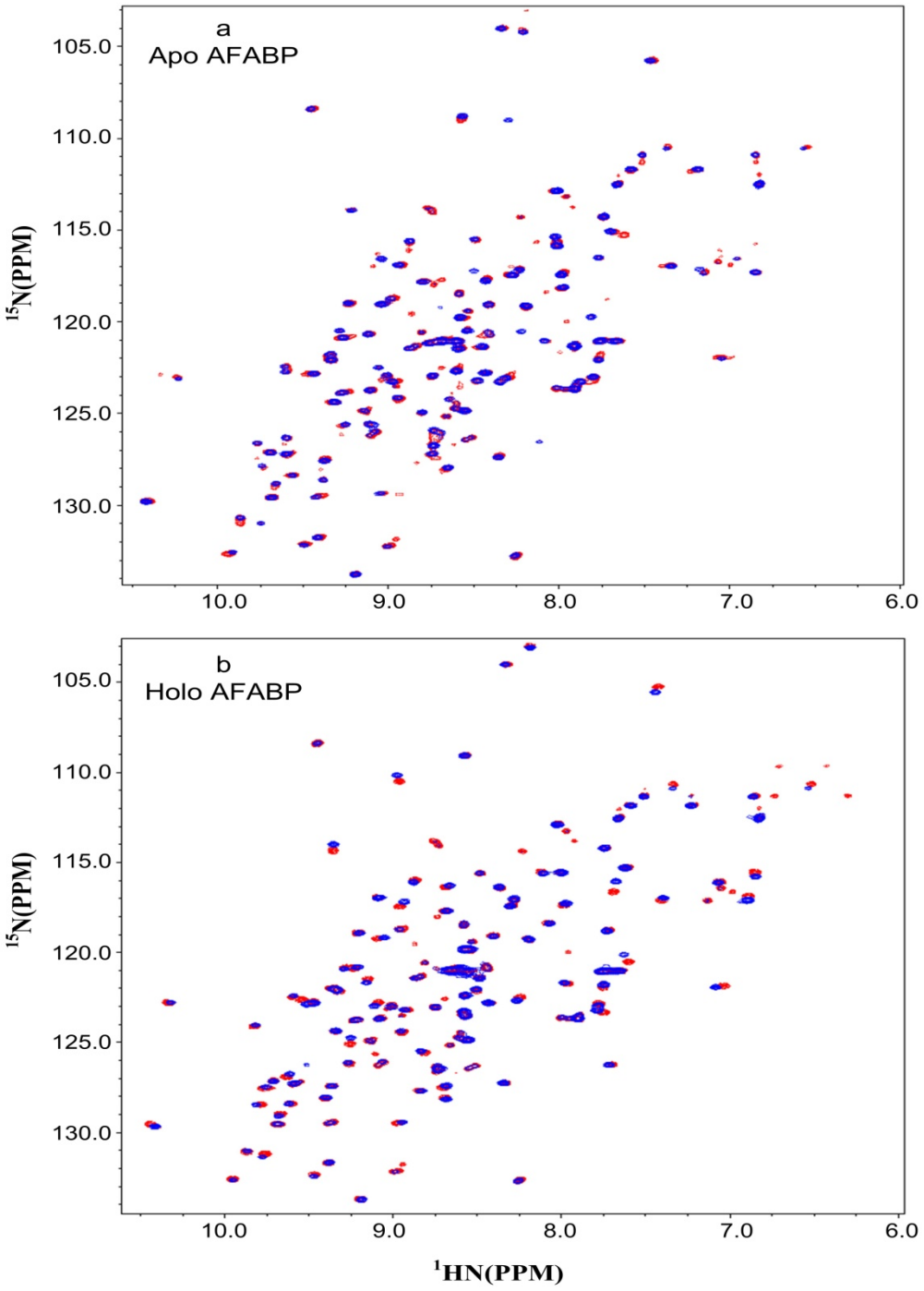

Figure V.12. (top) Superposition of apo AFABP [^{1}H-^{15}N] spectra recorded for linoleic acid titration (blue) and oleic acid titration (red) showing a larger number of extra peaks in the red spectrum relative to the blue. (bottom) Overlay of two holo AFABP spectra; holo (linoleic acid) is shown in blue, while holo (oleic acid) is shown in red. Both spectra show the majority of the apo peaks and holo peaks superimposed demonstrating that the proteins are similar in conformation except for the additional peaks in the apo sample that was used in the oleate titration.

Eight residues (Y19, A33, F57, E72, A75, L113, and V127) could not be unambiguously assigned. In the holo (linoleate) complex, the peaks corresponding to these latter residues move to the same location as in holo (oleate), but in a slightly different pattern (**Figure V.13**). Based on the pattern of chemical shift in holo (oleate), the holo (linoleate) peaks of some of these residues appear as two peaks fused together and forming a broadened peak. Therefore in the holo (linoleic acid) spectrum, the peaks demonstrate similar overlay of peaks to holo (oleic acid), but with a slight shift leading to uncertainty of assignments. Nevertheless, it is notable that the difference in the possible chemical shifts of these residues is modest. Therefore although it was not possible to confirm the assignments of these eight residues by simple transfer from the oleate ones, it was still possible to narrow the choices to one or two possibilities (marked by an arrow in **Figure V.13**) where the residue may shift to in the holo (linoleate) form.

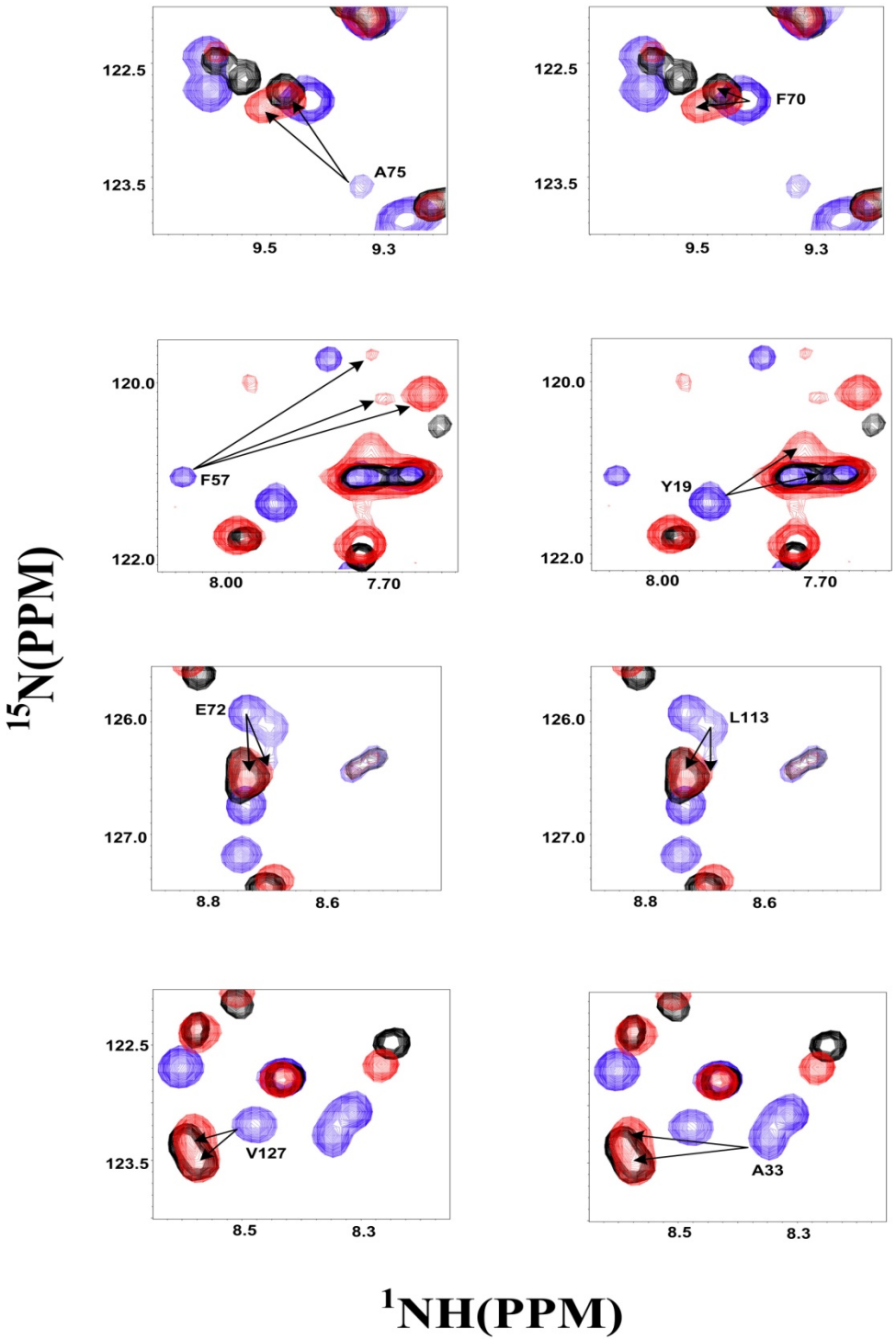

Figure V.13. Overlay of holo linoleate (orange), holo oleate (black), and apo (blue) AFABP, showing residues that are ambiguously assigned. Black arrows extend from apo peaks of each of the eight residues towards possible holo positions for that residue. The figure demonstrates that the chemical shift difference between possible holo assignments is modest.

The composite chemical shift perturbations (ΔPPM) between apo and holo states are plotted in **Figure V.14**. Chemical shift perturbations were omitted for 11 residues (D2, N15, F16, D17, F27, K37, G46, T56, G88, G89, and G110), as they remain unassigned either in apo, or holo or both states. These residues are given a negative value of -0.02.

For the purpose of this study, in order to investigate whether the eight ambiguously assigned residues affect our confidence in the determination of the perturbed area, the chemical shift perturbations were calculated for each of the residues between apo peaks and two (three for residue F57) possible holo peaks. The difference between those possibilities was calculated and then plotted on the chemical shift perturbation plot as an error bar in red color. It is apparent that chemical shift perturbation values of these ambiguous residues do not vary greatly between possible peak positions. Three residues (Y19, A33, and V127) show no difference in chemical shift perturbations, while F70, E72, A75, and L113 show slight differences ranging between 0.01 to 0.03 ppm, and the maximum difference is residue F57 with a difference in chemical shift perturbation of 0.06 ppm. This ambiguity does not change the pattern of perturbations in the plot between significant, moderate, and subtle changes, which gives us confidence to analyze the mapping of perturbed areas on the structure based on the chemical shift perturbation plot. By taking the difference in the chemical shift perturbations of the ambiguously assigned residues into consideration, the average is increased by 0.01 ppm and the value of the average above the standard deviation by

0.014 ppm. This in turn does not change the pattern of chemical shift perturbations in the plot.

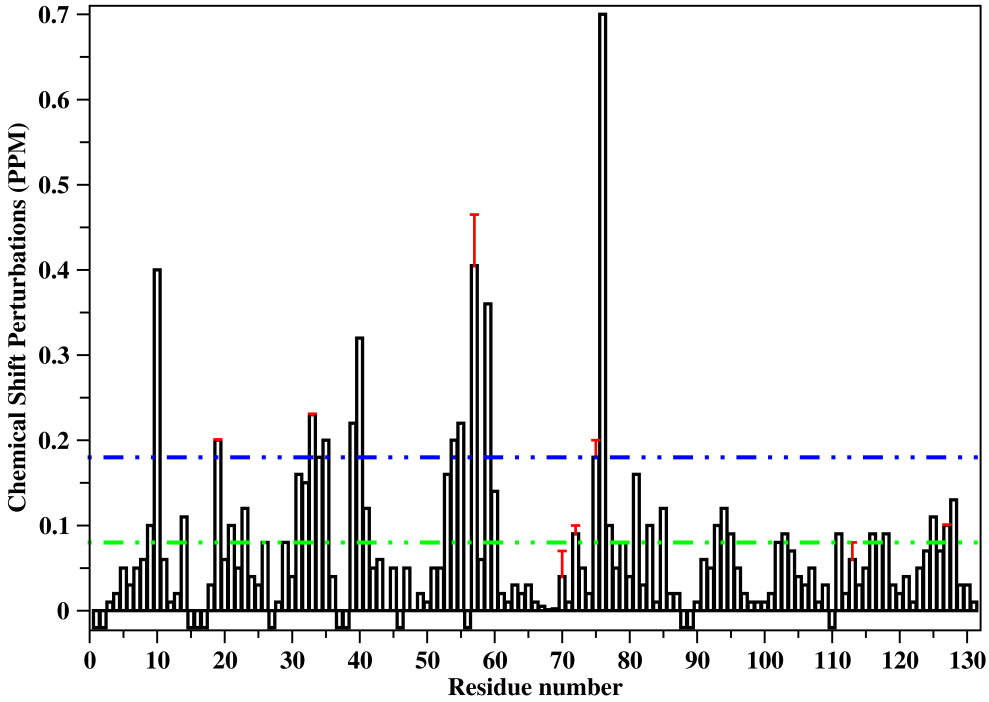

Figure V.14. Composite ^{1}H ^{15}N chemical shift perturbations plotted along the protein sequence for AFABP. The blue dashed line is set at one standard deviation above the average chemical shift perturbation, while the green dashed line is set at the average chemical shift perturbation of 0.08 ppm, The red error bars mark ambiguous residues and the extent of their ambiguity. The plot highlights the residues with significant, moderate and subtle perturbations. Negative values indicate residues that are unassigned in one or both protein forms.

A blue dashed line is drawn across the chart at 0.18 ppm, highlighting residues with significant perturbations (perturbations greater than one standard deviation (0.1) above the average (0.08)), while a green one is drawn at 0.08 ppm. Residues that lie between the red and green lines display moderate perturbations, while those below the green line demonstrate subtle ones. Thirteen residues demonstrate significant chemical shift perturbations (L10, Y19, A33, G34, M35, N39, M40, E54, S55, F57, N59, A75, and

D76). Residues D76, F57, and L10 display the highest deviations. D76 and L10 exhibit values of 0.70, and 0.4 ppm, respectively, while F57 displays a deviation value in the range of 0.40 to 0.47 ppm. Perturbations for the other eight residues lie in the range of 0.18 to 0.36 ppm.

The chemical shift perturbation plot shows that the most significant perturbations occur in the first 60 % of protein sequence **(Figure V.14)**. While residues 81, 88, 89, 110 are unassigned, the latter 40 % demonstrate modest perturbations. This trend could be highlighted by mapping the chemical shift perturbations and the unassigned residues onto the crystal structure of holo AFABP **(Figure V.15)**. The highest perturbations are observed near the defined portal area, particularly between β_A and α_I, α_{II}-β_B loops, and β_C-β_D, β_E-β_F turns, while the rear side of the β- barrel displays only moderate perturbations.

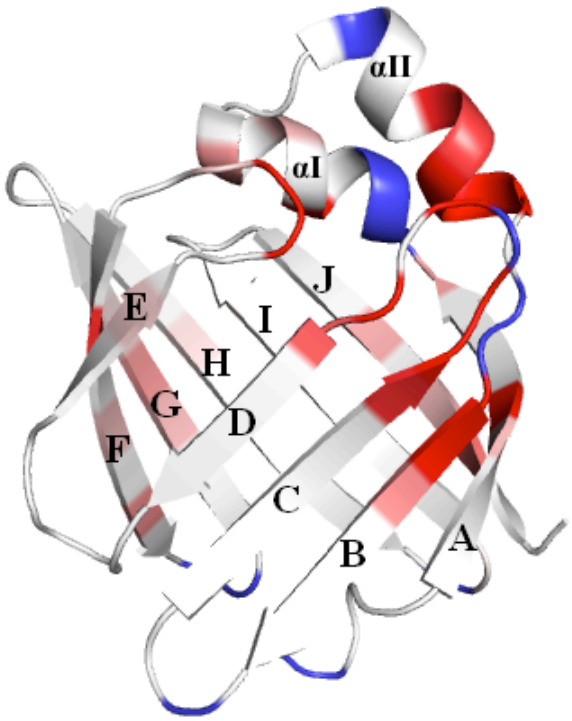

Figure V.15. Chemical shift perturbation mapping. The chemical shift perturbations are mapped onto the x-ray structure of holo AFABP (PDB: 2Q9S, Gillilan *et al.* 2007). The protein residues are colored based on a color gradient spanning from white to red to represent an increase in chemical shift perturbation with a minimum and a maximum cutoff of 0.08 and 0.18, respectively, while unassigned residues are colored blue. The 3D structure is labeled to demonstrate β-strands (A-J) and helices αI and αII. Ligand is not shown.

3. Discussion

By titrating linoleic acid into AFABP, it was possible to identify the binding exchange mechanism and binding region of the ligand. Transferring the assignments from previously studied holo AFABP (oleate) to holo AFABP (linoleate) was facilitated by similar chemical shift changes of both holo proteins with respect to apo AFABP. Eight residues were ambiguously assigned. Nevertheless, the chemical shift perturbation difference between possible holo peaks for the latter eight residues were subtle and did not demonstrate a significant effect on the pattern of chemical shift perturbation plot. In

order to confirm the assignments of those eight residues, 3D experiments could be performed. Nevertheless, it was possible to identify the ligand binding site, which will be discussed in detail below. Although the protein concentration was probably overestimated in the titration, by studying the stepwise titration points, it was possible to observe two sets of HN crosspeaks corresponding to both apo and holo states of the protein in the same spectra, indicating a slow exchange mechanism.

(a) Titration Analysis

1) Exchange Rate and Ligand Stoichiometry

By stepwise observation of the HSQC spectra at each titration point, single backbone resonances corresponding to residues in apo form could be noted at the first point. At the addition of the first aliquot of 0.1 equivalents of linoleate, a second set of resonances corresponding to holo peaks started appearing with a relatively weak intensity compared to apo resonances. At the following titration points, resonances corresponding to holo protein continued to grow while those corresponding to apo protein continued to shrink. Upon the addition of 0.4 equivalents of linoleate, the apo peaks completely disappeared from the spectrum, and the holo peaks plateaued in intensity at 0.5 equivalents but remained in the same holo positions until the end of the titration. Since the holo peaks did not continue to shift upon addition of linoleate, it is concluded that AFABP does not demonstrate a preholo state of the protein as observed for titration of LFABP with oleate (He *et al.,* 2011). Disappearance of the apo peaks and the observation of a plateau in intensity of holo peaks indicate saturation of the protein with ligand. The peak intensities of each set of resonances should be proportional to the ratio

of bound to free protein in each titration point. Therefore, the absence of apo peaks in 0.4 and above equivalents implies that the protein concentration was over-estimated. The coexistence of two sets of resonances corresponding to apo and holo protein forms in indicative of slow exchange on the NMR time scale.

2) Mapping the Binding Site

By utilizing the chemical shift perturbation method and mapping, thirteen residues (L10, Y19, A33, G34, M35, N39, M40, E54, S55, F57, N59, A75, and D76) demonstrated significant perturbation values greater than one standard deviation above the average (0.18 ppm) (**Figure V.16**). The eight ambiguously assigned residues did not affect the pattern of chemical shift perturbation plot or the mapping. Although the definitive assignments of these residues would need to be confirmed through 3D NMR experiments, it was possible to identify two (and in one case, three) possible holo peaks for each residue. These peaks were very close in the spectrum and therefore had minor differences in ppm. That property in turn allowed for confident use of the chemical shift perturbation data to identify the binding site upon ligand addition. Collectively, the thirteen highly perturbed residues comprise the binding site, which can be described as a contiguous localized area, involving the loops and turns connecting β_A and α_I, α_{II}-β_B, β_C-β_D, and β_E-$\beta_{F,}$ and coinciding with the defined portal area (helix αII (27-35) and β-turns between β-strands β_C-β_D (55-58), and β_E-β_F (74-78)) (Xu *et al.* 1993; Reese-Wagoner *et al.* 1999). Although the backside of the protein (β-strands β_F-β_J) is mainly unaffected by the ligand binding, the front side of the protein (β-strands β_A-β_D and helix αII) is

predominantly the most perturbed, specifically near the location of the ligand on the 3D structure. However, AFABP does not go through a global conformational change upon binding to linoleate.

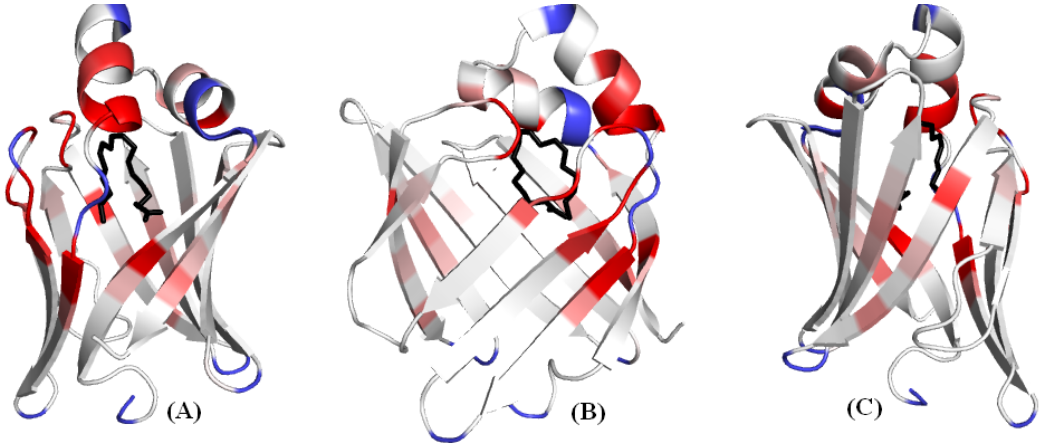

Figure V.16. Visual representations of the chemical shift perturbation plot. The chemical shift perturbations were mapped onto the x-ray structure of holo AFABP in complex with linoleate (PDB: 2Q9S, Gillilan *et al.* 2007). The protein residues are colored based on a color gradient spanning from white to red colors to represent an increase in chemical shift perturbation with a minimum and a maximum cutoff of 0.08 and 0.18, respectively, while unassigned residues are colored blue. Alternate views of AFABP-oleate complex (B), and (C) are rotated by 90°, and 180° about the Y-axis relative to (A) to facilitate viewing the positioning of the ligand inside the protein cavity. Ligand is shown in black.

Several of the highly perturbed residues are involved in hydrophobic interactions with the ligand. Using the crystal structure of the holo (linoleate) complex (pdb: 2Q9S, Gillilan *et al.* 2007) as an input, a LigPlot schematic representation (Wallace *et al.* 1995) (**Figure V.17**) shows eight residues interacting hydrophobically with linoleate (V25, A33, P38, S53, F57, D76, I104, C117) and one residue (Y128) forming an H-bond with the ligand.

Three of the nine interacting residues (A33, F57 and D76) demonstrate significant perturbation and interact hydrophobically with the ligand. At least one neighbouring residue to those three demonstrates significant perturbation as well. These adjacent residues (G34, M35, N39, M40, E54, S55, and A75) may be affected by the hydrophobic interactions between interacting residues with the ligand. The remaining three residues (V25, C117, and Y128) show only subtle chemical shift perturbations.

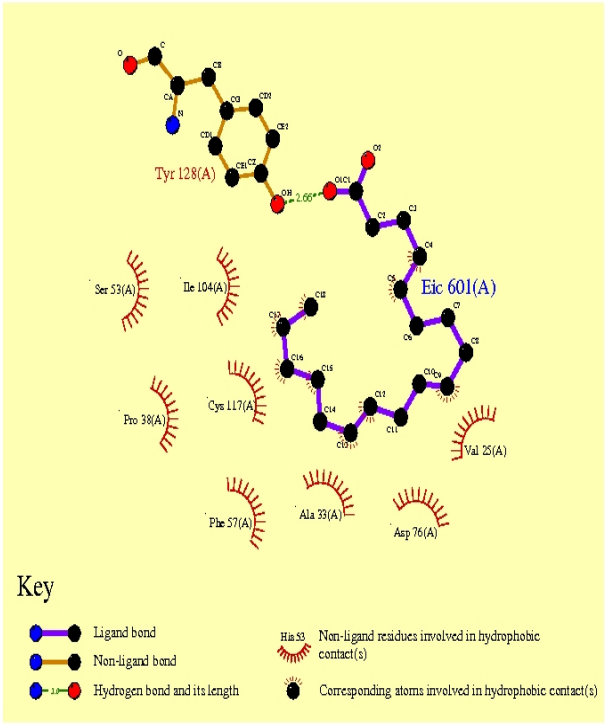

Figure V.17. LigPlot schematic diagram illustrating polar and non-polar interactions between linoleate and protein residues.

By studying the holo protein crystal structure (pdb: 2Q9S, Gillilan *et al.* 2007), the tail of linoleate is observed to fold back and form a U-shaped structure inside the protein cavity, leading to a short distance (3.7 Å) between the tail and the carboxylate

head. Consequently, both the ligand's tail and its carboxylate head extend towards N39 and M40. While the ligand's tail is in closer proximity to the backbone of the two residues, their amide groups lie at distances of 8.5 Å and 7.8 Å, respectively, from the carboxyl groups. Therefore, observation of chemical shift perturbation for those two residues agrees with the positioning of the ligand in the crystal structure of the holo complex.

With the exception of T56, which is unassigned, and K58, which shows subtle perturbation, residues S55 and F57 along with their neighboring residues S53, E54, N59, and T60 undergo either moderate or significant perturbations. Together these residues coincide with part of the defined portal, and form a contiguous perturbed region.

Contrasting effects of ligand binding are observed for residues F57 and K58. While K58 shows a subtle perturbation (0.06 ppm), F57 undergoes a significant perturbation of a value between (0.40 to 0.47 ppm). The position of the F57 side chain, in the holo (linoleate) complex is slightly different from apo (**Figure V.18)**, while the K58 side chain remained in the same location, except for a slight rotation. Despite lying in the portal region within 6.9 Å from the ligand and residing between two significantly perturbed residues (F57 and N59), it is not easily understood why the chemical environment of K58 was not affected by the presence of the ligand and therefore did not show significant perturbation.

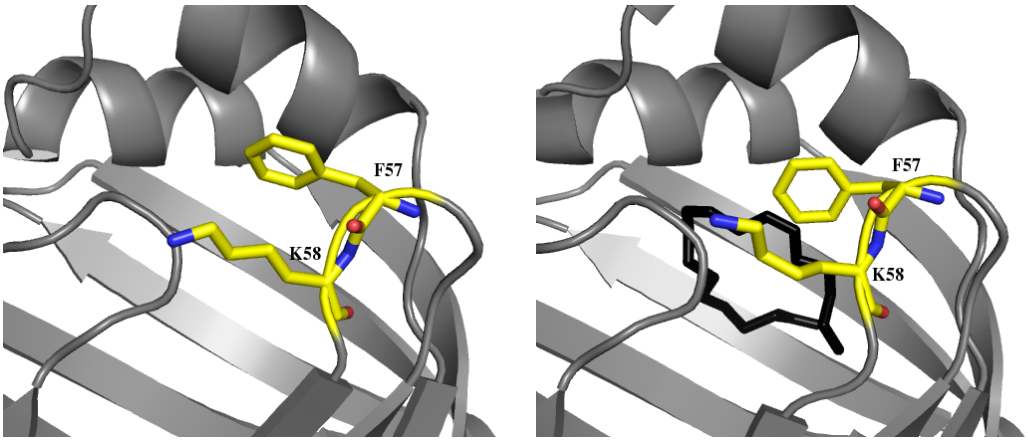

Figure V.18. Apo (left) and holo linoleate (middle) and holo oleate (right) AFABP to compare the position of the F57 ring. Ligands are shown in black in the holo complexes.

Both D76 and A75 reside in close proximity to the two double bonds of linoleate (less than 7 Å away from the ligand's four carbons involved in the double bond), and undergo significant chemical perturbations. The amide group of D76 is closer to both of the ligand's two double bonds than A75. The linoleate C10, which is involved in the ligand's double bond, is the closest to both residues, and lying within 4.3 and 5.4 Å of residues D76 and A75, respectively. The significant chemical shift perturbation found for both residues (0.7 ppm for D76, and 0.2 for A75) is likely to result from the effect of proximity and from their interactions with the electron cloud of the π orbital, thus leading to a change in the chemical environment of their respective amide groups.

The amide nitrogen of L10 was shown to form a hydrogen bond with the carbonyl group of P38 in holo (linoleate) AFABP, which is missing in the apo protein (**Figure V.19**). The distance between these atoms involved in hydrogen bonding is shortened to 2.4 from 3.6 Å in holo (linoleic acid) compared with apo, The presence of that hydrogen

bond between $P38_{co}$ and $L10_N$ in holo compared with apo could be the reason for the change in chemical environment of the amide nitrogen of L10 residue.

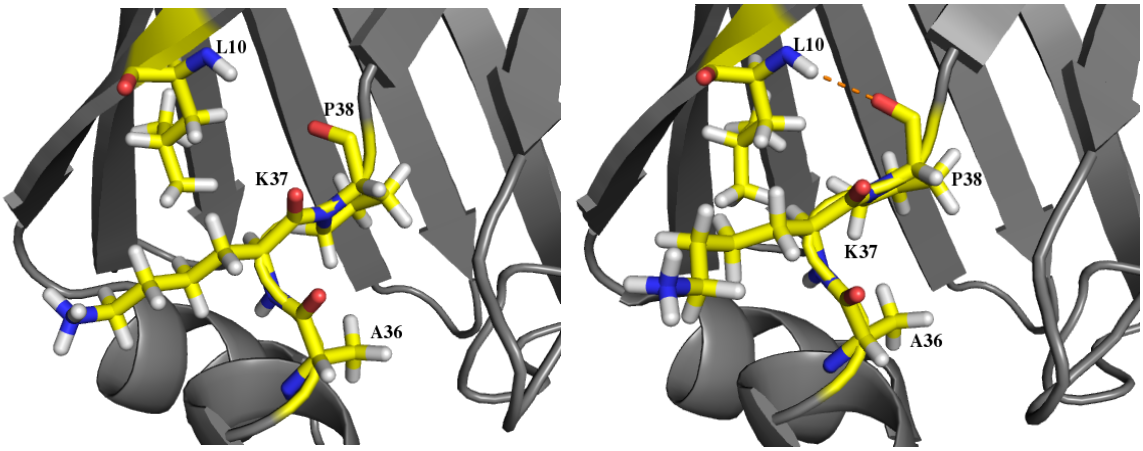

Figure V.19. Comparative PyMOL representation of apo and holo (linoleate) structures, highlighting hydrogen bond formation in the holo complex but not in apo. Hydrogen bonding between L10 and P38 is shown in orange for holo AFABP while the ligand is not shown.

Finally, by studying the binding of linoleate to AFABP via chemical shift perturbation mapping, it was possible to highlight thirteen significantly perturbed residues interacting with the ligand via hydrophobic interactions or hydrogen bonding. The NMR studies, which were carried in solution, disclosed that the binding site is a contiguous localized area encompassing the loops and turns connecting β_A and α_I, α_{II}-β_B, β_C-β_D, and β_E-β_F of the defined portal.

(b) Conclusion

Studying the linoleate ligand binding of AFABP by solution state NMR at close to physiological conditions allowed for identification of the binding site, which is composed of thirteen significantly perturbed residues. Together these residues comprise

the binding site, which is described as a localized region involving part of the portal region. By studying the chemical shifts of the protein residues through the titration points, it was possible to identify two sets of HN cross peaks corresponding to apo and holo states of protein residues in the same spectrum. This observation is indicative of a slow exchange mechanism on the NMR time scale. Although it was possible to transfer all the assignments of holo (oleate) AFABP to holo (linoleate) AFABP, and eight ambiguously assigned residues did not interfere with chemical shift perturbation plot and mapping.

D. AFABP Binding Interactions with Troglitazone (TDZ)

1. Materials and Methods

(a) Preparation of NMR Samples

Uniformly ^{15}N labeled murine adipose fatty acid binding protein (mAFABP) was produced and purified as described previously in Chapter II. Unlabeled troglitazone (TDZ) was obtained from Enzo Life Sciences, Inc. (Plymouth Meeting, PA). Ethanol and HPLC-grade DMSO (dimethyl sulfoxide) were obtained from Sigma-Aldrich (St. Louis, MO).

Since TDZ is insoluble in aqueous media, an organic solvent was used to dissolve the ligand for each of the two titrations carried out to study the interaction with AFABP. In alternative procedures, a protein solution was added to dry TDZ obtained from ethanol evaporation or TDZ dissolved in DMSO was added to the aqueous protein solution.

1) Titration (1): Titrating AFABP with TDZ (dried from ethanol solution)

A 2.3 mM stock solution was prepared by dissolving 5 mg of TDZ in 5 ml of 100 % ethanol. The ligand equivalents were first added to a clean 5 mm NMR tube to allow evaporation of ethanol, followed by addition of 550 µl of 250 µM protein solution (10 % D_2O) to the NMR tube. In this way, the aqueous-insoluble ligand is introduced to the protein solution and should dissolve if it binds to AFABP; the ethanol organic solvent cannot influence the titration results. Ten titration points were recorded at 20 °C using

increments of 0.2 molar equivalent for the first six points, then 0.4 increment for the following two points, then 1.0 molar increment for the last point. At each titration point the protein solution was transferred into an NMR tube containing an additional increment of ligand after confirming evaporation of ethanol prior to protein transfer. Possible volume losses upon transfer were estimated as 10 %; therefore underestimation of protein concentration may have occurred with progressive ligand addition, resulting in a larger ligand to protein ratio than originally planned.

2) Titration (2): Titrating AFABP with TDZ (dissolved in DMSO)

This experiment was performed with two parallel procedures. Following previously published protocols (Bernard *et al.,* 2009), the first step was to carry out the titration of the ligand (dissolved in DMSO) into the protein. In order to establish the independent effect of the organic solvent on AFABP, a second blank experiment was conducted. The control experiment was performed with identical gradual additions of DMSO to the protein solution in the absence of ligand; the protein concentration and NMR acquisition and processing parameters were maintained constant. While DMSO has been shown to have no effect on particular proteins (Bernard *et al.* 2009), other literature suggests that DMSO could affect the tertiary structure of the protein (Bhattacharjya and Balaram 1997). In some cases a percentage as small as 0.05 % DMSO has been reported to induce protein instability and denaturation or aggregation (Tjernberg *et al.,* 2006). Therefore, it was important to perform the control (blank) experiment to isolate the effect of the organic solvent on the protein residues and subtract that effect from the ligand-DMSO titration.

Aliquots ranging from 0.6 to 93 µL from a 7.6 mM TDZ stock solution (5 mg TDZ dissolved in 1.5 ml DMSO) were added sequentially to a 5 mm NMR tube containing 400 µL (350 µM) apo AFABP in phosphate buffer (pH 7.4 with 10 mM Pi/ 150 mM KCl and 0.02 NaN_3) that was 10 % in D_2O. Aliquots of TDZ solution were added in small equivalents for the first points, and then increased gradually until the protein-to-TDZ ratio reached 1:15.0. A total of 19 points were recorded at the following molar ratios: 1:0, 0.05, 0.1, 0.25, 0.4, 0.5, 0.75, 1.0, 1.5, 2, 2.5, 3.0, 4.0, 5.0, 6.0, 7.0, 8.0, 10.0, 15.0. The total volume of ligand (dissolved in DMSO) was 278 µL as compared with a total volume of protein of 678 µL, respectively, accounting for 6.5 % DMSO at a 1:1.5 protein-to-ligand ratio and a maximum of 41 % DMSO in the protein solution at a ratio of 1:15.

Similarly, the control experiment was carried out with identical protein concentration, NMR recording parameters and DMSO percentages (0, 0.25, 0.5, 1.2, 1.8, 2.1, 3.4, 4.6, 6.5, 8.3, 10.3 and 12.3 %) corresponding to the ligand titration points at 1:0 – 1:3 protein-to-ligand molar ratios. A rationale for not performing experiments with higher percentages of DMSO to match the ligand experiment is explained in the discussion section.

(b) [^{1}H- ^{15}N] HSQC NMR Experiments

All ^{15}N-edited Heteronuclear Single-Quantum Coherence (HSQC) spectra were recorded on a Varian 600 MHz VNMRS spectrometer (Agilent Technologies, Santa Clara, CA) with a conventional 5 mm inverse detection triple resonance (HCN) probe.

Experiments for titrations (1) and (2) were measured with 32 and 64 transients, respectively. Both titrations were conducted at 20 °C with 128 and 1024 complex points in the indirect (t1) and direct (t2) dimensions, respectively. The sweepwidths in the direct ^{1}H and indirect ^{15}N dimensions were 15 ppm and 36 ppm, respectively. Thus, the digital resolution for titration (1) was 8.9 Hz/point (^{1}H) and 4.3 Hz/point (^{15}N), and 8.9 Hz/point (^{1}H) and 8.6 Hz/point (^{15}N) for titration (2). The water signal (4.821 ppm) was set on resonance in the proton dimension, and the ^{15}N carrier was set in the middle of the amide region (119 ppm).

NMR spectra were processed using NMRPipe (Delaglio *et al.* 1995) and were analyzed using NMRViewJ (Johnson 2004) software. Composite chemical shift perturbations for each backbone cross-peak were calculated with the formula $[(\Delta N/6.5)^2 + \Delta H^2]^{1/2}$ (Mulder *et al.* 1999), where ΔN and ΔH denote the chemical shift differences for ^{15}N and ^{1}H in ppm, respectively.

(c) Molecular Structures

Coordinates for apo and holo mAFABP were obtained from the Protein Data Bank (PDB) entries 1LIB (Xu *et al.* 1993) and 2QM9 (Gillilan *et al.* 2007), respectively, and displayed graphically with PyMOL software (The PyMOL Molecular Graphics System) (DeLano *et al.* 2005) and with LigPlot+ software (Laskowski and Swindells 2011). Figures were prepared with GIMP software (http://www.gimp.org/), and plots were prepared with Grace software (http://plasma-gate.weizmann.ac.il/Grace/).

2. Results

(a) Titration (1): Interaction between AFABP and dry TDZ from ethanol solution

Protein solution was added to the dried ligand while shaking to allow uptake of all ligand by the protein solution. Precipitation was observed as for previous titrations of oleate and linoleate, but in smaller quantity.

The HSQC spectra of apo AFABP show well resolved peaks and spectral dispersion typical of a well-folded protein. Upon the addition of ligand, starting from the second titration point (1:0.2) some of the peaks show broadening, leading to either disappearance or loss of intensity during subsequent steps of the titration. This observed broadening and eventual disappearance of the peaks upon addition of ligand is characteristic of some residues entering an intermediate exchange regime between two or more states. The relation between exchange rates and the chemical shift perturbation for fast, intermediate and slow exchange regimes was discussed earlier in the introduction to this chapter. This effect is illustrated in **Figure V.20 (bottom)** for G34, while G99 shows no perturbation due to ligand binding. **Table V.2** lists nine residues that disappear upon ligand binding due to exchange broadening effects.

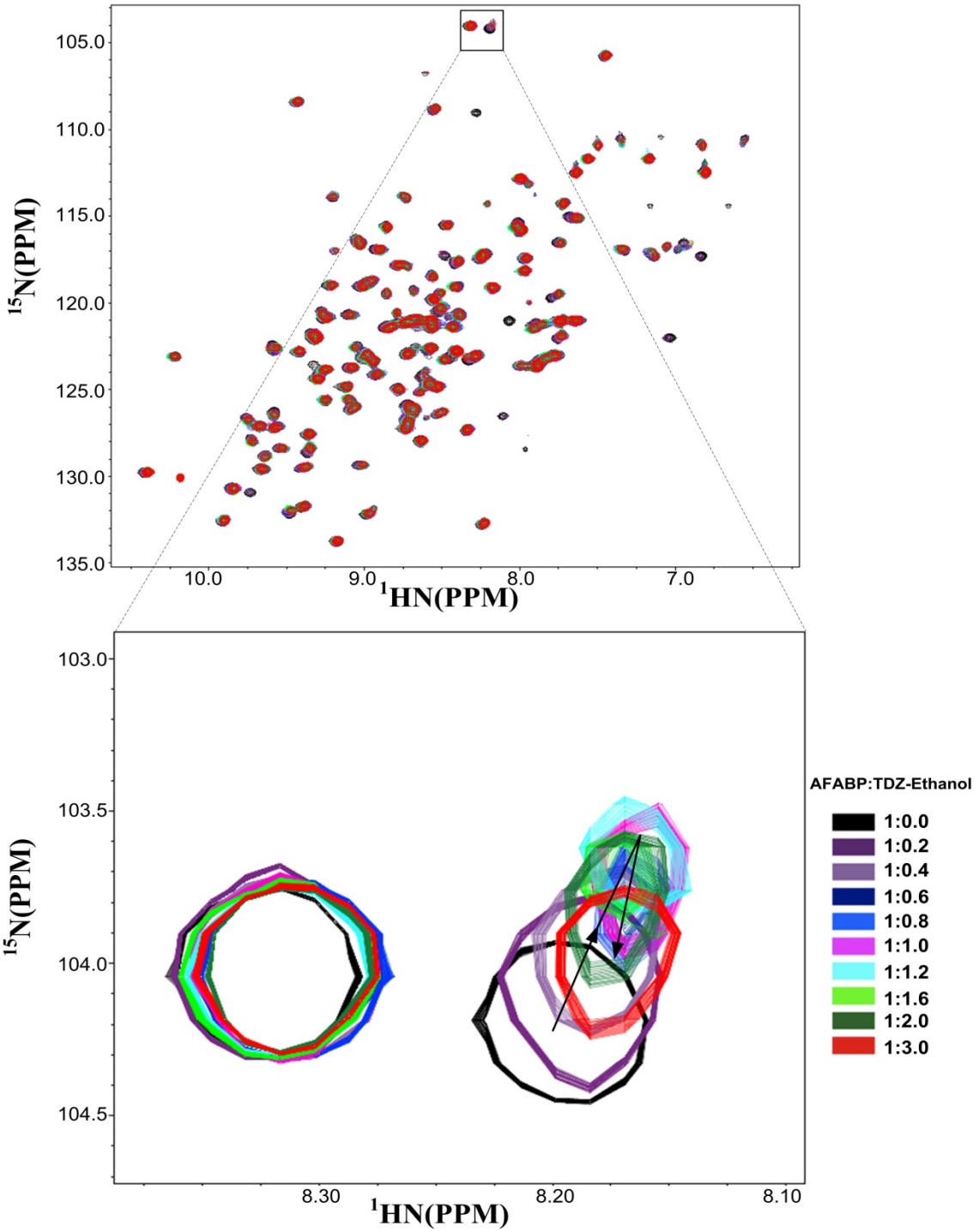

Figure V.20. (top) Expanded region of [^{1}H-^{15}N] HSQC spectra for titration points of AFABP with TDZ (from ethanol solution) at molar ratios of 1:0, 0.2, 0.4, 0.6, 0.8, 1.0, 1.2, 1.6, 2.0, and 3.0. (bottom) Expanded region showing residues G99 with no chemical shift perturbation throughout the titration and G34 exhibiting perturbation and intermediate exchange. The key illustrates the color designated for each spectrum. The maximum perturbation of G34 corresponds to 0.5 ppm ^{15}N (3.5 points) and 0.02 ppm ^{1}H (1.5 points).

Figures V.21 and V.22 show that upon the addition of ligand, residue G34 goes into intermediate exchange and decreases in peak intensity while showing a very subtle change in chemical shift (0.5 and 0.013 ppm in ^{15}N and ^{1}H dimensions, respectively) and peak intensity. Both effects continue to change upon addition of ligand increments until the molar ratio of protein-to-ligand reaches 1:1.2. At the 1:1.6 molar ratio the peak changes the direction of movement and starts to retract back towards the direction of the original apo position.

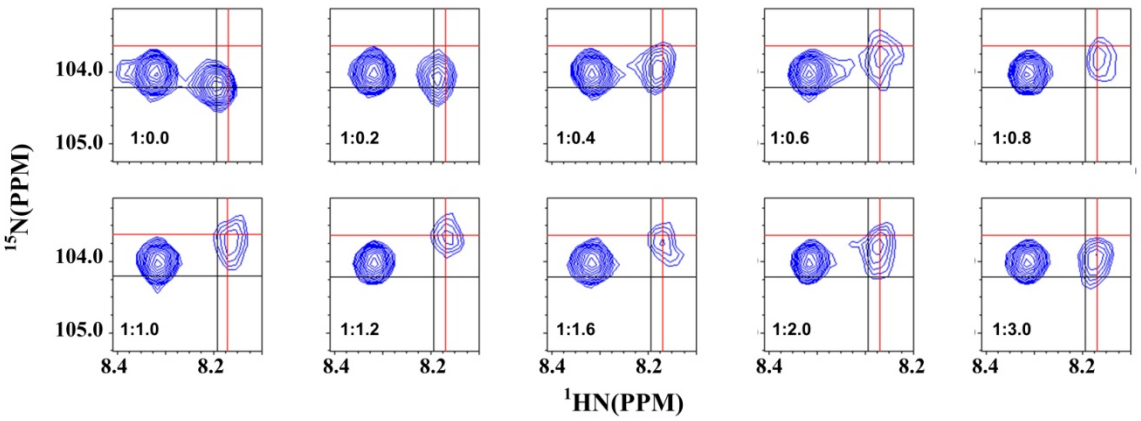

Figure V.21. Expanded regions of [^{1}H-^{15}N] HSQC contour plots for residue G34 in AFABP upon titration with TDZ (dried from ethanol). The apo peak is centered at the black cursor, and the position of the peak at the maximum perturbation at point (1:1.2) is centered at the red cursor. The plots show 10 titration points of protein to ligand ratios 1:0 - 1:3.0.

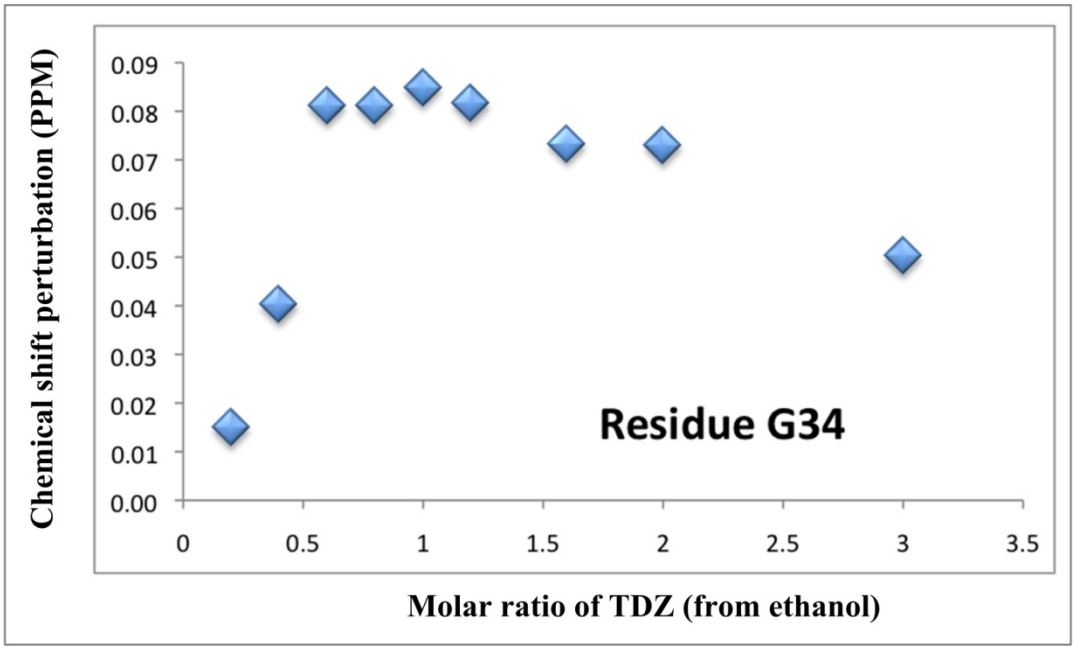

Figure V.22. Chemical shift variations for residue G34 during titration with TDZ from ethanol. Plot shows increase of perturbation followed by a slight decrease, which is demonstrated visually in the previous figure. The peak corresponding to the holo protein resonance that appears in the last three points was used in these calculations.

Many of the residues show subtle or no observable chemical shift changes throughout the titration, with the exception of 40 residues that go through intermediate exchange whereby the peaks exhibit broadening and loss of intensity throughout the titration points. Most of those 40 peaks could be traced throughout the titration, while others (nine, summarized in **Table V.2**) disappeared after gradual addition of the ligand. By examining the calculated chemical shift perturbations of the remaining 31 residues it is evident that the chemical shift differences between apo and molar ratio 1:1.6 protein-to-ligand are modest in comparison with those prevalent in the fatty acid ligand titrations. Additionally, the shift trend of the peaks is non-linear; in fact, many peaks reverse direction so that by the last point they migrate back in the direction of their original apo positions. In most cases it appears that the change in direction occurs either at 1:1.2 or 1:1.6 titration points.

It was not possible to trace the nine residues that disappear after the addition of the ligand, and investigation of the later titration points did not show any reappearing peaks that could be attributed to those residues. In fact the number of peaks observed at the later titration points (145 peaks at 1:3 protein-to-ligand) were fewer than at the first point (154 peaks) and did not increase after that point. The residues that exhibit intermediate exchange are likely to be those that are most affected by ligand binding, since the rate of exchange could be greater than the chemical shift perturbation initially but comparable to the chemical shift perturbation subsequently. Since it is not possible to quantify the perturbation for those nine residues, their behavior is analyzed qualitatively in the following sections.

As noted in Chapter IV, 96 % of the apo protein backbone resonance is assigned, with five unassigned residues (N15, F27, T56, G88, G110). Except for the residues that exhibit enough broadening to disappear from the spectrum (nine residues) and those unassigned (five residues), the peaks corresponding to the AFABP residues could be followed throughout the titration and therefore could be assigned for the protein at protein-to-ligand molar equivalents of (1:1.2) and (1:1.6). Residues Y19 and T103 were assigned provisionally. The peaks of both residues overlapped in the apo spectrum and then separated upon the addition of ligand, so they could not be assigned with certainty. Nonetheless, the chemical shift perturbation between the apo peak and the two new separated peaks upon the addition of the ligand is very similar. Therefore in order to calculate the chemical shift perturbations, each peak was assigned to a particular residue arbitrarily.

Since the maximum chemical shift changes occur at molar equivalents of 1:1.6, the composite chemical shift perturbations between apo and the point (1:1.6) were calculated, plotted and summarized in **Figure V.23**.

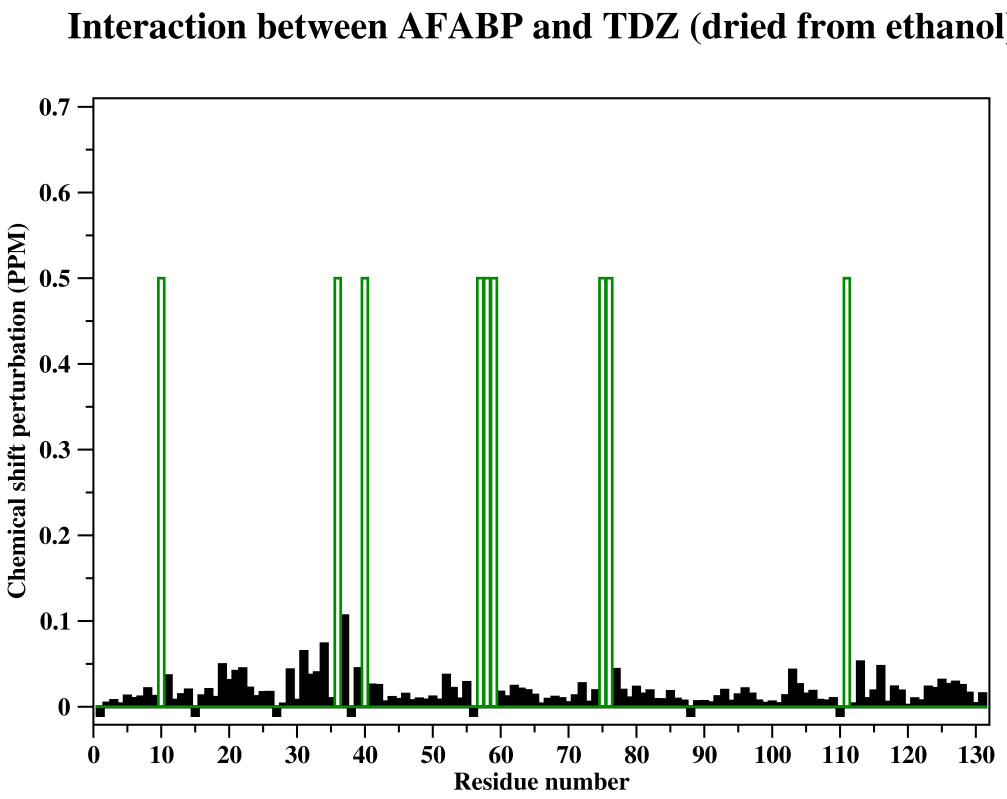

Figure V.23. Composite [^{1}H-^{15}N] chemical shift perturbations plotted along the protein sequence for AFABP. The perturbations were calculated for the molar ratio 1:1.6 protein-to-ligand. Residues that disappeared due to intermediate exchange broadening are assigned an arbitrary value of 0.5 ppm and highlighted in green color. The same scale is used as for fatty acid titrations (oleate and linoleate) described in previous sections of this chapter. The average value is intentionally omitted from the figure (see text). Negative values indicate unassigned residues. Residues Y19 and T103 are assigned provisionally as described in the text.

The average (0.02) plus standard deviation (0.02) was calculated to be 0.04 ppm, but was not drawn in **Figure V.23**. Since nine residues are omitted from the calculations because of exchange broadening and are presumed to show the largest chemical shift perturbations, the calculated average plus standard deviation could be misleadingly small.

Figure V.23 illustrates the chemical shift perturbations for those residues that were monitored throughout the titration, including a maximum observable chemical shift perturbation of 0.1 for residue K37.

For the fatty acid titrations (oleate and linoleate), the average plus standard deviation was of 0.18 ppm in both cases, with a maximum chemical shift perturbation of 0.7 ppm for D76 in both titrations. D76 is one of the residues that disappears upon gradual addition of the TDZ ligand, so it is not possible to compare chemical shift perturbation values among the three titrations. However, the location of the residues that are affected upon ligand binding in each of the three titrations will be compared later in this chapter. Mapping the chemical shift perturbations and the broadened residues onto the crystal structure will be presented in the discussion section.

(b) Titration (2): AFABP with TDZ dissolved in DMSO

The results of the titration of AFABP with TDZ from ethanol showed modest chemical shift perturbations (compared with titration of AFABP with other fatty acid ligands). Additionally, even though the titration reached a protein-to-ligand molar ratio of 1:3, the peaks continued to shift and showed no saturation. Moreover, the peak movement showed nonlinear behavior and changed direction toward the position of the original position of the apo peaks. Upon addition of the protein to the dried TDZ, some precipitation was observed; thus complete dissolution of the ligand could not be completely assured since it could be masked by the observed precipitation. For all these reasons, an additional titration was performed with a different solvent and technique to investigate the binding interactions between AFABP and TDZ.

In this second titration, TDZ was introduced into the protein solution after dissolution in DMSO, while a blank titration was also performed at identical protein concentration and NMR acquisition/processing parameters so that any effects of DMSO on the protein residues could be subtracted from the ligand effects.

HSQC spectra were recorded for the control experiment at each point equivalent to the titration of the ligand until the DMSO in the protein solution reached 6.5 % (equivalent to 1:1.6 protein-to-ligand molar ratio). Inspection of the NMR spectra showed a well folded protein with 20 residues showing subtle chemical shift changes by comparison with perturbations from the ligand experiment (with a maximum value of 0.03 ppm perturbation for residue L10 between apo and 6.5 % DMSO (1:1.5 protein-to-ligand molar ratio), while the remaining peaks exhibited no changes. **Figure V.24** shows an overlay of all blank points with DMSO at 0, 0.25, 0.5, 1.2, 1.8, 2.1, 3.4, 4.6 and 6.5 %, corresponding to the ligand titration points at 1:0 – 1:1.5 protein-to-ligand molar ratios.

Additional points with 8.3 %, 10.3 %, and 12.3 % DMSO (equivalent to molar ratios of 1:2, 1:2.5 and 1:3 protein-to-ligand) showed substantial broadening of all peaks in the spectrum that prevented clear determination of peak positions.

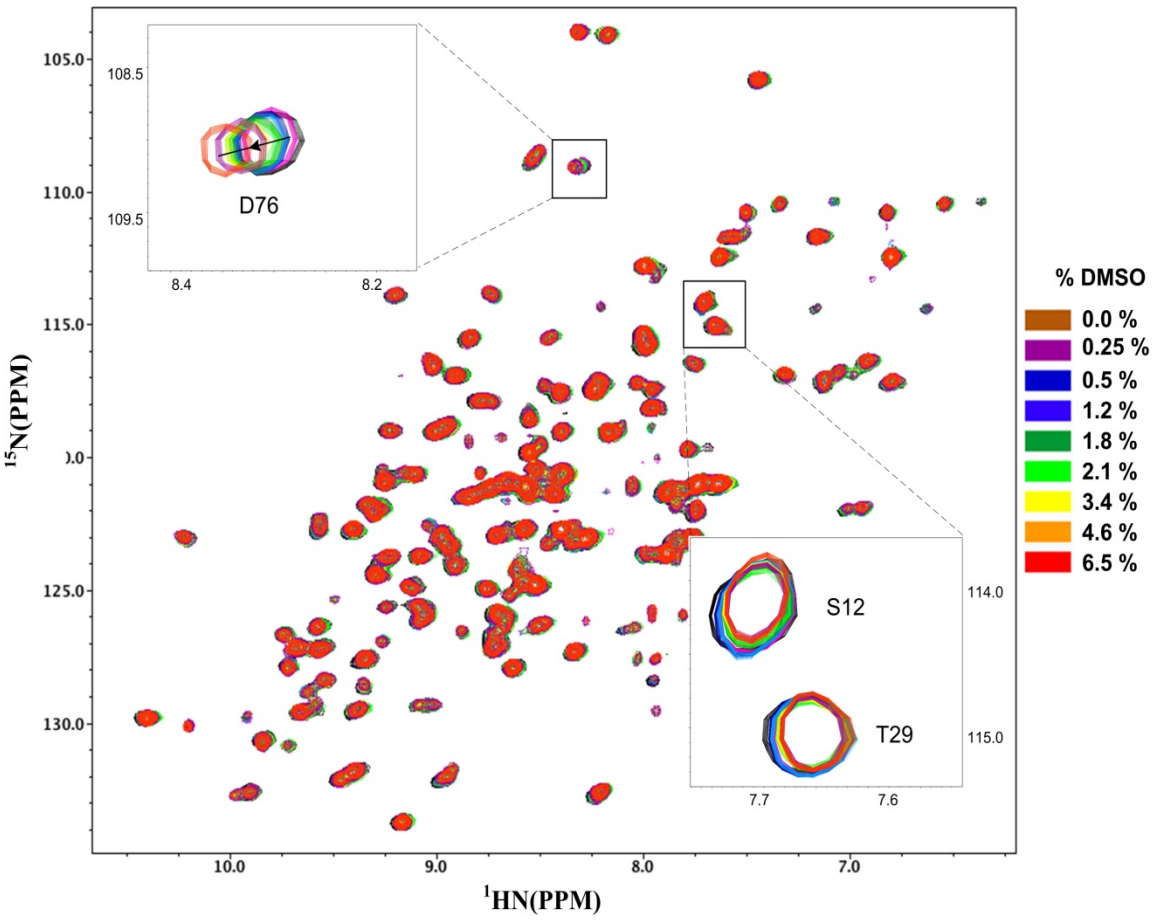

Figure V.24. Overlaid spectra of apo AFABP with stepwise addition of different DMSO percentages (0.0, 0.25, 0.5, 1.2, 1.8, 2.3, 3.4, 4.5 and 6.5 %) corresponding to that added for the ligand titration for TDZ at 1.0 - 1:1.5 protein-to-ligand molar ratios. The key shows colors used to display each point. Insets show different regions in the spectra that illustrate perturbation for residue D76 but not for residues S12 or T29.

The composite chemical shift perturbations were calculated between the apo and the last point recorded before strong broadening of the peaks in the control experiment (equivalent to 1:1.6 protein-to-ligand molar ratio). In this way the chemical shift perturbations were calculated for those residues that were affected by addition of DMSO at that point and could be subtracted from the composite chemical shift perturbations calculated for the ligand titration (described below).

Since AFABP has been reported to bind to only one molecule of ligand (Xu *et al.* 1992; Gillilan *et al.* 2007), the ligand experiment was designed originally to stop at a molar ratio of 1:3 (protein to ligand). However, the peaks were observed to continue to shift and showed no signs of saturation. Therefore the ligand titration was extended to higher molar ratios up to (1:15.0) in an attempt to assure completeness of the experimental procedure. However, all the peaks showed broadening and loss of intensity at later points of the titration, presumably due to the high proportion of DMSO added at these points. Preparation of a more concentrated ligand stock solution could have avoided addition of large volume aliquots at higher equivalents of ligand.

Even though 19 experiments were recorded for the TDZ in DMSO titration (1:0 - 15.0), the chemical shift perturbations could be compared for TDZ in DMSO (between apo and 1:1.5) and for TDZ from ethanol (between apo and 1:1.6) since the maximum chemical shift perturbation for both experiments was observed at these respective protein-to-ligand molar ratios (see discussion section).

Similar to the titration using TDZ from ethanol, an overlay of the spectra from addition of TDZ in DMSO shows well resolved peaks **Figure V.25 (top)**. Peaks corresponding to 50 residues decrease in intensity and some disappear at later points, indicative of an intermediate exchange mechanism. Twelve of these peaks experience so much broadening that they disappear and cannot be followed at later titration points. Exchange broadened and disappearing peaks in this titration are summarized in **Table**

V.2. Residue G34 in **Figure V.25 (bottom)** is given as an example to demonstrate the intermediate exchange regime and loss of intensity throughout the titration.

As for titration (1), some peaks show nonlinear directionality in movement, with the peaks returning toward the direction of the apo position for the later titration points. This change in direction can be demonstrated for G34 in the previous figure and in **Figure V.26,** where the peak corresponding to D17 first moves down followed by a movement to the left across the titration points.

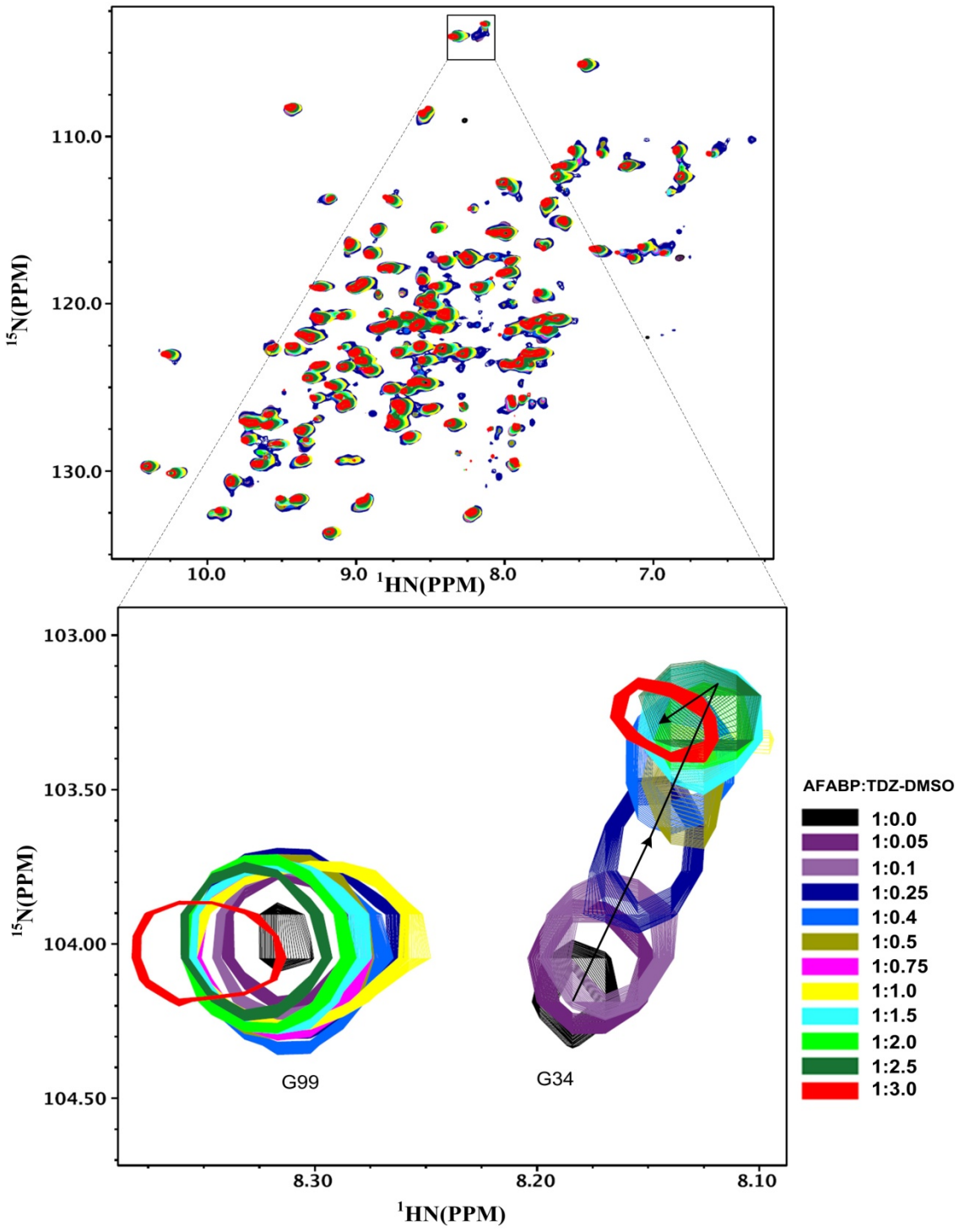

Figure V.25. (Top) An overlay of apo and holo points of the AFABP titration with TDZ (dissolved in DMSO). Color Key designates the color used at each titration point. (Bottom) Apo and holo peaks of residues G99 and G34 go into intermediate exchange and exhibit a change in direction of the peak from residue G34. The maximum perturbation of G34 corresponds to 0.9 ppm ^{15}N (12 points) and 0.064 ppm ^{1}H (5 points).

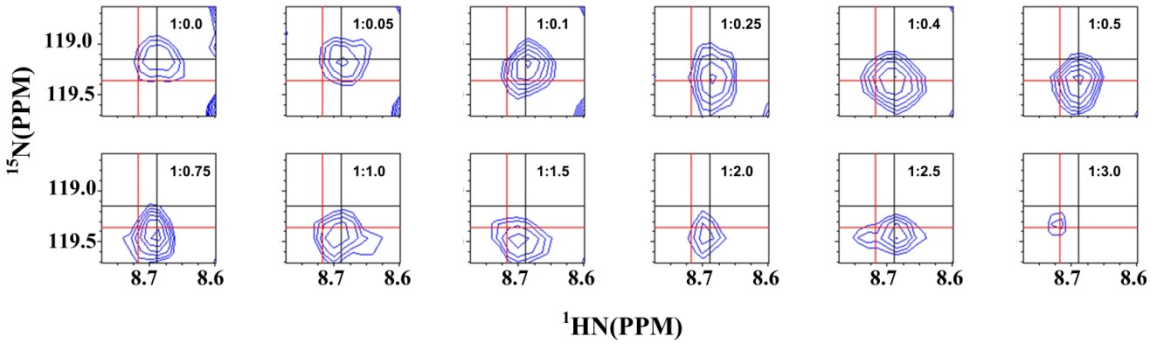

Figure V.26. Expanded region of [^{1}H-^{15}N] HSQC contour plots for residue D17 in AFABP upon titration with TDZ dissolved in DMSO. The apo peak is centered at the black cursor, and the holo (1:3.0) peak is centered at the red cursor. The plots show 10 titration points of protein-to-ligand ratios 1:0 - 1:3.0.

The composite chemical shift perturbations between apo and the titration point (1:1.5) were calculated, plotted and presented in **Figure V.27**. Chemical shift perturbations were omitted for twelve residues where the peaks disappear due to broadening upon the addition of the ligand and five unassigned residues. The twelve disappearing residues are given an arbitrary value of 0.5 ppm and highlighted in green color since they are presumed to be the most affected due to ligand binding. Similar to the TDZ in ethanol titration, residues that are unassigned are shown with a negative value of -0.01. Similar to the TDZ from ethanol titration, the average (0.03) plus standard deviation (0.03) that was calculated to be 0.06 is misleading since it does not include those nine disappearing residues that are most likely to be highly perturbed. Residue G34 shows the maximum observable perturbation of 0.15 ppm in this titration. The mapping of perturbed and disappearing residues on the crystal structure of holo (TDZ) AFABP will be presented in the discussion section.

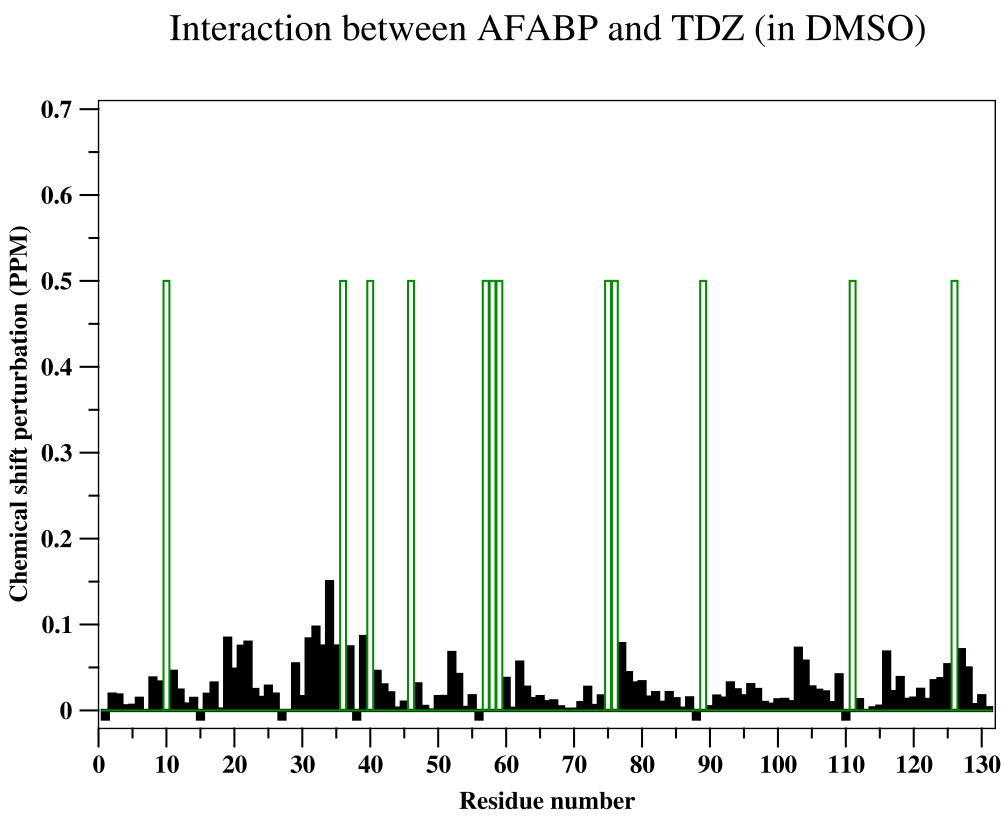

Figure V.27. Composite [^{1}H-^{15}N] chemical shift perturbations plotted along the protein sequence for AFABP. The perturbations were calculated for the molar ratio 1:1.6 protein-to-ligand. Residues that disappeared due to intermediate exchange broadening are assigned an arbitrary value of 0.5 ppm and highlighted in green color. The same scale is used as titrations (oleate and linoleate) illustrated in previous sections of this chapter. The average value is intentionally omitted from the figure (see text). Negative values indicate residues that are unassigned. Residues Y19 and T103 were assigned provisionally as described in the text.

3. Discussion

In order to study the effect of troglitazone (TDZ) on AFABP, two titration procedures were carried out. In each of those titrations, an organic solvent was used to introduce the ligand into the protein solution. In the first titration, TDZ was dissolved in ethanol; then the organic solvent was evaporated prior to addition of the protein solution onto the dried ligand to eliminate solvent effects on AFABP. In the second titration, TDZ was dissolved in DMSO and a blank experiment was performed in order to evaluate and subtract the solvent effect from the ligand-solution titration.

(a) Binding of TDZ from Ethanol

Throughout the titration of AFABP with TDZ dried from ethanol, nine residues exhibited broadening and loss of intensity upon gradual addition of ligand, indicative of an intermediate exchange mechanism (**Table V.2**). These resonances, which did not reappear at later stages of the titration, are presumed to exhibit a large chemical shift perturbation due to ligand binding and thus correspond to the most interesting backbone sites.

The chemical shift perturbation observations and mapping of the perturbed and disappearing residues onto the crystal structure of holo (TDZ) AFABP (Gillilan *et al.* 2007) define the binding site location (**Figure V.28**). The location of six of the nine disappearing residues (colored red) and most of the perturbations (shown by the thickness of the sausage) overlap with the portal region involving α_{II} (27-35) and turns between β_C-

β_D (55-58) and β_E-β_F (74-78) (Reese-Wagoner *et al.* 1999). While A36 and M40 lie close to the portal region, residues L10 and D111 lie outside of the portal region and may be perturbed due to other factors as discussed below.

Table V.2 Summary of intermediate exchange-broadened peaks in titrations of AFABP with TDZ dried from ethanol and TDZ dissolved in DMSO. Residues that disappear in only one titration are underlined.

	AFABP – TDZ dried from Ethanol titration	AFABP – TDZ dissolved in DMSO titration
Disappearing peaks	9 residues: L10, A36, M40, F57, K58, N59, A75, D76, D111	12 residues: L10, A36, M40, G46, F57, K58, N59, A75, D76, G89, D111, R126

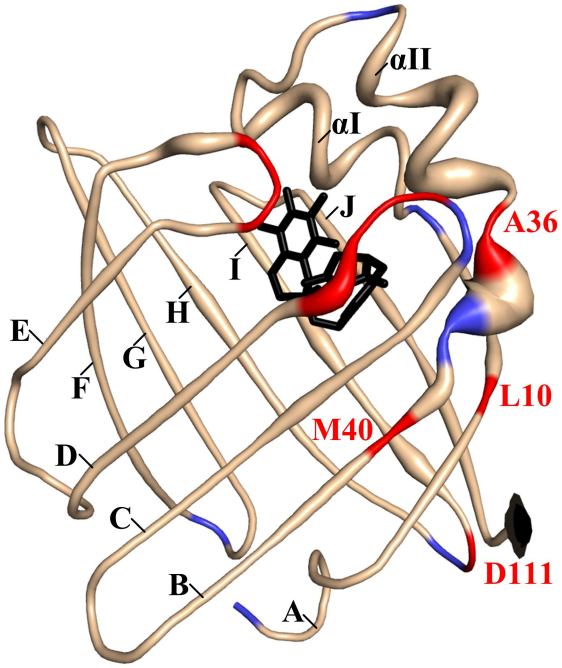

Figure V.28. Sausage/putty representation showing the chemical shift perturbations of AFABP titration with TDZ dried from ethanol mapped onto the x-ray structure of holo AFABP (PDB: 2QM9, Gillilan et al 2007). The thickness of the sausage plot is proportional to the value of perturbation for each residue. The minimum and maximum cutoff for the thickness of the putty are 0.0 and 0.7, respectively, similar to the oleate and linoleate titrations for comparative analysis. Unassigned residues are colored purple, while exchange broadened residues are colored red. Ligand position in the crystal is displayed in black.

Additionally, many peaks exhibited continuous but nonlinear shifts in peak position, even returning back in the direction of the apo location and failing to show saturation upon addition of ligand. The change in direction of peak movement is observed to start after 1:1.5 molar ratio of protein-to-ligand (at which point the maximum chemical shift perturbation occurs for most residues). Beyond this molar ratio the chemical shift perturbation decreases in magnitude as the peaks go back toward the apo position. These phenomena cannot be attributed to the ligand dissociating from the binding site when added in excess. TDZ was reported to bind tightly with AFABP with a dissociation constant of 17 nM (Gillilan et al 2007) and therefore all available ligand should be bound to the protein and cannot dissociate at the 200 – 700 μM concentration range used in this experiment. Thus it is not clear why the peaks retract back toward the apo position.

At the first points of adding the protein to the dried ligand, ligand crystals were observed to swirl around the solution, then eventually disappear as an indication of ligand's crystal dissolution, hence protein uptake. At the following points, as some precipitation occurred, it is possible that any ligand precipitation was masked by protein precipitation and could not be monitored visibly. Protein precipitation and loss of protein volume while performing the titrations are both factors that could contribute to changes in the protein-to-ligand molar ratios but are difficult to assess when they are combined. These factors may lead to discrepancies between actual and calculated protein-to ligand molar ratios in the sample. While the protein may not be saturated at a high added molar

ratio of ligand due to unavailability of the ligand in solution, this does not explain why the peaks retract back and do not keep moving in the same direction.

(b) Binding of TDZ dissolved in DMSO

For the titration of AFABP with TDZ dissolved in DMSO, two experiments (ligand and control blank) were planned to be performed successively for molar ratios of 1:0 – 1:3.0 in order to subtract the DMSO effect from the ligand titration and therefore analyze the sole TDZ binding effect on the protein. While performing the ligand experiment, the protein behaved very well with addition of the DMSO-ligand mixture: the spectra did not show any global broadening which would indicate solvent effects on the protein such as unfolding. Upon examining successive spectra (up to the protein to ligand molar ratio 1:3) that did not show saturation but demonstrated continuous movement of the peaks, the experiment was extended to a protein to ligand molar ratio of 1:15.0. At that ratio, all the peaks exhibited extensive broadening due to the high proportion of added DMSO. The peaks that disappeared did not reappear with excess added ligand. Although the peaks continued to move gradually back towards the apo peak position, they did not reach the position of the apo peaks. This indicates that the protein did not reach ligand saturation as mentioned for the TDZ-ethanol titration.

Even though the control blank titration was planned to be performed in the same molar ratios as the ligand experiment (up to 41 % DMSO), the spectra showed extensive broadening suggestive of protein destabilization starting at a molar ratio of 1:2.0 (8.3 % DMSO). The experiment was stopped at a molar ratio of 1:3.0 (with the last two spectra

showing extensive broadening). Maximum chemical shift perturbation of residues was observed at 1:1.5 molar ratio protein-to-ligand, after which the peaks started to move back toward the apo position, so it was possible to subtract the DMSO effect from the ligand titration at that ratio. The well behaved protein in the ligand titration and tolerance of the protein to large percentages of DMSO in solution validated the use of this solvent to introduce the TDZ ligand and make corrections for its presence in the protein solution. However, it was unexpected to see the protein exhibiting such a global broadening with the addition of DMSO alone since the protein spectra looked well resolved upon addition of a large proportion of TDZ-DMSO in solution.

Figure V.29 shows that the broadening effect of 12.3 % blank-DMSO (**e**) (1:3.0 protein-to-ligand molar ratio) is slightly more profound than the broadening effect of TDZ-DMSO at 41 % DMSO (**c**) (1:15.0 protein-to-ligand molar ratio). It is possible that the ligand coupled with DMSO protects the protein from the effects of the solvent: for instance by dissolving TDZ, DMSO may be interacting with the ligand and becomes less available to interact or destabilize the protein. This possible explanation offers a reason why the titration of TDZ dissolved in DMSO exhibits an effect that is different from the blank experiment. Additionally, the TDZ-DMSO aliquot additions and experiments were completed within a three-week time frame and the TDZ was kept solubilized for a longer time than the DMSO in the stock solution until the last TDZ-DMSO NMR spectrum was recorded. Since the manufacturer's MSDS (material safety data sheet) advises keeping the ligand solubilized for no longer than a week, it is possible that the ligand stability and

properties were affected in the TDZ-DMSO leading to the observed behavior in this titration.

Mapping the chemical shift perturbations and the residues which go into intermediate exchange onto the holo (TDZ) crystal structure (Gillilan *et al.* 2007) shows qualitatively the location of these residues that are most affected by ligand binding (**Figure V.30**). Together, the disappearing residues and those exhibiting the largest observable perturbations constitute the binding site. Some of the disappearing residues (F57, K58, A75, D76) and many perturbed ones are localized at α_{II} (27-35) and turns between β_C-β_D (55-58) and β_E-β_F (74-78) i.e. in the portal region (Reese-Wagoner *et al.* 1999). A36 and N59 are neighboring to the portal region, and disappearing residues L10, M40 and R126 are located in the middle of β-strands β_B and β_J, respectively, that is close to the ligand location in the crystal structure. However, residues G46, G89 and D111 exist in β-turns between β_B-β_C, β_F-β_G and β_H-β_I and are not in close proximity to the ligand in the crystal structure. The location of the perturbed residues could be interpreted as those that constitute the binding site and lie in close proximity to the ligand, and several that lie far from the ligand (G46, G89 and D111) and are presumed to be perturbed due to a conformational change in the protein.

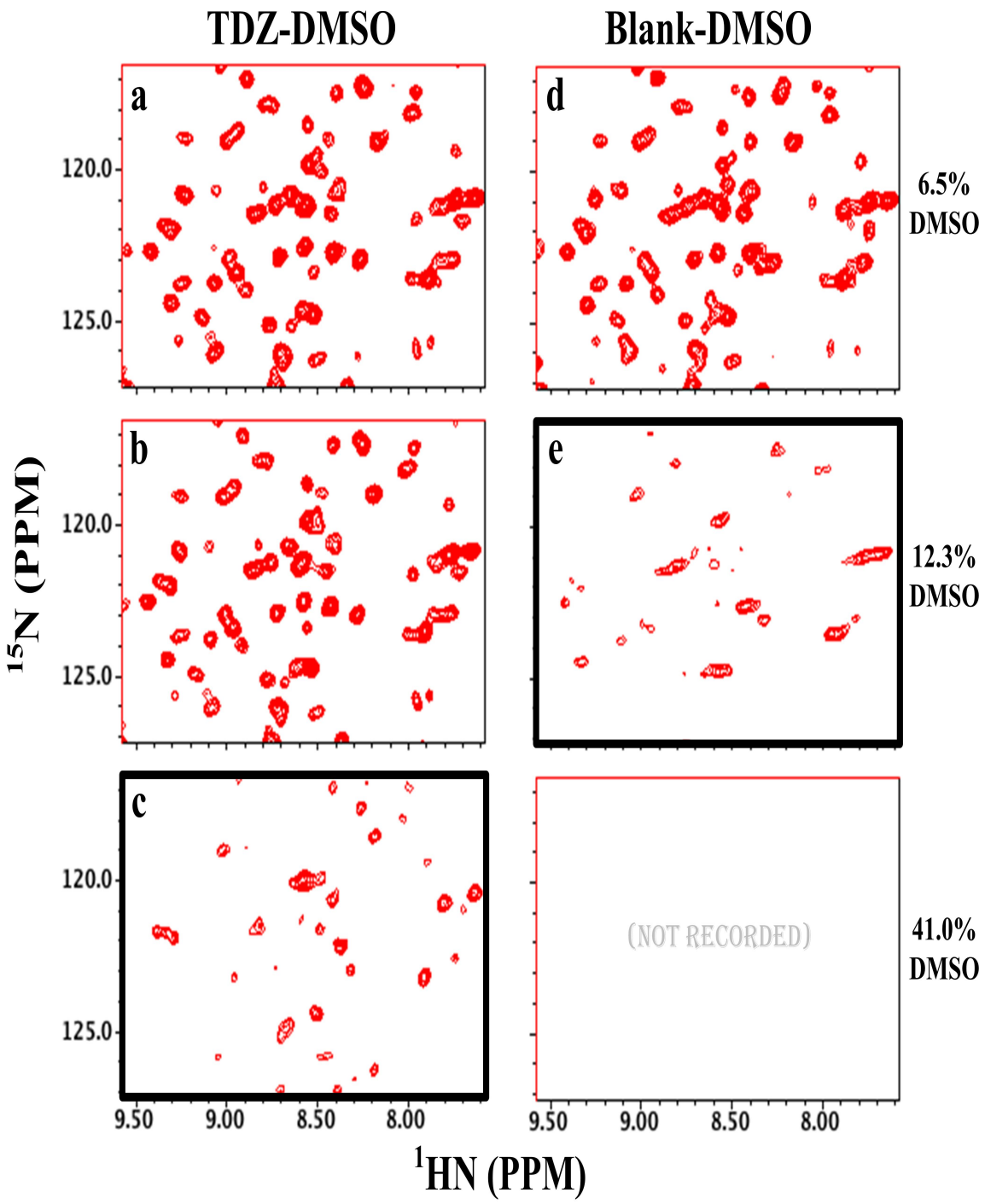

Figure V.29. Expanded regions of HSQC spectra for AFABP with TDZ ligand experiment (left side) with molar ratios of (a) 6.5 %DMSO, (b) 12.3 %DMSO, (c) 41 % DMSO, and blank control experiment (right side) (d) 6.5 % DMSO, (e) 12.3 % DMSO. The spectra demonstrate the more severe deterioration of protein quality in the blank experiment as compared with the experiment containing ligand dissolved in DMSO. 6.5, 12.3 and 41 % DMSO correspond of protein-to-ligand molar ratios 1:1.5, 1:3.0 and 1:15.0, respectively. (c) and (e) are highlighted for comparison.

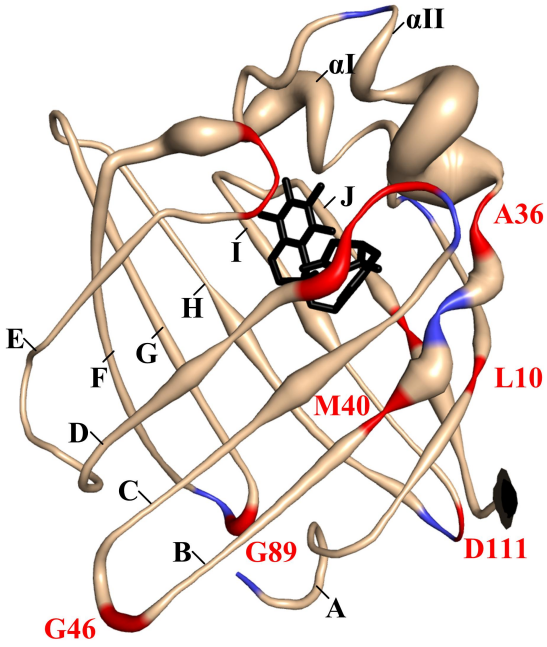

Figure V.30. Sausage/putty representation showing the chemical shift perturbations of titrating AFABP with TDZ dissolved in DMSO mapped onto the x-ray structure of holo AFABP (PDB: 2QM9, Gillilan et al 2007). The thickness of the sausage plot is proportional to the value of perturbation of each residue. The minimum and maximum cutoff for the thickness of the putty and the color gradient are 0.0, and 0.7, respectively, similar to the oleate and linoleate titrations for comparative analysis. Unassigned residues are colored blue, while exchange broadened residues are colored red. Ligand is displayed in black.

(c) Contrasting TDZ Titrations

By comparing the titrations using TDZ dried from ethanol and TDZ dissolved in DMSO, it seems that, qualitatively, TDZ in DMSO has a more profound effect on AFABP than TDZ dried from ethanol. While the observed differences in the magnitude of the chemical shift perturbation between the two titrations are subtle, three additional disappearing residues (G46, G89 and R126) are observed in TDZ-DMSO. These differences are highlighted by a chemical shift perturbation plot (**Figure V.31**). Although the difference is very small (maximum of 0.07 ppm), the differences between the two

titrations can be observed and are discernible in the α_{II} region (residues 27-35) and in the last one third of the protein sequence.

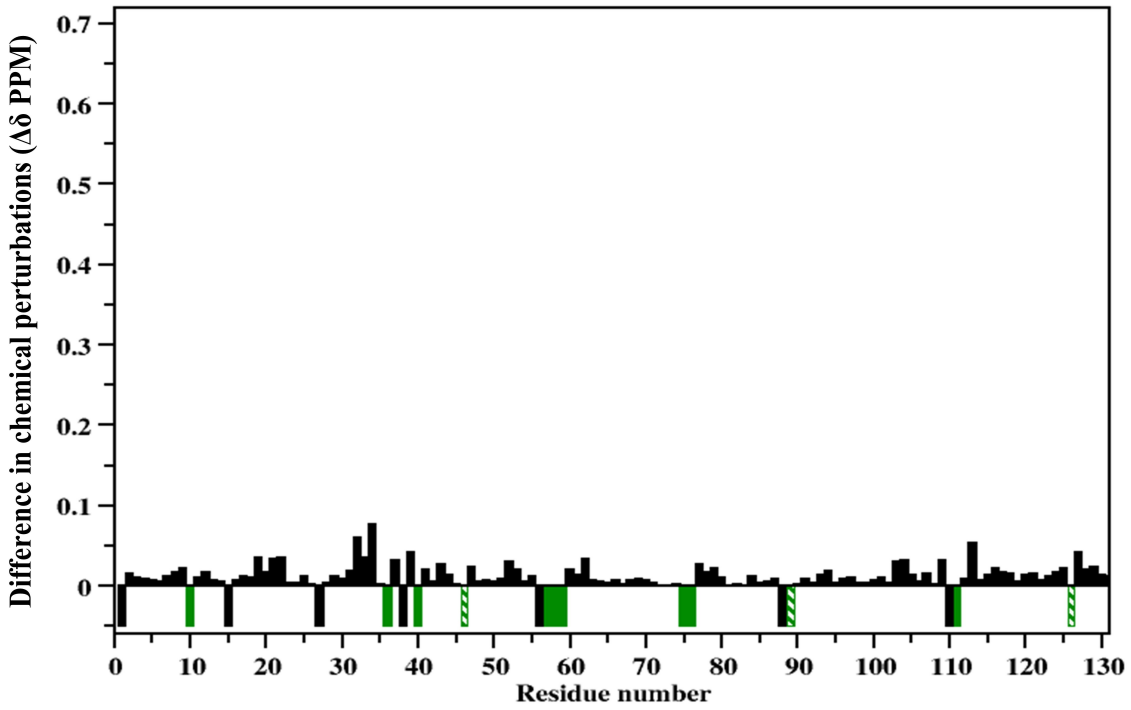

Figure V.31. The difference in chemical shift perturbations (ΔδPPM) between titrations of TDZ dried from ethanol and TDZ dissolved in DMSO, with the AFABP protein sequence plotted on the x-axis. Disappearing and unassigned residues are assigned a negative value. Disappearing residues in both titrations are represented in solid green, while disappearing residues in TDZ-DMSO only are colored striped green. Unassigned residues are colored black. The vertical scale is set to facilitate comparison with the fatty acid titrations illustrated in Figures V.23 and V.27.

In both TDZ titrations, the residues that exhibit the largest measurable perturbations together with those that broaden constitute the binding region. Nonetheless, the observation of three perturbed protein residues that are located far from the position of the ligand in the crystal structure suggests additional conformational changes upon ligand binding: for instance D111 is located in the β-turn connecting β_H-β_I,

whereas the remaining perturbed residues constitute a single defined locus. Some of these perturbed residues are located in the portal region, which involves helix α_{II} (27-35) and turns between β-strands β_C-β_D (55-58), and β_E-β_F (74-78) (Xu *et al.* 1993; Reese-Wagoner *et al.* 1999). **Figure V.32** shows that the location of the perturbations is very similar as judged from both titrations. Qualitatively the TDZ-DMSO displays more disappearing residues than TDZ-ethanol. Differences between the perturbations observed in the two titrations, judged by comparing the thickness of the sausage representations in **Figure V.32**, are evident mainly in the α_{II} helix (as also seen in the chemical shift difference plot, **Figure V.31**) but these differences in magnitudes of perturbations are subtle since they are less than 0.1 ppm (**Figure V.31**). G46, G89 and R126 disappear exclusively in the TDZ-DMSO titration and are located in the β turns connecting β_C-β_D and β_F-β_G, respectively (**Figure V.32.b**). It is not understood why these three residues behave differently in the two TDZ titrations, but it is clear that the TDZ has a different effect than the dried ligand, in some way associated with the presence of DMSO.

Despite the differences noted above, there are many similarities between the two TDZ titrations. Even though three residues exchange-broaden and disappear in the TDZ-DMSO titration exclusively, nine residues exchange broaden extensively such that they disappear upon gradual ligand addition in both TDZ titrations, suggesting that the effect of TDZ binding in both titrations is largely similar. Moreover, residues that show the largest observable perturbations demonstrate a comparable magnitude of perturbation. This similarity in the magnitudes of TDZ perturbations is highlighted upon roughly

comparing them with higher magnitudes of the chemical shift perturbations for the fatty acid titrations (a standard deviation above the average of 0.18 ppm for FA chemical shift perturbation compared with 0.04 and 0.06 for TDZ-ethanol and TDZ-DMSO, respectively; see following sections). Despite small variations in magnitudes between the two TDZ titrations, it is possible to consider that the two titrations are fairly similar in overall effect and magnitude.

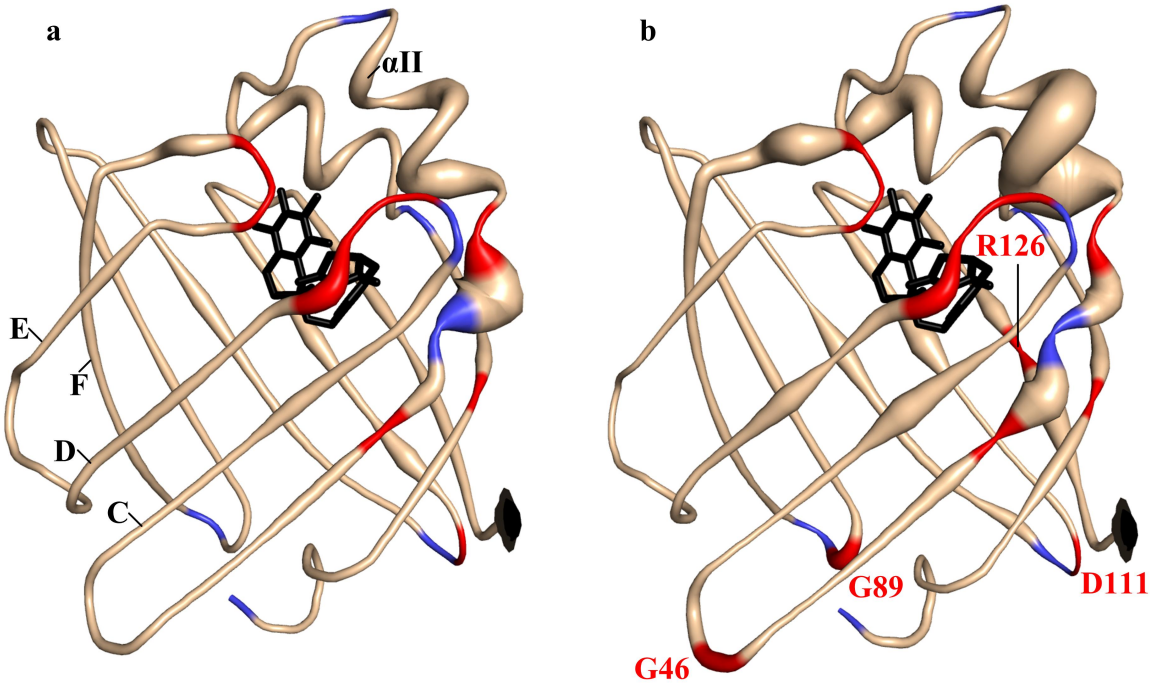

Figure V.32. Sausage/putty representation showing the chemical shift perturbations of titrating AFABP with TDZ dried from ethanol (a) and TDZ dissolved in DMSO (b) mapped onto the x-ray structure of holo AFABP (PDB: 2QM9, Gillilan *et al.* 2007). The thickness of the sausage plot is proportional to the value of perturbation of each residue. The minimum and maximum cutoffs for the thickness of the putty are 0.0, and 0.7, respectively, similar to the oleate and linoleate titrations for comparative analysis. Unassigned residues are colored blue, while exchange broadened residues are colored red. Ligand is colored black.

(d) Structural Rationale for TDZ Perturbations

It is possible to combine results from both TDZ titrations (TDZ-ethanol and TDZ-DMSO) to assess the structural effect of TDZ binding on AFABP. Nine residues disappear in both titrations (L10, A36, M40, F57, K58, N59, A75, D76, D111) and three (G46, G89 and R126) disappear only in the TDZ-DMSO titration. It is possible to then deduce that those nine disappearing residues are definitely affected due to the TDZ binding, while the three disappearing only in TDZ-DMSO are less certain. Therefore a binding site defined by the combined results comprises nine disappearing residues and possibly the three additional residues (**Figure V.33**).

By mapping the affected residues, the binding site could be defined. These nine residues are observed to be within close proximity to TDZ in the protein crystal (**Figure V.33**). Three additional ambiguous residues are affected by the binding, while two of the three ambiguous ones (colored magenta) lie far from the ligand and could possibly be perturbed due to either a secondary effect or a confomational changes induced in the protein by the ligand binding. A binding pocket can be observed surrounding the ligand and localized near those ten residues. Since TDZ is a bulky ligand, perturbations are seen to span the turns connecting β-strands β_C-β_D and β_E-β_F. and in β-strands β_A and β_B but It was expected to observe more perturbations in the ligand binding site that would relate to the bulkiness of the ligand.

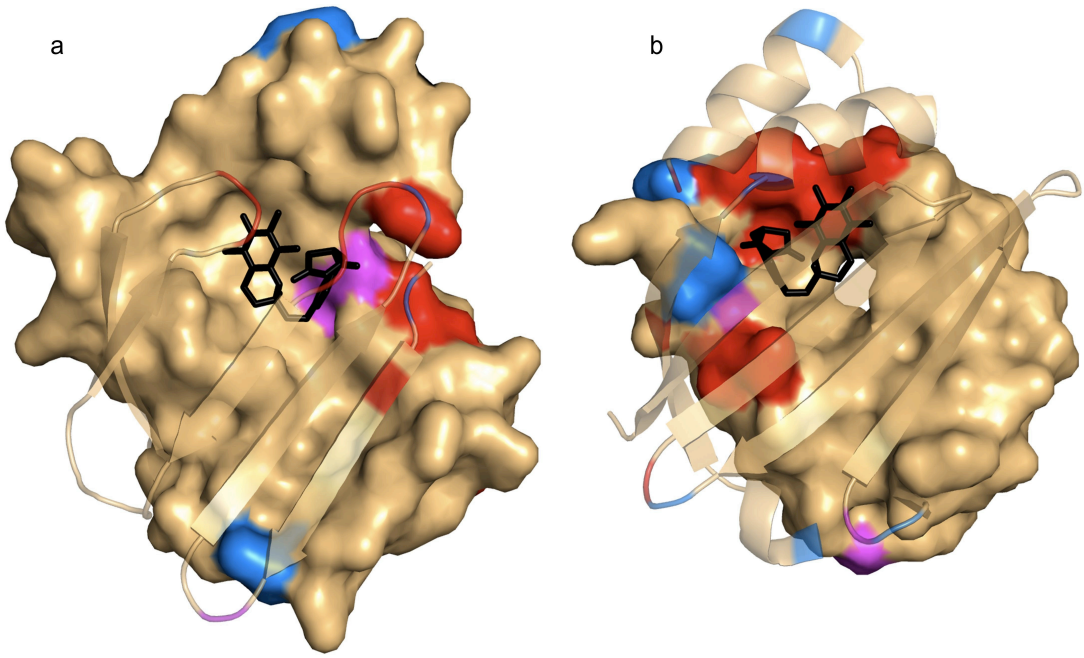

Figure V.33. Surface representations of the mapping of residues (in red) presumed to be highly affected in TDZ titration on the x-ray structure of holo (TDZ) AFABP (PDB: 2QM9, Gillilan *et al.* 2007). Residues that disappear in only one titration and are therefore considered ambiguously affected by ligand binding are colored in magenta, while unassigned residues are displayed in blue.

By comparing our NMR results to published X-ray data for the holo (TDZ) structure, it becomes clear that some of our data agree with the published information (Gillilan *et al.* 2007) while others do not. Many of the disappearing residues lie in close contact with the thiazolidinedione ring of TDZ in the crystal structure and may be affected directly or indirectly by the position of the ligand inside the binding cavity. For instance, the distances between those nine highly affected residues and the ligand (**Table V.2**) were measured for the published holo (TDZ) crystal structure using PyMOL (**Table V.3**) in order to assess the proximity of these residues to the ligand in the crystal structure. Some residues, such as F57, K58, N59, A75 and D76, lie within 6 Å from the ligand in the crystal structure and should be affected by ligand binding, while some of our

highly affected residues lie far from the ligand (G46, G89 and D111). It is possible that the amide groups of these residues are affected as a secondary effect and not directly by interacting with the ligand in solution or that the TDZ location differ in solution and crystals.

Table V.3 Shortest amide nitrogen – ligand carbon distances between residues that disappear from our NMR titration data and ligand in published crystal structure of holo (TDZ) AFABP (Gillilan *et al.* 2007).

Residue Type and number	X-ray Distance (Å) between N of residue & the nearest atom of the ligand
L10	8.9
A36	8.3
M40	7.0
G46	22.3
F57	5.5
K58	4.3
N59	5.1
A75	6.0
D76	5.1
G89	18.6
D111	17.8
R126	7.6

While the two crystal structures were obtained under different crystallization conditions, a comparison of the apo AFABP (Xu *et al.* 1993) and holo (TDZ) AFABP

(Gillilan *et al.* 2007) crystal structures showed substantial similarities in overall fold that permit us to compare them. A novel hydrogen bond was found to be formed between the amide nitrogen of residue L10 and carbonyl group of P38 in the holo structure but not in apo-AFABP (**Figure V.34**). This newly formed hydrogen bond agrees with our solution-state NMR observations of a significant change in the local environment of residue L10 when the ligand is bound, leading to a large chemical shift perturbation.

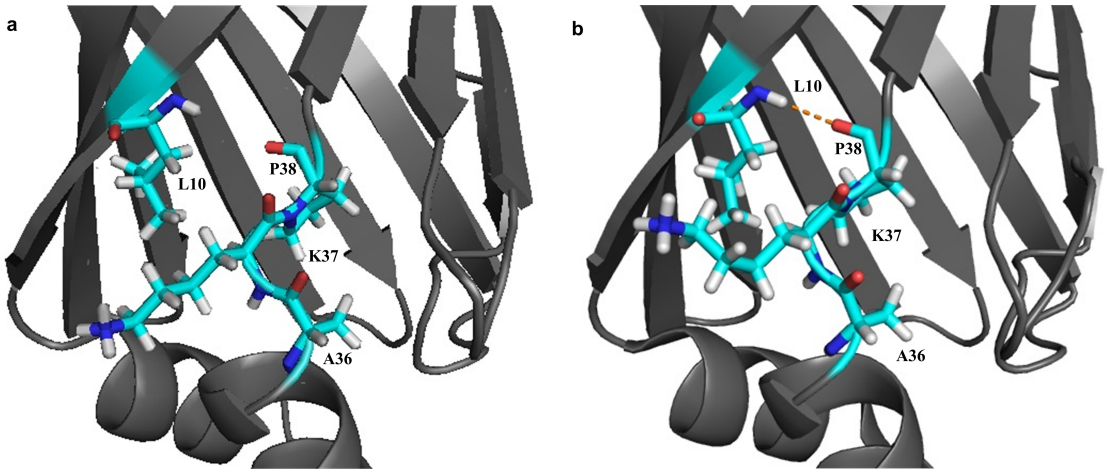

Figure V.34. Comparative PyMOL representations of apo (left) and holo TDZ (right) AFABP structures, demonstrating the presence of hydrogen bond uniquely in the holo complex. The hydrogen bond between $L10_N$ and $P38_{CO}$ is colored red, but the ligand is not shown in the figures.

A LigPlot schematic representation was used to provide a 2D view of the residues that are involved with the ligand binding via hydrogen bonding or hydrophobic interactions (Laskowski *et al.* 2011), where **Figure V.35** is based on the holo (TDZ) AFABP crystal structure (Gillilan *et al.* 2007). 15 residues interact with the ligand hydrophobically and three residues interact with the ligand via hydrogen bonding (**Table V.4**).

Table V.4 Summary of residues that interact with TDZ via hydrophobic interaction and hydrogen bonding based on LigPlot data.

Residues that make hydrophobic interactions based on LigPlot data	Residues that interact via hydrogen bonding based on LigPlot data
15 residues: F16, Y19, M20, V25, P38, E54, F57, K58, A75, D76, R78, I104, C117, R126 and Y128	3 residues: S53, S55 and T60

Among the 15 residues that are shown to make hydrophobic contacts with TDZ from LigPlot analysis, our NMR data show that four residues (F57, K58, A75 and D76) are highly affected by ligand in both TDZ titrations, while one more (R126) disappears only for TDZ dissolved in DMSO. The remaining residues identified by LigPlot (excluding P38) show only subtle chemical shift perturbations.

In the crystal structure, S53 and T60 form hydrogen bonds with two oxygen atoms in the thiazolidinedione (TZD) ring, while S55 interacts via formation of a hydrogen bond with the TZD ring's nitrogen atom. These three residues show very subtle perturbations in the NMR titrations of TDZ (less than 0.07 ppm). Even though the distances between their hydroxyl groups and the ligand hydrophilic groups are 2.5, 8.6 and 2.6 Å for S53, S55 and T60, respectively, our NMR measurements are sensitive to changes in chemical environment at the amide groups of each residue and not at the side chains. Whereas hydrogen bond formation involving the amide group of L10 led to a large chemical shift perturbation, hydrogen bond formation through the side chains of S53, S55, and T60 did not produce a change in the chemical environment of their respective amide groups in either titration.

As noted above, some of the x-ray data involving the holo (TDZ) AFABP agree with our NMR data, but others do not. Some of the disappearing residues lie in close proximity in the crystal structure and therefore are in agreement between the data. Additionally, while residue L10 disappears in the titration, and forms a novel hydrogen bond in the crystal stuucture data, other disappearing residues lie far from the ligand on the crystal structure. Despite being similar in location, the ligand binding site obtained from NMR titration data appears more localized in comparison with the one obtained from the crystal sturucture, which is larger and includes more residues. Studying the binding by NMR allowed for investigation of the AFABP-ligand interaction and location in solution and close to physiological conditions for the protein, while the structural information previously reported on the holo (TDZ) AFABP sheds light on the protein in crystal form and under conditions with low ionic strength (Gillilan *et al.*).

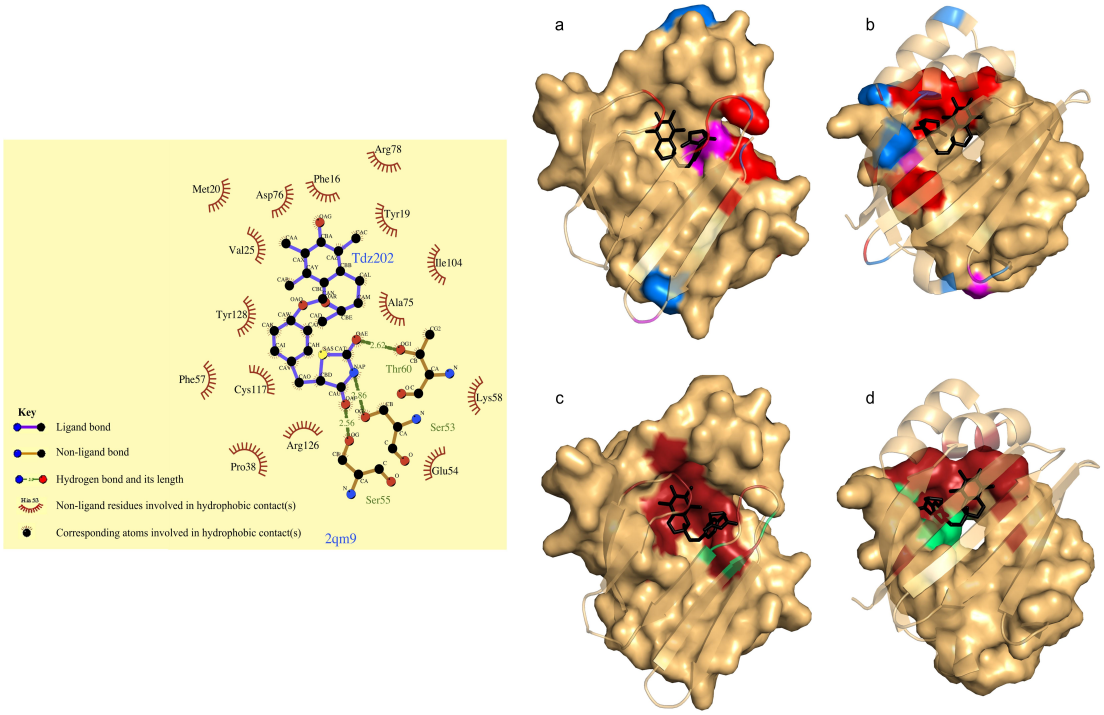

Figure V.35. (left) Schematic representation from LigPlot showing residues that are involved with ligand binding, based on AFABP (TDZ) holo crystal structure (PDB 2QM9; Gillilan *et al.*, 2007). (a and b) Mappings of the involved residues on holo (TDZ) crystal structure from the NMR data in red and magenta and unassigned residues are colored blue. (c and d) LigPlot data is displayed in surface representation where affected residues are shown in deep red and residues deduced to interact by hydrogen bonding with the ligand in green.

Mapping of these residues on the holo (TDZ) crystal structure reveals their location on the tertiary structure of the holo protein (**Figure V.35, c and d**). By comparing the LigPlot predictions derived from the crystal structure (**Figure V.35**, **c and d**) and the perturbations observed in solution by NMR (**Figure V.35 a and b**), both similarities and differences are noted. The binding site locations deduced from LigPlot analysis of the crystal structure data and from our NMR data look roughly similar. Nevertheless, from the NMR data, the binding site appears to be smaller: the α-helices appear unaffected in solution, while α_I is involved in the binding based on LigPlot

information. Moreover, while residues F57, K58, A75 and D76 on the β-turns are similarly involved in the binding, residues on the back face of the protein are affected in the crystal structure, but are not perturbed in solution. Additionally, it appears that the protein demonstrates an indirect effect due to ligand binding, witnessed by the chemical changes that occur at distant sites from the ligand.

Since we are studying the protein in solution, the protein and the ligand have more freedom to demonstrate an indirect effect due to ligand binding or to undergo a conformational change versus studying the protein in crystal form. Studying the holo protein crystal precludes flexibility that would allow some conformational changes for a protein in solution.

In addition to these contrasts in binding locus, Gillilan *et al.* reported that it was possible to saturate the protein with TDZ during the crystallization process, contrasting with our failure to observe protein saturation despite adding excess ligand in both TDZ titrations. While similarities are observed between our NMR data and the crystal structure, their crystallization conditions were in low salt and 5 % ethanol buffer and very different from the near-native medium of protein in solution. This could result in differences in the bound structure between the crystal structure and in solution, which may lead to changes in chemical environment of the residues in solution that are not seen based on the crystal structure or vice versa. Since we are studying the protein in solution by NMR, it was important to keep in mind when comparing with published crystal

structure data that some ligand-protein proximities are not picked up by NMR shift perturbations if the chemical environment of the residues' NHs are not affected. Additionally, some perturbations are secondary to the binding and thus may occur at distant sites in addition to those at the binding interface.

In summary, the TDZ titration allowed us to define a locus that is involved in the binding. Nine residues were highly affected by the binding and three ambiguously affected. Some of these residues are close to the ligand in the crystal; they define the binding pocket, which is small in size compared with the bulkiness of the ligand. Moreover, the NMR defined binding site was restricted in the β barrel and did not involove the α helices. Additionally, when compared with the structure, the defined binding site obtained from our NMR data appeared similar but smaller in size. Finally some affected residues of the protein were in far from the ligand and may be attributable to either a secondary and indirect effect of ligand binding or to a conformational change.

E. Comparative Analysis of Oleate, Linoleate and TDZ Interactions with AFABP

After performing titrations of the three ligands (oleate, linoleate and TDZ) (**Figure V.36**) on AFABP, it was important to compare the three modes of binding in light of their contrasting metabolic consequences.

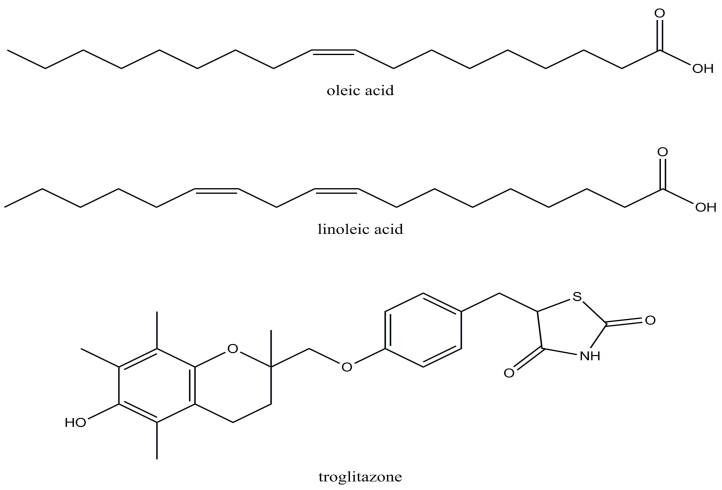

Figure V.36. Structure of the three ligands: oleic acid, linoleic acid and troglitazone.

The titrations were performed using different protein concentrations and molar ratios, but it is possible to compare the bound states of the protein since in the fatty acid titrations the protein was fully saturated. While the two TDZ titrations (using TDZ evaporated from ethanol and TDZ dissolved in DMSO) did not reach full saturation with ligand, it was still possible to assess the effect of the ligand binding on the protein. In both titrations, extra ligand was added that reached more than 1:3 protein to ligand molar ratio. Since the stoichiometry of ligand to protein is 1:1 in AFABP, and since AFABP is reported to have high affinity to TDZ (K_d is 17 nM, (Gillilan *et al.* 2007)), this molar

ratio is well above that required for saturation of protein. Comparing the data from the three ligand titrations helped to identify the residues that are most affected by each ligand and therefore to determine the respective binding regions.

1. Structural Comparison of Oleate, Linoleate and TDZ Binding with AFABP

Pairwise comparisons between titration of AFABP with different ligands were done in order to assess the implications of each binding on the protein.

(a) Comparison between Oleate and Linoleate Titrations

The composite chemical shift perturbation calculations and mapping on the respective holo crystal structures highlighted the differences and similarities between the binding of each ligand with AFABP. The composite chemical shift perturbation calculations showed an average of 0.08 ppm and a standard deviation of 0.1, making the standard deviation plus average equal to 0.18 in both titrations. Eleven and thirteen residues were significantly perturbed in the oleate and linoleate titrations, respectively (**Figure V.37 a and b**). The eleven perturbed residues in the oleate titration (L10, Y19, A33, M35, N39, M40, S55, F57, N59, A75 and D76) are similarly perturbed in the linoleate titration in addition to two residues (G34 and E54) that are above the perturbed threshold only in linoleate. However, those two residues are very close to being significantly perturbed for oleate as they have magnitudes of perturbations (0.17 and 0.16) ppm, respectively, that are close to the average plus standard deviation of (0.18

PPM), as shown in **Figure V.37**. The difference between the chemical shift perturbations in the two titrations after the data were normalized is shown in (**Figure V.37c**). The differences are very modest, highlighting the similarities between the two fatty acid titrations.

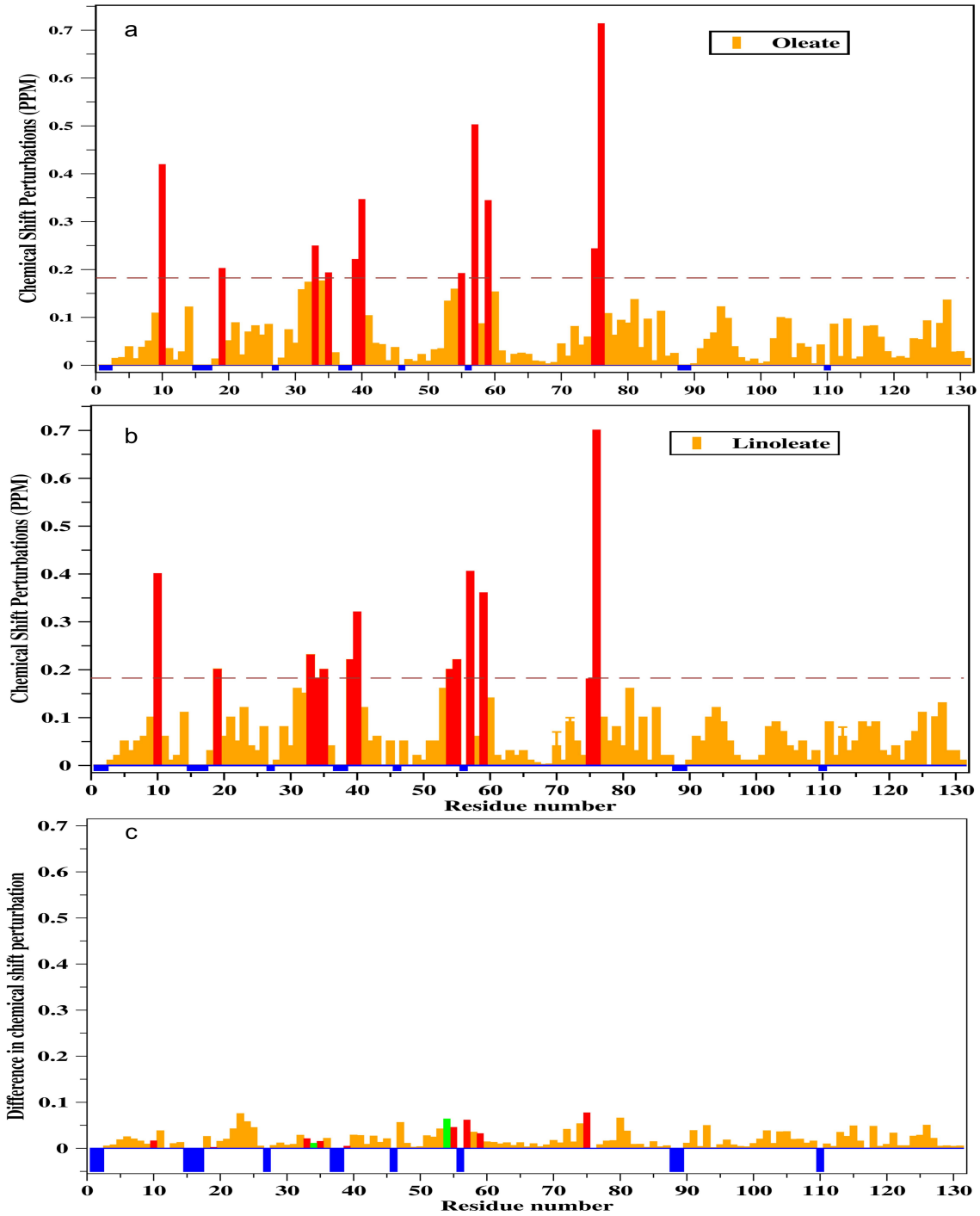

Figure V.37. Plots showing chemical shift perturbations for oleate (a) and linoleate (b). Significantly perturbed residues are colored red, while unassigned ones are displayed in blue and assigned a negative value. Dashed line is drawn across each plot at 0.18 ppm respresenting one standard deviation above the average. (c) Normalized chemical shift perturbation difference between oleate and linoleate titrations. Same color scheme is used as in (a) and (b), with those residues significantly perturbed only in linoleate titration colored in green.

Mapping of the perturbed residues on the crystal structure shows that the binding of those two fatty acid titrations affects similar locations on the protein (**Figure V.38**). The two additional residues (G34 and E54) are in the same region as the other eleven common to both oleate and linoleate. Therefore the two titrations are very similar and define a similar binding site with AFABP despite the fact that the two fatty acids elicit two contrasting functional behaviors of AFABP based on published reports (Gillilan *et al.* 2007).

Mapping the perturbations of both fatty acid titrations on the published crystal structures shows the ligand binding site deduced in solution to be localized in proximity to the ligands in the crystals. However, even though the two fatty acids are both composed of 18 carbons, in the two published crystal structures the ligand conformations in the protein cavity are not similar: oleate adopts a nearly straight extended form while linoleate is configured in a U-shaped form. Despite this difference in reported spatial orientations, the two ligands interacted similarly with AFABP in solution, and the binding interface is almost identical in solution except for the addition of two extra residues with enhanced perturbation in the linoleic acid titration. As mentioned previously, these two residues have similar magnitudes in both titrations except that they are slightly above one standard deviation above the average threshold for linoleate versus slightly below that threshold for oleate.

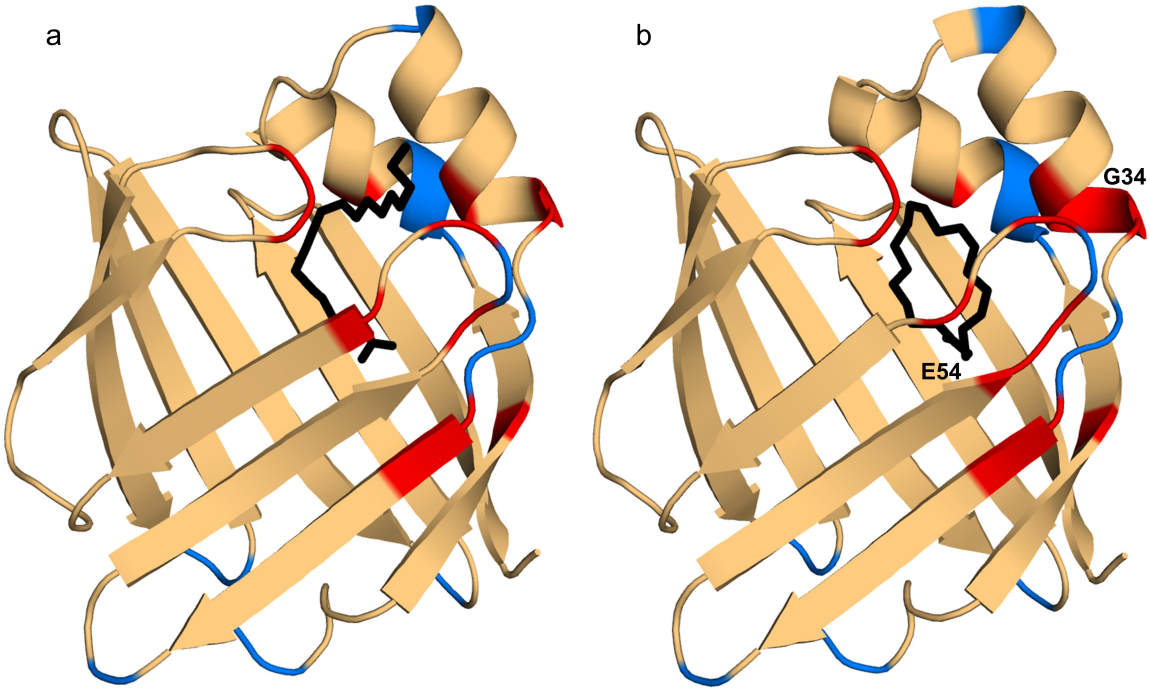

Figure V.38. Mapping of the chemical shift perturbations for oleate (a) and linoleate (b) titrations on crystal structure of holo (oleate, PDB: 1LID) and (linoleate, PDB: 2Q9S), respectively. Highly affected residues are colored red while unassigned residues are colored blue. Ligands are shown in black.

Residue F57 has been found to be present in an extended open conformation in the oleate X-ray crystal structure versus a closed one in linoleate (**Figure V.39).** Published reports state that residue F57 is of great importance for translocation of AFABP into the nucleus (Gillilan *et al.* 2007). It is presumed to perform this function upon binding to activating ligands (such as linoleate and Troglitazone) when its side chain is positioned in a closed conformation. This is presumed to allow F57 side chain interaction with V32, which in turn allows the residues involved in the nuclear localization signal (NLS, defined by residues K21 on α_I and R30 and K31 on α_{II}), (Ayers *et al.* 2007) to become revealed and therefore activate the NLS of the protein (Gillilan *et al.* 2007). However, residue F57 shows comparable magnitude of perturbation (0.5 and

0.44 ppm) in both solution-state NMR titrations of oleate and linoleate. It is interesting that the magnitude of perturbation of this residue is similar in both titrations despite the contrasting side chain displacement and orientation of residue F57 in the linoleate and oleate holo-AFABP X-ray crystal structures and similar location of F57 in apo and holo-linoleate proteins.

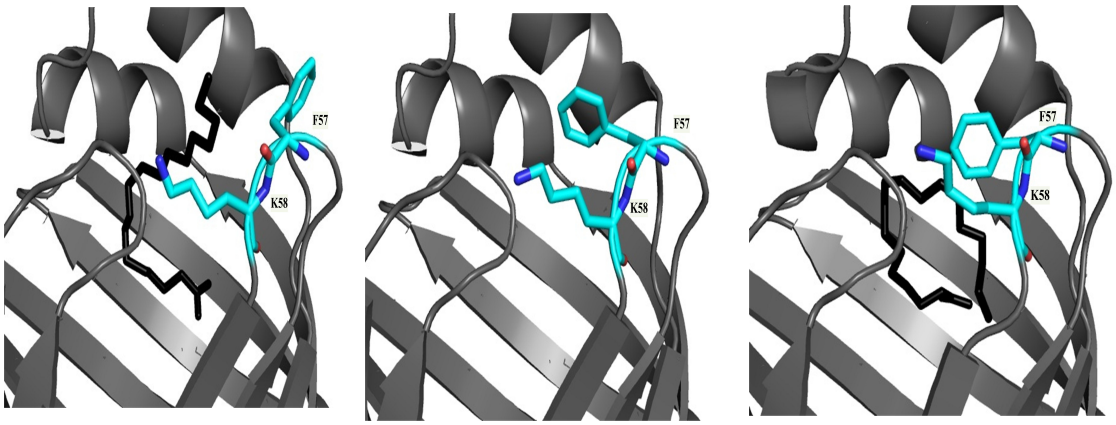

Figure V.39 position of F57 in apo AFABP (middle) and holo (oleate) AFABP (left) and holo (linoleate) AFABP (right) X-ray crystal structures.

In solution, the residues that are affected by the binding and hence define the binding site are very similar even though the conformations of the fatty acids are different in the published crystal structures (**Figure V.40**). Neither the oleate nor the linoleate NMR data are in full agreement with the position of the ligand in their respective crystal structures. Thus the positions of the ligand in the crystal structures are not in full agreement with the identified binding pocket deduced from the titration. The perturbed residues from the oleate and linoleate titrations form a contiguous region surrounding the location where a U-shaped linoleic acid is positioned in the crystal structure. The position of oleic acid in the crystal structure extends so that the carboxylate is buried in the cavity and the carbon tail protrudes out from the gap between α helix α_{II} and β-turns

connecting β-strands β_C-β_D and β_E-β_F. Neither structure of the crystallized ligands fit perfectly with the locus identified for their respective binding site identified by NMR (**Figure V.40**), but both binding sites are identical. Therefore a question arises differences in the position of the ligands in solution compared with the crystal structure.

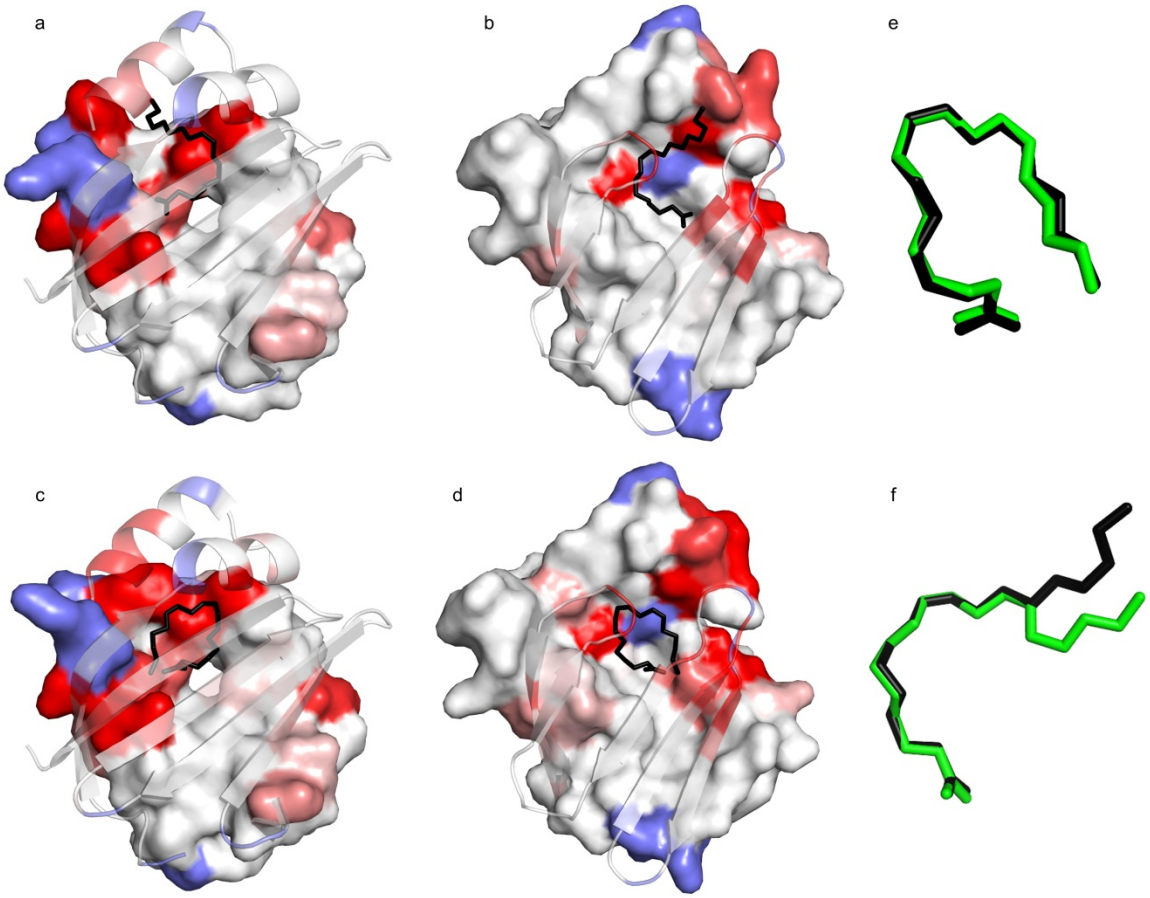

Figure V.40. Mapping of significant chemical shift perturbations from the oleate titration (colored red) on the crystal structure of holo (oleate) AFABP (a) and (b) and holo linoleate (c) and (d). Mapping of the chemical shift perturbations of all residues is displayed in a color gradient from red to white to represent large to small perturbations, while unassigned residues are colored blue. (b) and (d) are rotated 180° relative to (a) and (c), respectively. Oleic and linoleic acids are displayed in black inside their respective holo protein crystal cavities. Oleic acid (green) rotated to fit the conformation of linoleic acid (black) is shown in (e) while linoleic acid rotated to fit the conformation of oleic acid is shown in green (f) compared with linoleic acid (black).

Since the assignments were identified only for holo (oleate) AFABP and then were transferred to the holo (linoleate) AFABP spectrum, it was important to rule out that

the similarity in perturbations is an artifact of the transfer of assignments to linoleate-liganded protein. The holo (linoleate), and holo (oleate) spectra, give us confidence that the two proteins behave in a similar way: **Figure V.41** shows such similar chemical shift positions for the respective holo proteins that they could be almost confused as the same spectra. There were only eight ambiguously assigned resonances (discussed previously), which were accounted for while calculating the chemical shift perturbations. The similarity between the oleate and linoleate spectra gives us confidence in transferring the assignments from holo (oleate) to holo (linoleate) AFABP and allows for mapping of the perturbations onto the 3D structures of the holo proteins.

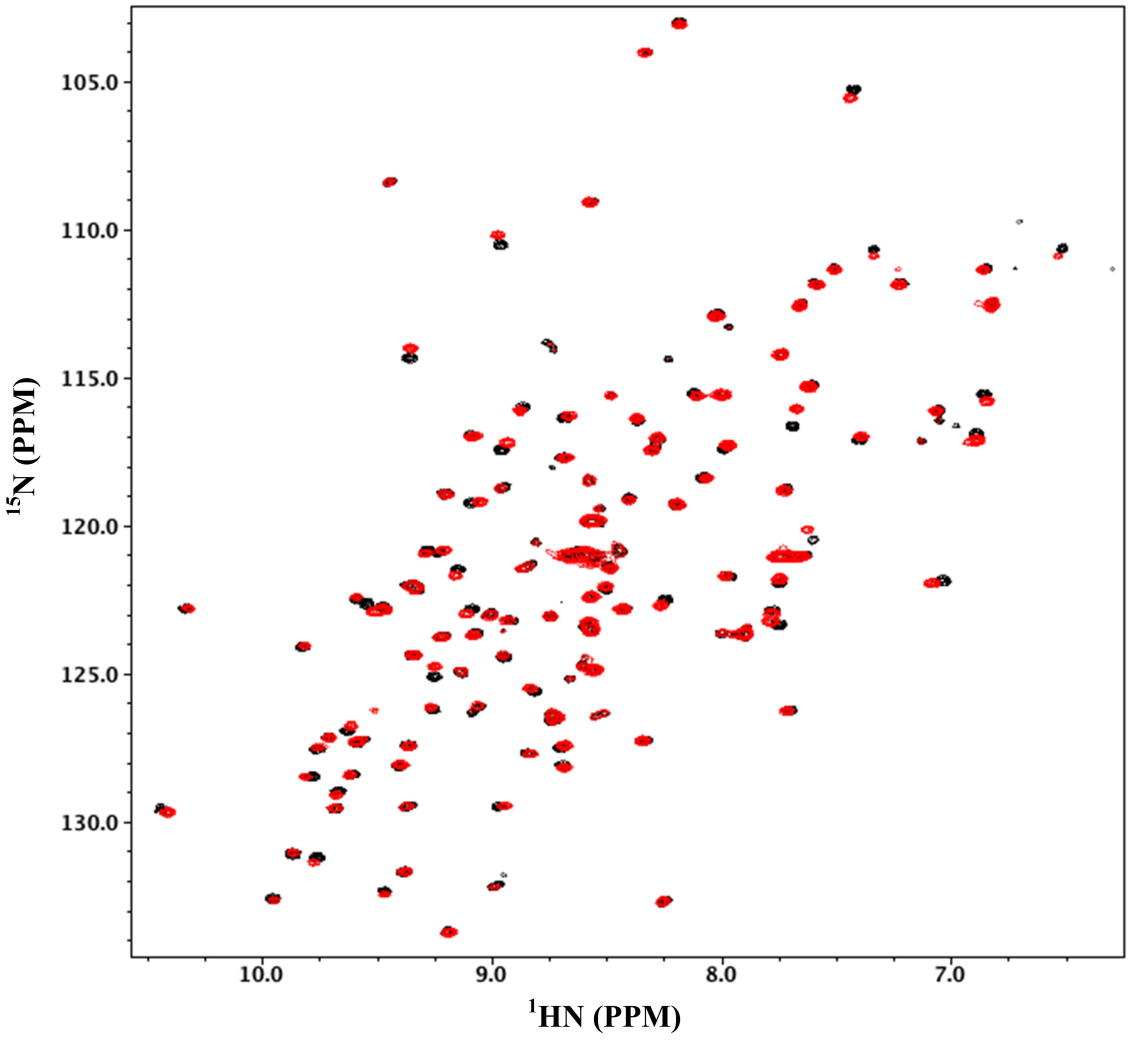

Figure V.41. Overlaid spectra of holo (oleate) and holo (linoleate) AFABP in black and red, respectively. The spectra show almost identical perturbations from holo (not shown) as witnessed by the overlapping spectra.

This similarity between the perturbations from the two fatty acid titrations suggests that the positions of the ligands in the protein cavity are also similar. While oleate and linoleate were crystallized in extended and U-shaped conformations respectively, we explored different scenarios that involved rotating the single bonds in oleate and linoleate to see whether both ligands could adopt similar conformations in solution. Using PyMOL and rotating single bonds, we found that the hydrocarbon chain

of oleate could rotate to make an almost perfect fit with linoleate (**Figure V.40.e**). Given that linoleate possesses a second double bond at C12, it was also possible to rotate linoleate to extend out of the cavity. It was possible to fit the first half of linoleate including the carboxyl group and leading to C11 with the conformation of oleate in the crystal structure perfectly, but the remaining hydrocarbon chain cannot fit with oleate due to the presence of a second double bond that restricts the angles and bond orientations (**Figure V.40.f**). Since the oleate and linoleate chemical shift perturbations form an identical contiguous binding pocket when mapped onto the tertiary crystal structure, it may be deduced that oleate and linoleate adopt identical conformations inside the cavity in solution. The extended fatty acid configuration is then disfavored for the holo proteins in solution because it cannot be adopted for both oleate and linoleate, and because it is in poorer accord with the chemical shift perturbation results. The common fatty acid conformation could be U-shaped like the linoleate conformation or intermediate between the oleate extended form and the linoleate U-shaped form. To produce protein crystals with favorable diffraction characteristics, buffers, buffer conditions, salt concentrations and the pH values are often changed dramatically. These conditions may favor particular structural motifs or conformations that may not be present in solution or under physiological conditions.

Based on our NMR titration data, it appears that oleate and linoleate have identical binding sites and the ligands adopt similar conformations in solution, despite having been reported to elicit different behavior of AFABP in the nucleus. The binding sites and modified oleate conformation are proposed in **Figure V.42**.

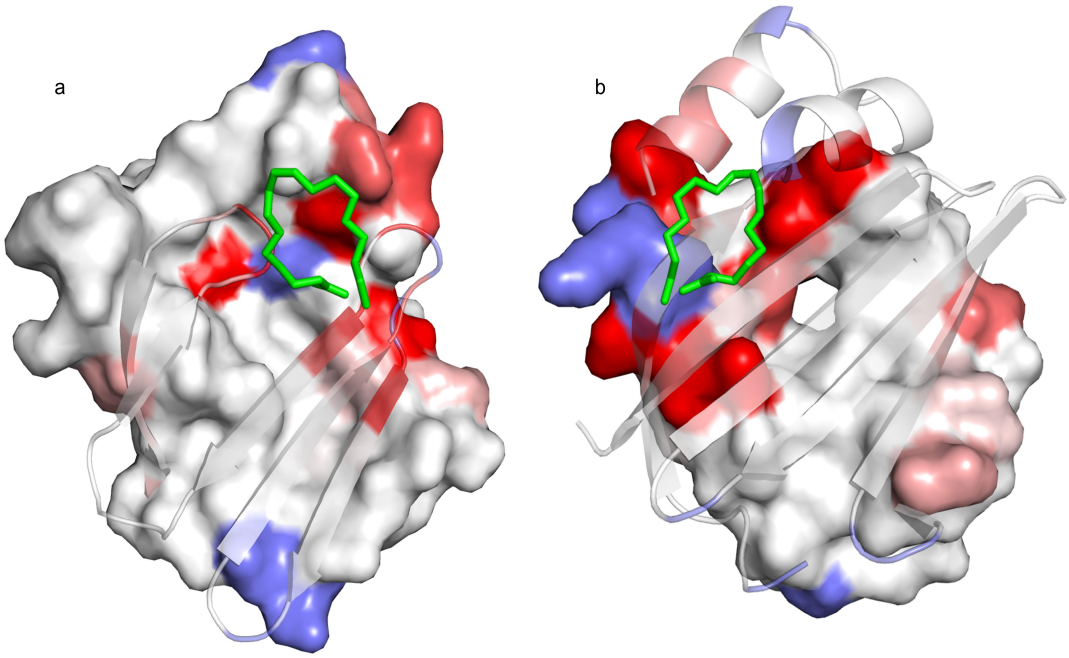

Figure V.42. Mapping of chemical shift perturbations of oleate titrations on the published crystal structure of holo (oleate) AFABP (PDB: 1LID). Oleate (shown in green) was rotated to fit inside the cavity as a proposed conformation in solution. The position of the ligand has been adjusted to fit the proposed binding site.

(b) Comparison between Linoleate and TDZ Titrations

By comparing the chemical shift perturbations from linoleate and TDZ titrations, it is possible to observe the differences and similarities between the locations of the most perturbed residues in the protein sequence by mapping the perturbations on the X-ray crystal structure. We are using linoleate as a proxy for oleate, since their effects on AFABP in solution are so similar. Additionally, linoleate and TDZ are reported to produce similar functional effects on AFABP, making it interesting to compare the effect for binding of those two ligands on the protein and investigate the commonalities and the differences. From the chemical shift perturbations it is clear that similar number of residues is affected by each ligand. However the location of these residues and the degree of localization are two stark differences between the linoleate and the TDZ ligand binding (**Figure V.43**). Thirteen residues (**Table V.5**). are perturbed in the linoleate titration constituting a binding site localized mainly on the two α-helices and the turns connecting the β-strands β_C-β_D and β_E-β_F. However, in the TDZ titration, nine residues are affected, plus three additional ambiguous ones, where a small binding site is localized on the turns connecting the same β-strands but not spanning the α-helices of the protein (**Figure V.44**). Moreover, in the TDZ titration, some perturbed residues are distant from the ligand and the binding site. These residues may experience a secondary effect of the binding of TDZ and possibly show perturbations due to a conformational change in the protein. This latter effect was not observed in the linoleate titration, where the binding site is tightly defined and lies in close proximity to the ligand location repored from the crystal structure.

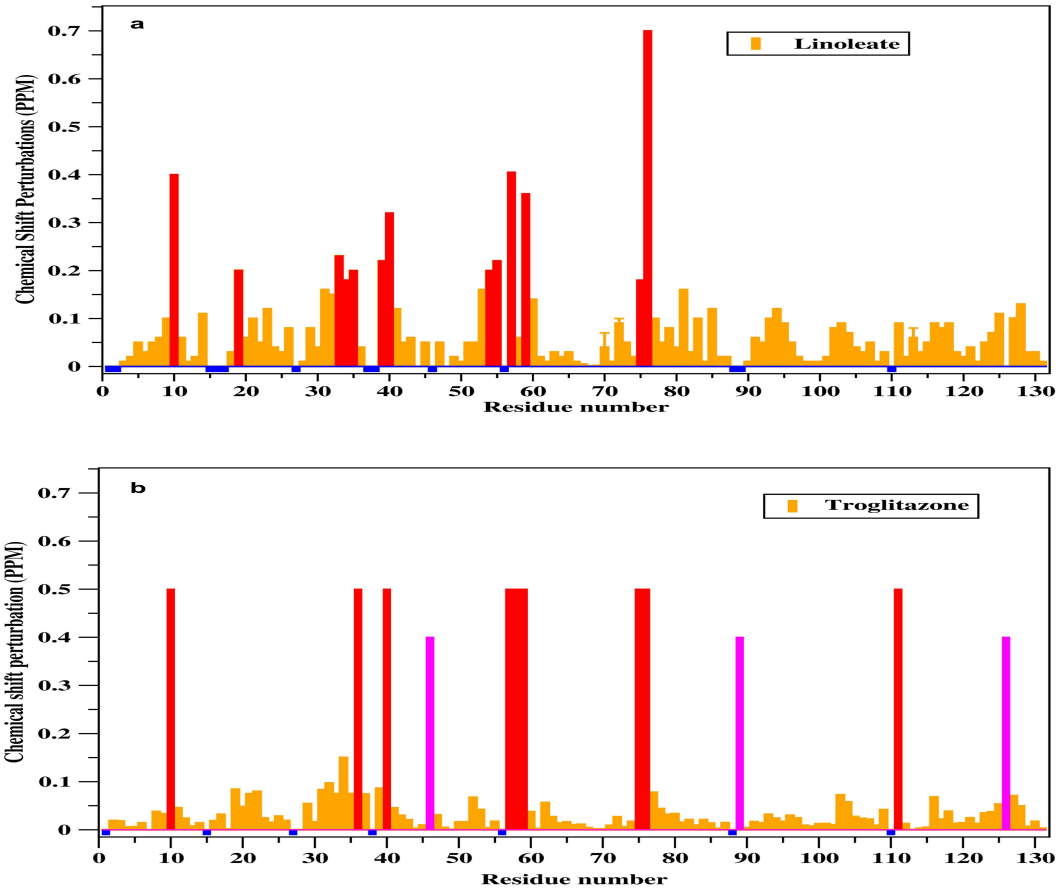

Figure V.43. Plots showing chemical shift perturbations for linoleate (top) and TDZ (bottom). Significantly perturbed residues are colored red, while unassigned ones are displayed in blue and assigned a negative value. Disappearing residues in the TDZ titration are assumed to be the most affected, and are assigned arbitrary values of 0.5 ppm, whereas ambiguously affected residues in the TDZ titration are assigned 0.4 ppm and shown in purple.

Considering that both linoleic acid and TDZ are activating ligands, our solution NMR data do not reveal common elements of molecular structure that account for this similar functional behavior. This difference between the linoleic acid and TDZ titrations in the location of the residues affected and specifically the absence of ivolvement for the α-helices in the TDZ binding leaves unexplained the mechanism by which these ligands produce a functional similarity on AFABP, specifically the hypothesis that ligands exert

their effect on the protein via unmasking residues of the nuclear localization signal (NLS) located on the α_{II} helix.

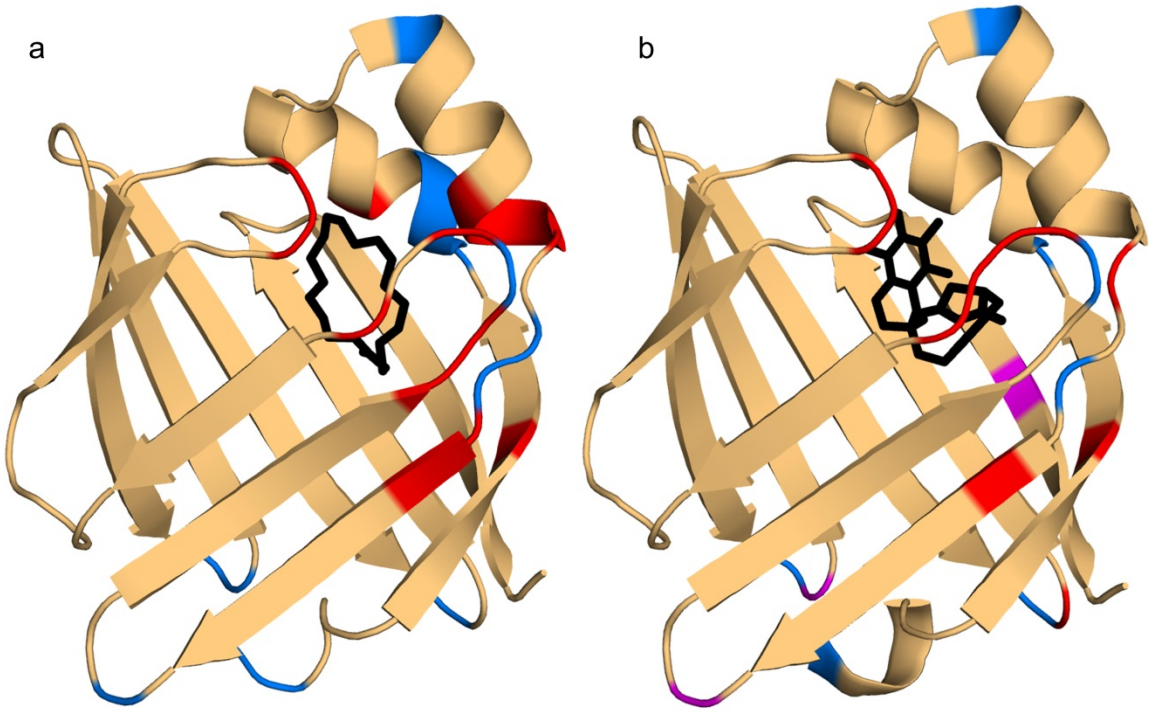

Figure V.44 . Mapping of the chemical shift perturbations for linoleate (left) and TDZ (right) titrations on crystal structure of holo (linoleate, PDB: 2Q9S) and (TDZ, PDB: 2QM9), respectively. Perturbed residues are colored red while ambiguously affected residues in TDZ titrations are colored purple. Unassigned residues are colored blue while the ligands are displayed in black color.

(c) Conclusion

As summarized in **Table V.5**, there are 11 and 13 residues that are most affected in the oleate and linoleate titrations, respectively. Nine residues disappear and are presumed to be the most affected in the TDZ titration with the addition of three (G46, G89 R126) that are identified provisionally because they were affected in only one of the TDZ titrations.

From our NMR data, while the two fatty acids have an identical effect on the AFABP, TDZ has a dissimilar effect that is difficult to correlate with the ligand size and location. Instead of observing a large binding pocket relative to the ligand size and location, the chemical shift perturbation data indicated a smaller binding pocket that does not involve the helices in addition to showing scattered indirect environment chemical changes at distant protein sites. These findings contrast with published data showing that, in contrast to oleate, TDZ and linoleic acid evoke similar functional behavior for AFABP. While it is possible for two ligand to bind differently but have similar finctional consequences, the solution-state NMR data do not offer a clear rationale for how each of these ligand exerts its effect on the protein.

Table V.5 Summary of residues most affected by ligand binding from the three ligand titrations (oleate, linoleate and TDZ).

	Residues that are most affected
Oleate titration	**11 residues: L10, Y19, A33, M35, N39, M40, S55, F57, N59, A75, and D76**
Linoleate titration	**13 residues: L10, Y19, A33, G34, M35, N39, M40, E54, S55, F57, N59, A75, and D76**
TDZ titrations	**9 common residues: L10, A36, M40, F57, K58, N59, A75, D76 and V111** **3 ambiguously affected residues: G46, G89 and R126**

2. Critical Assessment of Hypotheses for Ligand Modulation of AFABP Function

Our results from the three solution-state NMR titrations of oleate, linoleate and troglitazone with AFABP shed light on the locus for each ligand and structure of each protein-ligand complex (**Figure V.45**). Pairwise comparison of the data showed that oleate and linoleate have a nearly identical effect on the protein, as they interact with similar residues and have nearly identical binding sites, while TDZ has a dissimilar impact from the fatty acids (**Figure V.45**). Comparison of linoleic acid with TDZ shows that their respective binding sites are similar in location but differ in extent, despite their proposed similar activating and nuclear localizing functions. Even though intermediate exchange phenomena and solubility issues limited the scope of the TDZ study, the observed binding site for the TDZ interaction appeared differently located and localized; the α- helices are not affected by TDZ binding and the protein show a secondary effect that is far from the ligand binding site. However, from the fatty acid titration data, both fatty acids are likely to exist in a U-shaped conformation in solution, though their position inside the protein cavity differs somewhat from that found in the crystal structures. Our structural results suggest that the two fatty acids will affect the protein similarly and in a different manner than TDZ, that is, our molecular comparisons do not account for activating versus inactivating functional trends. Therefore it seems that this binding step is not where the protein discriminates between the two different ligands to produce contrasting functions.

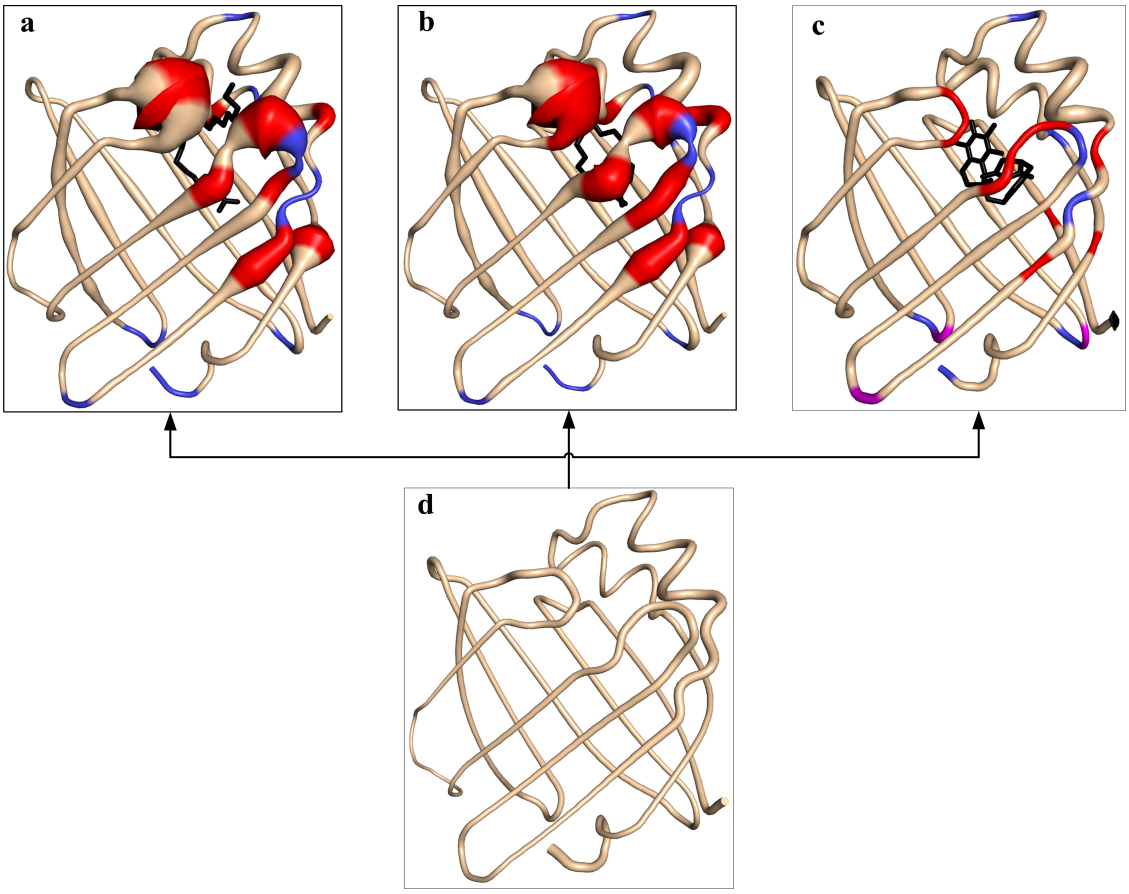

Figure V.45. Mapping of chemical shift perturbations of (a) oleate, (b) linoleate, (c) TDZ. Residues demonstrating large perturbation or disappearance are colored red and unassigned residues shown in blue. Residues that are ambiguously affected in TDZ titration are colored magenta. Apo AFABP is shown below (d) as a reference. The minimum and maximum cutoff for the thickness of the sausage putty are 0.0 and 0.7, respectively for comparitive analysis. Mapping was done on holo and apo structures (PDB: 1LID, 2Q9S, 2QM9 and 1LIB for (a), (b), (c) and (d), respectively.

While NMR allows study of the effect of ligand binding on the chemical environment of affected residues in solution, it is possible that the functional role of these ligands is not evident from simple pairwise interactions with AFABP that are reported by chemical shift perturbations. Since linoleate and TDZ ultimately lead to the activation of PPAR while oleate by contrast appears not to lead to its activation, it would be interesting to examine the effect of ligand binding on the AFABP/ PPARγ ligand assembly. That

plan is facilitated by the fact that the two proteins are currently being expressed and purified in our lab. By labeling one protein while the other remains unlabeled, it should be possible to identify the effect of one protein on the other. Specifically, complexing apo and holo AFABP with PPARγ simultaneously could probably give more insight to the role of each ligand in the interaction of this protein assembly.

It should also be noted that, Gillilan *et al.* claimed that linoleate and TDZ binding elicit their functional effects on the protein by inducing a specific homodimer conformation that facilitates translocation of AFABP into the nucleus, while oleate elicits a contrasting functional effect by inducing a different homodimer formation that localizes the protein in the cytosol (Gillilan *et al.* 2007). Our solution-state NMR data do not support the dimerization hypothesis of AFABP put forth by Gillilan *et al.* based on data from crystals produced in different solvents and salt conditions. Our size exclusion results for the three holo proteins (Chapter III) do not support dimer formation; instead the monomeric form of the protein is shown to be predominant (≥ 85 %) for both apo and holo forms. These observations include experiments done at low ionic strength to match some of the experiments done by Gilillan *et al*. Additionally, SLS experiments performed on the his-tagged holo (oleate) protein yielded an absolute molecular weight of 17 kDa, corresponding to a monomer.

Moreover, we saw no signs of dimerization in respective [^{1}H ^{15}N] HSQC spectra of apo and holo AFABP. Dimerization of a 15 kDa protein might be expected to result in peak broadeneing for resonances corresponding to those residues involved at the dimer

interface. Depending on the rate of chemical exchange between the dimer and monomer forms in solution, it may be possible to see such dimerization by NMR. If there is slow exchange between dimer and monomer protein forms, extra peaks corresponding to the residues in the dimer form may be visible in the HSQC spectrum unless the one form is predominant in the solution, while fast exchanging monomer and dimer forms of the protein will be averaged into a single peak. While extra peaks that we reported were often in holo positions and could not be assigned to any of AFABP residues due to loss of connectivity in the 3D experiments, the experiments for apo and holo showed a good signal and were performed using normal spectroscopic parameters. Loss of connectivity is thus not likely to be attributable to a larger complex for which T_2 relaxation causes the NMR signal to be diminished.

It is interesting that Gillilan *et al.* formulated this hypothesis to explain activating versus non activating ligands based on information from the protein crystal structures with these ligands, combined with fluorescence studies to observe protein localization in the nucleus versus the cytosol. However, a clean cut link and comparison between functional activation of PPAR and these ligands has not been defined. While TDZ, linoleate and oleate bind PPAR, the binding affinity and activation of the receptor are not similar. While TDZ is a synthetic activator, upon comparing oleate and linoleate binding and activity to PPAR it seems that linoleate is a better binder and activator for PPAR than oleate (Krey *et al.* 1997). However, direct comparison of linoleate and TDZ activity on the receptor has not been demonstrated.

Although Gillilan *et al.* used the structural information obtained from the crystal structures of AFABP complexed with these ligands to devise their activating versus inactivating functional rationale, their localization experiments using green fluorescent protein fused with AFABP to show nuclear localization upon binding of activating ligands are not complete. For instance, they show that AFABP localizes into the nucleus upon addition of an activating ligand (ANS), but they did not show the effect of oleic acid as a non activating ligand. They also showed that TDZ nuclear localization failed to occur upon mutation of F57, but did not demonstrate nuclear localization of wild type holo TDZ AFABP. A direct link between structural - functional effects of these ligands is required to be classified as activators versus non-activators, whereas Gillilan *et al.* appear to base their classification on structural features of the ligand binding made by different groups using different crystallization conditions rather than offering a clean comparison of the two dimerization models.

In sum, the mode of action of PPAR and its activation and repression remains incompletely specified. The structural rationale behind the activation of this functionally significant protein assembly is still unclear. While studying the effect of ligand on the protein complex of PPAR and AFABP is important, this study of AFABP-ligand interactions lays the foundation from which to unravel the impact of ligands on the biological function of the AFABP-PPAR. In order for this big protein assembly should be studied in depth, protein pairs should be studied independently, both in presence and in absence of ligands. Under order to assess the bigger picture, the protein pairs should be studied extensively in conditions close to physiological including salt concentrations.

It is possible that the activating versus non-activating effect of ligands on PPAR is influenced by the presence of PPAR itself, but in order to turn speculations into facts, more studies should be done on PPAR with activating and non-activating ligands and the PPAR-AFABP complex with the same ligands as well.

References

Adida, A. and Spener, F. (2006). "Adipocyte-type fatty acid-binding protein as inter-compartmental shuttle for peroxisome proliferator activated receptor gamma agonists in cultured cell." *Biochim Biophys Acta* **1761**(2): 172-181.

Akerstrom, B. (1992). "Role of alpha 1-microglobulin in immune response and inflammation." *Folia Histochem Cytobiol* **30**(4): 183-186.

Akerstrom, B. and Logdberg, L. (1990). "An intriguing member of the lipocalin protein family: alpha 1-microglobulin." *Trends Biochem Sci* **15**(6): 240-243.

Andrews, P. (1962). "Estimation of molecular weights of proteins by gel filtration." *Nature* **196**: 36-39.

Andrews, P. (1964). "Estimation of the molecular weights of proteins by Sephadex gel-filtration." *Biochem J* **91**(2): 222-233.

Ayers, S. D., Nedrow, K. L., Gillilan, R. E. and Noy, N. (2007). "Continuous nucleocytoplasmic shuttling underlies transcriptional activation of PPARgamma by FABP4." *Biochemistry* **46**(23): 6744-6752.

Banaszak, L., Winter, N., Xu, Z., Bernlohr, D. A., Cowan, S. and Jones, T. A. (1994). "Lipid-binding proteins: a family of fatty acid and retinoid transport proteins." *Adv Protein Chem* **45**: 89-151.

Bax, A. and Ikura, M. (1991). "An efficient 3D NMR technique for correlating the proton and ^{15}N backbone amide resonances with the alpha-carbon of the preceding residue in uniformly ^{15}N/^{13}C enriched proteins." *J Biomol NMR* **1**(1): 99-104.

Bayer, E. A. and Wilchek, M. (1990). "Application of avidin-biotin technology to affinity-based separations." *J Chromatogr* **510**: 3-11.

Bernard, C., Gely, S., Bourhis, J. M., Morelli, X., Longhi, S. and Darbon, H. (2009). "Interaction between the C-terminal domains of N and P proteins of measles virus investigated by NMR." *Febs Lett* **583**(7): 1084-1089.

Bhattacharjya, S. and Balaram, P. (1997). "Effects of organic solvents on protein structures: observation of a structured helical core in hen egg-white lysozyme in aqueous dimethylsulfoxide." *Proteins* **29**(4): 492-507.

Blaner, W. S. (1989). "Retinol-binding protein: the serum transport protein for vitamin A." *Endocr Rev* **10**(3): 308-316.

Boord, J. B., Maeda, K., Makowski, L., Babaev, V. R., Fazio, S., Linton, M. F. and Hotamisligil, G. S. (2004). "Combined adipocyte-macrophage fatty acid-binding protein deficiency improves metabolism, atherosclerosis, and survival in apolipoprotein E-deficient mice." *Circulation* **110**(11): 1492-1498.

Cavaggioni, A., Sorbi, R. T., Keen, J. N., Pappin, D. J. C. and Findlay, J. B. C. (1987). "Homology between the Pyrazine-Binding Protein from Nasal-Mucosa and Major Urinary Proteins." *Febs Lett* **212**(2): 225-228.

Cavanagh, J., Fairbrother, W. J., Palmer, A. G., Skelton, N. J. and Rance, M. (2007). Protein NMR Spectroscopy, 2nd Edition, Principles and Practice

Consortium, U. (2012). "Reorganizing the protein space at the Universal Protein Resource (UniProt)." *Nucleic Acids Res* **40**(D1): D71-D75.

Constantine, K. L., Friedrichs, M. S., Wittekind, M., Jamil, H., Chu, C. H., Parker, R. A., Goldfarb, V., Mueller, L. and Farmer, B. T., 2nd (1998). "Backbone and side chain dynamics of uncomplexed human adipocyte and muscle fatty acid-binding proteins." *Biochemistry* **37**(22): 7965-7980.

Cowan, S. W., Newcomer, M. E. and Jones, T. A. (1990). "Crystallographic refinement of human serum retinol binding protein at 2A resolution." *Proteins* **8**(1): 44-61.

Davies, G. F., McFie, P. J., Khandelwal, R. L. and Roesler, W. J. (2002). "Unique ability of troglitazone to up-regulate peroxisome proliferator-activated receptor-gamma expression in hepatocytes." *J Pharmacol Exp Ther* **300**(1): 72-77.

Delaglio, F., Grzesiek, S., Vuister, G. W., Zhu, G., Pfeifer, J. and Bax, A. (1995). "Nmrpipe - a Multidimensional Spectral Processing System Based on Unix Pipes." *Journal of Biomolecular Nmr* **6**(3): 277-293.

DeLano, W. and Lam, J. (2005). "PyMOL: A communications tool for computational models." *Abstracts of Papers of the American Chemical Society*(230): U1371-U1372.

Devchand, P. R., Keller, H., Peters, J. M., Vazquez, M., Gonzalez, F. J. and Wahli, W. (1996). "The PPARalpha-leukotriene B4 pathway to inflammation control." *Nature* **384**(6604): 39-43.

Esadze, A., Li, D. W., Wang, T. Z., Bruschweiler, R. and Iwahara, J. (2011). "Dynamics of Lysine Side-Chain Amino Groups in a Protein Studied by Heteronuclear ^{1}H-^{15}N NMR Spectroscopy." *Journal of the American Chemical Society* **133**(4): 909-919.

Ferrage, F., Zoonens, M., Warschawski, D. E., Popot, J. L. and Bodenhausen, G. (2003). "Slow diffusion of macromolecular assemblies by a new pulsed field gradient NMR method." *J Am Chem Soc* **125**(9): 2541-2545.

Flower, D. R. (1993). "Structural relationship of streptavidin to the calycin protein superfamily." *Febs Lett* **333**(1-2): 99-102.

Flower, D. R. (1996). "The lipocalin protein family: structure and function." *Biochem J* **318 (Pt 1)**: 1-14.

Flower, D. R., North, A. C. and Attwood, T. K. (1993). "Structure and sequence relationships in the lipocalins and related proteins." *Protein Sci* **2**(5): 753-761.

Fruchart, J. C., Duriez, P. and Staels, B. (1999). "Peroxisome proliferator-activated receptor-alpha activators regulate genes governing lipoprotein metabolism, vascular inflammation and atherosclerosis." *Curr Opin Lipidol* **10**(3): 245-257.

Furuhashi, M. and Hotamisligil, G. S. (2008). "Fatty acid-binding proteins: role in metabolic diseases and potential as drug targets." *Nat Rev Drug Discov* **7**(6): 489-503.

Gillilan, R. E., Ayers, S. D. and Noy, N. (2007). "Structural basis for activation of fatty acid-binding protein 4." *J Mol Biol* **372**(5): 1246-1260.

Glatz, J. F., Janssen, A. M., Baerwaldt, C. C. and Veerkamp, J. H. (1985). "Purification and characterization of fatty-acid-binding proteins from rat heart and liver." *Biochim Biophys Acta* **837**(1): 57-66.

Glatz, J. F. C., Luiken, J. J. F. P. and Bonen, A. (2010). "Membrane Fatty Acid Transporters as Regulators of Lipid Metabolism: Implications for Metabolic Disease." *Physiological Reviews* **90**(1): 367-417.

Gottlicher, M., Widmark, E., Li, Q. and Gustafsson, J. A. (1992). "Fatty acids activate a chimera of the clofibric acid-activated receptor and the glucocorticoid receptor." *Proc Natl Acad Sci U S A* **89**(10): 4653-4657.

Grzesiek, S. and Bax, A. (1992). "Correlating Backbone Amide and Side-Chain Resonances in Larger Proteins by Multiple Relayed Triple Resonance Nmr." *Journal of the American Chemical Society* **114**(16): 6291-6293.

Grzesiek, S. and Bax, A. (1992). "An Efficient Experiment for Sequential Backbone Assignment of Medium-Sized Isotopically Enriched Proteins." *Journal of Magnetic Resonance* **99**(1): 201-207.

Haunerland, N. S., F. (2003). "Properties and physiological significance of fatty acid binding proteins." *Lipobiology* **33**: 99-122.

Hawlicka, E. (1995). "Self-diffusion in multicomponent liquid systems." *Chemical Society Reviews* **24**(5): 367-377.

He, Y., Estephan, R., Yang, X. M., Vela, A., Wang, H., Bernard, C. and Stark, R. E. (2011). "A Nuclear Magnetic Resonance-Based Structural Rationale for Contrasting Stoichiometry and Ligand Binding Site(s) in Fatty Acid-Binding Proteins." *Biochemistry* **50**(8): 1283-1295.

Hirayama, K., Akashi, S., Furuya, M. and Fukuhara, K. (1990). "Rapid confirmation and revision of the primary structure of bovine serum albumin by ESIMS and Frit-FAB LC/MS." *Biochem Biophys Res Commun* **173**(2): 639-646.

Hohoff, C. and Spener, F. (1998). "Fatty acid binding proteins and mammary-derived growth inhibitor." *Fett-Lipid* **100**(6): 252-263.

Hotamisligil, G. S. (2006). "Inflammation and metabolic disorders." *Nature* **444**(7121): 860-867.

Hsu, K. T. and Storch, J. (1996). "Fatty acid transfer from liver and intestinal fatty acid-binding proteins to membranes occurs by different mechanisms." *J Biol Chem* **271**(23): 13317-13323.

Hunt, C. R., Ro, J. H., Dobson, D. E., Min, H. Y. and Spiegelman, B. M. (1986). "Adipocyte P2 gene: developmental expression and homology of 5'-flanking sequences among fat cell-specific genes." *Proc Natl Acad Sci U S A* **83**(11): 3786-3790.

Ibrahimi, A., Teboul, L., Gaillard, D., Amri, E. Z., Ailhaud, G., Young, P., Cawthorne, M. A. and Grimaldi, P. A. (1994). "Evidence for a common mechanism of action for fatty acids and thiazolidinedione antidiabetic agents on gene expression in preadipose cells." *Mol Pharmacol* **46**(6): 1070-1076.

Iwahara, J., Jung, Y. S. and Clore, G. M. (2007). "Heteronuclear NMR spectroscopy for lysine NH3 groups in proteins: Unique effect of water exchange on ^{15}N transverse relaxation." *Journal of the American Chemical Society* **129**(10): 2971-2980.

Johnson, B. A. (2004). "Using NMRView to visualize and analyze the NMR spectra of macromolecules." *Methods Mol Biol* **278**: 313-352.

Kay, L. E., Ikura, M., Tschudin, R. and Bax, A. (1990). "Three-dimensional triple-resonance NMR Spectroscopy of isotopically enriched proteins. 1990." *J Magn Reson* **213**(2): 423-441.

Kim, H. K. and Storch, J. (1992). "Free fatty acid transfer from rat liver fatty acid-binding protein to phospholipid vesicles. Effect of ligand and solution properties." *J Biol Chem* **267**(1): 77-82.

Kim, H. K. and Storch, J. (1992). "Mechanism of free fatty acid transfer from rat heart fatty acid-binding protein to phospholipid membranes. Evidence for a collisional process." *J Biol Chem* **267**(28): 20051-20056.

Kohanski, R. A. and Lane, M. D. (1990). "Monovalent avidin affinity columns." *Methods Enzymol* **184**: 194-200.

Krey, G., Braissant, O., L'Horset, F., Kalkhoven, E., Perroud, M., Parker, M. G. and Wahli, W. (1997). "Fatty acids, eicosanoids, and hypolipidemic agents identified as ligands of peroxisome proliferator-activated receptors by coactivator-dependent receptor ligand assay." *Mol Endocrinol* **11**(6): 779-791.

Laemmli, U. K. (1970). "Cleavage of structural proteins during the assembly of the head of bacteriophage T4." *Nature* **227**(5259): 680-685.

LaLonde, J. M., Bernlohr, D. A. and Banaszak, L. J. (1994). "X-ray crystallographic structures of adipocyte lipid-binding protein complexed with palmitate and hexadecanesulfonic acid. Properties of cavity binding sites." *Biochemistry* **33**(16): 4885-4895.

Laskowski, R. A. and Swindells, M. B. (2011). "LigPlot+: multiple ligand-protein interaction diagrams for drug discovery." *J Chem Inf Model* **51**(10): 2778-2786.

Lehmann, J. M., Moore, L. B., Smith-Oliver, T. A., Wilkison, W. O., Willson, T. M. and Kliewer, S. A. (1995). "An antidiabetic thiazolidinedione is a high affinity ligand for peroxisome proliferator-activated receptor gamma (PPAR gamma)." *J Biol Chem* **270**(22): 12953-12956.

Likic, V. A., Juranic, N., Macura, S. and Prendergast, F. G. (2000). "A "structural" water molecule in the family of fatty acid binding proteins." *Protein Sci* **9**(3): 497-504.

Likic, V. A. and Prendergast, F. G. (2001). "Dynamics of internal water in fatty acid binding protein: computer simulations and comparison with experiments." *Proteins* **43**(1): 65-72.

Lucke, C., Huang, S., Rademacher, M. and Ruterjans, H. (2002). "New insights into intracellular lipid binding proteins: The role of buried water." *Protein Sci* **11**(10): 2382-2392.

Lucke, C., Qiao, Y., van Moerkerk, H. T., Veerkamp, J. H. and Hamilton, J. A. (2006). "Fatty-acid-binding protein from the flight muscle of Locusta migratoria: evolutionary variations in fatty acid binding." *Biochemistry* **45**(20): 6296-6305.

Makowski, L., Boord, J. B., Maeda, K., Babaev, V. R., Uysal, K. T., Morgan, M. A., Parker, R. A., Suttles, J., Fazio, S., Hotamisligil, G. S. and Linton, M. F. (2001). "Lack of macrophage fatty-acid-binding protein aP2 protects mice deficient in apolipoprotein E against atherosclerosis." *Nat Med* **7**(6): 699-705.

Marcelino, A. M., Smock, R. G. and Gierasch, L. M. (2006). "Evolutionary coupling of structural and functional sequence information in the intracellular lipid-binding protein family." *Proteins* **63**(2): 373-384.

Marion, D., Driscoll, P. C., Kay, L. E., Wingfield, P. T., Bax, A., Gronenborn, A. M. and Clore, G. M. (1989). "Overcoming the overlap problem in the assignment of ^{1}H NMR spectra of larger proteins by use of three-dimensional heteronuclear ^{1}H-^{15}N Hartmann-Hahn-multiple quantum coherence and nuclear Overhauser-multiple quantum coherence spectroscopy: application to interleukin 1 beta." *Biochemistry* **28**(15): 6150-6156.

Marley, J., Lu, M. and Bracken, C. (2001). "A method for efficient isotopic labeling of recombinant proteins." *J Biomol NMR* **20**(1): 71-75.

Matarese, V. and Bernlohr, D. A. (1988). "Purification of murine adipocyte lipid-binding protein. Characterization as a fatty acid- and retinoic acid-binding protein." *J Biol Chem* **263**(28): 14544-14551.

Meadus, W. J., MacInnis, R. and Dugan, M. E. (2002). "Prolonged dietary treatment with conjugated linoleic acid stimulates porcine muscle peroxisome proliferator activated receptor gamma and glutamine-fructose aminotransferase gene expression in vivo." *J Mol Endocrinol* **28**(2): 79-86.

Mesgarzadeh, A., Pfeiffer, S., Engelke, J., Lassen, D. and Ruterjans, H. (1998). "Bound water in apo and holo bovine heart fatty-acid-binding protein determined by heteronuclear NMR spectroscopy." *Eur J Biochem* **251**(3): 781-786.

Mulder, F. A. A., Schipper, D., Bott, R. and Boelens, R. (1999). "Altered flexibility in the substrate-binding site of related native and engineered high-alkaline Bacillus subtilisins." *Journal of Molecular Biology* **292**(1): 111-123.

Oeemig, J. S., Jorgensen, M. L., Hansen, M. S., Petersen, E. I., Duroux, L. and Wimmer, R. (2009). "Backbone and sidechain ^{1}H, ^{13}C and ^{15}N resonance assignments of the human brain-type fatty acid binding protein (FABP7) in its apo form and the holo forms binding to DHA, oleic acid, linoleic acid and elaidic acid." *Biomol NMR Assign* **3**(1): 89-93.

Onate, S. A., Tsai, S. Y., Tsai, M. J. and O'Malley, B. W. (1995). "Sequence and characterization of a coactivator for the steroid hormone receptor superfamily." *Science* **270**(5240): 1354-1357.

Ong, D. E. (1987). "Cellular retinoid-binding proteins." *Arch Dermatol* **123**(12): 1693-1695a.

Ory, J., Kane, C., Bernlohr, D. and Banaszak, L. (1995). "Structural and Biochemical-Characterization of Portal Mutants of Adipocyte Lipid-Binding Protein." *Faseb J* **9**(6): A1394-A1394.

Rademacher, M., Zimmerman, A. W., Ruterjans, H., Veerkamp, J. H. and Lucke, C. (2002). "Solution structure of fatty acid-binding protein from human brain." *Mol Cell Biochem* **239**(1-2): 61-68.

Reese-Wagoner, A., Thompson, J. and Banaszak, L. (1999). "Structural properties of the adipocyte lipid binding protein." *Biochimica Et Biophysica Acta-Molecular and Cell Biology of Lipids* **1441**(2-3): 106-116.

Richards, F. M. (1990). "Avidin-biotin technology. Reflections." *Methods Enzymol* **184**: 3-5.

Richieri, G. V., Ogata, R. T. and Kleinfeld, A. M. (1994). "Equilibrium-Constants for the Binding of Fatty-Acids with Fatty-Acid-Binding Proteins from Adipocyte, Intestine, Heart, and Liver Measured with the Fluorescent-Probe Adifab." *J Biol Chem* **269**(39): 23918-23930.

Ruterjans, H., Lucke, C., Rademacher, M., Zimmerman, A. W., van Moerkerk, H. T. B. and Veerkamp, J. H. (2001). "Spin-system heterogeneities indicate a selected-fit mechanism in fatty acid binding to heart-type fatty acid-binding protein (H-FABP)." *Biochem J* **354**: 259-266.

Sacchettini, J. C., Hauft, S. M., Van Camp, S. L., Cistola, D. P. and Gordon, J. I. (1990). "Developmental and structural studies of an intracellular lipid binding protein expressed in the ileal epithelium." *J Biol Chem* **265**(31): 19199-19207.

Sacchettini, J. C., Scapin, G., Gopaul, D. and Gordon, J. I. (1992). "Refinement of the structure of Escherichia coli-derived rat intestinal fatty acid binding protein with bound oleate to 1.75-A resolution. Correlation with the structures of the apoprotein and the protein with bound palmitate." *J Biol Chem* **267**(33): 23534-23545.

Saltiel, A. R. and Kahn, C. R. (2001). "Insulin signalling and the regulation of glucose and lipid metabolism." *Nature* **414**(6865): 799-806.

Scapin, G., Gordon, J. I. and Sacchettini, J. C. (1992). "Refinement of the structure of recombinant rat intestinal fatty acid-binding apoprotein at 1.2-A resolution." *J Biol Chem* **267**(6): 4253-4269.

Schaap, F. G., van der Vusse, G. J. and Glatz, J. F. (2002). "Evolution of the family of intracellular lipid binding proteins in vertebrates." *Mol Cell Biochem* **239**(1-2): 69-77.

Scheja, L., Makowski, L., Uysal, K. T., Wiesbrock, S. M., Shimshek, D. R., Meyers, D. S., Morgan, M., Parker, R. A. and Hotamisligil, G. S. (1999). "Altered insulin secretion associated with reduced lipolytic efficiency in aP2-/- mice." *Diabetes* **48**(10): 1987-1994.

Snyder, S. H., Sklar, P. B. and Pevsner, J. (1988). "Molecular mechanisms of olfaction." *J Biol Chem* **263**(28): 13971-13974.

Sorof, S. (1994). "Modulation of mitogenesis by liver fatty acid binding protein." *Cancer Metastasis Rev* **13**(3-4): 317-336.

Storch, J. and Corsico, B. (2008). "The emerging functions and mechanisms of mammalian fatty acid-binding proteins." *Annu Rev Nutr* **28**: 73-95.

Storch, J. and Thumser, A. E. (2000). "The fatty acid transport function of fatty acid-binding proteins." *Biochim Biophys Acta* **1486**(1): 28-44.

Sun, T., Chance, R. R., Graessley, W. W. and Lohse, D. J. (2004). "A Study of the Separation Principle in Size Exclusion Chromatography." *Macromolecules* **37**(11): 4304-4312.

Tan, N. S., Shaw, N. S., Vinckenbosch, N., Liu, P., Yasmin, R., Desvergne, B., Wahli, W. and Noy, N. (2002). "Selective cooperation between fatty acid binding proteins and peroxisome proliferator-activated receptors in regulating transcription." *Mol Cell Biol* **22**(14): 5114-5127.

Thompson, J. D., Gibson, T. J., Plewniak, F., Jeanmougin, F. and Higgins, D. G. (1997). "The CLUSTAL_X windows interface: flexible strategies for multiple sequence alignment aided by quality analysis tools." *Nucleic Acids Res* **25**(24): 4876-4882.

Tjernberg, A., Markova, N., Griffiths, W. J. and Hallen, D. (2006). "DMSO-related effects in protein characterization." *J Biomol Screen* **11**(2): 131-137.

Tontonoz, P., Hu, E. and Spiegelman, B. M. (1994). "Stimulation of adipogenesis in fibroblasts by PPAR gamma 2, a lipid-activated transcription factor." *Cell* **79**(7): 1147-1156.

Ulrich, E. L., Akutsu, H., Doreleijers, J. F., Harano, Y., Ioannidis, Y. E., Lin, J., Livny, M., Mading, S., Maziuk, D., Miller, Z., Nakatani, E., Schulte, C. F., Tolmie, D. E., Wenger, R. K., Yao, H. Y. and Markley, J. L. (2008). "BioMagResBank." *Nucleic Acids Res* **36**: D402-D408.

Vassileva, G., Huwyler, L., Poirier, K., Agellon, L. B. and Toth, M. J. (2000). "The intestinal fatty acid binding protein is not essential for dietary fat absorption in mice." *Faseb J* **14**(13): 2040-2046.

Veerkamp, J. H., Peeters, R. A. and Maatman, R. G. (1991). "Structural and functional features of different types of cytoplasmic fatty acid-binding proteins." *Biochim Biophys Acta* **1081**(1): 1-24.

Wallace, A. C., Laskowski, R. A. and Thornton, J. M. (1995). "LIGPLOT: a program to generate schematic diagrams of protein-ligand interactions." *Protein Eng* **8**(2): 127-134.

Wang, Y. W., Teraoka, I., Hansen, F. Y., Peters, G. H. and Hassager, O. (2010). "A Theoretical Study of the Separation Principle in Size Exclusion Chromatography." *Macromolecules* **43**(3): 1651-1659.

Whitaker, J. R. (1963). "Determination of Molecular Weights of Proteins by Gel Filtration on Sephadex." *Anal Chem* **35**(12): 1950-&.

Wootan, M. G., Bernlohr, D. A. and Storch, J. (1993). "Mechanism of fluorescent fatty acid transfer from adipocyte fatty acid binding protein to membranes." *Biochemistry* **32**(33): 8622-8627.

Wuthrich, K. (1986). NMR of proteins and Nucleic Acids. New York, Wiley.

Xu, Z., Buelt, M. K., Bernlohr, D. A. and Banaszak, L. J. (1992). "Crystal-Structures of the Apo-Adipocyte and Holo-Adipocyte Lipid-Binding Protein." *Faseb J* **6**(1): A288-A288.

Xu, Z. H., Bernlohr, D. A. and Banaszak, L. J. (1993). "The Adipocyte Lipid-Binding Protein at 1.6-a Resolution - Crystal-Structures of the Apoprotein and with Bound Saturated and Unsaturated Fatty-Acids." *J Biol Chem* **268**(11): 7874-7884.

Yao, S., Howlett, G. J. and Norton, R. S. (2000). "Peptide self-association in aqueous trifluoroethanol monitored by pulsed field gradient NMR diffusion measurements." *J Biomol NMR* **16**(2): 109-119.

Young, A. C., Scapin, G., Kromminga, A., Patel, S. B., Veerkamp, J. H. and Sacchettini, J. C. (1994). "Structural studies on human muscle fatty acid binding protein at 1.4 A resolution: binding interactions with three C18 fatty acids." *Structure* **2**(6): 523-534.

Yu, S. and Reddy, J. K. (2007). "Transcription coactivators for peroxisome proliferator-activated receptors." *Biochim Biophys Acta* **1771**(8): 936-951.

Zhang, O., Kay, L. E., Olivier, J. P. and Forman-Kay, J. D. (1994). "Backbone ^{1}H and ^{15}N resonance assignments of the N-terminal SH3 domain of drk in folded and unfolded states using enhanced-sensitivity pulsed field gradient NMR techniques." *J Biomol NMR* **4**(6): 845-858.

Zimm, B. (1948). "The Scattering of Light and the Radial Distribution Function of High Polymer Solutions." *The Journal of Chemical Physics* **16**(12): 7.

Zimmerman, A. W., van Moerkerk, H. T. and Veerkamp, J. H. (2001). "Ligand specificity and conformational stability of human fatty acid-binding proteins." *Int J Biochem Cell Biol* **33**(9): 865-876.

Zimmermann, H., Braun, N., Kegel, B. and Heine, P. (1998). "New insights into molecular structure and function of ectonucleotidases in the nervous system." *Neurochem Int* **32**(5-6): 421-425.

Zuiderweg, E. R. (2002). "Mapping protein-protein interactions in solution by NMR spectroscopy." *Biochemistry* **41**(1): 1-7.